THÈSE

Présentée à l'Université de Lille 1

Sciences et Technologies

pour obtenir le grade de

DOCTEUR

Spécialité : Molécules et Matière Condensée

Présentée par

Prashant RAJBHANDARI

le 29 Octobre 2013

Advanced NMR characterization of the effect of Al_2O_3, B_2O_3 and SiO_2 doping on low-T_g phosphate based glass.

Jury:

Gilles SILLY	Professeur, Université Montpellier II	Rapporteur
Thierry CARDINAL	DR CNRS, ICMCB Bordeaux	Rapporteur
Ronan LEBULLENGER	MDC, Université de Rennes	Examinateur
Herve VEZIN	DR CNRS, LASIR, Lille	Examinateur
Lionel MONTAGNE	Professor, Université Lille 1	Directeur
Gregory TRICOT	MDC Université Lille 1	Co-encadrant

Acknowledgements

First of all, I would like to thank my PhD supervisors, Mr. Lionel Montagne and Mr. Gregory Tricot, for supporting me during these past 3 years. My utmost and sincere thanks go to Lionel for his continued support, guidance and encouragement throughout this project.

My heartfelt thanks go to Mr. Gregory Tricot without whom this work would not have been completed. He is someone with full of good sense of humor and one of the smartest people I know. I hope that I could be as lively, enthusiastic and energetic as him and to someday be able to command an audience as he can. He has not only inspired me with his scientific advices, insightful discussions and suggestions, but also taught me how to make an effective presentation in a science community. Besides science, I also have an opportunity to learn so many things from him, among which the integration of professionalism, humor, friendliness and patience even during difficult times is the one for which I will forever be thankful.

There are many people from the laboratory who have contributed their expertise to allow the project to mature. I gratefully thank the entire people of Unité de Catalyse et Chimie du Solide (UCCS). My special thanks go to Mr. Julien Trébosc not only for his proficient manipulation of NMR spectrometer that impresses me favorably but also for imparting his knowledge at the same time. I am also grateful to Mr. Bertrand Doumert, Mr. Bertrand Revel and Mr. Xing Yu for their guidance and help as and when required during the experiments. Many thanks to Ms. Veronique Alaimo and Mr. Maxence Vandewalle for always being kind to me at all circumstances at the glass preparation room. I will specially remember the humor that I used to share with Mr. Maxence- ‘the big smile on his face’. I sincerely thank Ms. Annick Rubbens, Ms. Nora Djelal, Ms. Lawrence Burlyo, Mr. Jeremy Maton, Mr. Edward Capoen and Ms. Claudine Devynck for their kind support. The hilarious way of sharing experiences and wisdom at the same time from Mr. Laurent Delevoye has always awaken me up and thus cannot be forgotten.

Acknowledgements

I am also highly thankful to my colleagues Mr. Thomas Lemesle, Ms. Sandra Castanié and Ms. Esperanza Pavon for helping me in all the difficult tasks of mine during the entire period. Working with such fabulous colleagues and their amicable environment made me feel these 3 years so short.

Over the years, it's a great luck of mine to have friends like Jusal, Firealem, Matteo, Giuliano, Thomas, Sandra, Esperanza, Kelly, Freddy, Carla, Almaz, Maryna, Olga and Era who always stayed by my side during all my moments of joy and sorrow. Their contributions are more valuable than anything. Many thanks to Florent, Renald, Guillaume, Clement, Ana Gil, Vincent, Nathalie, Anne-lise and all for their warm company.

An honorable mention goes to my family (my parents, my brothers and sisters) for their understandings and support on me in completing this thesis. Especially, I have no words to express my appreciation to my wife Dhira Shrestha, unconditional love and persistent confidence in me, has taken a load off my shoulder. I owe her my deepest gratitude for her patience and endurance. Special thanks to the newest additions to my family, my daughter Rhea for desperately awaiting for us to be united.

Finally, I would like to thank everyone who has directly or indirectly supported this work, as well as expressing my apology for being unable to mention here personally one by one.

Table of contents

Table of contents

Chapter C: Investigation of the zinc sodium pyrophosphate glasses: effect of the Zn/Na ratio on the properties, stability and network structure

Table of contents

Chapter F: Discussion about the doping effect

General introduction

Developing glasses presenting simultaneously a low glass transition temperature (T_g < 400°C) and high thermal and chemical stabilities is an exciting topic in glass science. Low T_g is indeed usually associated to a glass network exhibiting low energy bonds and a low degree of polymerization. Hence, it seems that stability and low T_g are contradictory and that low-T_g glasses are easily crystallized or attacked by water whereas stable glasses exhibits very high thermal characteristics. Therefore, numerous papers have been devoted in the last decades to formulations searching for the best low-T_g/stability compromises. They have been motivated by the wide range of technical applications that could benefit from these materials. In addition to classical low temperature applications like sealing glasses for electronic devices, protective coatings for aeronautical applications, refractory adhesives, overcladding materials for glass fibers, glass-polymer alloys matrices, these materials could also be used as or biomaterials and to confine volatile radioactive wastes.

Classical silica based oxide glasses usually present high T_g and the very important amount of modifier oxide required to decrease the T_g under 400°C leads to depolymerized structure and unstable glasses. Different network former oxides have thus been considered for the development of low-T_g and stable materials. Interesting compositions were formulated from the PbO-B_2O_3 or PbO-ZnO-B_2O_3 systems (Dietz 1972, Tawansi 1988 and Zivanovic 2000). Unfortunately, the toxicity of lead oxide, used in very high proportion in these glasses, forced the glass community to find alternative compositions. Phosphate glasses were presented as a credible alternative. Many patents have been published from the Corning society about P_2O_5-based compositions presenting low-T_g and acceptable stability (Aitken 1990, 1993, 1994(a), 1994(b), 1996 and Beall 1991(a), 1991(b), 1992). The formulations are very complex and can be based on more than 15 different oxides, some of them being used at very low proportions. Usually, the papers contain many formulations accompanied by observed and measured properties. Moreover, stability is usually considered as the water attack resistance and there is only sparse information about the resistance against crystallization, even if this property governs some of the above-

mentioned low temperature applications. No systematic investigations, trying to clearly establish structure/properties/compositions relationships, are available in the literature.

However, we believe that this important glass science topic could greatly benefit from investigations (i) taking into account the structural point of view, (ii) focusing on the exact role and structure of the oxides used in minor proportions (denoted as dopants in the following) and (iii) investigating both chemical (resistance against water) and thermal (resistance against crystallization) stabilities. This is the starting point of the work presented in this Ph-D manuscript.

Of course, the system investigated here was simplified to enable efficient investigation. Among all the systems presented in the numerous patents, the zinc alkali pyrophosphate system (ZnO- M_2O- $33.4P_2O_5$, M=Li, Na and K) catches our attention owing to its excellent properties and low-T_g values. This is why we carried out a systematic study of the macroscopic properties (T_g, density (ρ), molar volume (V_M)), chemical and thermal stabilities and local and medium range order structure of this composition line, to assess the relevancy of that system for the development of low-T_g and stable glasses. Then, one doping element was introduced in low amounts (1-4 mol%) in the formulations to investigate its effect on the properties, stabilities and structure. Among all the doping elements used in the literature (Al^{3+}, B^{3+}, Fe^{3+},Ga^{3+}, Si^{4+}, Ti^{4+}, Mo^{6+}), three dopants were used in this study. We have chosen to analyze the effect of Al-, B- and Si-doping procedure owing to the important number of papers dealing with these elements. Another criteria leading to this choice was that the main technique used for the structural characterization presented here is the Nuclear Magnetic Resonance (NMR) spectroscopy. Indeed, this technique will allow for an efficient characterization of the doping elements though ^{27}Al, ^{11}B and ^{29}Si MAS-NMR analysis. In addition, it is well known that ^{31}P MAS-NMR is the technique of choice for the structural characterization of the phosphate network. In addition to 1D analysis, 1D/2D correlation NMR has also been used to analyze the interaction between the phosphate network and the doping elements. If the use of correlation NMR in mixed network phosphate glasses (containing significant amount of P_2O_5 and other oxides like B_2O_3 or Al_2O_3) is routinely applied nowadays, the very low amounts of dopant was considered for a long time as a strong limitation for the application of correlation NMR techniques. However, the development of very stable and robust techniques makes this investigation a challenging (but no more impossible)

topic. The only drawback of NMR within this study will be its inefficiency of investigating the zinc environment.

The global objective of this work is thus to investigate the effect of Al-, B- and Si-doping of low-T_g phosphate glasses developed within the zinc alkali pyrophosphate system. This work will contribute to understand how the doping elements enter into the network, change the glass structure and modify the properties and stabilities of the materials. Supported formulations leading to phosphate glasses presenting optimized low-T_g and stability compromise could then be derived from this work and will possibly open the way for new applications.

This work is divided in 6 chapters:

(i) the first part is devoted to the state of the art. Generalities on oxide glasses, phosphate glasses and low-T_g phosphate glasses will be presented. Doping in phosphate glasses will also be discussed. We will explain how the zinc alkali phosphate system was chosen from all the systems presented in the different patents;

(ii) the second chapter deals with the methods and techniques used in this work. The glass preparation using the standard melt-quenching method is described in the first part. The techniques used to determine the macroscopic properties (thermal analysis, pycnometer, X-ray diffraction, viscosimetry) and stabilities are exposed in the second part. Then, the Raman and NMR spectroscopic techniques employed to analyse the structure are presented in the third part. A particular emphasis has been given to the 1D/2D NMR correlation methods used in this work;

(iii) the third chapter is dedicated to the base zinc sodium pyrophosphate composition line. Glasses within the (66.6-*x*)ZnO- *x*Na_2O- 33.4P_2O_5 system have been prepared and systematically characterized. The impact of the Zn/Na substitution on the macroscopic properties (T_g, ρ and V_M) and on the chemical and thermal stabilities has been investigated. The local- and medium- range orders of the phosphate structure are then analysed by means of Raman and 1D ^{31}P NMR and 2D ^{31}P DQ-SQ NMR, respectively. The extent of disorder in the spectroscopies of glass network has been

derived from the complete set of analysis and discussed. Optimum formulations presenting the best low-T_g/stability have been derived and will be used in the following chapter for the doping procedures;

(iv) the fourth chapter presents the Al-, B- and Si-doping procedures and their effect on the macroscopic properties and stabilities. The role of each dopant on the glass characteristic is discussed based on the complete sets of results. In addition to the T_g, ρ, V_M and chemical and thermal stabilities, the impact of doping on the viscosity has also been investigated by using the parallel-plates viscosimetry method. Finally, preliminary structural study was obtained by Raman and 1D MAS-NMR techniques. If the Si-doping procedure can be explained using the 1D ^{29}Si MAS-NMR results, ^{27}Al and ^{11}B NMR analyses only provide information about the coordination state. No clear information about the P/dopant interactions can be derived from these analyses in case of the Al- and B-doping procedures;

(v) the fifth chapter presents the structural results obtained by 1D/2D ^{31}P/X correlation NMR with X=^{27}Al and ^{11}B. Definitive and supported conclusions about the presence of P-O-X bonds are derived from the X/^{31}P 2D correlation maps edited with the ^{31}P{X} D-INEPT technique. The chemical environment adopted by the doping elements was analysed using the X{^{31}P} REDOR and X DQ-SQ techniques. The complete sets of data allow describing the modifications of the phosphate network as well as the exact chemical environment adopted by the dopant elements within the glass structure;

(vi) structure/properties relationships governing the doped low-T_g phosphate glasses investigated here are discussed in the sixth and last chapter. Formulation benefitting from the information provided by this work is finally presented. Perspectives coming from that work are also discussed.

References

Aitken, B. *US Patent 5.021.366*, 1990.

Aitken, B. *US Patent 5.256.604*, 1993.

Aitken, B. *US Patent 5.153.151*, 1994(a).

Aitken, B. *US Patent 5.286683*, 1994(b).

Aitken, B, G Beall, and J Dickinson. *US Patent 5.529.961*, 1996.

Beall, G, and C Quinn. *US Patent 5.071.795*, 1991a.

Beall, G, J Dickinson, and C Quinn. *US Patent 4.933.172*, 1991b.

Beall, G, J Dickinson, and R Morena. *US Patent 5.122.484*, 1992.

Dietz, R L, *US Patent* 3.703.386, 1972.

Tawansi, A, I A Gohar, D Holland, and N A El-Shishtawl, *J. Phys. D: Appl. Phys.* 21(1988): 607-613.

Zivanovic, V D, N S, Blangojevic, S R Grujic, L C, Karanovic, and B R Bozovic, *J. Serb. Chem. Soc.* 65(12) (2000): 891-898.

Chapter A

State of the art

This chapter brings together the literature data related to our thesis work. After a general presentation of vitreous materials, a part of this chapter will be devoted to phosphate glasses and their general characteristics. More specific information about phosphate glasses presenting low glass transition temperature and acceptable stability will be then presented. The last part will deal with doping in phosphate glasses. Finally, the global strategy of this work, derived from this chapter, will be exposed in the conclusion.

I. Glass

Glass is a transparent solid that we see around us on a regular basis. It is among the most ancient materials in human history. The history of creating glass can be traced back to 3500 BC in Mesopotamia, when glasses were used as tool or to design containers. Despite of being known for such a long time, it seems paradoxical that our knowledge of their structure is far from being complete. The challenge of studying disordered solids is due to the lack of spatial periodicity typical of crystals. In spite of the difficulties, glass science has made decisive progress in the last five decades. Glass is no longer solely a material of primary technological value for architecture, transport, lighting or packaging. New types of glass have been discovered and played an increasing role in modern optics (lasers), electronics, opto-electronics, energy conversion, in medicine (biomaterials) and they are even used to confine radioactive wastes. So it constitutes a fascinating group of materials both from the fundamental and applied standpoints. Glass science thus encompasses all the different aspects found in materials science and necessitates knowledge in various fields of physics, chemistry and mechanics (Shelby 2005).

Many definitions have been proposed to characterize a glass. A proper definition can be obtained if two parameters (the amorphous structure and the glass transition) are taken into account.

I.1. Structural aspect

The strictest form of structure in a solid is lattice periodicity that implies *long-range order* (LRO). Given pattern (arrangement of atoms in a unit cell) is repeated in the three spatial dimensions again and again to form a translationally invariant tiling, as depicted for crystalline SiO_2 in *Fig. 1.1*. In contrast to the crystalline state, the amorphous state is characterized by the absence of LRO, and is thus evidenced by the absence of Bragg peaks in X-ray diffraction. Nevertheless, if amorphous compounds lack LRO, the elementary building units are similar than in crystalline compounds. This limited order is called short range or local order (SRO). From the structural point of view, we can say that glasses are non-crystalline solids without LRO (Shelby,

2005). So, a structural definition may be proposed as: "Glass is a non-crystalline solid." Following this view, the terms "non-crystalline solid," "amorphous solid" and "glass" are synonymous. The definition encompasses all the amorphous products and cannot be used to clearly define what a glass is.

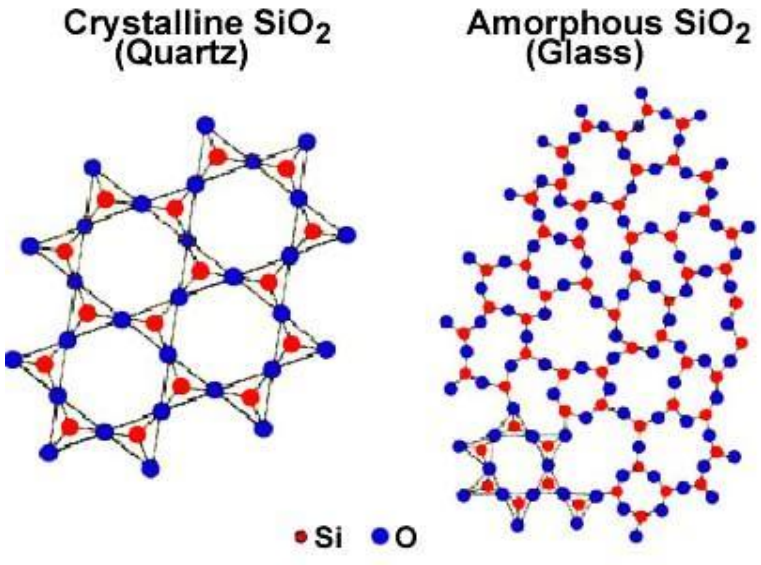

Fig. 1.1 2D representations of the ordered (left side) and amorphous (right side) structures of SiO_2 compounds.

I.2. Glass transition temperature (T_g)

Glass is usually produced by cooling a liquid so quickly that crystallization does not have time to occur. As the temperature decreases, the continuous increase of viscosity results in a progressive freezing of the liquid to its final solidification. Modification of volume versus temperature is reported in *Fig. 1.2*, in case of a liquid that crystallizes and in case of a glass forming liquid. Starting with a liquid at an elevated temperature, the lowering of the temperature first causes a contraction. When the point of solidification (T_m) is reached, two phenomena may occur:

(i) the liquid crystallizes and a discontinuity can be observed in the curve, corresponding to the crystallization phenomena. When the liquid is completely crystallized, the

temperature decreases and the crystalline solid contracts again, the slope of the curve being now less intense than that for the initial liquid.

(ii) the liquid does not crystallize and passes to a supercooled state. The representative point follows an extension of the liquid curve and passes T_m without discontinuity. The decrease in the temperature first causes a contraction of the supercooled liquid with a coefficient identical to that of the original liquid. The viscosity of the liquid increases continuously as the temperature decreases. Then, the slope of the curve decreases to become close to that of the crystalline solid. This break in cooling curve marks the passage from a supercooled liquid to a glass. The temperature for which the curve slope changes is called the glass transition temperature and is denoted as T_g. Glass transition corresponds to a viscosity in the neighborhood of 10^{13} dPa.s (Zarzycki, 1982).

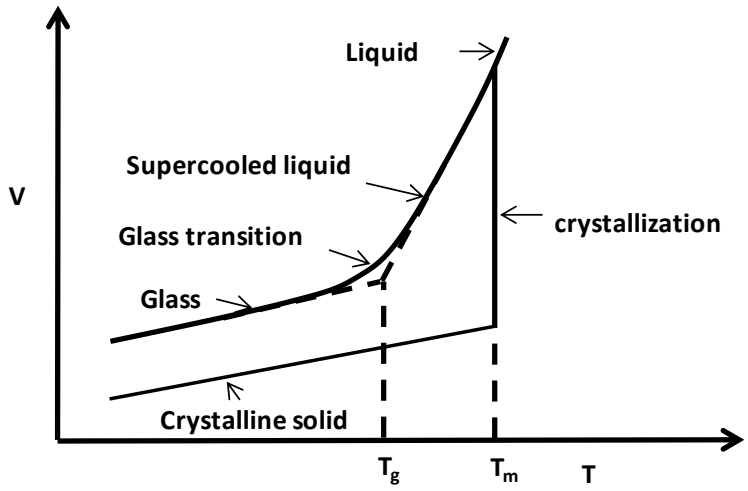

Fig. 1.2 Variation of the specific volume (V) versus temperature (T).

The T_g can be efficiently determined by using thermal analysis. The glass transition phenomenon is highlighted through a weak second order transition due to a change in the heat capacity (C_p) between the solid and the supercooled liquid (*Fig. 1.3*). However, T_g values depend on the heating rate used in the measurement and on the complete sample thermal history and cannot thus be considered to be an exact property of the glass. We can, however, think of T_g as a

useful indicator of the approximate temperature where the supercooled liquid converts to a solid on cooling or the solid converts to viscous liquid on heating (Zarzycki, 1982).

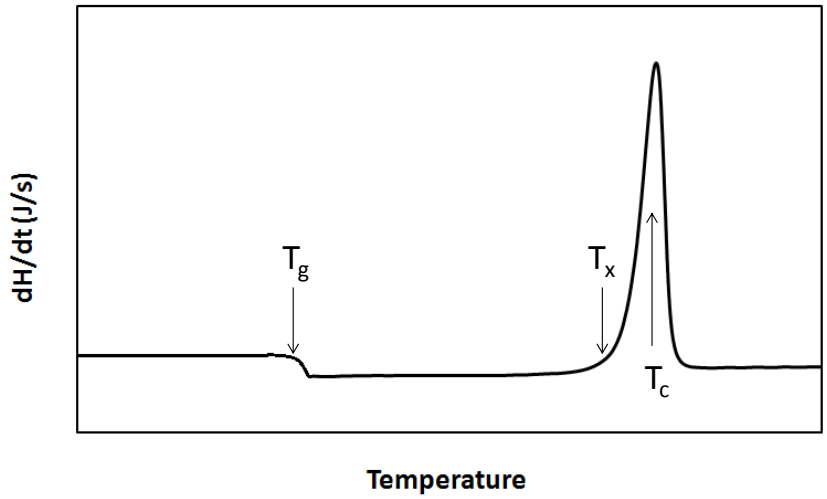

Fig. 1.3 Schematic representation of thermal analysis of glass, T_g being glass transition temperature T_x being onset of crystallization temperature and T_c being crystallization temperature.

I.3. General definition

The apparently simple structural definition presented in the part I.1 is too general. Although glass is truly a non-crystalline solid, all non-crystalline solids are not necessarily glasses (gels for example which can sometimes be transformed into glass by appropriate thermal treatment without being melted). The operational definition that requires glasses to be prepared from supercooled liquid quenching is of little help since there is no reason not to consider as glasses those materials, which are prepared by other processes like sol-gel. A general definition was given in 1982 by Zarzycki:

'*A glass can be defined as a non-crystalline solid exhibiting the phenomenon of glass transition.'*

Any amorphous material, inorganic, organic, or metallic, formed by any techniques, which exhibits glass transformation behavior is a glass and the corresponding physical state is called the vitreous state (Zarzycki 1982).

I.4. Classification of the oxides used in glass science

Glasses are mainly categorized into two types: natural and artificial glasses. The former is formed by natural process, e.g. vitreous phase in volcanic rocks (Zarzycki 1982), *tectites* by meteor impact (O'Keefe 1970) or by the skeleton of some deep water sponges (*monoharpis*) (Levi 1989) etc. The artificial glasses formed by men by using different substances that are classified in accordance to the used elements. Chalcogenide glasses are composed of As-Se, Ge-Se combinations, halide glasses are prepared from halogen containing compounds like BeF_2 and $ZnCl_2$ and metallic glasses contain metals like Ni-Nb, Cu-Zn. The most important glass category is the oxide based glasses that represents more than 95% of the glass production.

The tendency of a particular oxide to form glasses has been investigated using many parameters. For simple oxides with formula A_mO_n, the ratio of ionic radii r_A/r_O is considered as main criteria (Goldschmidt, 1926). Smekal suggests that glass-forming liquids should possess structures allowing the formation of complexes permitting mixed types of bonding (Smekal 1951). Sun used bond strength as a parameter of glass formation. According to his theory, the melts with high bond strengths are considered good glass formers upon cooling as they possess high viscosity and difficult to reform into ordered lattice (Sun 1947). Similar pattern with electronegativity/ion size was noted by Stanworth (Stanworth 1952).

The most important contribution in this research comes from Zachariasen in 1932 (Zachariasen, 1932). The basic idea was derived from the observation that the mechanical properties of glasses are similar to those of crystals of the same composition. Hence Zachariasen concluded that the atoms in a glass should be linked together by the same forces as in crystals and that the local order in glasses should be similar. Several rules were derived from these assumptions that allow Zachariasen to classify the oxides in three categories: the network-forming, the network-modifying and the intermediate oxides.

Network forming oxides: these oxides are mandatory to form glasses since they form the vitreous network. They have to be used in significant amounts in the formulation. The glass network is then constituted by interconnected network-forming polyhedra through the formation of X-O-X bonds where X is the forming element. All the polyhedra create the 3D disordered

network that can be considered as the structural backbone of the materials. The most important network-forming oxide is the silicon oxide (SiO_2). The other network forming oxides are reported in *Tab. 1.1*.

Network modifiers: an oxide that does not participate directly to the network but depolymerizes the network through the rupture of X-O-X bonds is called modifying network oxide. The replacement of a strong covalent X-O-X bond by two ionic $X\text{-}O^{-}\ ^{+}M$ linkages can be expressed by the following expression:

$$X\text{-}O\text{-}X + M_2O \longrightarrow X\text{-}O^{-} \cdots\cdots {}^{+}M + M^{+} \cdots\cdots O\text{-}X$$

The network-modifying oxides that are usually used in glass science are alkali or alkaline-earth oxides.

Intermediates: certain oxides can function either as network-forming or network-modifying depending on the proportions they are used in the glass compositions and on the elements that they are associated with. Lead, aluminium or zinc oxides are known to be intermediate oxides.
The main oxides used in glass science are classified and reported in *Tab. 1.1*:

Tab. 1.1 Classification of the oxides.

Glass formers	Modifiers	Intermediates
SiO_2, GeO_2, B_2O_3, P_2O_5, As_2O_3, As_2O_5, V_2O_5	Li_2O, Na_2O, K_2O, CaO, BaO	Al_2O_3, PbO, ZnO, CdO, TiO_2

Zachariasen also proposed that the structure should consist in an extended three-dimensional network made up of well-defined small structural units (SRO) that are linked together in a random way (no LRO). The structural model derived from this assumption is called random network model and is reported in *Fig. 1.4*. In 1985, a modified random network model was proposed by Greaves (Greaves 1985), where the distribution of network modifying cations

in the glass is not expected to be purely random. Instead, the network modifying cations cluster together to form ion channels within the glass network, as illustrated in *Fig. 1.5*.

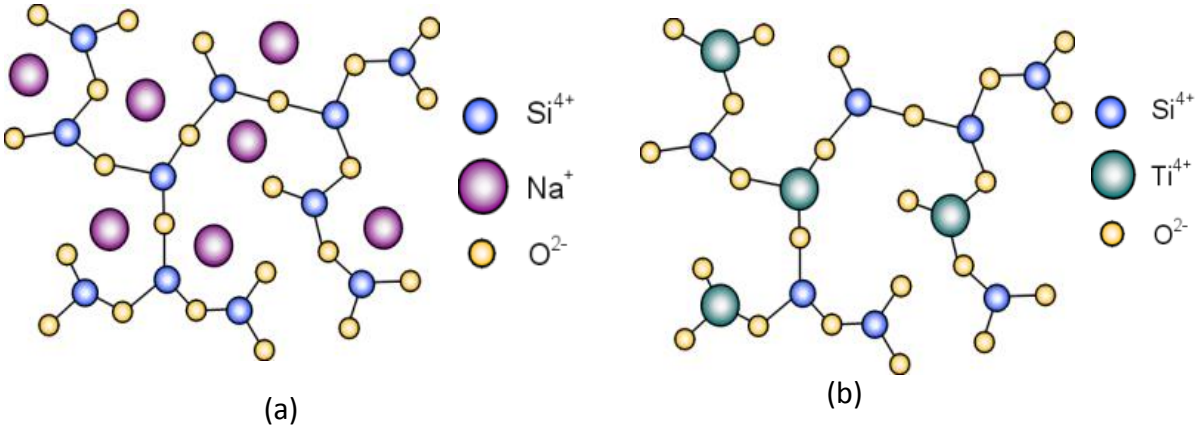

.

Fig. 1.4 Two-dimensional schematic representation of a disordered network (Zachariasen 1932 and Warren 1932). (a) Glass with added sodium as a network modifier. (b) Glass with added titanium as an intermediate.

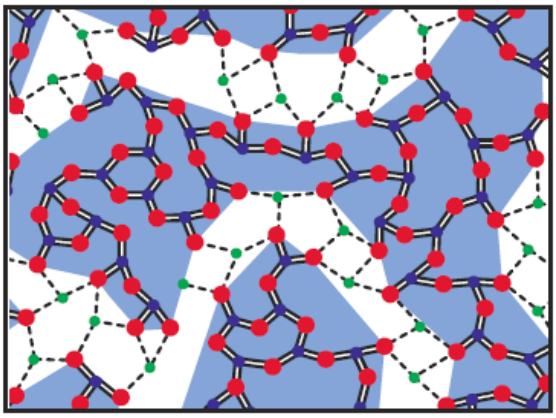

Fig. 1.5 The modified random network model, proposed by Greaves (Greaves 1985), where network modifying cations (green/small circles) form channels in the glass. The silicon (blue/medium circles) and oxygen (red/large circles) form a polymerized random network.

In oxide based glasses field, silicates glasses are the most important materials, representing more than 95% of the industrial glass products tonnage. However, other network forming oxide based glasses have emerged out as potential technical alternatives to silicate glasses for some applications. The phosphate glasses, based upon the P_2O_5, oxides will be discussed in detail in the next part.

II. Phosphate based glasses

II.1. Generalities

Compared to silicate glasses, phosphate based glasses are characterized by:

- low thermal characteristics. Glass transition temperature but also preparation, softening, processing or crystallization temperatures are lower than in case of silicates;
- high thermal expansion coefficients;
- UV transparency;
- high ability of solubilizing oxides. Oxides with very low solubility in silicate melts can be inserted at significant amounts in phosphate melts;
- poor chemical and thermal stability. Phosphate glasses are easily attacked by water and are quickly affected by crystallization at temperature above T_g.

The properties of the phosphate glasses are associated to its structure at molecular level. Therefore it is important to review the chemical nature of the phosphorus pentoxide as well as the structure of the phosphate based glasses.

II.2. The PO_4^{3-} basic unit

The basic building block of crystalline and amorphous phosphates is the PO_4^{3-} tetrahedra that results from the formation of sp^3 hybrid orbitals by the P outer electrons ($3s^2\ 3p^3$). The fifth

electron is promoted to a 3d orbital where strong π-bonding molecular orbitals are formed with oxygen 2p electrons (Cruickshank 1961 and Mitchell 1969) thereby forming a double bond P=O (Van Wazer 1958). Despite of the higher charge of the cation (P^{5+}) than that of the other glass formers (Si^{4+}, Ge^{4+}, B^{4+}), the crosslinking of the tetrahedra is then reduced to three (*Fig. 1.6*).
Due to the higher charge of phosphorus ion, the electrostatic field around the phosphorus is the highest among the network former elements (z/a^2 (P^{5+}) = 2.16 10^{20} m^{-2}; z/a^2 (Si^{4+}) = 1.54 10^{20} m^{-2} and z/a^2 for trigonal boron (B^{3+}): = 1.39 10^{20} m^{-2}). The phosphate glasses are thus largely acidic and high anion acceptors due to the strong electrostatic field of P^{5+} ions (Duffy 1971). This is why phosphate glasses can accept several oxides in larger quantities than silicate glasses.

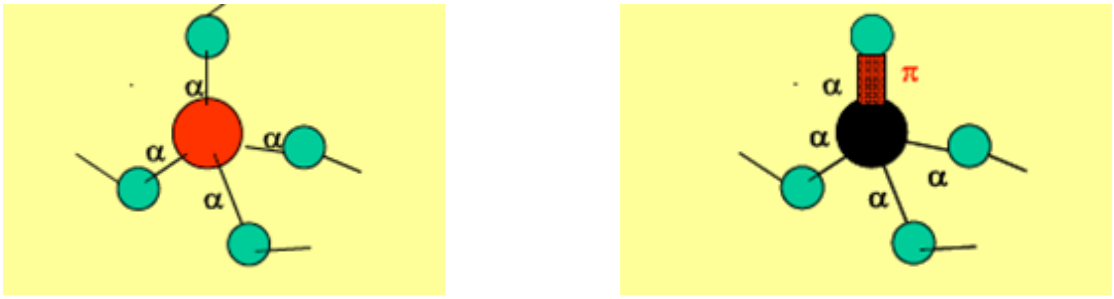

SiO_4^{4-} entity- 4 bridging oxygen atoms PO_4^{3-} entity -3 bridging oxygen atoms

Fig. 1.6 Comparison of structural entity in P_2O_5 and SiO_2 systems.

II.3. Structure and nomenclature

The phosphate tetrahedra are linked through covalent bridging oxygens to form various phosphate anions. The phosphate tetrahedra are classified using the Q^n terminology developed for silicate glasses by Lippmaa, where "n" represents the number of bridging oxygens per tetrahedral (Lippmaa 1980). When applied to phosphate, the nomenclature can be used to distinguish 4 different units (from Q^3 to Q^0) (*Fig. 1.7*) since Q^4 cannot be formed due to the P=O bond presence (Van Wazer 1950) (*Fig. 1.7*).

The different sites can be described as follows:

- Q^3 is a phosphate tetrahedron connected to three other phosphate tetrahedra forming a three-dimensional network. The glasses containing Q^3 species are called *ultraphopshates*;

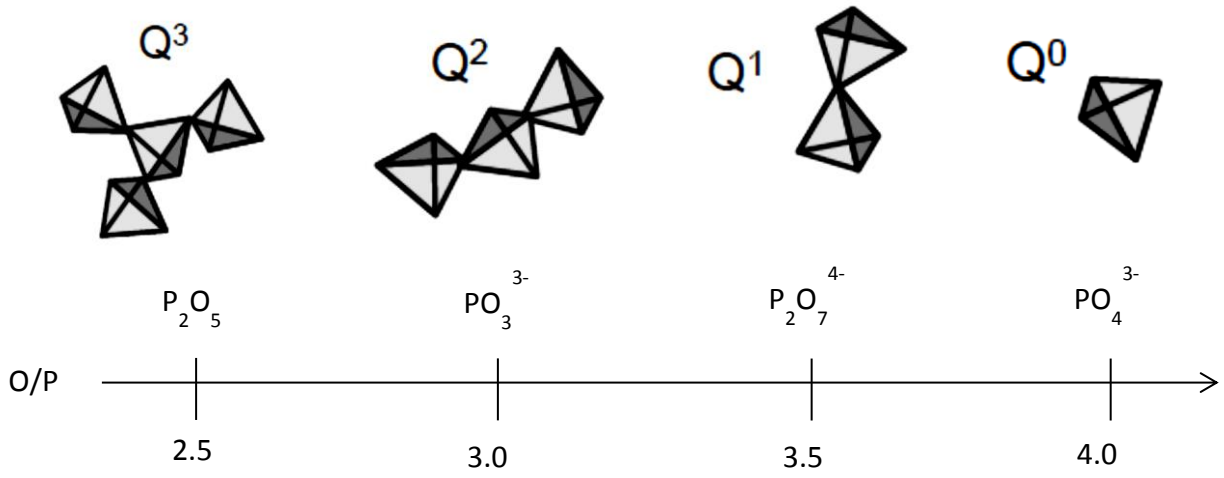

Fig. 1.7 Q^n speciation observed in phosphate glasses and corresponding O/P ratio (Van Wazer 1950).

- Q^2 is a phosphate tetrahedra connected to two other phosphate tetrahedra giving rise to chains (*polyphosphates*) or cycles *(metaphosphates)*;

- Q^1 is a phosphate tetrahedron connected to one other phosphate tetrahedron, generally found at the end of the phosphate chains or in the form of dimers.

- Q^0 is an isolated PO_4^{3-} anion (*monophosphate* or *orthophosphate*) and is not connected to any other phosphate tetrahedron.

The prevalence of any particular Q^n species is dependent on the network modifying oxide content in the glass composition. In pure P_2O_5 glass ([O]/[P] = 2.5), the Q^3 species will be the only phosphate group present forming a highly cross-linked phosphate network as confirmed by neutron diffraction studies (Suyuza 1998 and Hoppe 1998). However, ultra-phosphate glasses

possess compositions in the range of $0< x <0.5$ where x is the mol. % of metal oxide, and are defined by the presence of Q^3 tetrahedra but may also contain Q^2 species. The evolution of a cross-linked Q^3 network to the chain-like Q^2 network of a metaphosphate is confirmed by ^{31}P NMR spectroscopy on sodium phosphate glasses (Kirkpatrick 1995). An increase of the Q^2 peak at the expense of the Q^3 peak was observed as the Na_2O concentration increased from 5 to 50 mol%.

The addition of metal cations, so that $[M_2O] = [P_2O_5]$ ($[O]/[P] = 3.0$ (where M is any mono- or di-valent cation) will make Q^2 the only species present, hence producing non-branched phosphate chains, theoretically of infinite length (Van Wazer 1958). These phosphates are named metaphosphates. The addition of any more M_2O will introduce terminating Q^1 species, decreasing the chain length (Van Wazer 1950).

When the concentration of M_2O is twice that of P_2O_5 ($66.6MO\text{-}33P_2O_5$) ($[O]/[P] = 3.5$), the terminating Q^1 species is dominant and the structure is supposed to be formed by dimers (or pyrophosphate). Nevertheless, the ^{31}P NMR spectra of lead or zinc pyrophosphate compositions reveal the presence of Q^2 and Q^0 sites in significant amounts (Brow 1995). The presence of both sites was explained by Q^1 disproportionation reactions that occur during the reorganization of the melts quenched to prepare the glasses.

$$2Q^1 \longleftrightarrow Q^0 + Q^2$$

If the concentration of M_2O is at least three times higher than that of P_2O_5 ($[O]/[P] = 4.0$) then the non-bridging Q^0 (orthophosphate) species is dominant.

Fig. 1.8 shows the distribution of tetrahedra determined from the NMR spectra from a series of zinc phosphate glasses (Brow 1995). As previously noticed in case of the pyrophosphate compositions, the study shows that the structure of glasses can be more complex than expected.

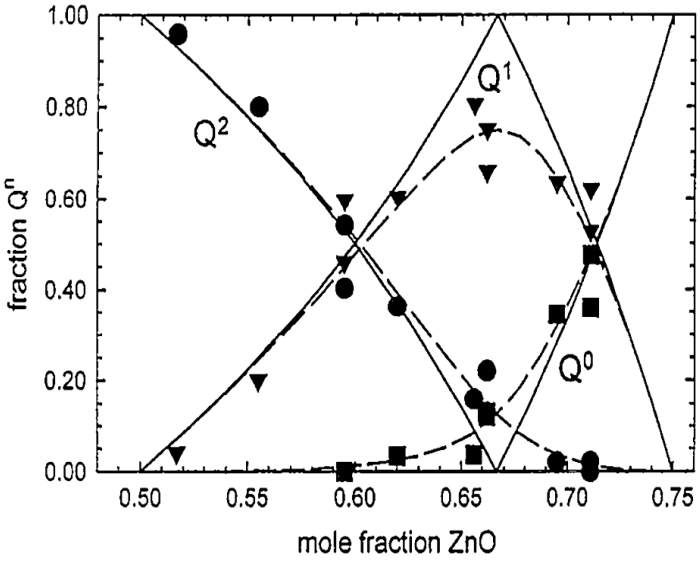

Fig. 1.8 The effect of composition on the Q^n distributions determined by ^{31}P MAS-NMR (closed symbols). The solid lines are the predicted (Brow 1995). The solid lines present predicted Q^n distributions, whereas the dashed lines are predicted accounting for experimental distribution.

II.4. Applications of phosphate glass

Here are reported some applications in which phosphate glasses have been used in place of silicate based materials. If the applications benefit from the properties of the phosphate network previously described, it is noteworthy that the poor stability strongly restricts their use in many other technical domains.

Compared to silicate glasses, phosphate glasses can easily solubilize rare earth metals and are material of choice for high power laser applications (Weber 1990) and many optical devices (Harada 2006). Major advances have been made with glass laser compositions based on phosphate systems and Nd_2O_3 (Myers 1975) to overcome inherent disadvantages of silica systems. In addition, the interest in alkaline phosphate glasses stemmed from their high transparency for ultraviolet radiations (Brow 2000). Phosphate glasses containing fluoride, which have been doped with rare earth ions, have shown great promise for optical and laser applications due to their low absorption at certain frequencies (Ebendorff-Heidepriem 2000, Ebendorff-Heidepriem 2002 and Philipps 2001).

Another important use of phosphate glasses is the application as biomaterials based on calcium phosphate system. Calcium phosphate materials have some outstanding ability to fill bone defects as synthetic material, because of their similarity in composition to bone mineral and osteoconductivity. It may also offer a potential for hard tissue surgery because of their solubility behavior, since this property can be controlled by their chemical composition (Franks 2000, Dias 2003, Al-Noaman 2013 and Hill 2011). The lack of durability of some phosphate glasses was utilized to find a cure for trace element deficiencies in cattle and sheep (Allen 1978, Allen 1984 and Allen 1985). Similarly Ti-containing quaternary phosphate glass system, as a transporter for strontium ion delivery to cells, has been investigated (Lakhkar 2011).

A major concern with radioactive waste disposal is the possibility of radioactive nuclides escaping from the storage site and contaminating the biosphere. In order to prevent such environmental contamination, the immobilization of radioactive waste materials in confinement matrix has been under investigation for many years. At the present time, borosilicate glass is the generally accepted confinement matrix (IAEA 1992). Unfortunately, many of the radioactive wastes contain components that are either insoluble or incompatible with borosilicate glasses. Alternatively, phosphate glasses have ability to dissolve larger quantities of several oxides (like Cr_2O_3, ThO_2, MoO_3) than the silicate matrix and have been considered as potential alternatives. Due to the very poor durability of conventional phosphate glasses, the compositions described here contain high amounts of reticulating oxides as Al_2O_3 or Fe_2O_3. These oxides produce a highly reticulated network leading to a spectacular improvement of the stability, accompanied by a significant increase of T_g (Brow 1993, Donald 2004, Nishida 1999 and Mogus-Milankovic 2007). Iron phosphate glass has come to the forefront of this application as a possible solution. A group led by Day has developed an iron phosphate glass containing 40 mol% of Fe_2O_3 with excellent chemical durability, which is able to accept different types of nuclear waste at very high loading (up to six times more waste per unit volume than borosilicate glasses) (Day 1998, Mesko 2000, Huang 2004, Huang 2005, Kim 2004 and Donald 2006).

Sealing materials are used in many technical applications. For many purposes, it is desirable to maintain the sealing temperature as low as possible. This is particularly true in electrical and electronic articles where thermally sensitive parts or coatings (Ye 2009) are

commonly employed. Phosphate glasses are therefore attractive as glass-metal seals and metal to metal sealing glasses (Morena 2000) due to their low melting temperature, low viscosity and high thermal expansion coefficients (Wei 2001). Considerable attention has been paid to lead glasses as low temperature sealing glasses since it has low softening temperature. However, due to toxicity reason, lead has to be replaced by some other elements, like a mixture of ZnO and SnO oxides (Aitken 1993).

The last example is a textbook case in which phosphate glasses have been used for their low thermal characteristics. Many other applications (low temperature protective coatings, confinement matrix for volatile wastes, preparations of organic/inorganic materials) would benefit from the development of glasses presenting a low T_g (between 300 and 400°C). Unfortunately, this kind of glass generally presents a very poor stability, in opposition to the glasses used to confine radioactive waste.

To summarize, two kinds of phosphate glasses can be distinguished depending on the targeted applications:

(i) the low T_g formulations (T_g < 400°C) suitable for low temperature applications but presenting a poor stability and,

(ii) the high T_g formulations (T_g> 400°C) presenting a very good durability but also a high T_g that make them unsuitable for low temperature applications.

This work focuses on the first category. The next part will thus be dedicated to the most valuable systems described in literature that present low thermal characteristics combined with acceptable stability.

II.5. Low-T_g phosphate glass

Lead phosphate glasses had been studied since the mid 1950's as PbO was the only oxide that reduces the dissolution rate and T_g at the same time (Peng 1991 and Liu 1996). Later lead-iron phosphate glass was introduced and characterized in detail by Sales and Boatner in the mid

1980's (Sales 1984). While lead-iron phosphate glasses appear to offer advantages of reduced preparation temperature and improved chemical durability compared to borosilicate glass, their lead content was considerable (40-60 wt%), posing the potential for excessive toxic releases from the glass matrix. Therefore, it was desirable to prepare a lead-free glass for many applications. Sn (Morena 2000), Zn (Ray 1973), Cd (Hussin 2002), Cu (Shih 1999), Sb (Zhang 2008), Mo (Bih 2002 and Santagneli 2007), W (Maczka 2006) or Ba (In 2003) oxides have since been considered as potential alternatives for the preparation of lead-free phosphate glasses with low T_g and acceptable stability. It is noteworthy that many patents have been deposited by the Corning society about that topic, assessing the relevancy of that research domain (Aitken 1990, 1993, 1994(a), 1994(b), 1996, Beall 1991(a), 1991(b) and Beall 1992).

Very interesting results were obtained with Sn, Cu and Zn elements. Unfortunately, the two former elements can be submitted to redox reactions during the melting stage and thus require controlled melting atmospheres. Finally, the best alternative to lead appears to be the zinc element.

Zinc oxide based materials are attractive due to their nontoxicity, nonhygroscopic nature and low cost. Combined with phosphorous oxide, zinc gives rise to interesting systems such as $ZnO\text{-}P_2O_5\text{-}TeO_2$ (Mosner 2011), $ZnO\text{-}Bi_2O_3\text{-}P_2O_5$ (Irak 2007) or $ZnO\text{-}Sb_2O_3\text{-}P_2O_5$ (Koudelka 2007) with T_g reported to be close to 400 °C. Corning proposed several patents with durable phosphate compositions with low melting and processing temperatures. The best results were obtained on zinc phosphate glasses containing alkali and alkaline earth metal oxides (Ray 1973, Quinn 1995, Varshneya 1994, Quinn 1992, Beall 1990 and Beall 1991 (a)). The formulations are very complex and contain a lot of oxides (more than 15), some being used in minor proportions.

To summarize, the proposed formulations contain:

- ZnO in the range of 60-30 mol%. Generally, ZnO is partially substituted by other divalent ions like Ba, Sr, Pb or Mg. The higher the divalent ions content, the higher the T_g.

- Alkali oxides (Li_2O, Na_2O, K_2O, Rb_2O) in the range 5-40 mol%. The amount of alkali oxide has a direct impact on the T_g and on the durability, an increase of the alkali oxide content leading to a T_g and stability decreasing. In many patents, alkali oxides are used in combinations and give rise to the well-known mixed alkali effect that decreases the T_g.

- P_2O_5 in the range of 30-38 mol%. This particular concentration range leads to pyrophosphate (Q^1) structure. Glasses with higher P_2O_5 contents contain longer chains (Q^1/Q^2) that are more sensitive to water attack. Lower P_2O_5 contents produce glasses containing isolated phosphate species (Q^0) that can hardly produce disordered network alone. Therefore, the pyrophosphate structure can be considered as the most stable structural feature.

- Reticulating oxides in small proportions (>5 mol%). The role of these oxides is to improve the glass stability. Al_2O_3, Fe_2O_3, B_2O_3, MoO_3, SiO_2 and TiO_2 are the most commonly used reticulating oxides. These oxides have to be used in low proportions to keep the T_g below the 400°C boundary. Even if it is well established that insertion of reticulating oxides (denoted as dopant in the following) in very small proportions could significantly change the macroscopic properties of materials, there is no clear information about the mechanism of insertion and the true nature of the doping moieties. The next part will focus on general literature concerning doping in phosphate glasses.

II.6. Doping of phosphate glasses

A dopant, also called a doping agent, is an element that is inserted into a material in low concentrations in order to alter material properties. In phosphate glasses, rare earth oxides, Al_2O_3, Fe_2O_3, B_2O_3, MoO_3, SiO_2 and TiO_2 are some commonly used dopants that produce dramatic change in the properties of the material. In many cases, rare earth elements are used to only confer optical properties of the glasses. Some of the examples considering laser glass

applications are: Sm_2O_3 (5 mol%) in $BaO-Al_2O_3-P_2O_5$ (Xianfeng 2006), Nd_2O_3 (3 mol%) in $BaO-Al_2O_3-K_2O-P_2O_5$ (Xu 2011), Er_2O_3/Yb_2O_3 (0.5-5 mol%) in $Li_2O-TiO_2-Al_2O_3-Li_2O-P_2O_5$ system (Ming 2012), Tb_2O_3 (0.5-5 mol%) in $BaO-B_2O_3-Al_2O_3-K_2O-P_2O_5$ (Zhang 2012) and Dy_2O_3 (0-3 mol) $PbO-ZnO-P_2O_5$ (Amjad 2013). It is noteworthy that these systems also consist small amount (5 mol%) of Al_2O_3, B_2O_3, and TiO_2, however their effect on glass stability has not been prioritized in the papers.

Many problems regarding low T_g and stability exist in the glass applications. For instance, the immobilization of hazardous and volatile radionuclide, including Technetium and Iodine, not only requires stable glass with low processing temperature but also long-term stability (high chemical durability). The stability of phosphate system for the above application is usually improved by adding 3-8 mol% Fe_2O_3 in $Na_2O-Al_2O_3-P_2O_5$ (Donald 2006), 5 mol% of Al_2O_3 in $Fe_2O_3-P_2O_5$ system and 1-5 mol% of TiO_2 in $Na_2O-CaO-P_2O_5$ (Kiani 2010). The increase in stability of these glasses is usually explained by the replacement of P-O-P bonds by P-O-Fe, P-O-Al and P-O-Ti bonds respectively. However, the addition of Al_2O_3, Fe_2O_3 and TiO_2 produce very high T_g glasses and are therefore not suitable when low processing temperature is required.

A considerable improvement on thermal stability of the phosphate glasses with B_2O_3 loading has also been reported. For instance, the thermal stability of sodium aluminophosphate (used for nuclear waste confinement) was markedly improved by the addition of up to 10 mol% of B_2O_3 (Donald 2006). But, surprisingly, the study reports that the chemical durability of these glasses decreased with the increase in B_2O_3 content though the addition of B_2O_3 is well known to improve the chemical stability. Other example includes the addition of less than 10 mol% of B_2O_3 to improve the poor thermal stability of $BaO-P_2O_5$ system for the optical applications (Harada 2004 and Takebe 2006). The addition of B_2O_3 (0-10 mol%) to $SnO-P_2O_5$ system produces stable low temperature sealing glasses (Lim 2010). Moreover, the combination of small quantity of Al_2O_3 (< 1 mol%) and B_2O_3 (< 2 mol%) in glass phosphate composition with many other components was also reported to produce relatively durable phosphate glass (Marino 2001).

If the addition of TiO_2, Fe_2O_3, Al_2O_3 and B_2O_3 on stability of the phosphate glass is consistent, effect of SiO_2 does not provide clear information on stability of glass. Some said that SiO_2 (2-25 mol %) addition did not necessarily exhibit improved thermal stability on P_2O_5-Fe_2O_3 glasses (Marasinghe 2000) while others showed that insertion of Fe_2O_3 with substantial quantity of SiO_2 (2-25 mol%) to Fe_2O_3-P_2O_5 system produced alteration in thermal behavior of the glass (Russo 2008). The addition of 0.5-8 mol% of SiO_2 to SnO-CaO-P_2O_5 system improved the chemical durability of the glass (Hong 2010). Moreover, a study by Bingham claimed that the addition of small quantity of SiO_2, Al_2O_3 and B_2O_3 (< 5 mol%) on P_2O_5-Fe_2O_3 glasses showed dramatic improvement on their thermal stability in the order Al_2O_3 > SiO_2 > B_2O_3 (Bingham 2006).

The stability of the glasses in all these studies are indeed improved with the Fe_2O_3, Al_2O_3, B_2O_3 and SiO_2 additions. However the increase in T_g at the same time restricts the use of high amounts. The doping for thermal stability in low-T_g glasses has not yet been studied with any rigour. To our knowledge, the glass formulations with optimum quantity of B_2O_3, Al_2O_3 and SiO_2 to improve the stability while keeping their T_g value low have not been documented. This is therefore the main aim of our work.

III. Conclusion

The final purpose of this work is to understand how the doping elements change the properties and the structure of low-T_g phosphate glasses. The global strategy to achieve this work has been constructed from the data reported in this chapter.

First, a simple system allowing for the preparation of low-T_g phosphate glasses was derived from the literature. It turns out that zinc alkali pyrophosphate constitutes a very promising system allowing for the preparation of low-T_g materials. A more detailed analysis of the literature data indicates that pyrophosphate structure should be preferred in order to optimize

the glass stability. Our based system was finally designed by using Na_2O as single alkali oxide. Therefore, the based system that will be investigated in this work will be the (66- *x*)ZnO- *x* Na_2O-33.4P_2O_5 composition line. The impact of the Zn/Na ratio on the properties, structure and stability will be investigated in details.

Second, the doping elements used in this study have been chosen according to the properties we want to improve. Al_2O_3, B_2O_3 and SiO_2 have already been used to increase the chemical or thermal stability of general phosphate glasses. Therefore, these three doping elements will be used to determine their effect on low-T_g phosphate glasses within this work. We have decided to limit the doping elements in the glasses to 4 mol% in order to keep the T_g under the 400°C boundary. It is noteworthy that these three elements can be efficiently probes by nuclear magnetic resonance through ^{27}Al, ^{11}B and ^{29}Si NMR experiments.

The next chapter will focus on the glass preparation, on the methods used to determine the macroscopic properties and on the spectroscopic techniques employed to analyze in details the structure of the base and the doped compositions.

References

Aitken, B. *US Patent 5.021.366*, 1990.

Aitken, B. *US Patent 5.256.604*, 1993.

Aitken, B. *US Patent 5.153.151*, 1994 (a).

Aitken, B. *US Patent 5.286683*, 1994 (b).

Aitken, B, G Beall, and J Dickinson. *US Patent 5.529.961*, 1996.

Allen, W M, B F Sansom, C B Mallinson, R J Stebbings, and C F Drake. *Vet. Rec.* 116(7) (1985): 175-177.

Allen, W M, B F Sansom, C F Drake, and D C Davies. *Vet. Sci. Commun.* 2(1) (1978): 73-75.

Allen, W M, B F Sansom, P T Gleed, C B Mallinson, and C F Drake. *Vet. Rec.* 115(3) (1984): 55-57.

Al-Noaman, A, N Karpukhina, and S C F Rawlinson. *J. Non-Cryst. Solids.* 364 (2013): 85-91.

Amjad, R, M R Sahar, S K Ghoshal, M R Dousti, and R Arifin. *Opt. Mater.* 35 (5) (2013): 1103-1108.

Beall, G H, and C J Quinn. *US patent 4940677*, 1990.

Beall, G H, J E Dickinson, and C J Quinn. *US Patent 4996172*, 1991 (a).

Beall, G, J Dickinson, and C Quinn. *US Patent 4.933.172*, 1991(b).

Beall, G, J Dickinson, and R Morena. *US Patent 5.122.484*, 1992.

Bih, L, A Nadiri, and J Aride. *J. Therm. Anal. Cal* 68 (2002): 965-972.

Bingham, P A, R J Hand, and S D Forder. *Mater. B.* 41 (2006): 1622-1630.

Brow, R K. *J. Am. Ceram. Soc.* 76 (1993): 913-918.

Brow, R K. *J. Non-Cryst. Solids.* 263/264 (2000): 1-28.

Brow, R K, D R Tallant, S T Myers, and C C Phifer. *J. Non-Cryst. Solids.* 191 (1995): 45-55.

Cruickshank, D W.J. *J. Chem. Soc.* 69(2) (1961): 5486.

Day, D E, Z Wu, and C S Ray. *J. Non-Cryst. Solids.* 241 (1998): 1.

Dias, A G, M A Lopes, I R Gibson, and J D Santos. *J. Non-Cryst. Solids.* 330 (2003): 81-89.

Donald, I W, and B L Metcalfe. *J. Non-Cryst. Solids.*348 (2004): 118.

Donald, I W, B L Metcalfe, S K Fong, and L A Gerrard. *J. Non-Cryst. Solids.* 352 (2006): 2993-3001.

Duffy, J A, and M D Ingram. *J. Am. Chem. Soc.* 93 (1971): 6448.

Ebendorff-Heidepriem, H, and D Ehrt. *Opt. Mater.* 15(1) (2000): 7-25.

Ebendorff-Heidepriem, H, and D Ehrt. *Opt. Mater.* 19(3) (2002): 351-363.

Franks, K, I Abrahams, and J C Knowles. *J. Mater. Sci-Mater. Med.* 11 (2000): 609-614.

Goldschmidt, V M. "Skrifter Norske Videnskaps Akad. (Oslo)." *I. Math. Naturwiss. KI, Nr 8,7,* 1926: 156.

Greaves, G N. *J. Non-Cryst. Solids.* 71 (1985): 203-217.

Harada, T, H In, H Takebe, and K Morinaga. *J. Am. Ceram. Soc.* 87 (3) (2004): 408-411.

Harada, T, H Takebe, and M Kuwabara. *J. Am. Ceram. Soc.* 89 (1) (2006): 247-250.

Hill, R G, and D S Brauer. *J. Non-Cryst. Solids.* 357 (24) (2011): 3884-3887.

Hong J, D Zhao, J Gao, M He, H Li, and G He. *J. Non-Cryst. Solids.* 356 (2010): 1400-1403.

Hoppe, U, G Walter, A Barz, D Stachel, and A C Hannon. *J. Phys : Condens. Mater.* 10 (1998): 261.

Huang, W H, D E Day, C S Ray, C W Kim, and S T D Reis. *Glass. Sci. Technol.* 77(5) (2004): 203-210.

Huang, W H, N Zhou, D E Day, and C S Ray. *J. Inorg. Mater.* 20(4) (2005): 842-850.

Hussin, R, D Holland, and R Dupree. *J. Non-Cryst. Solids.*298 (2002): 32-42.

IAEA, Vienna. "International Atomic Energy Agency (Vienna), Design and operation of high level waste vitrification and Storage Facilities." *Technical Report Series No 339*, 1992.

In, H, H Takebe, and K Morinaga. *J. Ceram. Soc. Jpn.* 111 (2003): 426-429.

Irak, j, L Koudelka, J Pospisil, P Mosner, L Montagne, and L Delevoye. *J. Mater. Sci.* 42 (2007): 8592-8598.

Kiani, A, L S, Cahill, E A Neel, J V Hanna, M E Smith, and J C Knowles. *Mater. chem. Phys.*120 (2010): 68-74.

Kim, C W, and D E Day. *Abstr. Pap. Am. Chem. S.* 227 (2004): U1044-U1045.

Kirkpatrick, R J, and R K Brow. *Solid State Nucl. Mag.* 5(1) (1995): 9-21.

Koudelka, L, J Jirak, P Mosner, L Montagne, and L Delevoye. *Phys. Chem. Glasses: Eur. j. glass. Sci. Technol.* 48 (2007): 33-38.

Lakhkar, N, E A Abou Neel, V Salih, and J C Knowles. *J. Biomater. Appl.* 25 (8) (2011): 877-893.

Levi, C, J L Barton, C Guillemet, E Le Bras, and P Lehuede. *J. Mater. Sci. Lett.* 8 (1989): 337.

Lippmaa, E, M Magi, A Samson, G Engelhardt, and A R Grimmer. *J. Am. Chem. Soc.* 102 (1980): 4889-4893.

Liu, H S, P Y Shih, and T S Chin. *Phys. Chem. Glasses* 37(6) (1996): 227.

Maczka, M, B Macalik, J Hanuza, and J Bukowska. *J. Non-Cryst. Solids.* 352 (2006): 5586-5593.

Marasinghe, G K, M Karabulut, X Fang, C S Ray, D E Day, D L Caulder, J J Bucher, N M Edelstein, D K Shuh, and P G Allen, *Ceram. Trans.*107 (2000) 115.

Mesko, M G, D E Day, and C B Bunker. *Waste Manage.* 20(4) (2000): 271-278.

Ming, C, et al. *Opt. Mater*.35 (2) (2012): 244-247.

Mitchell, K A R. *Chem. Rev.* 69(2) (1969): 157.

Mogus-Milankovic, A, V Licina, S T Reis, and D E Day. *J. Non-Cryst. Solids.* 353(27) (2007): 2659-2666.

Morena, R. *J. Non-Cryst. Solids.* 263/264 (2000): 382-387.

Mosner, P, k Vosejpkova, and L Koudelka. *J. Non-Cryst. Solids.* 522(1-2) (2011): 155-160.

Myers, J D, and C S Vollers. *U.S Pat. No. 4,075,120*, (1975).

Nishida, T, and K Maki. *J. Radioanal. Nucl. Ch.* 242 (2) (1999): 557-560.

O'Keefe, J, and W Weiss-Kirchner. *Glastechn. Ber.* 43 (1970): 199.

Peng, Y B, and D E Day. *Glass. Technol.* 32(5) (1991): 166.

Philipps, J F, T Topfer, H Ebendorrf-Heidepriem, D Ehrt, and R Sauerbrey. *Appl. Phys. B-Lasers. O.* 72(4) (2001): 399-405.

Quinn, C J, J E Dickinson, and G H Beall. *Int. Congr. on Glass: Bull. Spanish. Soc. Ceram. Glass.* 31 (C4) (1992): 79.

Quinn, C J, P D Frayer, and G H Beall. *Sci. Technol in: G. H. Beall, Proc. XVII Int. Congr. on Glass, Beijing, China*, 1995 (Oct. 9-14).

Ray, N H, J N C Laylock, and W D Robinson. *Glass. Technol.* 14 (1973): 55-59.

Russo, D O, D S Rodriguez, J M Rincon, M Romero, and C J R Oliver. *J. Non-Cryst. Solids*. 354(2008): 1541-1548.

Sales, B C, and L A Boatner. *Science* 226 (1984): 45-48.

Santagneli, S H, et al. *J. Phys. Chem.* 111 (2007): 10109-10117.

Shelby, J E. "Introduction to Glass Science and Technology." *The Royal Society of Chemistry* (2nd edition), 2005: 1-3.

Shih, P Y, S W Yung, and T S Chin. *J. Non-Cryst. Solids.* 244 (2-3) (1999): 221-222.

Smekal, A. *J. Soc. Glass. Tech.* 35 (1951): 411T.

Stanworth, J. *J. Soc. Glass. Tech.* 36 (1952): 217T.

Sun, K. *J. Am. Ceram. Soc.* 30 (1947): 277.

Suyuza, K, D L Price, C K Loong, and S W Martin. *J. Non-Cryst. Solids.* 232-234 (1998): 650-657.

Takebe, H, T Harada, and M Kuwabara. *J. Non-Cryst. Solids.* 352 (2006): 709-713.

Van Wazer, J R. *J. Am. Ceram. Soc.* 72 (1950): 644-647.

Van Wazer, J R. *Phosphorus and its Compounds, Interscience, New York* 1 (1958): 93.

Varshneya, A K. "Fundamentals of Inorganic glasses, Academic Press, New York." 1994: 116.

Warren, B E. *J. Am. Ceram. Soc.* 54 (1932): 3841.

Weber, M J. *J. Non-Crysts. Solids.* 123 (1990): 208-222.

Wei, T Y, Y Hu, and L G Hwa. *J. Non-Crysts. Solids.* 288(1-3) (2001): 140-147.

Xianfeng, M, Z Qitu, L Chunhua, and X Zhongzi. *J. Rare Earth.* 24 (1) (2006): 211-214.

Xu Y, S Li, L Hu, and W Chen. *J. Rare. Earth*. 29 (6) (2011):614-617.

Ye. *Patent No: US 7494692 B2*,(2009).

Zachariasen, W H. *J. Am. Chem. Soc.* 54 (1932): 3841.

Zarzycki, J. "Glass and the Vitreous state." (1982).

Zhang, B, Q Chen, and L Song. *J. Non-Crysts. Solids.*254 (2008): 1948-1954.

Zhang, L, M Peng, G Dong, and J Qiu. *Opt. Mater.* 34 (7) (2012): 1202-1207.

Chapter B

Experimental procedures and techniques.

The materials and techniques employed for the preparation and characterization of the glasses are presented in detail in this chapter. The first section describes the method of preparation of glasses. The second section deals with the methods used for the characterization of the macroscopic properties of the glasses. In the third section, the spectroscopic techniques used for the structural analysis (Raman and solid-state Nuclear Magnetic Resonance) are presented.

I. Glass preparation

All the glasses were prepared with the melt-quenching technique. The required amounts of precursors such as ZnO, Na_2CO_3, $(NH_4)_2HPO_4$, $Al(OH)_3$, $B(OH)_3$ and SiO_2 were weighed and mixed thoroughly using porcelain mortar and pestle. The batches were designed in order to produce 5 g of glass. The origin and purity of each chemical product are reported in *Tab. 2.1*.

Tab. 2.1 List of oxides and salts:

Chemicals used	Mol. Wt (g/mol)	Society	Purity
ZnO	81.40	Prolabo	99+ %
Na_2CO_3	105.98	Acros	99.5+ %
$(NH_4)_2HPHO_4$	132.07	Acros	99+ %
$Al(OH)_3$	78.0	Riedal-de Haen	63-67 % (as Al_2O_3)
$B(OH)_3$	61.83	Riedal-de Haen	99.5+ %
SiO_2	60.08	Carl Roth	99+ %
^{29}Si-100% enriched SiO_2	60.98	Carl Roth	99+%

The mixtures were then transferred to a Pt-Au5 crucible and were thermally treated at 600°C for 2 hours, under slow heating rate of 1°C/minute in an electric furnace to remove NH_3, H_2O and CO_2.

The batches were melted at 900°C-1150°C for 20 minutes to 3 hours (depending upon the composition) with intermediate stirring ensuring the melt homogeneity. The temperature and melting time for each composition were optimized to limit the P_2O_5 volatilization that can occur at high temperature. The melts were finally quenched on a brass plate under standard atmosphere to prepare transparent glasses. Nevertheless some compositions require to be quenched between two brass plates to avoid crystallization (these special cases will be mentioned in the manuscript). The weight loss ($\Delta m/m$) occurring during the preparation was also measured for each composition to check for the P_2O_5 volatilization. Melting procedure was performed again if $\Delta m/m > 2\%$. All the prepared glass samples were kept in a desiccator to prevent them from moisture.

Due to the low natural abundance of ^{29}Si isotope (4.7%), the SiO_2 doped glasses analyzed by NMR were prepared with ^{29}Si 100% enriched SiO_2. To limit the use of very expensive enriched SiO_2, the syntheses were designed to produce 1 gram of glass. Comparison of spectroscopic signature was used to assess for the glass homogeneity compared to the glasses obtained by standard preparation procedure.

II. Macroscopic properties

II.1. Thermal analyses

Differential Scanning Calorimetry (DSC) measures the temperatures and heat flow associated with transitions in materials as a function of time and temperature. The technique provides qualitative and quantitative information about physical and chemical changes that involve endothermic or exothermic processes or changes in heat capacity using minimal amounts of sample. Heat flow within the samples is measured from the temperature difference (ΔT) with an inert reference material (Al_2O_3) that indicates heat flow is proportional to the temperature difference (*Fig. 2.1*).

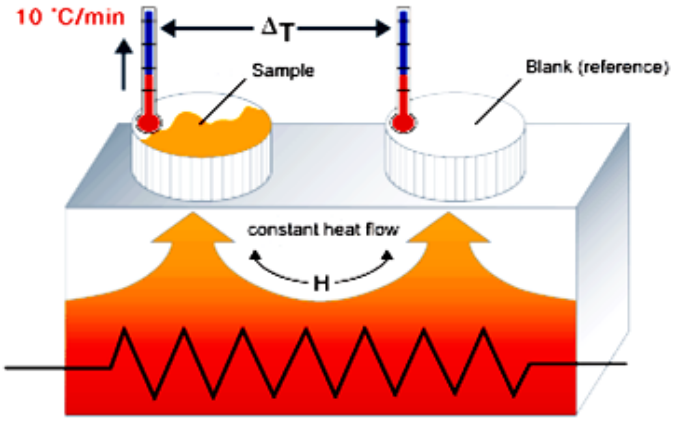

Fig. 2.1 Principle of Differential Scanning Calorimetry (DSC).

Application to this work: Differential scanning calorimetry (DSC) was used to determine the glass thermal characteristics like glass transition (T_g), beginning of crystallization (T_x) and maximum of crystallization (T_c) temperatures.

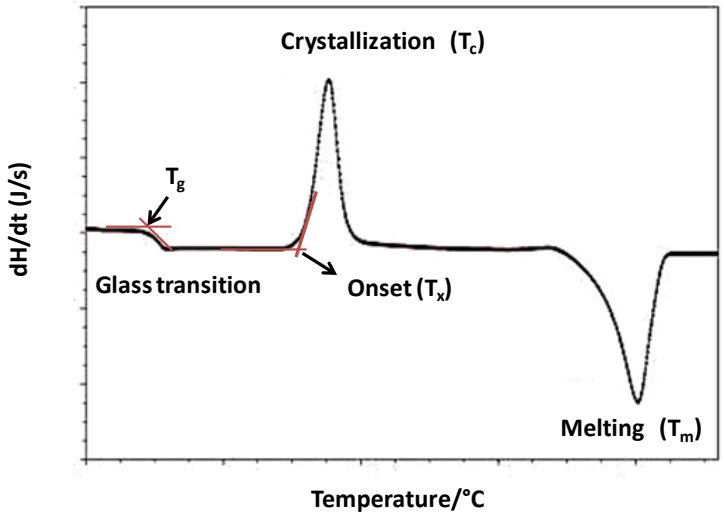

Fig. 2.2 Thermogram pattern obtained from Differential Scanning Calorimetry showing onset temperatures T_g,T_x,T_c and T_m.

A typical DSC curve obtained on a glass is shown in *Fig. 2.2* with the characteristic temperatures used in this study. DSC analysis was carried out using a Setaram Evo131 DSC apparatus. 30 mg of crushed glass sample powder of 40-80 µm granulometry were placed into an aluminum pan and heated from 25 °C to 600 °C at the rate of 10°C/min under an inert atmosphere.

II.2. Density

Densities were determined on powders using a helium gas pycnometer. The device consists of two chambers, one to hold the sample and a second chamber of fixed internal volume (known via calibration).

The working equation of a gas pycnometer is:

$$V_s = V_c + \frac{V_r}{1 - \frac{P_1}{P_2}}$$

where V_s is the sample volume, V_c is the volume of the empty sample chamber, V_r is the volume of the reference volume, P_1 is the first pressure (i.e. in the sample chamber only) and P_2 is the second (lower) pressure after expansion of the gas into the combined volumes of sample chamber and reference chamber. The volume V_s and thus the density (ρ) of glass powders are then determined by the following equation:

$$\rho = m/V_s$$

where ρ is the density of the glass, m is the mass of the glass powder (measured) and V_s the volume of the sample.

Application in this work: The glass densities were determined using a Micromeritics AccuPyc II 1340 helium gas pycnometer. The density of a sample is measured five times and the estimated the error was approximately ±0.005 g/cm^3. From the density measurements, molar volume was determined using the following equation:

$$V_m = M_m/ \rho$$

where M_m is molar mass of the sample and ρ is density.

II.3. X-ray diffraction

X-rays can be scattered from a crystal lattice according to the Bragg's law:

$$n\lambda = 2d \sin\theta$$

where 'n' is an integer determined by the order given, and λ is the wavelength.

The condition for maximum intensity contained in Bragg's law (*Fig. 2.3*) allows us to calculate details about the crystal structure, or if the crystal structure is known, to determine the the crystal with the help of above equation.

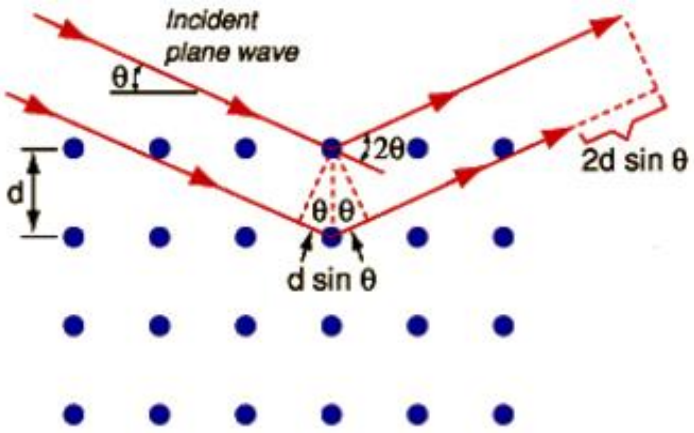

Fig. 2.3 Bragg's law.

Application to this work: The X-Ray Diffraction (XRD) technique was used in this work to check the amorphous nature of the prepared glasses and to identify the nature of the phases formed during the crystallization process. XRD patterns were obtained using a Bruker D-8 Advance diffractometer. The acquisitions were recorded for 2θ =10° to 80°, with 0.02° scan step and 0.4 s step time. The phase identifications were carried out with the JCPDS-2009 database**.**

II.4. Chemical durability test

The chemical durability represents the resistance of the glass sample against the attack by water, generally under its liquid form. This property can be investigated through many tests performed on powder or bulk samples, under different conditions of temperatures (from room temperature to boiling water), using different times (from hours to months) and under static or dynamic conditions (in dynamic conditions, water is periodically renewed to avoid saturation). The chemical durability can be simply related to weight losses measurements performed on the glass samples to follow the global solubilization of the material but much more deep insights can be obtained by following the concentration evolution of given elements in the released liquid. This latter technique allows a characterization of the dissolution mechanism deeper than the first one but is also much more time-consuming.

Application in this work: A quick glass dissolution test was derived from the literature and the conditions were adapted to our system (Donald, 2006). 1 g of glass was crushed between 400 to 1000 µm granulometry size. The powder was then weighed before being placed in savillex vessels filled with 150 mL of distilled water. The vessels were kept inside an oven at 90 °C for 24 hours. The solution was then filtered and the residue was dried at 100 °C for 24 hours before being weighed again. The normalized weight loss was finally calculated and related to the chemical durability, the lower the weight losses, the better the chemical durability. The experiment was repeated three times on a sample and the estimated error was ±1.5 to 5%.

II.5. Thermal stability

For glasses, thermal stability is the property to resist against crystallization when submitted to high temperature ($T > T_g$). The thermal stability can be associated to Angell parameter (K_A) which is the difference between the onset of crystallization and the glass transition temperature (T_x-T_g). The parameter K_A expresses the stability of supercooled liquid against crystallization, with high K_A values indicating very thermally stable glass. We used this parameter to support a quick screening of the formulations investigated in this study; however it does not take into account many information like the heat of crystallization, the possibility of multiple crystallization or activation energy. Therefore, we completed the work with crystallization kinetic performed under isothermal treatments. Proportion of crystalline phase was deduced from ^{31}P MAS-NMR analysis and used to follow the kinetics.

Application in this work: The onset of crystallization (T_x) and glass transition temperature (T_g) of the samples were derived from the DSC results to assess for the thermal stability. For isothermal treatment, the glass samples were submitted to thermal treatment at temperature above T_g. Solid state ^{31}P MAS-NMR was performed on the samples and the spectra obtained were deconvoluted by using DMfit software. Finally, the relative portion of crystalline phase was determined and expressed versus time to probe the crystallization kinetics.

II.6. Viscosity

Viscosity is a fundamental property in glass science. Viscosity represents the resistance against shear deformation versus time. The time rate of deformation is given by Newton's law of viscosity

$$\sigma = \eta \gamma$$

where η represents viscosity coefficient and thus defined as proportionality constant between the shear stress and the velocity of angular deformation γ. The unit of measurement is Pa.s.

There is no single technique that can be utilized to measure the viscosity of glass over the entire range. The different techniques allowing for the viscosity measurements are reported in *Tab 2.2*.

Tab.2.2 Viscosity measurement by various techniques.

Methods	Viscosity values (ranges)
Stokes' falling sphere/bubble rise	$< 10^4$ Pa.s
Margules rotating cylinder	$< 10^6$ Pa.s
Parallel plate	$< 10^5$ Pa.s $< \eta < 10^9$ Pa.s
Penetration viscometer	$< 10^5$ Pa.s $< \eta < 10^9$ Pa.s
Fiber elongation	$< 10^5$ Pa.s $< \eta < 10^{15.5}$ Pa.s
Beam bending	$< 10^7$ Pa.s $< \eta < 10^{12}$ Pa.s
Disappearance of stress	$< 10^{11}$ Pa.s $< \eta < 10^{14}$ Pa.s

Application to this work: The glasses viscosity has been studied in the range of 10^5 to 10^9 Pa.s (highlighted in *Fig. 2.4*) using a parallel-plate viscometer Physica MCR 101. The experiments were conducted on cylindrical samples presenting 6 mm diameter (d) and 3 mm height (h) dimensions. The cylinders were obtained after polishing annealed glass samples. Direct contact

with the parallel plates has been avoided by employing thin Pt foil. The continuous change in the sample height with increasing temperature (dh/dt) was recorded and viscosity was calculated with the following expression (Varshneya 1994):

$$\eta = \frac{2\pi . M . g . h^5}{3V . \frac{dh}{dt} . (2\pi . h^3 + v)}$$

where *M* is load, *g* gravity acceleration, *h* is height of the sample and *dh/dt* is deformation rate.

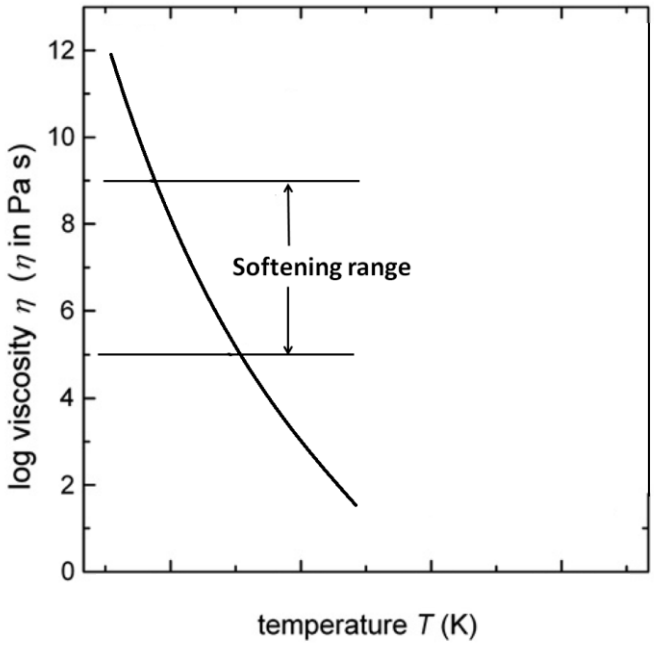

Fig. 2.4 Viscosity of the glasses measured at softening range 10^5-10^9 Pa.s by parallel plate viscometer.

III. Structural analyses

Glasses present a much more formidable challenge to structure elucidation when compared to crystalline solids. Owing to the lack of long-range periodicity in the glassy state,

diffraction techniques are not useful, and structural concepts typically emerge from the joint interpretation of numerous complementary spectroscopic experiments. In this study, Raman spectroscopy has been used as a preliminary structural analysis and the selective nuclear magnetic resonance (NMR) technique has been employed to selectively investigate the phosphate network and the doping elements.

III.1. Raman spectroscopy

The Raman spectroscopy is a non-destructive technique base on photon diffusion. The Raman effect occurs when photon impinges upon a molecule and interacts with the electric dipole of that molecule. The photon then excites the molecule from the ground state to a virtual energy state. When the molecule relaxes, it emits a photon and returns to a vibrational state. Usually, the photons are elastically scattered (the molecule returns to the ground state) and the frequency is unchanged (Rayleigh scattering) (*Fig. 2.5*). However in some cases (1 over 10^7), the scattering is not elastic and the molecule relaxed to a different vibrational state. The emitted photons present thus a different frequency. If the final vibrational state of the molecule is more energetic than the initial state, then the emitted photon will be shifted to a lower frequency, giving rise to the Stokes shift. If the final vibrational state is less energetic than the initial state, then the emitted photon will be shifted to a higher frequency and is designated as the anti-Stokes shift. Raman shifts are expressed in wave number, as from the following formula:

$$\Delta\omega(cm^{-1}) = \left(\frac{1}{\lambda_0(nm)} - \frac{1}{\lambda_1(nm)}\right) \times \frac{10^7(nm)}{(cm)}$$

Where, $\Delta\omega$ is the Raman shift expressed in wavenumber, λ_0 is the excitation wavelength and $\lambda_1$is the Raman spectrum wavelength. The unit chosen for expressing wave number is cm^{-1}.

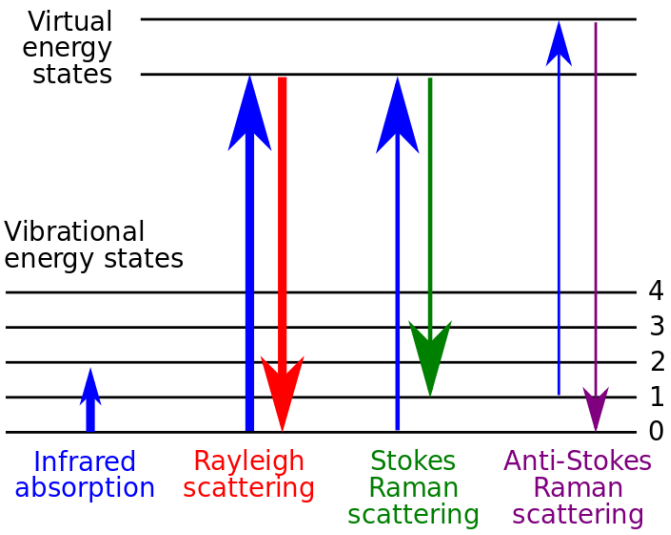

Fig. 2.5 Energy level diagram showing the states involved in Raman signal.

Tab. 2.3 Raman bands and proposed peak assignments for Zn-phosphate glasses.

Frequency cm^{-1}	Assignment	Speciation
704	POP_{sym} stretch (bridging oxygen)	Q^2
757	POP_{sym} stretch (bridging oxygen)	Q^1
969	$(PO_4)_{sym}$ stretch (nonbridging oxygen)	Q^0
1048	$(PO_3)_{sym}$ stretch (nonbridging oxygen)	Q^1
1138	P-O stretch	Q^1 chain terminator
1206	$(PO_2)_{sym}$ stretch (nonbridging oxygen)	Q^2

It is known that both the asymmetric and symmetric stretching vibrations characteristics of phosphate lattices are active in Raman spectra. However, the Raman spectra are dominated by intense bands related to the symmetric stretches. Literature data available on the frequency ranges related to the corresponding vibrations of the phosphate glasses are presented, in concise form (Brow1995), in *Tab. 2.3*. From this technique, the useful information for the preliminary structural characterization of the glass such as Q^n speciation and identification of P=O, P-O-P bonds can be obtained.

Application to this work: The samples were analyzed by Raman scattering using a XY800 Dilor spectrometer equipped with a Spectra Physics krypton ion laser. To record our spectra, we used the macroscopic stage and excited the sample with the 647.1 nm line with a low power (< 25 mW). A liquid nitrogen cooled charge coupled device constitutes the multichannel detector. The Labspec software was used for the acquisition and processing of the data. Each spectral range was recorded with four accumulations of 60 s and a resolution of 0.5 cm^{-1}.

III.2. Solid state nuclear magnetic resonance

The structural characterization reported in this work is mainly based on the solid-state NMR spectroscopy technique. 1D and 2D ^{31}P NMR was employed to characterize in details the structure of the phosphate network and ^{27}Al, ^{11}B and ^{29}Si NMR afford valuable information about the environment of the doping elements. In spite of the low amounts of dopant in the samples, correlation techniques were also used to probe the interactions between the doping elements and the phosphate network. After a brief discussion about the basic principles and a short presentation of the interactions involved in the NMR phenomenon, the chapter will focuses on the structural information obtained by NMR on the four elements previously mentioned (P, Al, B, Si). Finally, the correlation techniques employed within this study will be presented with a particular emphasis on the structural data derived from the correlation spectra.

III.2.1. Basic principles of NMR

Nuclear magnetic resonance is a phenomenon in which nuclei in a magnetic field absorb and re-emit electromagnetic radiation. The energy depends on the strength of the magnetic field and the magnetic properties of atom. However all nuclei are not observable, only nuclei with non-zero nuclear spin (I) are active. These nuclei have a magnetic moment $\vec{\mu}$ which can be expressed as:

$$\vec{\mu} = \gamma \hbar \vec{I}$$

where, γ is the gyromagnetic ratio

Ђ is Planck constant.

$\vec{I}$ is spin angular momentum.

The nuclei, for example, with I = 1/2 have two possible spin states: spin-up and spin-down. In the absence of external magnetic field, these states are degenerate. But if these nuclei are placed in a magnetic field ($\overrightarrow{B_0}$), the nuclear magnetic moment will interact with this field mean the two states are no longer degenerate. This leads to the distribution of spin population into 2I+1energy levels (for all nuclei). The interaction is thus called Zeeman interaction and is expressed by:

$$H = -\vec{\mu}\overrightarrow{B_0} = -\gamma\hbar\vec{I}\,\overrightarrow{B_0}$$

Usually z axis is chosen to be along $\overrightarrow{B_0}$, and the above expression reduces to:

$$H_z = -\gamma\hbar I_z B_0$$

The Zeeman energy corresponding to 2I+1, possible energy levels are,

$$E_m = -m\gamma\hbar B_0$$

where, m is the magnetic quantum number m =I, I-1,…

For any spin, the 2I+1 possible levels of energy are equidistant, and the energy difference between two states is given by (Mackenzie 2002) (*Fig. 2.6*):

$$\Delta E = \gamma\hbar B_0$$

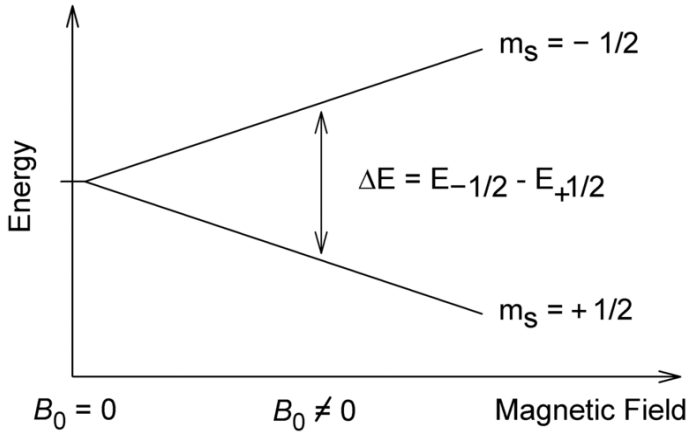

Fig. 2.6 Energy level diagram of a spin -1/2 nucleus showing the Zeeman interaction and its dependence upon static magnetic field B_0.

III.2.2. NMR pulse

In principle, NMR involves the perturbation of the alignment of the nuclear spins, under external magnetic field, by employing a radio frequency (RF) pulse. The evolution of the magnetization after the RF field is applied is called relaxation *Fig. 2.7*.

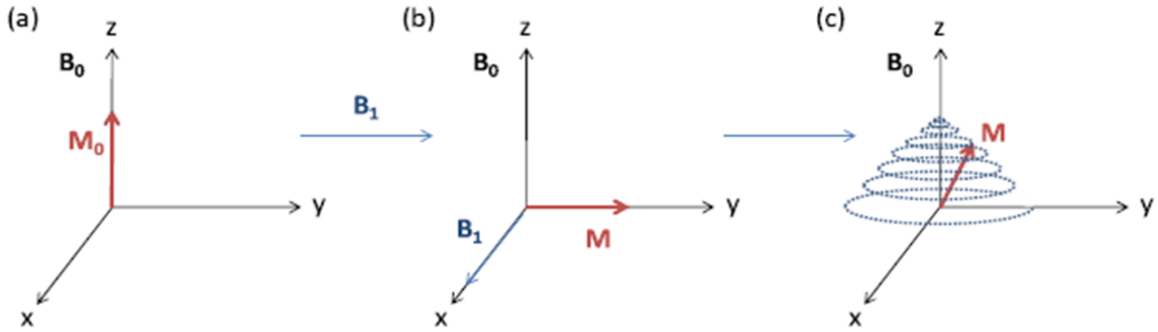

Fig. 2.7 Evolution of the magnetization before (a), during (b) and after (c) applying an RF field B_1.

When the RF pulse is applied, the nuclear magnetization falls out of the alignment and precesses around B_0 which is called Larmor frequency:

$$\omega_0 = \gamma B_0$$

After the RF pulse, the magnetization M is returned to its equilibrium position B_0 by following relaxation phenomena.

T_1: also referred as the longitudinal relaxation time (or spin-lattice). It characterizes the time for the nucleus to return to equilibrium of magnetization along the z axis.

The waiting time between two successive experiments must be long enough (3 to 5 times T_1) so that all the spin system is considered returned to equilibrium. This is very important condition to obtain spectrum for quantitative analysis.

T_2: referred as transverse relaxation time (or spin-spin). The value of T_2 is actually observed as decay time of the NMR signal or free induction decay (FID). A nucleus with a long T_2 relaxation time gives rise to a very sharp NMR peak in the FT-NMR spectrum whereas nuclei with shorter T_2 values give rise to broad FT-NMR peaks.

III.3. Interactions

All the interactions involved in the NMR technique are reported below and briefly discussed.

Tab.2.4 List of Interactions.

Interaction	Origin	Information	Typical Size (Hz)
Zeeman	Interaction between nuclear spin and static magnetic field	Selection of nucleus	10^7-10^9
Dipolar	Through space spin-spin interaction	Spatial proximity, distance	10^3-10^4
Chemical shielding	Interaction between magnetic field B_0 and electron clouds	Coordination, distance and the nature of the first neighbor	10^2-10^5
Quadrupolar (I>1/2)	Interaction of nuclear quadrupolar moment with the electric field gradient	Geometry of a site and symmetry	10^3-10^7
Indirect Spin (J-coupling)	Spin-spin coupling via bonding electrons	Connectivities through chemical bonding	1-10^3

III.3.1. The chemical shift

The chemical shift originates from the interaction between the electron cloud surrounding the nucleus and the external static field B_0. This interaction will give rise to a local magnetic field, proportional to B_0, defined as

$$B_{local} = \sigma . B_0$$

where σ is the shielding constant.

As a consequence, the true magnetic field (B_{eff}) felt by the nuclei comes from the superimposition of B_0 and B_{local}:

$$B_{eff} = B_0 - B_{loc} = (1-\sigma)B_0$$

and, the true resonance frequency will be given by:

$$\nu = (1-\sigma)\nu_0$$

nuclei in different chemical environments will thus present different resonance frequencies owing to their different shielding constants coming from their different electro clouds. This difference is expressed through the chemical shift values (δ_{CS}) defined as:

$$\delta = \frac{\upsilon - \upsilon_{ref}}{\upsilon_{ref}} . 10^6$$

where, υ_{ref} is the frequency resonance of a reference sample. The chemical shift is given in ppm and is not dependent on the employed B_0 (and is thus not dependent on the spectrometer used for the analysis).

III.3.2. Dipolar interaction

The dipole interaction arises from the through-space coupling between two magnetic dipoles and gives thus information about the spatial proximity between two nuclei. Classically the energy of two interacting dipoles μ_1 and μ_2 separated by a distance r, is given by the following expression:

$$E = \frac{\mu_0}{4\pi}\left[\frac{\vec{\mu_1}\vec{\mu_2}}{r^3} - 3\frac{\vec{\mu_1}\vec{r}.\vec{\mu_2}\vec{r}}{r^5}\right]$$

After simplification, the magnitude of the dipolar interaction between two nuclei I and S can be expressed as:

$$\omega_D = \frac{\mu_0}{4\pi}\frac{\gamma_I \gamma_S \hbar}{r_{IS}^3}$$

where γ_I and γ_S are the gyromagnetic ratios of I and S spins, respectively. The interaction intensity is thus governed by the distance ($1/r^3$) and by the gyromagnetic ratios. The values will thus be important in case of high γ nuclei like ^{1}H and ^{19}F. When I=S, the interaction is denoted as homo-nuclear dipolar interaction. When I and S are of different nature, the interaction is called hetero-nuclear dipolar interaction.

III.3.3. Scalar interaction

The scalar interaction originates from the mediation between two nuclei through the bonding electrons and thus traces the chemical connectivity between the two nuclei. This interaction is characterized by the J-coupling values. J-coupling originates from the interaction between two nuclei by means of the bonding electrons. In liquid NMR, the J-coupling results in the formation of multiplets from which the number of neighbors can be deduced. In solid state NMR, the J-coupling magnitude is negligible compared to the other interactions and does not allow for its determination on 1D analysis.

III.3.4. Quadrupolar interaction

This interaction occurs for spin > ½, which represent more than 2/3 of the periodic classification. In opposition to spin ½, for which the electrical charge inside the nucleus adopt a spherical distribution, it can be shown that the electrical charge distribution within quadrupolar nucleus is non-spherical, this configuration giving rise to a nuclear electric quadrupole moment (eQ), as depicted in *Fig. 2.8*. The quadrupolar interaction actually comes from the interaction between this nuclear electric quadrupole moment and the electric field gradient (eq) created around the nucleus by the chemical environment. Since the electric field gradient is formed in case of completely non-symmetric electrostatic environment, the quadrupolar interaction is very sensitive to symmetry.

This interaction thus can be considered as null in case of cubic environment (like for ^{23}Na in NaCl cubic structure) but it can also reach very important values (comparable to the Zeeman effect) in case of distorted environment. In these cases, the quadrupolar interaction leads to very broad and asymmetric NMR signals that strongly disturb the spectra analysis.

Two parameters are used to characterize the signals: the quadrupolar constant (C_Q given in MHz) that represents the interaction amplitude and the asymmetry parameter (η in the range of 0-1) representing the asymmetry character. It is noteworthy that the mathematical treatment of the quadrupolar interaction leads to an analytical expression containing two terms of significant

importance: the first order and the second order terms (due to their lower values, only the first order term is significant for the other interactions). The relevance of these two terms will be discussed in the following section (III.4).

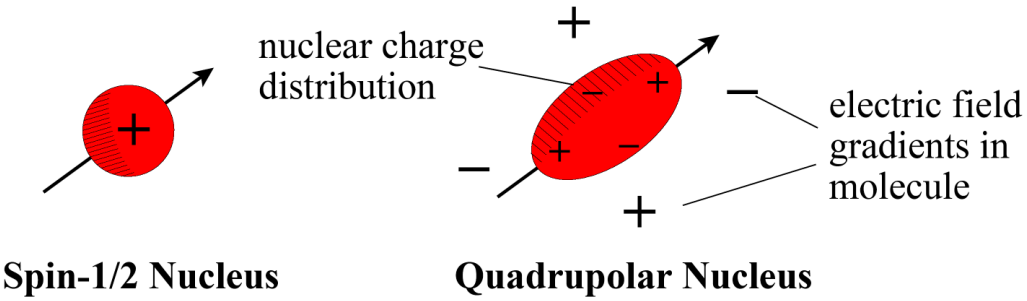

Fig. 2.8 Comparison of a spin ½ nucleus and quadrupolar nucleus (I>1.2)

III.4 Magic angle spinning (MAS)

The interactions described in the previous part contain isotropic and anisotropic contributions. The latter one is dependent to the microcrystalline orientation in respect to B_0, different orientations leading to different values. In liquid state, the very rapid Brownian motions (compared to the NMR time scale) lead to an averaging of the anisotropic part and the spectra are dominated by the isotropic character of the interactions. Such motions do not exist in case of solids. Therefore, NMR performed on solids and especially on powders (which can be considered as a mixture of micro-crystallites with all the possible orientations in respect to B_0) produces very broad signal arising from the superimposition of all the NMR signals coming from each orientation. The obtained spectra are complicated to interpret and structural information can hardly be derived from these analyses.

In 1958, Andrew proposed a technique, called Magic Angle Spinning (MAS), to improve the solid state NMR resolution. The basic idea was to mimic the Brownian movements occurring in liquids. The movement applied to the solids is a rotation and is characterized by its spinning frequency (denoted as $\omega_R/2\pi$) and by the angle between the rotation axis and B_0 (denoted as θ).

$$\omega(\alpha,\beta) = \omega_{iso} + \omega_{aniso}(\alpha,\beta).(3cos^2\theta - 1)$$

Under rotation conditions, it has been shown that the anisotropic part was modulated by a polynomial proportional to $(3\cos^2\theta-1)$ as shown in the above expression. If the θ angle is adjusted to the values of 54.74°, then the $(3\cos^2\theta-1)$ polynomial is equal to 0. The effect of the anisotropic part is thus averaged out and the spectra present the isotropic contributions. Technically, the powder is loaded into a cylinder made out of zirconia (called rotor), which can be inclined (at the θ angle) and rapidly spun about its symmetry axis (*Fig 2.9*).

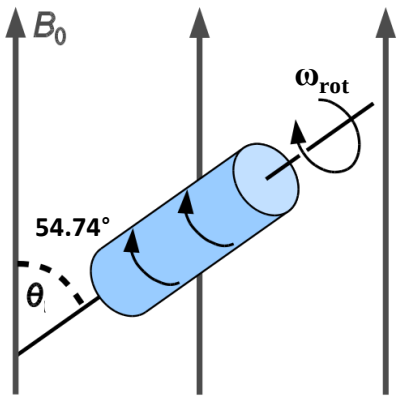

Fig. 2.9 Schematic representation of the Magic Angle Spinning technique.

The spectra obtained are thus free out of the anisotropic contributions and present narrow signals with optimized resolution. However, the MAS technique has two main limitations:

(i) the anisotropic part is completely averaged out only if the spinning frequency (ω_{rot}) is greater than the anisotropic part amplitude. If not, this latter is only modulated by the rotation that gives rise to additional signals, appearing periodically for every multiple of spinning frequency on both sides of the isotropic signal. This signals are called spinning sidebands. The lower the spinning frequency, the higher the number and intensity of the spinning sidebands, as reported in *Fig. 2.10*.

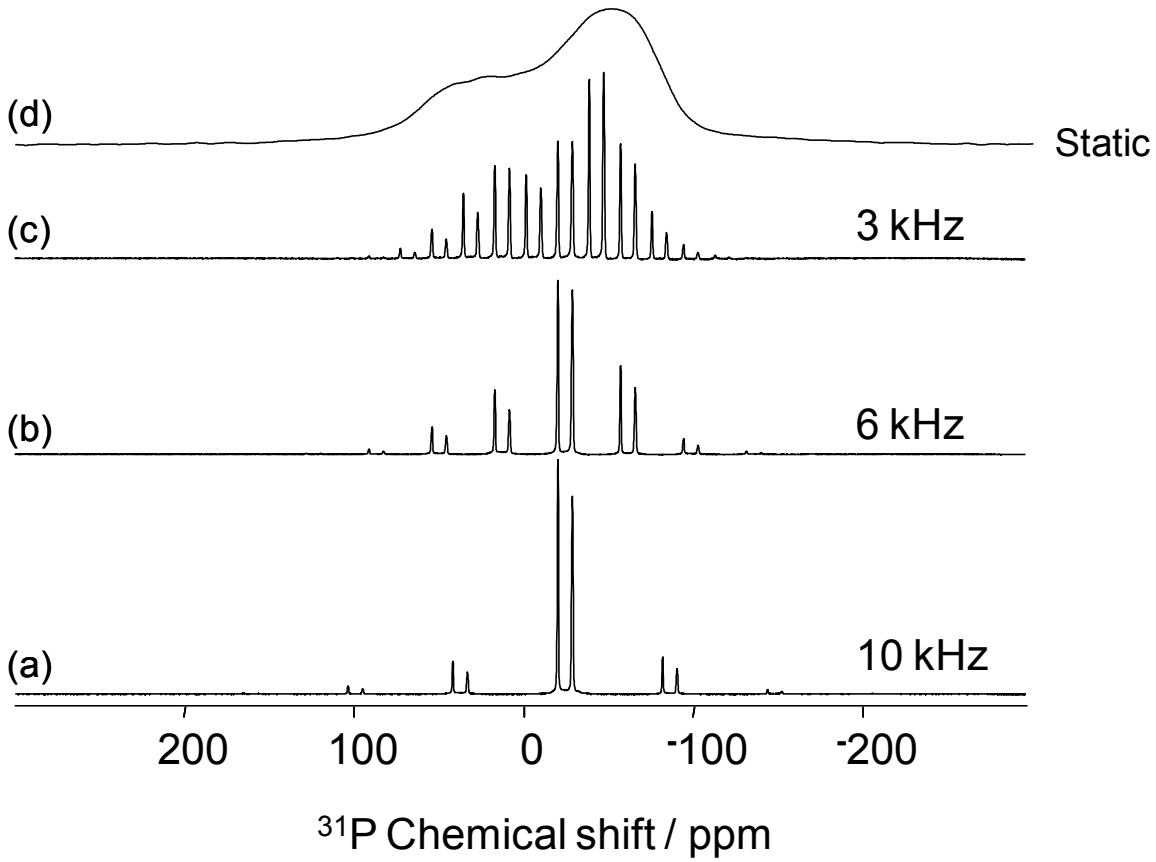

Fig. 2.10 ^{31}P NMR of $NaAlP_2O_7$ showing lower number of spinning side bands as the spinning frequency is increased 10KHz (a), 6KHz (b), 3KHz (c) and 0KHz (d).

(ii) as previously mentioned, the quadrupolar interaction reaches values comparable to the Zeeman effect leading to terms of significant importance in the analytical expression of the frequency. If the first order term (modulated under rotation conditions by $(3\cos^2\theta-1)$) can be efficiently averaged out by the MAS technique, the second order term is modulated by another polynomial that is partially reduced when $\theta = 54.74$.

$$P_2(cos\theta) = \frac{1}{2}(3cos^2\theta - 1)$$

$$P_4(cos\theta) = \frac{1}{8}(35cos^4\theta - 30cos^2\theta + 3)$$

Therefore, the MAS technique has only a reducing effect on the quadrupolar interaction. The acquired spectra can present characteristic features originating from the quadrupolar interaction like non symmetric shape. Special techniques can be used to record high resolution spectra for quadrupolar nuclei. Since these techniques were not necessary within this work, they will not be discussed. It is also noteworthy that the second order term is inversely proportional to the external B_0 field. Experiments performed at high field will thus benefit from a better reduction of the quadrupolar effect and will thus present narrower and more resolved signals. This will be illustrated in the next part through the analysis of ^{11}B nucleus (I=3/2).

To summarize, the MAS technique, by mimicking the Brownian movement occurring in liquids, allows recording well resolved spectra with absent or limited impact of the anisotropic character of the interaction. In many cases, the spectra can be interpreted in terms of chemical shifts and does not contain any information about the dipolar interaction, which is a 100% anisotropic interaction.

In the next section, the information derived from the chemical shift of ^{31}P, ^{27}Al, ^{11}B and ^{29}Si will be discussed. Then, we will present how the dipolar interaction can be selectively re-introduced using specific pulse sequences that can provide valuable information about spatial proximity between two nuclei.

IV. Application of 1D solid state MAS-NMR

This work has benefitted from information provided by ^{31}P, ^{27}Al, ^{11}B and ^{29}Si 1D MAS-NMR experiments. The NMR parameters (spin, natural abundance, Larmor frequency and relative sensitivity (compared to ^{13}C assigned to 1) are reported in *Tab. 2.5*. The Larmor frequency is given for a static magnetic field of 9.4 T since all the experiment were performed using a spectrometer developing this field.

Tab.2.5 Characteristics of the nuclei for NMR experiments.

Isotope	Spin	Natural abundance (%)	Larmor Frequency @ 400 MHz	Rel. Sens. ^{13}C =1
^{31}P	1/2	100	162	379.3
^{27}Al	5/2	100	104.3	101.2
^{11}B	3/2	80.42	128.4	151.2
^{29}Si	1/2	4.7	79.47	2.1

Tab. 2.5 indicates that ^{31}P nucleus is perfectly suitable for NMR investigation. The high sensitivity of ^{27}Al and ^{11}B will allow recording good signal to noise ratio spectra within reasonable experimental times in spite of the low amount in the glass formulation ($\leq$ 4 mol%). As previously mentioned, the low natural abundance of ^{29}Si that could have been a strong limitation to this study has been overcome by the preparation of 100% ^{29}Si enriched samples.

The structural information deduced when 1D MAS-NMR is applied to these nuclei is discussed in the following. It is noteworthy that all the 1D experiments have been performed on a 9.4 T Bruker AVANCE III spectrometer equipped with a 4-mm triple channel probe operating at a spinning frequency of 10-12.5 kHz.

IV.1. ^{31}P MAS-NMR

Owing to its ½ spin, its 100% natural abundance, its high Larmor frequency (161.9 MHz at 9.4 T), its reasonable relaxation times (120 s) and its wide chemical shift range, ^{31}P is a perfect nucleus for NMR investigations. The chemical shift values observed on the 1D analysis of phosphorus compounds is governed by two parameters:

(i) The Q^n speciation: different chemical shift ranges can be determined depending on the Q^n speciation. Isolated Q^0 units present high values chemical shifts (deshielding effect) and the chemical shift decreases with the network reticulation up to the Q^3 chemical shift range. This evolution only requires the phosphate network to be associated with identical chemical elements.

(ii) The neighbors chemical nature: at constant phosphate unit structure (fixed Q^n species), the chemical shift will be governed by the chemical nature of the associated elements. A linear correlation has been determined between the chemical shift and the electrostatic field strength (z/a^2) of the associated element in binary systems.

The effect of these two parameters is illustrated in *Fig. 2.11* where the chemical shift ranges observed in different binary phosphate systems are reported. If the signal assignment is obvious on binary systems from the figure, analysis of complex systems containing more than two oxides with different valency is much more complicated. For example, if a signal observed at -15 ppm in a Na_2O-Al_2O_3-P_2O_5 system can be assigned either to a Q^2 surrounded by sodium, a Q^0 surrounded by aluminium or can also be associated to a Q^1 surrounded by both elements (Brow 1990). Therefore, information about the real chemical environment of phosphorous is necessary for a supported assignment on complex systems.

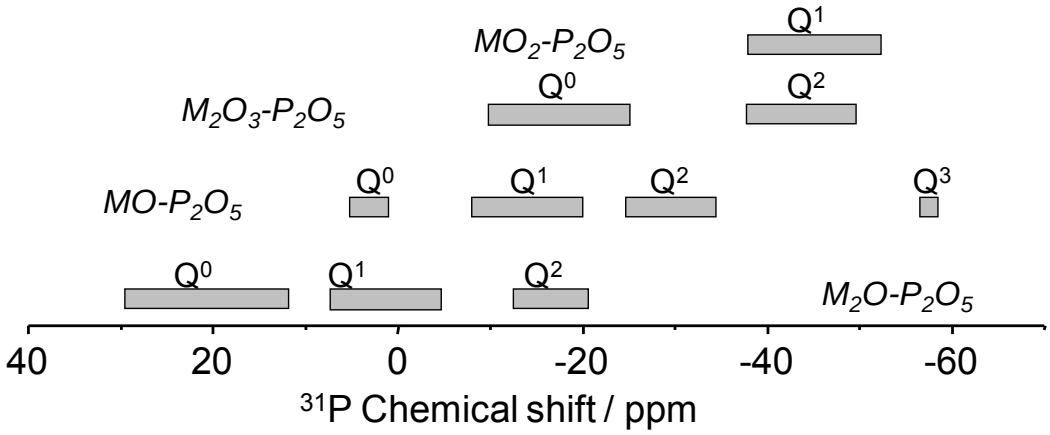

Fig. 2.11 ^{31}P isotropic chemical shift/ppm ranges for each $Q^{(n)}$-species in different binary phosphate systems.

In this work, the ^{31}P 1D MAS-NMR analysis were performed at 162 MHz. The spectra were recorded using single pulse acquisition with a 2.25 µs pulse length (corresponding to a 45° angle and a 60 kHz radiofrequency field (rf strength) and 16-32 accumulations. Quantitative spectra were obtained by using relaxation time (rt) of 120 and 300 s for the amorphous sand crystalline samples, respectively. ^{31}P MAS-NMR spectra were deconvoluted using the DMFit software (Massiot 2002). All the chemical shifts are referred to H_3PO_4 as 0 ppm.

IV.2. ^{27}Al MAS-NMR

Despite being a quadrupolar nuclei I=5/2, ^{27}Al is a very favorable nucleus for NMR spectroscopy since it has a natural abundance of 100 %, high Larmor frequency and short relaxation times. Moreover, the spectra are usually affected by the quadrupolar interaction in a moderate way. Therefore, the spectra can be used to extract chemical information without the need of special precautions. Basically, the chemical shift gives information about the aluminium coordination states. Aluminium can be found in four-, five- and six-fold coordination, denoted as Al^{IV}, Al^{V} and Al^{VI} in the following. As depicted in *Fig. 2.12*, each coordination state can be distinguished through different and separated chemical shift ranges.

^{27}Al MAS-NMR gives thus access to the above mentioned structural information and can be used to quantitatively determined the proportions between the different Al^{M} species (M=IV, V or VI).

In this work, 1D ^{27}Al MAS-NMR spectra were acquired at a Larmor frequency of 104.3 MHz. The one pulse experiment were done using very short pulse length (1 μs) corresponding to a 10° angle and a rf strength of 30 kHz (determine on a liquid), 1024 accumulations and a rd o f 1s. All the chemical shifts are referred to $Al(NO_3)_3$ solution (1M) as 0 ppm. The 1D ^{27}Al spectra is deconvoluted with DmFit software to quantify 4-, 5-, and 6-coordinated Al-polyhedra. The relative proportion of 4-, 5- and 6-coordinated Al species were also determined, using DMfit software with Czjzek's model taking into account a distribution of the quadrupolar parameter (Czjzek 1981).

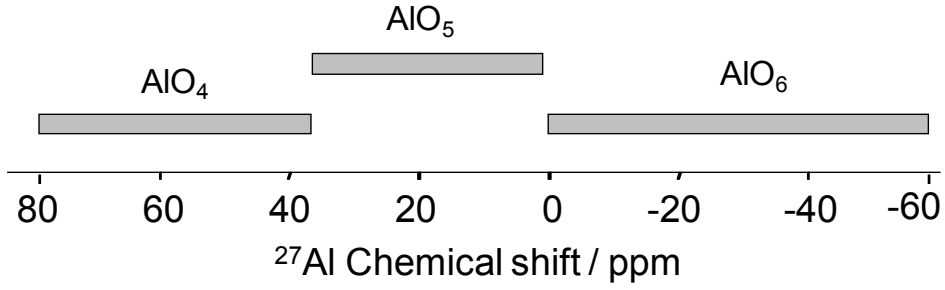

Fig. 2.12 ^{27}Al isotropic chemical shift in ppm ranges for different coordination states.

IV.3. ^{11}B MAS-NMR

^{11}B is a quadrupolar nucleus (I=3/2) with a good natural abundance (80.4%), a high Larmor frequency and short relaxation times. Boron can be found in three- and four- fold coordination states (denoted as B^{III} and B^{IV} in the following) in materials. The chemical shift is sensible to the boron coordination states and different chemical ranges have been determined (*Fig. 2.13*) that give access to this structural information. Nevertheless, the quadrupolar interaction has to be taken into account. The B^{IV} units are not strongly affected by this latter interaction owing to the high symmetric character of these species. B^{IV} units are thus characterized by almost symmetric peaks. The planar B^{III} species, that present a highly asymmetric character, are significantly affected by the quadrupolar interaction. The resulting signals are thus broad and present characteristic asymmetric features. At low magnetic field, when the effect of the quadrupolar interaction is important, the B^{III} signals is so broad that it superimposes with the B^{IV} signal giving rise to spectra with poor resolution. At higher field, the second order term is significantly reduced, leading to a narrowing of the B^{III} signal and to spectra with well separated B^{III} and B^{IV} resonances. *Fig. 2.14* shows the ^{11}B MAS-NMR analysis performed on a sodium borosilicate glass performed at 9.4 (a) and 18.8 (b) T and shows the effect of high field on the spectrum resolution. Depending on the systems under investigation, high field can be required to get detailed information about the borate speciation.

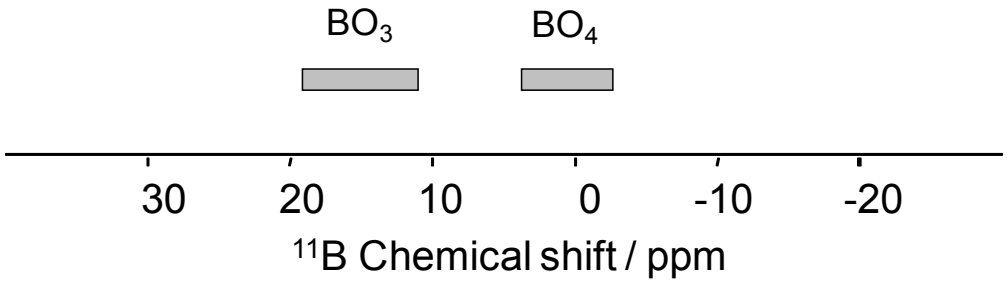

Fig. 2.13 ^{11}B Isotropic chemical shift/ppm ranges for different coordination states.

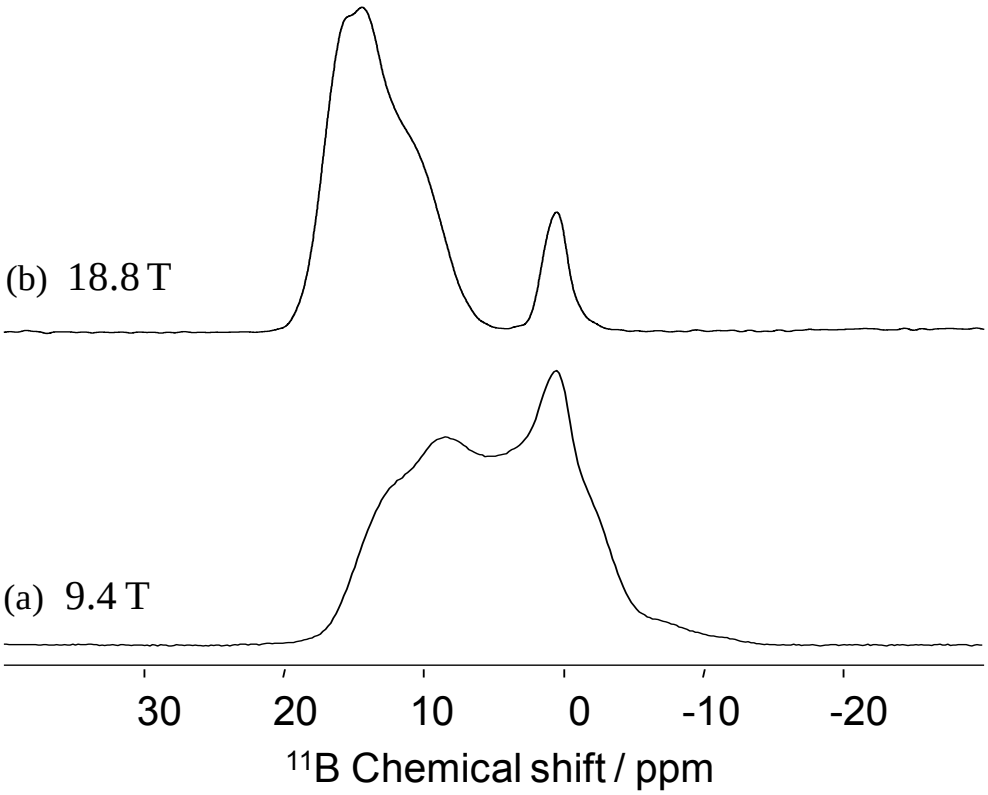

Fig. 2.14 ^{11}B isotropic spectra of sodium borosilicate glass at 9.4T (a) and 18.8 T (b).

In this work, 1D ^{11}B MAS-NMR spectra were acquired at a Larmor frequency of 128.4 MHz. The one pulse experiment were done using 1 µs pulse length, corresponding to a 15° angle and a rf strength of 40 kHz (determine on a liquid), 1024 accumulations and a rd of 2 s. The chemical shifts of ^{11}B are referenced to the secondary reference $NaBH_4$ at -42.06 ppm. The baseline was corrected by subtracting the background signal coming from the boron nitride stator of the probe.

IV.4. ^{29}Si MAS-NMR

^{29}Si is a spin 1/2, and is thus not concerned by the quadrupolar interaction. However, acquisitions are limited by its low natural abundance (4.7 %) and by the very long relaxation times (up to hours) leading to very time-consuming experiments. As for ^{31}P MAS-NMR, the ^{29}Si

chemical shift value is sensible to the Q^n configuration. As reported in *Fig. 2.15*, five chemical shift ranges have been determined corresponding to the five Q^n species (from Q^4 to Q^0) that can be obtained with the tetrahedral silicon units (Smith 1983).

In some rare cases, silicon can also adopt an octahedral coordination state leading to signal shifted to -195 to -215 ppm (Dupree 1987).

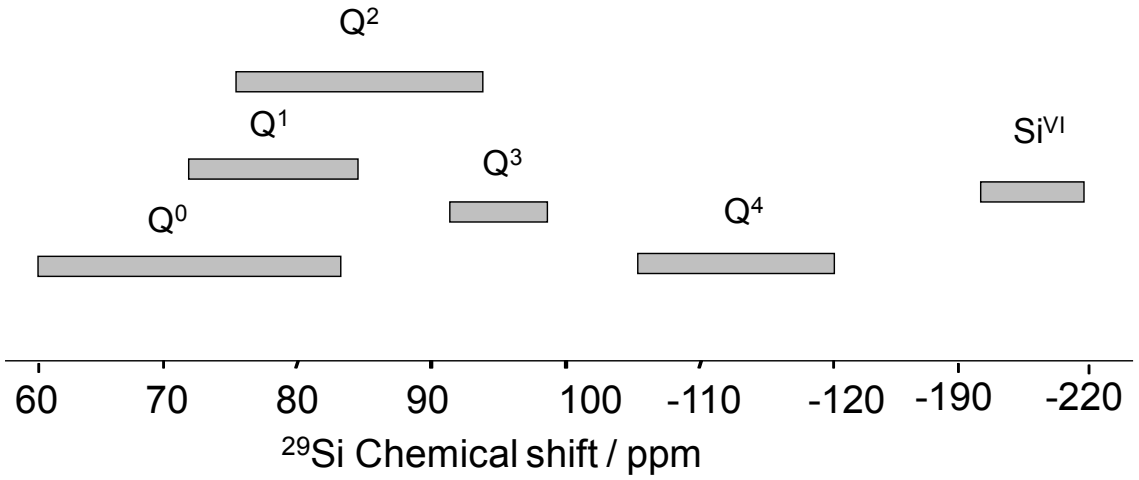

Fig. 2.15 Isotropic chemical shift ranges for each $Q^{(n)}$-species.

In this work, 1D ^{29}Si MAS-NMR spectra were acquired at a Larmor frequency of 79.47 MHz. The spectra were recorded using a single pulse experiment with a 3.25 µs pulse length, corresponding to 45° angle and a rf strength and a spectral width of 100 kHz. The spectra were acquired with 400-800 accumulation, depending on the SiO_2 proportion and an rd of 120 s. All the chemical shifts are referred to tetramethylsilane solution as 0 ppm.

V. Application of 2D solid state NMR

In order to complete the structural characterization of the materials and to understand the effect of the doping elements, advanced correlation NMR techniques were used. As previously

mentioned, the very low amounts of doping require the uses of stable, robust and easily optimized pulse sequences. The work has been based on three correlation techniques that are the X{^{31}P} REDOR, ^{31}P{X} D-INEPT and the DQ-SQ sequences, with X being the doping element (= ^{11}B or ^{27}Al). If the first sequence has already proven its efficiency in many investigations, the second one has been very recently developed. If the DQ-SQ experiment has been used for a long time in case of ^{31}P nuclei, we also employed in this work a slightly modified version suitable for the quadrupolar ^{27}Al and ^{11}B nuclei. Basics principles and structural information deduced from these correlation techniques will be discussed in this part. It is noteworthy that all the correlation NMR experiments have been done at 9.4 T with a 4-mm triple channel probe operating at a spinning frequency of 12.5 kHz.

V.1. D-INEPT (Refocused Insensitive nuclei Enhanced by Polarization Transfer)

This sequence will provide information about the interactions between the phosphate units and the doping polyedra, from which the presence of P-O-X linkages will be inferred or not. There are different sequences that can be used to investigate the P/X interactions like the Cross-Polarization (Hartmann 1962 and Caravatti 1982), the Hetero-nuclear Multiple Quantum Coherence (Lesage 1998) or the Insensitive Nuclei Enhanced by Polarisation Transfer (Morris 1979) techniques. In this work, we have worked with a slightly modified INEPT technique. Indeed, the original INEPT sequence is a scalar-based technique, but in our case, additional pulse schemes were inserted on the ^{31}P channel allowing for a through space magnetization transfer (Trebosc 2007). The sequence thus provides through space correlation information between P and the doping element. Compare to the standard scalar based sequence, Dipolar INEPT (D-INEPT) is much more sensible and will thus allow us to record analysis on doped samples within reasonable experimental times. Moreover, if spatial proximity does not necessarily and rigorously mean chemical connectivity, the proximity highlighted by these NMR methods has been shown to be selective enough to be representative of the chemical connectivity (Wullen 2007).

The D-INEPT pulse sequence used within this work is reported in *Fig. 2.16*. The first 90° pulse creates magnetisation for the X nucleus, which evolves during the delay t_1. A spin-echo

sequence is then applied to the X nuclei with a delay τ. Two synchronised 90° pulses are applied simultaneously to X and ^{31}P nuclei to create correlation signals. An additional spin-echo sequence (with an echo delay τ') is finally applied to both nuclei to refocus the signal. The acquisition of the FID for the ^{31}P nuclei is achieved during t_2. All along the sequence, dipolar recoupling pulse schemes are used on the ^{31}P channel to create through-space correlation signals.

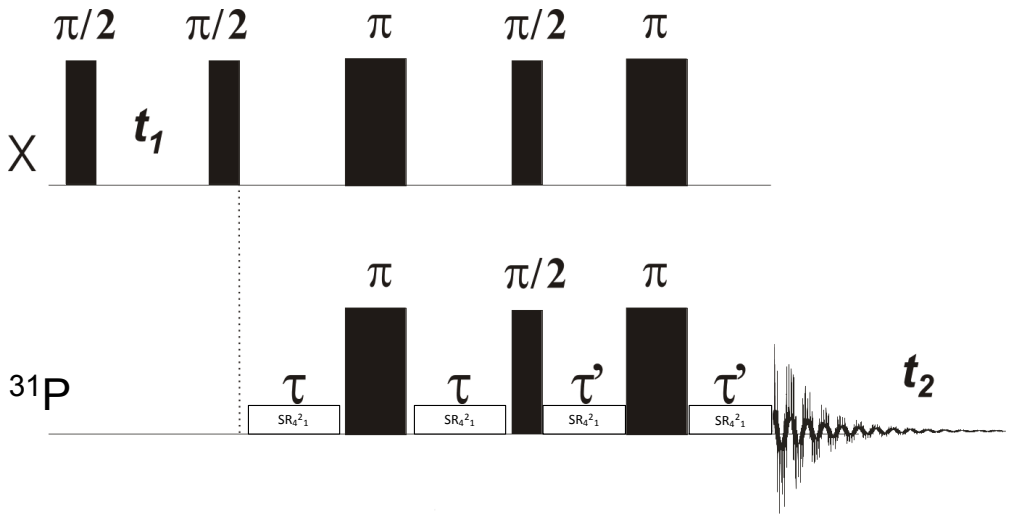

Fig. 2.16 ^{31}P{X} D-INEPT pulse sequence starting from the quadrupolar nucleus and detection on spin-1/2 nucleus.

The obtained ^{31}P{X} D-INEPT spectra will indicate the phosphate units that are closed to the doping elements and that are thus involved in P-O-X bonds. Comparison with standard 1D spectra will allow distinguishing P involved in P-O-X from P that are not connected to the doping elements.

All the experiments have been performed at 9.4 T. When X=Al, the experiments have been performed with 40 ×10^3 accumulations, a rd of 1 s and a rf field of 50 kHz and 28 kHz were used respectively for ^{31}P and ^{27}Al. The dipolar coupling was obtained with reintroducing SR4$^2_1$ technique (Lu 2013) irradiating ^{31}P with rf field of 25 kHz for 1 ms. When X=^{11}B, the experiments have been performed with 120 k accumulations, a rd of 2s and radiofrequency of 50 kHz and 32 kHz for ^{31}P and ^{11}B, respectively. For this, a recoupling power of 32 kHz for 1 ms was used.

V.2. REDOR (Rotational Echo Double Resonance)

In addition to the qualitative detection of the P-O-X bonds afforded by the D-INEPT technique, we also used the well known X{^{31}P} MAS-REDOR technique to quantitatively analyze the B/P interactions. The Rotational Echo DOuble Resonance (REDOR) technique was introduced by Gullion in 1989 (Gullion 1989) and will be used here to analyze the dipolar coupling between the X and ^{31}P nuclei. This information will then be used to extract the number of phosphorous attached to the doping elements, giving thus access to the nature of the $X(OP)_n$ structural units.

The REDOR principle is to compare 2 sets of signal intensity obtained on the X channel using spin-echo sequences (*Fig. 2.17*). In a first step, the S_0 signal set is measured under MAS conditions that completely suppress the X/P dipolar interaction. The S_0 signal is thus free of any dipolar coupling. Then, during the S signal acquisition, a set of π-pulse trains is sent to the ^{31}P channel during the middle of each rotor period that leads to the re-introduction of the X/P dipolar interaction. The S signal set is thus recorded under the influence of the reintroduced dipolar interaction. This latter affects the P atoms close to the B^{3+} ions and induces a signal dephasing, resulting in an intensity signal decrease.

The amplitude of the dipolar interaction can then be expressed through the normalized difference $(S_o\text{-}S)/S_o$. The evolution of this normalized difference versus the echo delay τ is called REDOR curves. In cases of multi-spins system, it has been shown that the evolution of the REDOR curves for $(S_o\text{-}S)/S_o < 0.2$ can be directly related to the dipolar interaction intensity and to the number of P attached to the X element. The higher the number of attached P, the quicker the evolution as depicted in *Fig.18* showing the REDOR curve obtained presenting $B(OP)_4$ and $B(OP)_3$ environments on crystalline borophosphate compounds (Raguenet 2011).

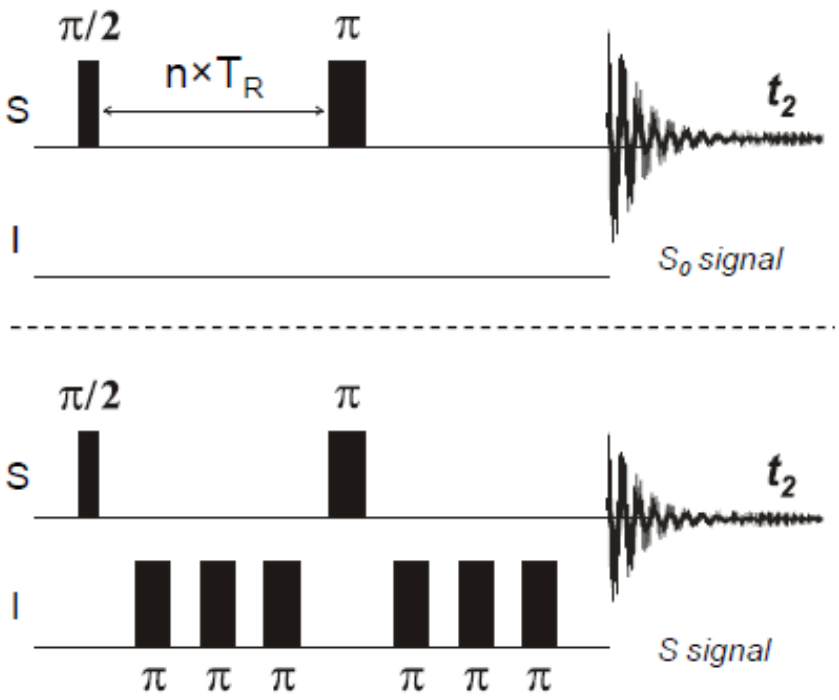

Fig. 2.17 REDOR pulse sequence.

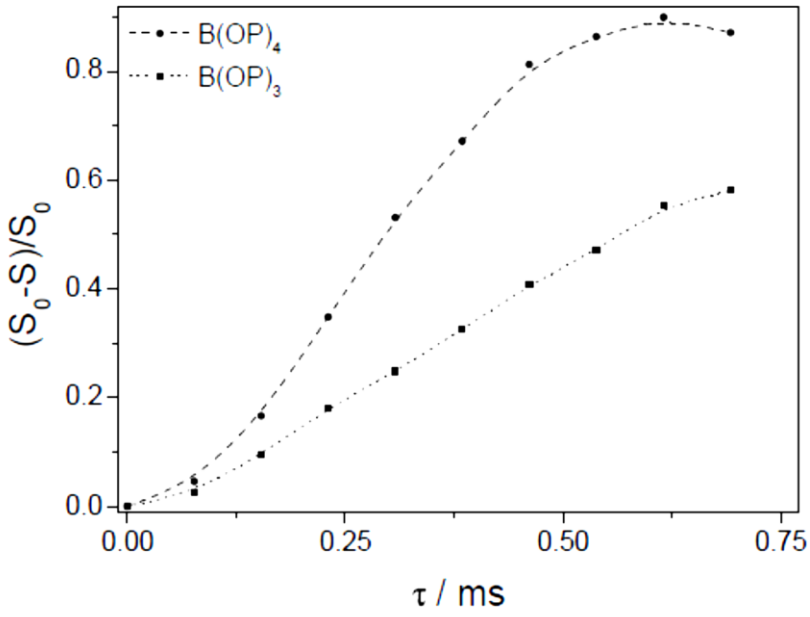

Fig. 2.18 REDOR curves for $B(OP)_4$ and $B(OP)_3$ environments.

All the X{^{31}P} REDOR experiments used in this work have been acquired at 9.4 T with a 4-mm probe operating at spinning frequencies of 8-15 kHz. When X=^{27}Al, the 90°-τ-180°- τ spin-echo sequence was performed using pulse lengths of 7 and 14 μs and a radiofrequency field of 15 kHz. The 18 sets of S_0 and S signals were recorded with 128 accumulations and a rd of 1s. When X=^{11}B, the spin echo was acquired with pulse lengths of 6 and 12 μs. The 26 S_0/S sets were acquired using 128 accumulations and a rd of 2 s. For both systems, the reintroduction of the heteronuclear dipolar interaction was performed by irradiating the ^{31}P channel with 180° pulse of 11 μs corresponding to a rf strength of 45 kHz.

V.3. DQ-SQ (Double Quantum-Single Quantum)

The DQ-SQ experiments has been widely used to analyze the through space interaction between the phosphate species in crystalline or amorphous phosphate based materials (Witter 1998). A typical DQ sequence is reported in *Fig. 2.19*. The first pulse block (called *excitation*) allows for the creation of DQ coherences that evolve during the evolution time t_1. Then, these coherences are converted into zero-quantum coherences using the same pulse block (called *reconversion*). The last 90° pulse transfers the magnetisation into observable single quanta coherence for signal acquisition. Since the DQ coherence can only be created in case of spatially closed phosphorous atoms, the correlation signals observed in the 2D spectra highlight spatial proximity.

A schematic DQ spectrum is reported in *Fig.2.20*. In the double-quantum dimension, the chemical shifts of the resonances are reported at twice their isotropic values. The diagonal spectrum is then plotted at (δ_X, $2\delta_X$). Two kinds of signal can be observed: diagonal peaks (δ_A, $2\delta_A$), which highlight spatial proximity between two phosphorous in the same site, and off-diagonal peak pairs, which highlight spatial proximity between two different phosphorous sites (for example, in the spectrum reported in *Fig. 2.20*, spatial correlation between P_A and P_B is highlighted by an off-diagonal peak pair at (δ_A, $\delta_A+\delta_B$) and (δ_B, $\delta_B+\delta_A$)).

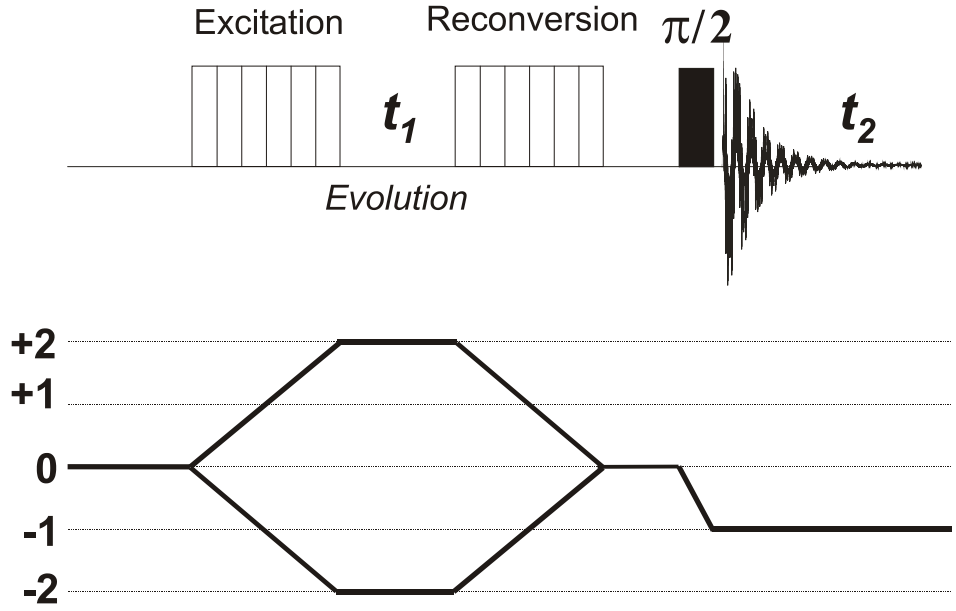

Fig. 2.19 DQ-pulse sequence.

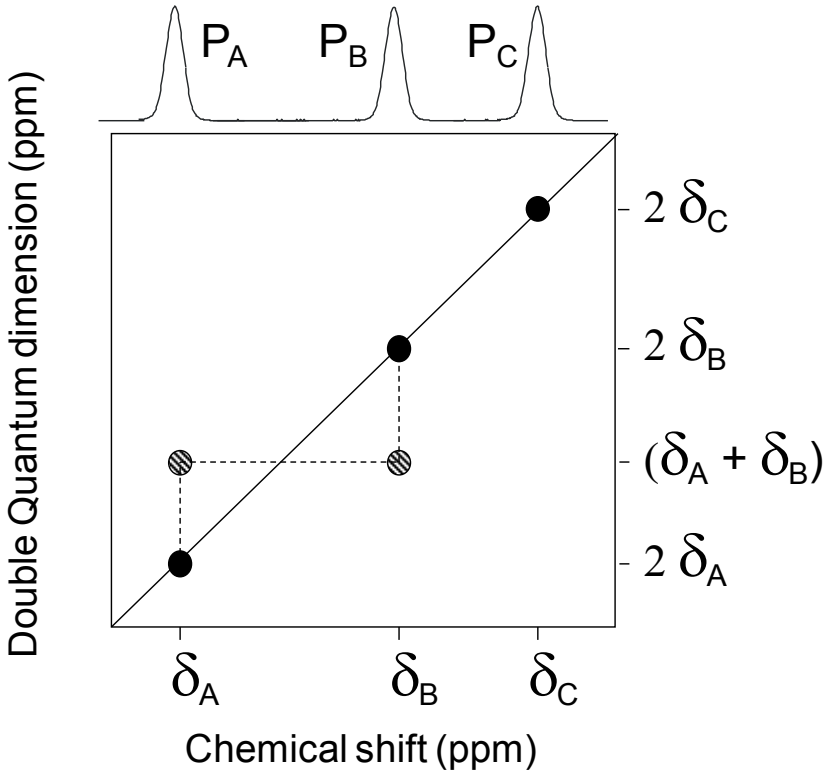

Fig. 2.20 Schematic 2D-DQ Spectrum.

This sequence was not suitable for quadrupolar nuclei since DQ coherence could be created by a single quadrupolar nucleus. As a consequence, the signal observed on the diagonal could not be used to trace spatial connectivity. Recently, the DQ-SQ sequence was slightly modified in order to produce 2D spectra that can be analysed without any ambiguity.

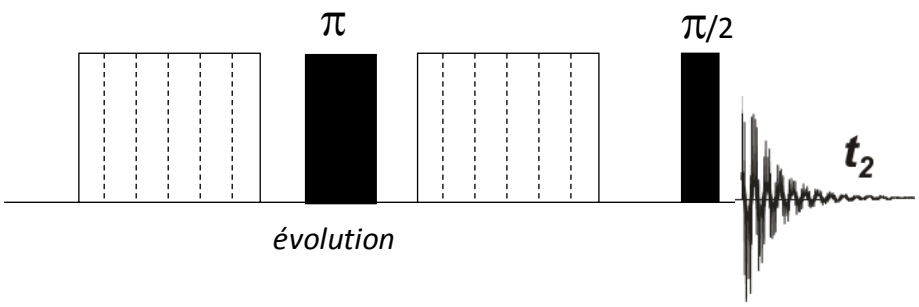

Fig. 2.21 {^{11}B or ^{27}Al} DQ-SQ pulse sequence with additional π pulse.

The sequence (*Fig. 2.21*) contains an additional 180° pulse that destroys all the DQ coming from a single nucleus, making thus of the observed diagonal signal a real evidence of spatial proximity between two different nuclei (Wang 2009).

In this work, the DQ-SQ experiment was used on ^{31}P to analyse the interaction between the different phosphate units and to analyse the MRO order in the glasses. The modified DQ-SQ was also employed to determine the presence of X-O-X linkages that could come from a dopant clustering or an incomplete solubilisation of the doping oxide within the glass structure.

The ^{31}P-DQ experiment was performed using BABA (back to back) DQ excitation and reconversion sequence. The ^{31}P-DQ experiment is carried out with rf field of 50 kHz for ^{31}P and relaxation delay of 30s. Eighty T_1 increments have been measured with 208 accumulations per slice. For both doping element X= ^{11}B and ^{27}Al, the experiments have been performed with 256, 512 and 1024 accumulations respectively for 1, 2 and 4 mol% of X_2O_3 respectively. When X= Al, a rd of 2 s and a rf field of 12.5 kHz was used with recoupling power of 7 kHz for 0.3 ms. Similarly, for X= B, a rf of 15 kHz was used with rd of 2s. The recoupling power and time used for the experiment were 3 kHz and 0.9 ms respectively.

References

Andrew, E R. *Progress Nucl. Mag Reson. Spectros.* 8 (1971): 1.

Andrew, E R. *Int. Rev. Phys. Chem.* 1 (1981): 195.

Brow, R K. *J. Am. Ceram. Soc.* 76 (4) (1993): 913-18.

Brow, R K, D R Tallant, S T Myers, and C C Phifer. *J.Non-Cryst. Solids.* 191 (1995): 45-55.

Brow, R K., R J Kirkpatrick and G L Turner. *J. Am. Ceram. Soc.* 73 (8) (1990): 2293-2300.

Caravatti, P, G Bodenhausen and R Ernst. *Chem.Phys.Lett.* 89 (1982): 363.

Czjzek, G, J Fink, F Gotz, H Schmidt, J M D Coey, J P Rebouillat, and A Lienard. *Rev. B.*23 (1981): 2513-2530.

Donald, I W. *J.Non-Cryst. Solids* 352 (2006): 2993-3001.

Dupree, R. *Nature,* 328 (1987): 416-417.

Gullion, T and J Schaefer. *J. Magn. Reson.* 81 (1989): 196.

Hartmann, S R and E L Hahn. *Phys. Rev.* 128 (1962): 2042.

Lesage, A, D Sakellariou, S Steuernagel and L Emsley. *J. Am. Chem. Soc.* 120 (1998): 13194.

Lu,X, J Trebosc, O Lafon and J P Amoureux. *Cryst. Eng. Comm.* DOI:10.1039/03ce40557e: 1-13.

Mackenzie, K J D and M E Smith. *Multinuclear Solid-State NMR of Inorganic Materials 6 Pergamon Elsevier Science, Materials Series,* 2002: 7-61.

Massiot, D, F Fayon, M Capron, I. King et. al. *Magn. Reson. Chem* 40 (1) (2002): 70-76.

Morris, G and R Freeman. *J. Am. Chem. Soc.* 101 (1979): 760.

Raguenet, B, G Tricot, G Silly, G Ribes, and A Pradel. *J. Mater. Chem.* 21 (2011): 17693.

Smith, K A, R J Kirkpatrick, E Oldfield, and D M Henderson. *Am. Mineral.* 68 (1983): 1206-1215.

Trebosc, J, B Hu, J P Amoureux, and Z Gan. *J. Magn. Reson.* 186 (2007): 220-227.

Varshneya, A K, "*Fundamentals of Inorganic Glasses"* (Academic Press, New York), 1994.

Wang, Q, B Hu, O Lafon, J Trebosc, F Deng, and J P Amoureux. *J. Magn. Reson.* 200 (2009): 251-260.

Witter, R, P Hartmann, J Vogel, and C Jager. *Solid State Nucl. Mag. Reson.* 13 (1998): 189-200.

Wullen, L V, G Tricot, and S Wegner. *Solid State Nucl. Mag. Reson.* 32 (2007): 44-52.

Chapter C

Investigation of the zinc sodium pyrophosphate glasses: effect of the Zn/Na ratio on the properties, stability and network structure.

As previously mentioned, the zinc alkali pyrophosphate composition line has been identified as a promising system for the development of low-T_g and stable phosphate glasses. In this part, we will first investigate the effect of Zn/Na substitution on the glass preparation and the macroscopic properties (density, molar volume, T_g, K_A, chemical durability). Then, the glass structure will be analyzed by Raman and ^{31}P NMR spectroscopies. The results will allow (i) determining the optimum formulations presenting a good compromise between low T_g and thermal/chemical stabilities and (ii) investigating the effect of sodium insertion on the structure. New insight onto the extent of disorder in the structure will be provided by 2D ^{31}P correlation NMR.

I. Preparation of the (66- *x*)ZnO- *x*Na_2O- 33.4P_2O_5 composition line

The (66- *x*)ZnO- *x*Na_2O- 33.4P_2O_5 was chosen as a simple and representative system allowing for the preparation of low-T_g and stable phosphate glasses. All the glasses exhibit an O/P ratio of 3.5 that should produce a structure dominated by dimeric $P_2O_7^{4-}$ structural units (Wazer, 1958). Indeed, this P_2O_5 content was found to be the optimum amount for the stability, since higher P_2O_5 contents produce structures with Q^2 and/or Q^3 units that are sensitive to water attack and lower P_2O_5 contents lead to glasses containing Q^0 that can hardly produce a disordered network alone. Keeping this fact in mind, the concentration of P_2O_5 was kept constant (33.4 mol%) in all the formulations, while ZnO has been progressively substituted by Na_2O (*Tab.3.1*).

All the glasses were prepared by the melt-quenching technique. Clear melts were obtained after the batches were treated at 900°C-1150°C for 15-20 minutes, suggesting that all of the zinc and sodium cations were solubilized homogeneously into the melt. It is noteworthy that the weight loss measurements are ≤ 2% for all the preparations, indicating that no significant volatility of P_2O_5 occurred during the glass preparation. For simplicity, a glass will thus be identified by its 'as-batched' composition in the following.

The formulations with $6.7 \leq x \leq 40$ were poured onto a brass plate at room temperature to produce clear and transparent glasses. Melts containing only ZnO ($x = 0$) as well as melts with high Na_2O contents ($x \geq 46.6$) partially crystallize during the quenching procedure. Therefore, these formulations were re-melted and quenched between two brass plates to increase the quenching rate and prevent the melt from crystallization. This procedure produced clear and transparent glasses for the $x = 0$ (pure zinc pyrophosphate) and $x = 46.6$ compositions. Melts with 53.3 mol% of Na_2O was still affected by crystallization during the quenching procedure, indicating that the maximum amount of Na_2O that can be inserted using our technical procedure was reached.

This conclusion was supported by the X-Ray Diffraction (XRD) analysis reported in *Fig. 3.1*. XRD was used to assess for the amorphous nature of the prepared sample. The characteristic

'amorphous hump' can be observed for the glasses with $0 \leq x \leq 46.6$, confirming thus their amorphous character previously deduced from their transparency. The XRD analysis also confirms that the $x = 53.3$ sample contains crystalline phase(s) after the quenching stage. The phase identification indicates that the sample contains sodium pyrophosphate crystalline compound $Na_4P_2O_7$.

This result shows that the limitation for the glass preparation in this system is actually related to the quenching rate and is not due to a limited sodium oxide solubilization within the phosphate melt. Sodium ions enter into the melt and combine with phosphorus but very high amount of sodium lead to the crystallization, probably due to the formation of pure sodium pyrophosphate units that cannot produce disordered structure. The similar precipitation of sodium pyrophosphate phase has been noticed in the binary sodium phosphate system with high amount of sodium (Weyl 1964). Ultra-fast quenching methods, like the twin roller technique (Varma 1987) could be used in order to increase the quenching rate (up to 10^6 $K.s^{-1}$), avoid crystallization and probably extent the composition line up to $x > 53.3$ mol%.

Tab. 3.1 Glass compositions in mol%, melting temperature and weight loss% of glasses prepared.

Sample	ZnO/mol%	Na_2O/mol%	P_2O_5/mol%	Melting/^oC	Wt. loss%	Remarks
$x = 0$	66.6	0	33.4	1150	2.0	Clear glass
$x = 6.7$	59.9	6.7	33.4	1000	1.6	Clear glass
$x = 13.3$	53.3	13.3	33.4	1000	0.76	Clear glass
$x = 20.0$	46.6	20.0	33.4	1000	1.3	Clear glass
$x = 26.6$	40.0	26.6	33.4	1000	1.4	Clear glass
$x = 33.3$	33.3	33.3	33.4	900	1.8	Clear glass
$x = 40.0$	26.6	40.0	33.4	900	1.7	Clear glass
$x = 46.6$	20	46.6	33.4	900	1.4	Clear glass
$x = 53.3$	13.3	53.3	33.4	900	1.9	Crystallized

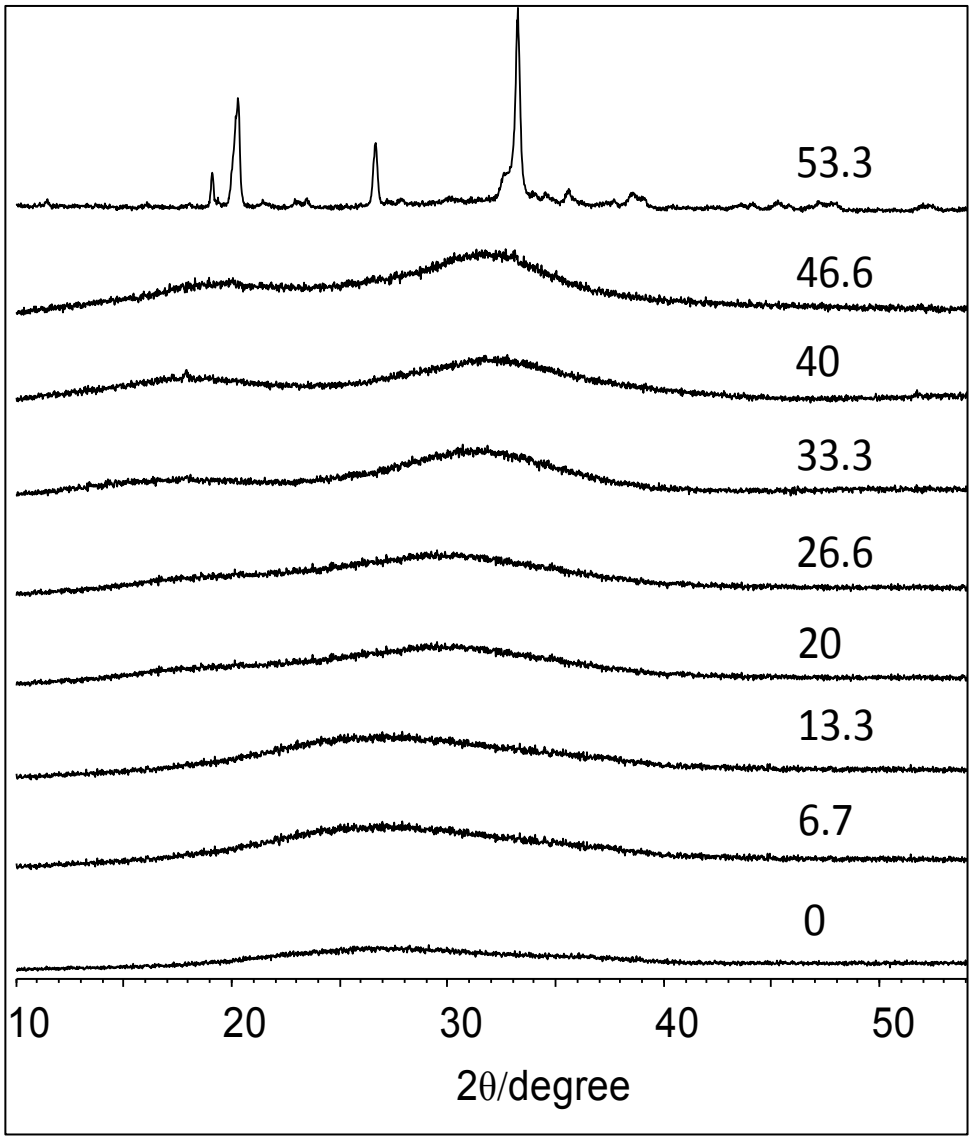

Fig. 3.1 XRD patterns of as quenched (66.6- x) ZnO- xNa_2O- 33.4P_2O_5 glasses where $0 \leq x \leq 53.3$.

Clear and transparent glasses were thus prepared in the (66-*x*)ZnO- *x*Na_2O- 33.4P_2O_5 composition line up to x = 46.6. The prepared compositions are reported in *Fig. 3.2* with filled and empty circles representing amorphous and partially crystalline formulations.

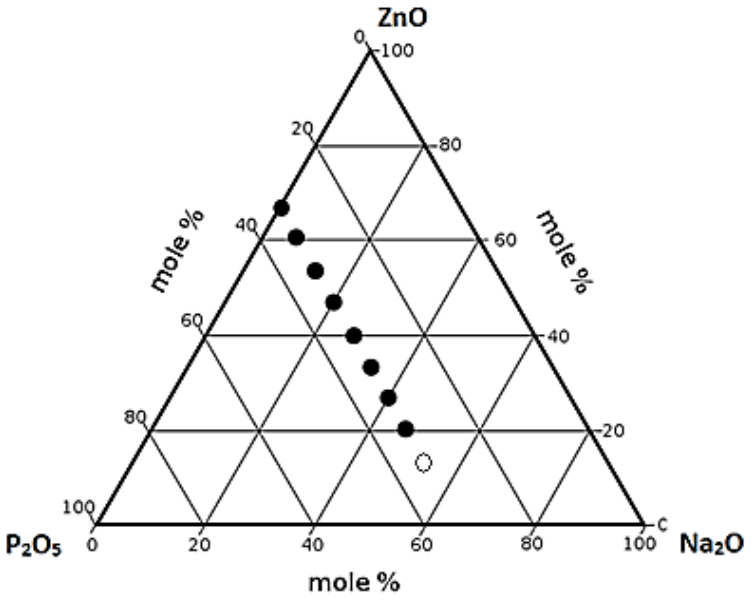

Fig. 3.2 Ternary Plot of ZnO-M_2O-P_2O_5 glasses prepared along the pyrophosphate line (% P_2O_5=33.4). Filled and empty circles represent amorphous and crystalline samples respectively.

II. Macroscopic properties of the (66.6-*x*)ZnO- *x*Na_2O- 33.4P_2O_5 system with $0 \leq x \leq 46.6$

In this section, the macroscopic properties of the (66.6-*x*)ZnO- *x*Na_2O- 33.4P_2O_5 system with $0 \leq x \leq 46.6$ have been measured in order to observe how the Zn/Na substitution improves or decreases the material properties and stabilities. From the results, compositions presenting a good compromise between low-T_g and stability will be derived and be used for the doping investigation described in chapter D.

II.1. Density and Molar volume

The densities and molar volume of the glasses are reported in *Tab. 3.2* and sketched versus the *x* content of the glasses in *Fig. 3.3*.

Density decreases when the Na_2O content increases in the formulations (*Fig. 3.3*). The density exhibits a linear and significant evolution since the values decreases from 3.498 $g.cm^{-3}$ (close to 3.5 $g.cm^{-3}$ as reported by Brow for identical composition (Brow 1995)) to 2.788 $g.cm^{-3}$ for the glass containing 46.6 mol% of Na_2O. Similar evolution of the density was observed upon Zn/alkali substitution in different phosphate based glass compositions (Montagne 1998 and Koudelka 2007b).

Tab. 3.2 Density and molar volume of the glass samples with different concentration of Na_2O.

.

Mol. % of Na_2O	ρ($g.cm^{-3}$) ±0.005	M_v ($cm^3.mol^{-1}$) ±0.1
x = 0	3.498	29.056
x = 6.7	3.385	29.642
x = 13.3	3.315	29.882
x = 20.0	3.217	30.388
x = 26.6	3.078	31.447
x = 33.3	3.005	31.673
x = 40.0	2.891	32.473
x = 46.6	2.788	33.217

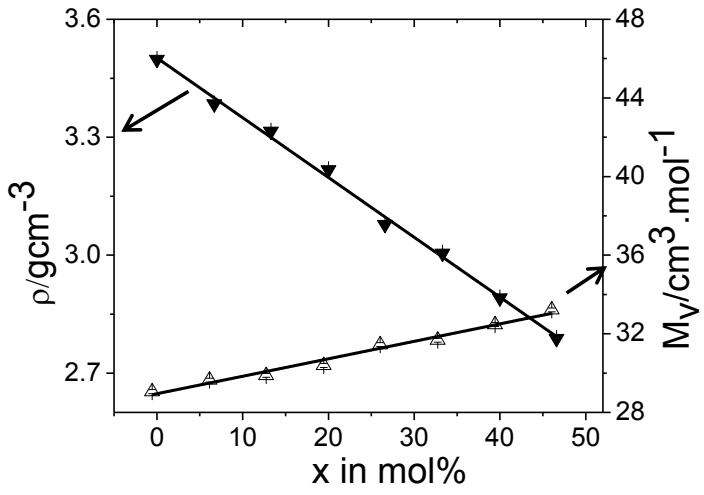

Fig. 3.3 The evolution of density (filled down triangle) and molar volume (up triangle) of the glass samples. (Error bars are smaller than the symbols used).

The substitution of ZnO by Na_2O means that two Na^+ ions compensate the charge of one Zn^{2+} ion. Globally, a zinc ion (M=65.83 u) is replaced by two Na ions (2*M= 2*22.98= 45.98 u) leading to a global decrease of the molecular weight of materials. At the same time, the global volume is also impacted by the substitution. Considering the covalent radius of Zn^{2+} (0.125 nm) and the ionic radius of Na^+ (0.10 nm), it appears acceptable to assume that the volume required to contain two Na^+ ions (that will compensate two $P\text{-}O^-$ bonds) is larger than the volume occupied by a single Zn^{2+} cation (required to compensate two $P\text{-}O^-$ bonds). Higher ionic character and higher polarity of Na-O bonds in comparison to the Zn-O bond could also contribute to this volume extension. The increase in the volume and the decreases in the global weight are perfectly in line with the observed decrease of the material density

This tendency is also reflected in the observed increase of the molar volume of these glasses. This increase has to be considered as a modest one (V_M is only increased by 4.16 cm^3/mol i.e, 15% between the x = 0 and x = 46.6 samples) compared to those in the literatures: 13.5 cm^3 $NaPO_3$-ZnO system (Montagne 1998), 20 cm^3/mol in $Ca(PO_3)_2$-B_2O_3 (Youssef 2000), 15 cm^3/mol in K_2O-ZnO-B_2O_3-P_2O_5 system (Koudelka 2007) and 15 cm^3/mol in P_2O_5-Fe_2O_3-FeO-Na_2O system (Bingham 2009), which showed the relevance of increase in molar volume to the significant evolution of the glass properties. Nevertheless, the modest increase in V_M in our system still indicates a larger free space in the structure of the glasses containing high amount of sodium oxide, the structure becomes more open due to the presence of two Na^+ ions in place of one Zn^{2+} ion.

II.2. Resistance against water attack

As described in chapter B, we have decided to use a quick glass dissolution (weight loss measurement on given granulometry powder in distilled water at 90°C for 24 h) test in order to perform a rapid and efficient screening of all the glass compositions. The chemical durability results of the samples are reported in *Tab. 3.3* and sketched in *Fig. 3.4*.

The weight loss increases significantly with the increase in proportion of sodium oxide, indicate that the Zn/Na substitution strongly alters the chemical durability. When the weight loss

of the pure zinc pyrophosphate can be considered as very weak (0.25 %), insertion of 46.6 mol% of Na_2O in the formulation leads to an almost complete dissolution characterized by weight loss value of 84.16 ±1.5%. This decrease in chemical durability with the increasing Na_2O content is a classical feature and is usually associated to a decrease in bonding forces inside the glass network. The covalent Zn-O(-P) bonds are replaced by more ionic Na^+ $^-$O(-P) linkages leading to a network weakening. The ionic bonds are more efficiently attacked by water that induces quicker bond breaking and solubilisation of the glasses.

Tab. 3.3 Dissolution test results after the samples were treated at 90 ^{0}C for 24 hours

Samples	Chemical durability (Wt.loss %)
$x = 0$	0.25 ± 0.01
$x = 6.7$	1.5 ± 0.1
$x = 13.3$	4.45 ± 1.5
$x = 20.0$	7.07 ± 1.5
$x = 26.6$	25.2 ± 3.5
$x = 33.3$	28.0 ± 3.5
$x = 40.0$	63.0 ± 5.0
$x = 46.6$	84.0 ± 5.0

However, the weight losses evolution exhibited by our system is far from being linear. Two domains can be distinguished according to the actual impact of Na_2O on this property:

(i) for low Na_2O contents ($x \leq 20$), the chemical durability is only marginally affected by the increase in Na_2O and the weigh losses slowly increase with the Na_2O contents, but never exceed 8 %. This domain is denoted as domain (I) in *Fig. 3.4.*

(ii) for Na_2O contents higher than 20%, the weight losses are strongly affected by the addition of sodium oxide in the formulation. Each addition leads to a significant decrease of the resistance against water attack. This domain is denoted as domain (II) in *Fig. 3.4.*

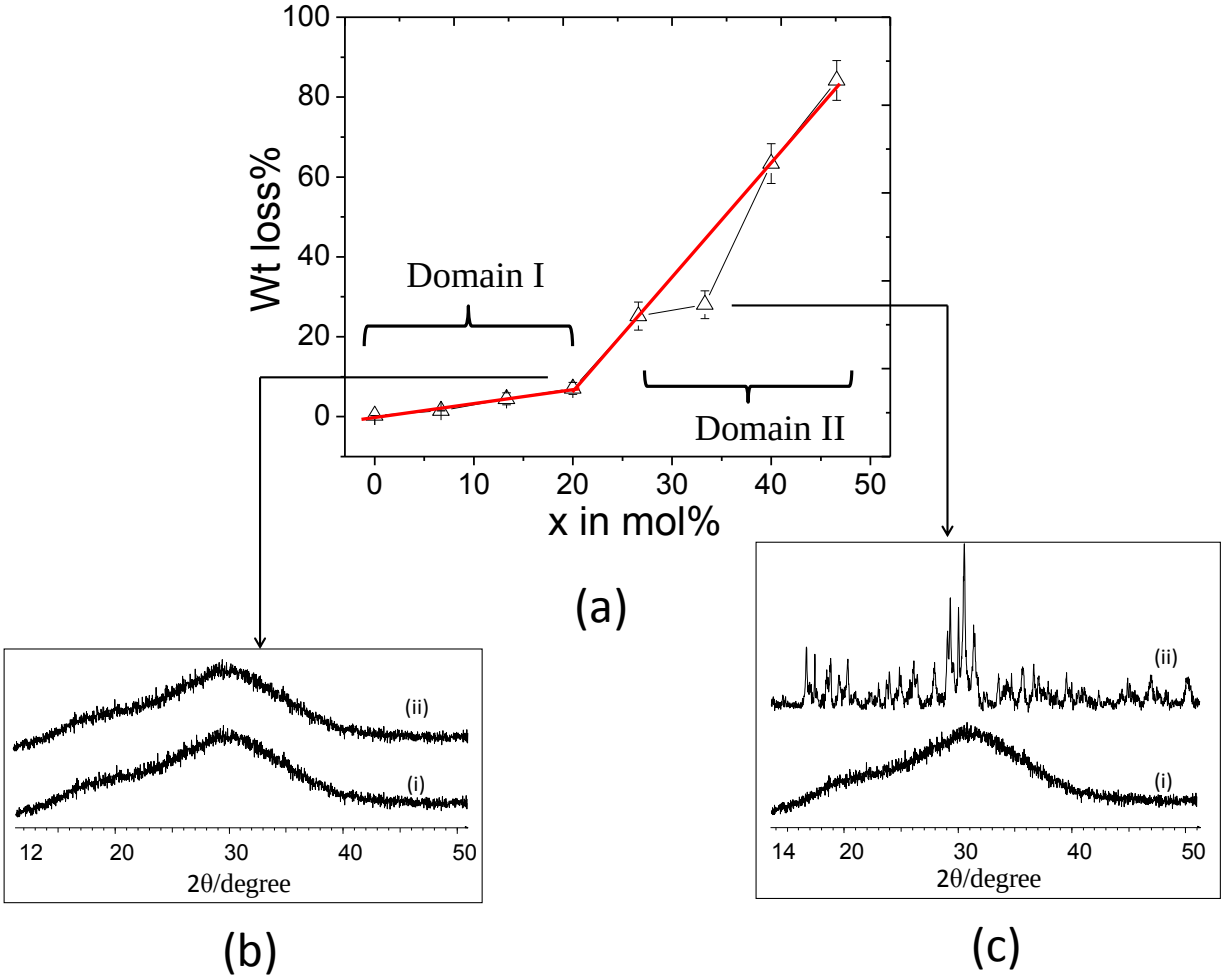

Fig. 3.4 Evolution of chemical durability of the glass samples (on the top) versus x in mol% (a). Inserts show X-ray diffractogram before (i) and after (ii) dissolution test, x = 20 (b) and x = 33.3(c).

The residual glass powder was analyzed after the tests in order to understand the origin of this two-domains evolution. XRD analyses, representative of each domain, have been performed on dried samples and are reported in *Fig. 3.4*. Clear difference can be observed between the residual powders of the two domains. At low Na_2O content, the powders still present an amorphous character, indicating that the material is still a glass. At high Na_2O content, the residual powders contain crystalline compounds, as indicated by the diffraction peaks observed on the XRD analysis. Even if the phase was not identified, this result indicates a completely different solubilisation mechanism for each domain. If a standard glass solubilisation, involving

bond breaking, can be assumed in the case of domain (I), the mechanism leading to domain (II) involved a much more deep change in the glass structure involving glass crystallization. It is noteworthy that similar two domains evolution of the chemical durability has also been observed in K_2O-ZnO-B_2O_3-P_2O_5 system (Koudelka 2007b). They have also reported that the domain with $\leq$ 20 mol% of K_2O showed relatively high chemical durability and the domain with > 20 mol% of K_2O presents steep decrease in resistance against water attack.

II.3. Thermal Characteristics

The glasses were investigated by thermal analysis to derive the T_g, T_x and T_c characteristics. All these parameters are reported in *Tab. 3.4* and the DSC analysis are reported in *Fig. 3.5*.

The glass transition temperature evolution is reported in *Fig. 3.6*. A continuous decrease of T_g is observed all along the Zn/Na substitution. The T_g of the binary zinc pyrophosphate (x = 0) is measured at 433 °C, in a perfect agreement with the values (432 °C) proposed by Brow (Brow 1995). The T_g decreases down to 288°C in case of the higher Na_2O content sample (x = 46.6). It is noteworthy that all the glass compositions, except the pure binary zinc phosphate glass, fulfill the low-T_g condition (T_g < 400°C), suggesting that this system is particularly relevant for our investigation.

The observed continuous decrease of T_g with the increase in sodium oxide content has been reported for many systems when divalent ions are substituted by mono-valent ones (Montagne 1998, Koudelka 2007a and Lakshmikantha 2012) and is mainly associated with the global weakening of bonding forces inside the glass structure (the stronger Zn-O bonds are substituted by weaker Na-O bonds), as previously mentioned.

Tab. 3.4 Thermal Characteristics (T_g, T_x, T_x-T_g and T_c) of the glass samples.

Sample	T_g/°C	T_x/°C	T_c/°C	$K_A = (T_x-T_g)$/°C
x = 0	433	505	532	72
x = 6.7	380	465	479	85
x = 13.3	358	455	475	97
x = 20.0	339	535	550	196
x = 26.6	320	458	490	138
x = 33.3	310	440	461	130
x = 40.0	300	422	445	122
x = 46.6	288	333	351	45

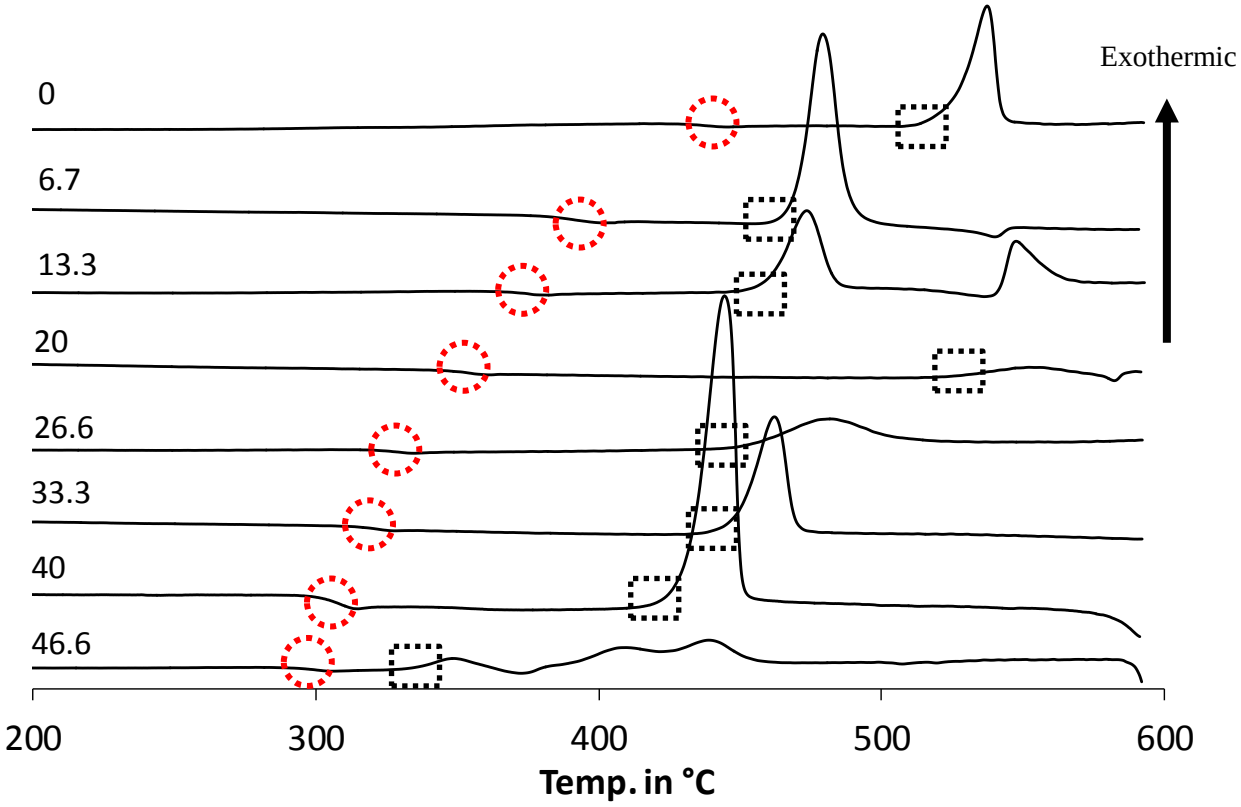

Fig. 3.5 DSC patterns of the glass samples.

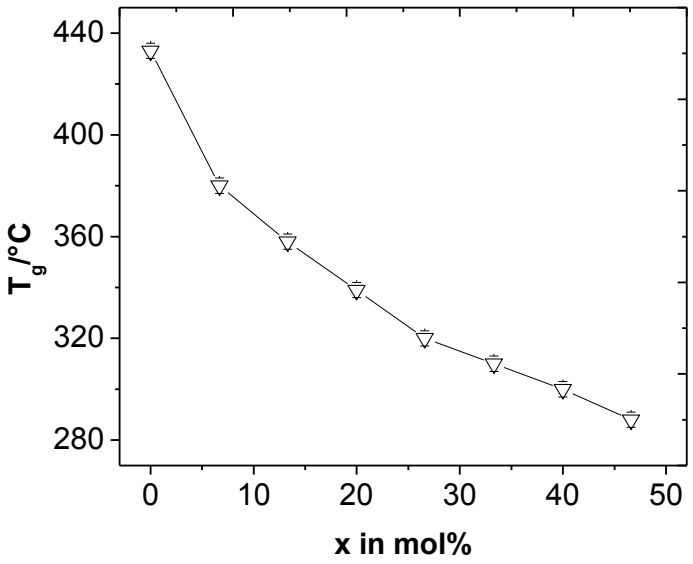

Fig. 3.6 Evolution of T_g vs Na_2O content in the glass samples.

Thermal stability was also derived from the DSC experiments and expresses through the Angell parameter, K_A (Cooper and Angell 1983), introduced in Chapter B. The difference between the onset of crystallization (T_x) and the glass transition temperature (T_g) for each glass was calculated (*Tab 3.4*) and the K_A evolution versus the Na_2O content is sketched in *Fig. 3.7*.

The K_A parameter experiences a non-linear evolution that can be separated in two domains: K_A first increases up to x = 20 and then decreases for higher Na_2O content. Nevertheless, it appears very complicated to explain the two domains evolution of K_A since this parameter is resulted from the monotonic decrease of T_g (*Fig. 3.6*) and systematic variations of T_x. The only information that can be related to the two-domains regime comes from the XRD analysis performed on the glasses annealed 3 h at T_c. The nature of the crystalline phase identified by XRD has been reported in *Tab. 3.5* for each composition. The samples with high ZnO content ($0 \leq x \leq 13.3$) contain pure zinc pyrophosphate compounds (the gamma and alpha forms, as major and minor components, respectively) in a good agreement with the results from Petrova (Petrova 1995). The samples containing high amounts of Na_2O ($26.6 \leq x \leq 46.6$) contain the sodium zinc pyrophosphate $Na_2ZnP_2O_7$ compounds (Belharouak 2000). The x =20 sample lies in the boundary between these two regions and is the first composition (the lowest Na_2O content composition) in which pure zinc pyrophosphate has been found as minor phase and

mixed zinc sodium pyrophosphate as a major phase. This turn in the crystallization process could be at the origin of the two-domain evolution observed in our system. It is noteworthy that no other mixed phases, likely to be formed during crystallization such as $Na_2Zn_5(PO_4)_3$ (Ji 2007), $NaZnPO_4$ (Elammani 1987), $NaZnP_3O_9$ (Abrahams 2000) have been identified in our analysis.

The eutectic point for $Zn_2P_2O_7$ -$Na_4P_2O_7$ system is obtained at 24 wt% of $Na_4P_2O_7$ (Majling 1974) (*Fig 3.8)*. It is noteworthy that the *x* = 20 formulation contains 27 wt% of $Na_4P_2O_7$ which is very close to the eutectic point. Thus the best glass forming ability presumably occurred at *x* = 20 since it is closer to the eutectic composition compared to other formulations in the composition line. Thus the high thermal stability of this glass may be as a result of best mixing of the components.

The main conclusion derived from the K_A evolution is that the *x* =20 sample exhibits the highest K_A values (196°C) of the composition line and presents thus the highest thermal stability. This result is also strongly supported by the crystallization enthalpy observed in the DSC curves. Indeed, *Fig. 3.5* indicates a very weak crystallization enthalpy for the *x* = 20 sample compared to the other compositions, the largest enthalpy being observed for the *x* =40 sample. The superiority in term of thermal stability of the *x* =20 sample over the other samples of the composition line has thus been supported by two independent parameters.

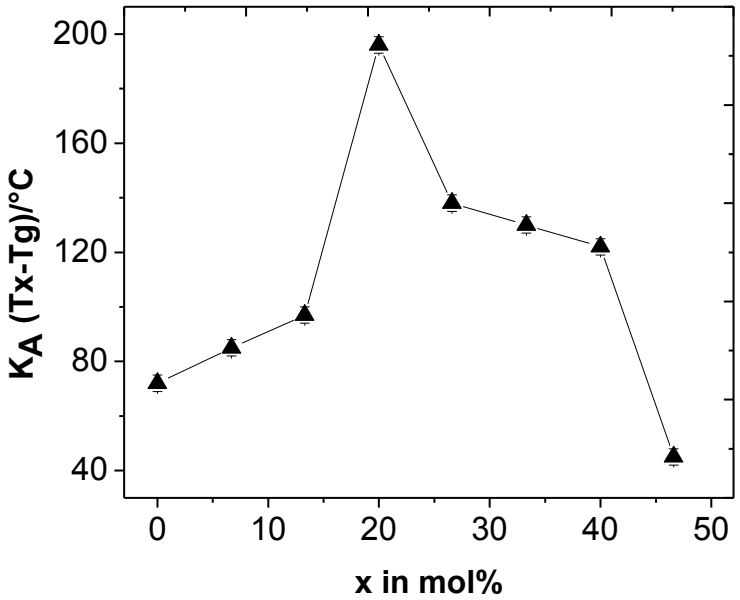

Fig. 3.7 Angell parameter K_A vs Na_2O content in the glass.

Tab. 3.5 Crystalline polymorphs observed from X-ray diffraction analyses.

Sample	Crystalline phase	
	Major phase	Minor
$x = 0$	γ-$Zn_2P_2O_7$	α-$Zn_2P_2O_7$
$x = 6.7$	γ-$Zn_2P_2O_7$	α-$Zn_2P_2O_7$
$x = 13.3$	$Na_2ZnP_2O_7$- γ-$Zn_2P_2O_7$	$Zn_2P_2O_7$
$x = 20.0$	$Na_2ZnP_2O_7$	$Zn_2P_2O_7$
$x = 26.6$	$Na_2ZnP_2O_7$	
$x = 33.3$	$Na_2ZnP_2O_7$	
$x = 40.0$	$Na_2ZnP_2O_7$	
$x = 46.6$	$Na_2ZnP_2O_7$	

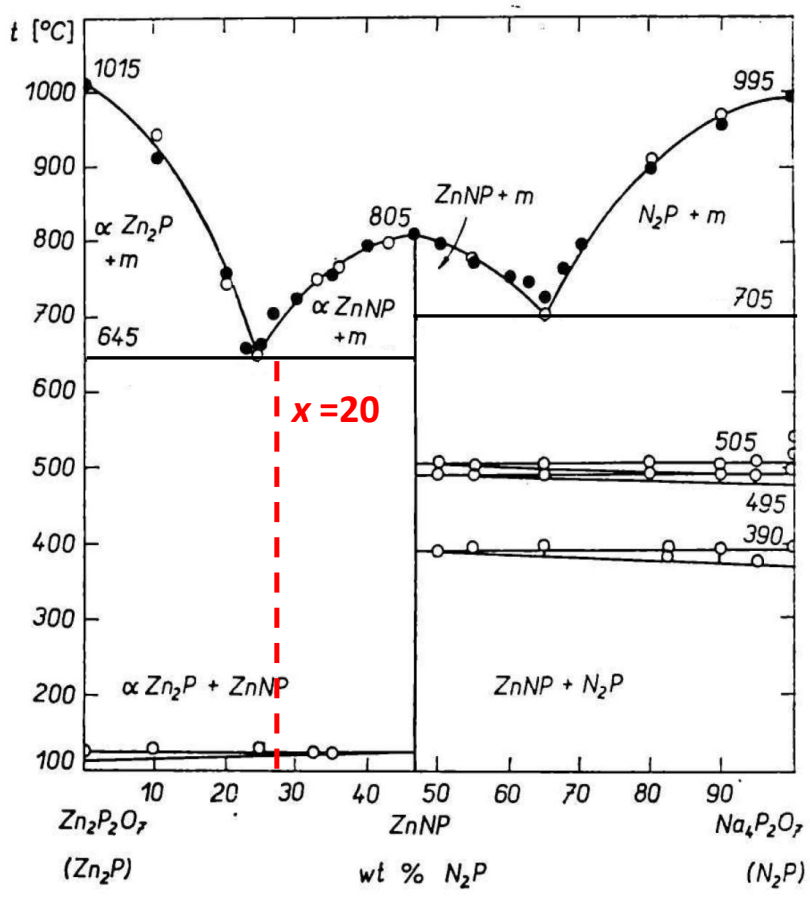

Fig. 3.8 Phase diagram of the system $Zn_2P_2O_7$-$Na_4P_2O_7$ system.

II.4. Discussion

The macroscopic properties have been determined in the (66- *x*)ZnO- *x*Na_2O- 33.4P_2O_5 composition line from pure zinc pyrophosphate (*x* = 0) to sample containing 46.6 mol% of sodium oxide.

From the results, it was concluded that the ZnO/Na_2O substitution induces a density and T_g decreases, due to the replacement of a single Zn^{2+} ion by two Na^+ ions near the vicinity of phosphate units and to a global weakening of the glass network resulting from the replacement of strong Zn-O(-P) bond by weak Na^+-O(-P) linkage, respectively. Moderate increases of the molar volume indicate that the free space is extended in case of high Na_2O amount compositions.

In addition to these classical features observed in phosphate systems where di- or tri-valent ion are replaced by mono-valent ones, unreported information about the chemical and thermal stabilities of the system were collected. We have shown that both stabilities were not affected in a linear way by the Zn/Na substitution but both adopts a two-domains regime. Surprisingly, both two-domain regimes share the same boundary composition which is the *x* = 20 sample. It appears that different dissolution and crystallization mechanisms occur for Na_2O contents lower and higher than 20 mol%. As reported in *Fig. 3.9*, when both chemical and thermal stabilities were compared, the *x* =20 sample is the composition presenting the best compromise between the thermal and the chemical stabilities. The associated T_g (339°C) is far below the boundary related to our topic, which was setup to 400°C, making of that particular composition the best low-T_g and stable formulation of the zinc sodium pyrophosphate composition line.

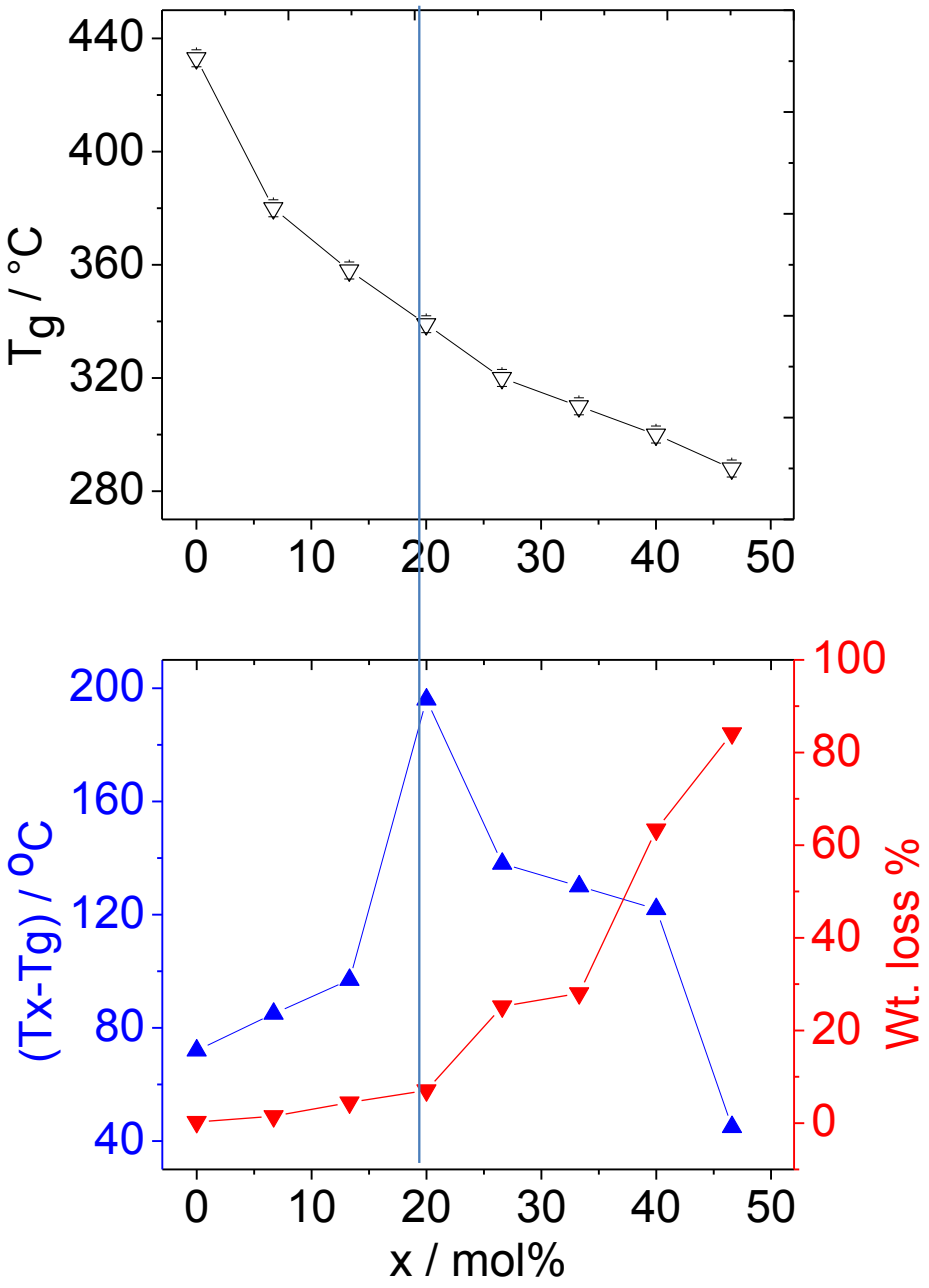

Fig 3.9 Evolution of T_g, Angell parameter (up triangles) and chemical durability (down triangles) of (66.6- x) ZnO- xNa_2O- 33.4P_2O_5 glasses.

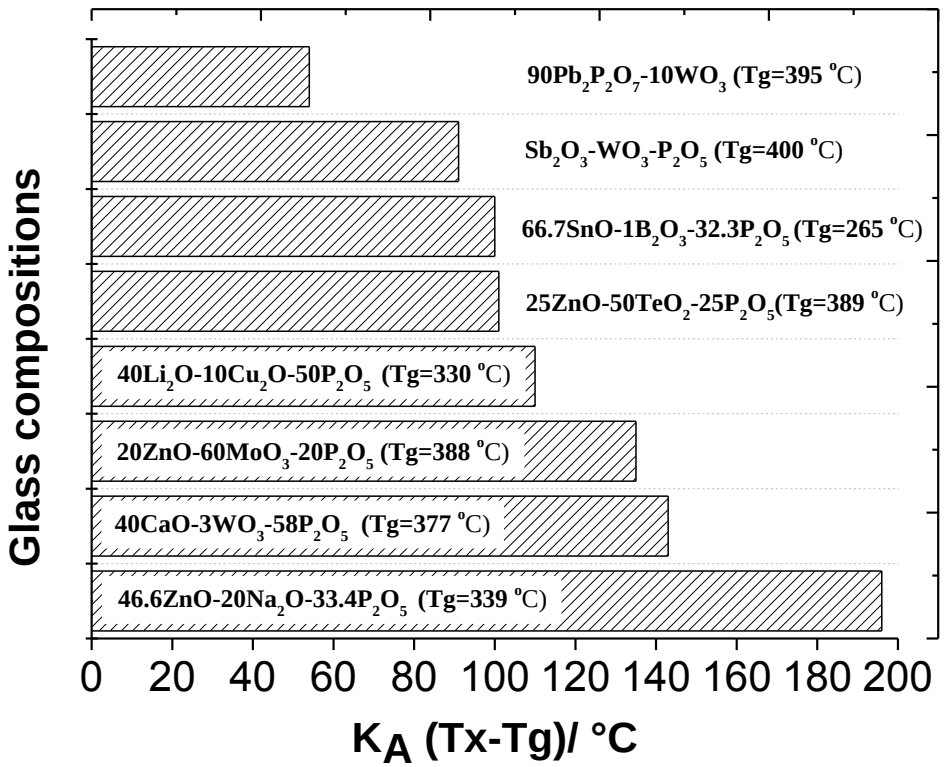

Fig. 3.10 Angell parameter of different phosphate-based compositions.

The characteristic of the x = 20 sample were then compared to other low-T_g phosphate systems described in the literature to confirm the relevancy of that system. Comparison of the chemical durability was complicated to establish due to the very different tests used in the literature and will thus not be discussed here. Angell parameter is an easier value to determine since it can be derived from standard DSC curves. Based on the literature we found (Subbalakshmi 2002, Nalin 2007, Lim 2010, Subcik 2010, Mosner 2011, Manzani 2011 and Mugoni 2013) and considering glass systems with T_g below 400°C, it appears that our formulation presents the highest K_A for a phosphate systems. As indicated in *Fig. 3.10*, K_A of other system does not exceed 150°C, whereas our system exhibits a K_A close to 200 °C. This result thus assesses for the relevancy of the zinc sodium phosphate system for the preparation of low-T_g and stable phosphate based glasses.

III. Structural characterization of the phosphate network of the (66.6- *x*) ZnO- *x*Na_2O- 33.4P_2O_5 composition line.

In addition to the evolution of properties, Raman and ^{31}P magic angle spinning solid state nuclear magnetic resonance (MAS-NMR) spectroscopies have been used to examine the impact of the Zn/Na ratio on the short and medium range order structure of the zinc sodium pyrophosphate glasses ($0 \leq x \leq 46.6$).

III.1. Raman spectroscopy

The *Fig. 3.11* shows Raman spectra of the prepared glasses. The Raman spectrum of the binary zinc pyrophosphate glass ($x = 0$) is comparable with those reported by Brow and Takebe (Brow 1995 and Takebe 2006) for similar zinc pyrophosphate composition. Four bands, at 755, 985, 1050 and 1142 cm^{-1} dominate the spectra. According to Stanford and Quinn, the 755 and 1050 cm^{-1} bands can be assigned to symmetric stretching modes of POP bonds and PO_3 unit Q^1 units, the 985 cm^{-1} Raman band is assigned to the symmetric stretching mode of non-bridging oxygen atoms in Q^0 tetrahedra and the 1142 cm^{-1} band is due to P-O stretching mode of Q^1 chain terminator (Stranford 1981, Quinn 1992).

When Zn^{2+} is substituted by Na^+, changes in the positions toward the lower frequency values can be observed for the main vibrational bands, accompanied by a decrease of the 755 and 1050 cm^{-1} bands broadness. The Raman bands at 755, 985, 1050 and 1142 cm^{-1} are shifted to 735, 970, 1038, and 1180 cm^{-1}, respectively with the sodium oxide shifts from 0 to 46.6 mol%.

The main conclusion of the Raman spectra is that the pyrophosphate Q^1 structure is the major structural features of the studied glasses. Also, high intensity band near 755 cm^{-1} confirms the presence of bridging oxygen P-O-P in $P_2O_7^{4-}$ structure. The shift in positions can be explained by the replacement of Zn^{2+} ions with higher field strength (0.44×10^{20} m^{-2}) by lower field strength Na^+ ion (0.19×10^{20} m^{-2}), indicating that both ions are homogeneously distributed around the different phosphate units. Finally, the presence of narrower bands suggests that the

extent of disorder decreases with the Zn/Na substitution. More specific insights onto the structure of the phosphate network will be given by using the selective NMR spectroscopy. It is noteworthy that no information has been derived on the zinc coordination state and its evolution all along the composition line. However, we can assume zinc to be four-fold coordinated since octahedral zinc has only been observed in case of ultra-phosphate compositions (Walter 2004) .

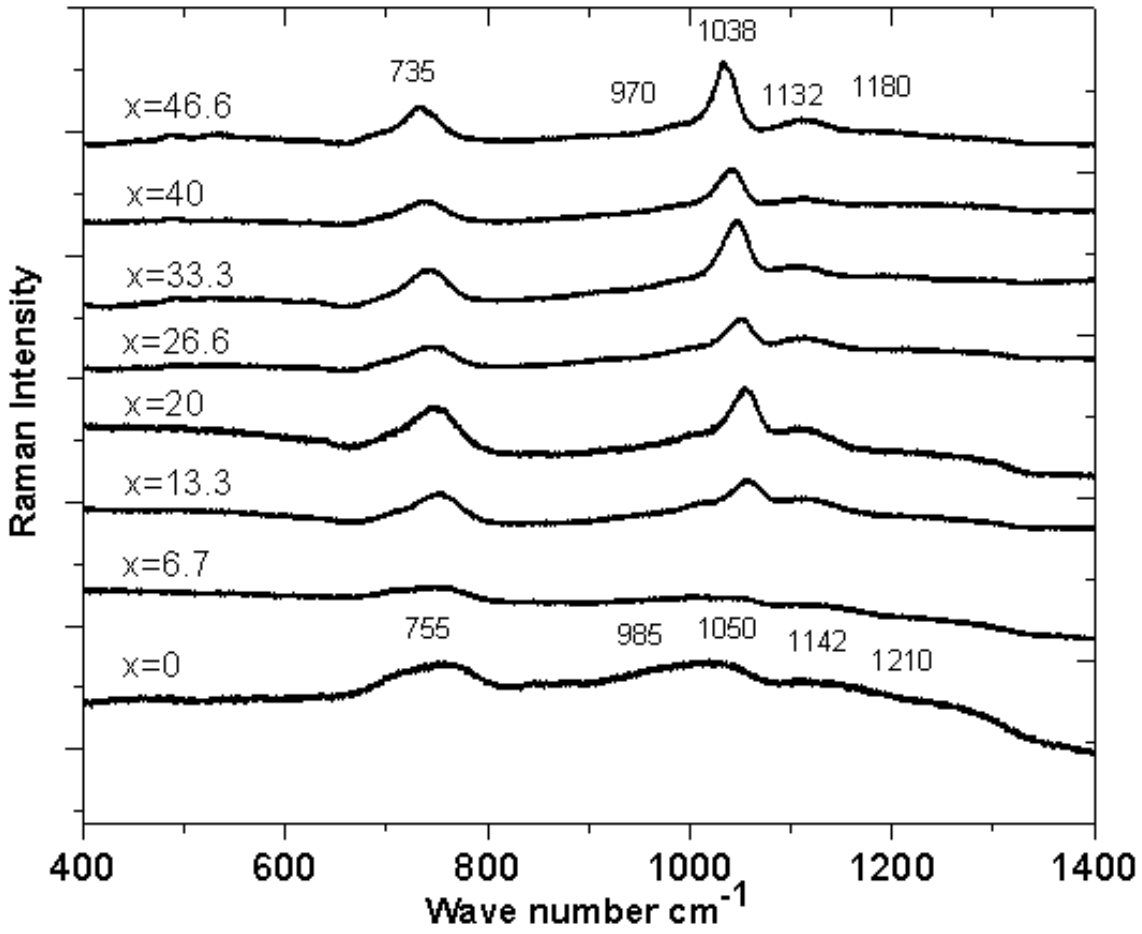

Fig.3.11 Raman spectra of (66.6- x) ZnO- xNa_2O- 33.4P_2O_5 with 46.6 ≤ x ≤ 0.

III.2. ^{31}P solid state NMR

The 1D ^{31}P MAS-NMR experiments performed on the zinc sodium pyrophosphate composition line are reported in *Fig. 3.12*. The spectrum of the pure zinc pyrophosphate (x = 0) appears to be composed by three signals: an intense one centered at -10.6 ppm accompanied by two lower intensity resonances at 3.7, and -28.4 ppm. The three signals have been assigned to Q^1, Q^0 and Q^2 species, respectively, in agreement with previous investigation (Brow 1995). The spectra of glasses with increasing sodium oxide contents also exhibit the above described '1 intense + 2 weak intense' components structure. The chemical shifts of the three signals continuously shift towards higher values and exhibit narrower features when the sodium oxide content increases.

The 1D ^{31}P NMR experiments indicates that the glass structure is essentially composed by Q^1 species as expected from the pyrophosphate composition (O/P=3.5) but also contains significant proportions of Q^0 and Q^2 sites. These Q^0 and Q^2 sites come from the disproportionation of Q^1 sites occurring within the melt as observed in zinc but also in several other binary phosphate systems (Brow 1995). This reaction follows the following equation:

$$2Q^1 \longleftrightarrow Q^2 + Q^0$$

and is characterized by the K_d parameter, defined as $[Q^2].[Q^0] /[Q^1]^2$

The chemical shift evolution, when Na_2O content increases, is explained by the difference in the electrostatic field strength of Na^+ and Zn^{2+} ions (0.19 and 0.44 10^{20} m^{-2}, respectively). As mentioned in chapter B, the chemical shift is sensible to this parameter. The progressive chemical shift evolution indicates that Zn^{2+} and Na^+ are homogenously distributed around the phosphate species, the latter progressively replacing the former.

Finally, the decrease of signal width with the Na_2O content can be analyzed as a global decrease of the disorder within the glass structure. Indeed, the width is usually related to the network bond length and angle distribution and its broadness suggests large distribution ranges. It appears thus that sodium oxide lead to a diminution of the distributions in our system that is perfectly in line with its pure network modifying nature compared to the intermediate zinc element.

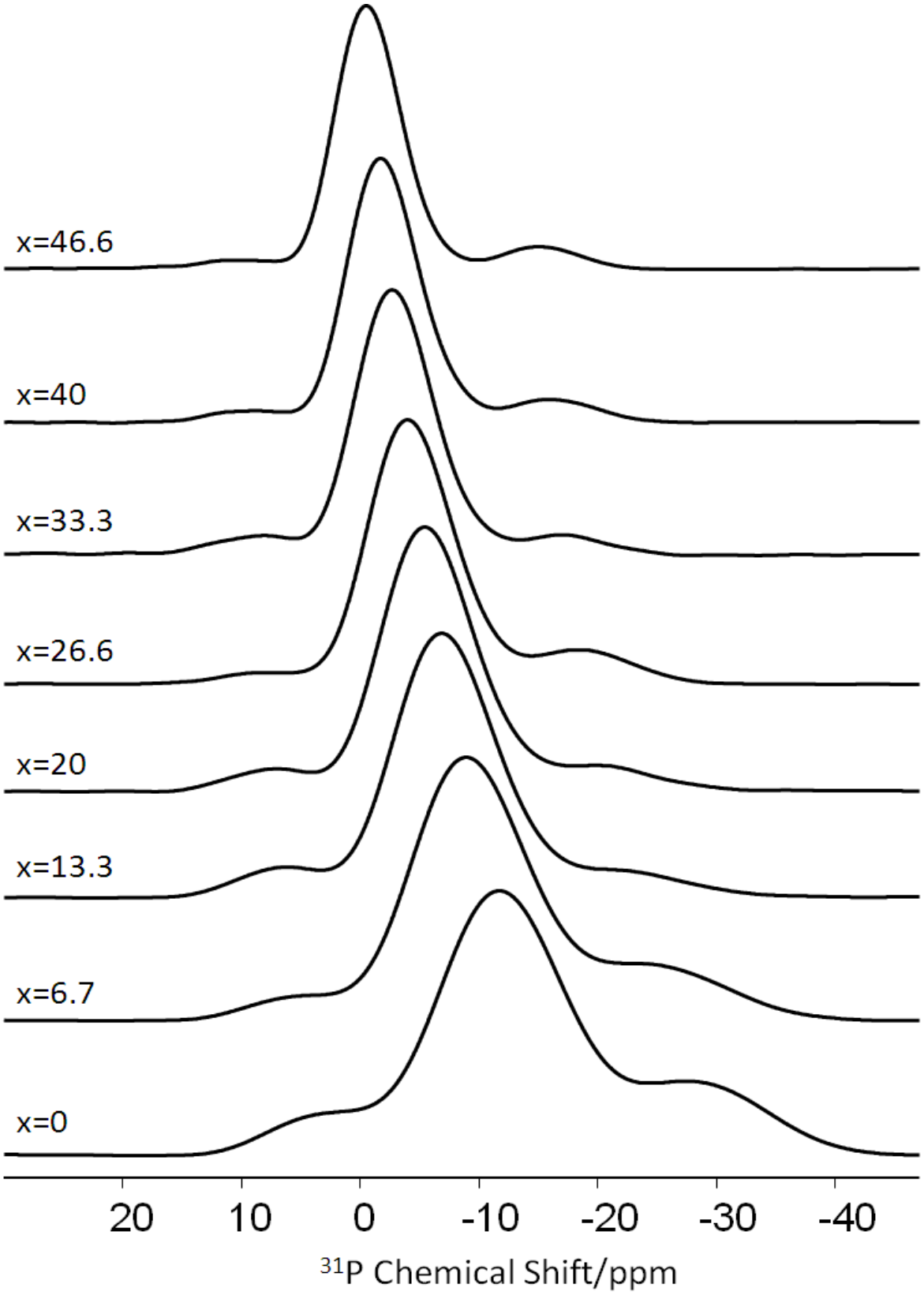

Fig. 3.12 ^{31}P solid state MAS NMR spectra of (66.6- x) ZnO- xNa_2O-33.4 P_2O_5 glasses with $46.6 \leq x \leq 0$.

The local order has thus been efficiently analyzed by 1D NMR. However, understanding the MRO requires additional information about the interaction between the different species. If the structure was supposed to be composed only by dimeric $P_2O_7^{4-}$ structural feature, the presence of Q^2 sites coming from the disproportionation should strongly impacted this 'theoretical structure'. Interaction of Q^2 with Q^1 could give rise to short phosphate chains, constitutes by 3 or more phosphate tetrahedra. If no Q^2/Q^1 interactions occur, the presence of Q^2 will lead to formation of cycles within the structure. The question of the phosphate network topology was addressed by using the 2D correlation ^{31}P DQ-SQ technique that shows spatial proximity (interpret as chemical connectivity in our case) between the different phosphate units. Particular emphasis will be paid to the Q^1/Q^2 interaction (highlighted by off diagonal in the 2D DQ-SQ spectra) since this parameter is the key point controlling the network topology, as previously explained. The 2D DQ-SQ spectra obtained on the x = 0, 20 and 46.6 samples are reported in *Fig. 3.13* (a), (b) and (c) respectively. The 2D spectra are accompanied by the extracted ^{31}P projections (horizontal axis) highlighting the Q^1-Q^2 and Q^1-Q^1 interactions.

The 2D spectra afford valuable information by highlighting the Q^1/Q^2 interactions through the presence of the off-diagonal correlation signals observed in the Q^1-Q^2 extracted slices. If this signal is obvious in the x = 0 and 20 samples, only a low intensity signal has been observed in case of the x = 46.6 sample, probably due to the low amount of the involved species. Another crucial information comes from the diagonal Q^1-Q^1 signal, observed in significant amounts in the three 2D spectra. This signal comes from one Q^1 phosphate connected to another Q^1 and thus forming a $P_2O_7^{4-}$ dimer. This signal is thus the precise signature of the principal structural features of the glass network.

Attentive comparison between the Q^1-Q^2 and Q^1-Q^1 extracted slices shows that the Q^1 species of both interaction schemes exhibit slightly different chemical shifts. The DQ allows thus to distinguish Q^1 involved in dimeric structure and Q^1 involved in phosphate chains containing at least 3 phosphate units. Although the two components were not discernible in the 1D spectra, the DQ experiments allow highlighting the presence of two different Q^1 species that will be defined in the following as $Q^{1,1}$ (a Q^1 connected to another Q^1 and forming a dimer) and $Q^{1,2}$ (a Q^1 connected to a Q^2 site and being involved in a phosphate chain). The extracted slices were used to extract the chemical shift and the width of the $Q^{1,1}$ and $Q^{1,2}$ species and will be used as input

parameter to properly fit the 1D ^{31}P spectra. Analysis of the fit and of the derived relative proportions between the different units (Q^0, Q^2, $Q^{1,1}$ and $Q^{1,2}$) will then be used to discuss in detail the MRO structure of our glasses.

It is noteworthy that the Q^0 species have never been observed in any correlation signals that support their isolated character. Very weak intensity Q^2-Q^2 correlation signals was also observed in the $x = 0$ sample only. Although this information is a very important one, since it suggests the presence of cycles or chains forming by at least 4 phosphate units, the very low intensity signal did not allow us extracting chemical shift and width of these particular species. In the following fits, the Q^2 will thus be considered as a single unit and be simulated with only one component. No direct distinction will be made in the fit between Q^2 involved in $P_3O_{10}^{5-}$ trimer (that does not appear in the Q^2-Q^2 correlation signal) and Q^2 involved in cycle or chains containing at least 4 phosphate units.

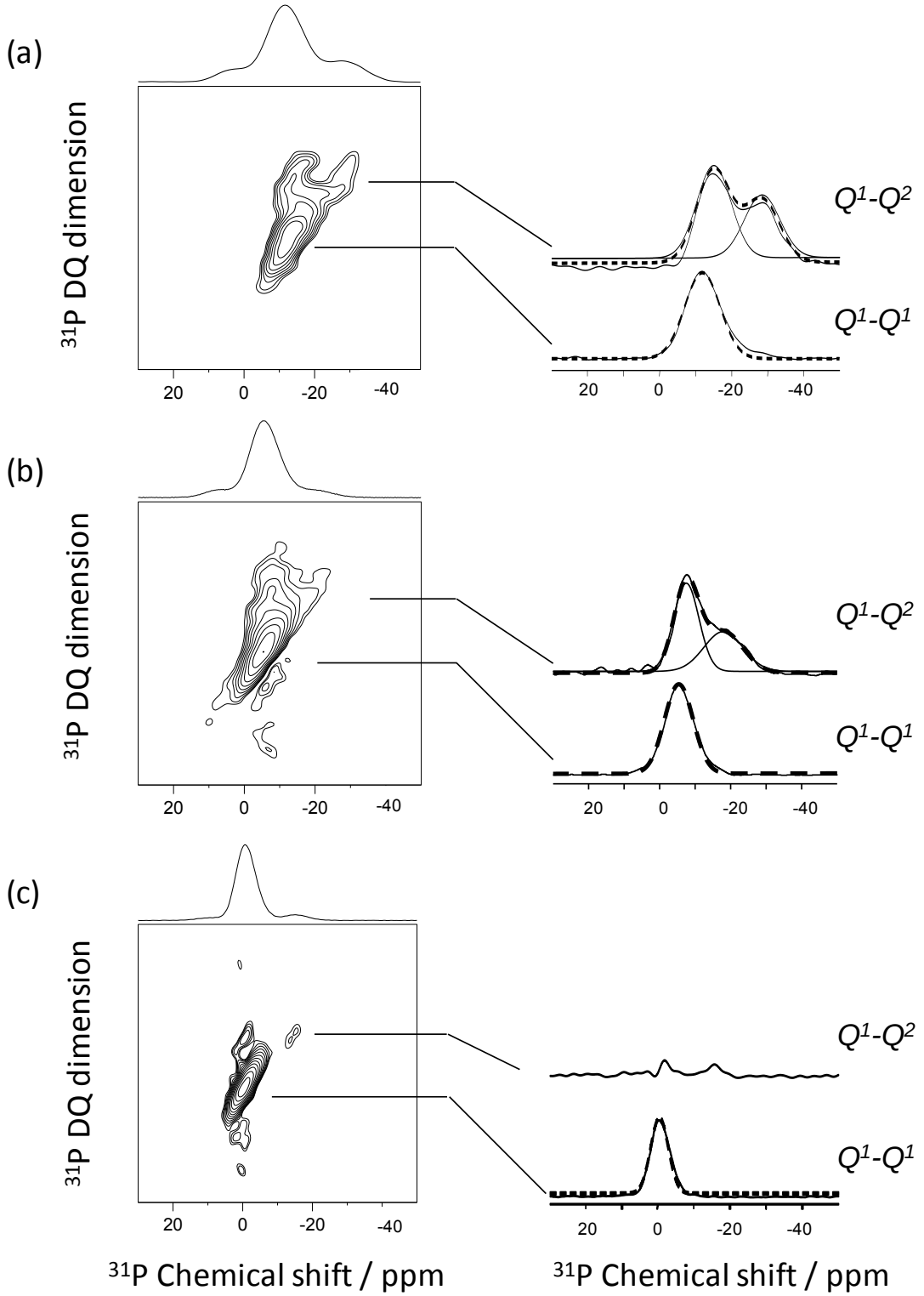

Fig. 3.13 ^{31}P-^{31}P 2D DQ spectra of the glass samples (a) x = 0 (b) x = 20 (c) x = 46.

Tab. 3.6 Chemical shifts, full width at half maximum and relative peak and spinning sideband areas, extracted from the simulation of the spectra of Fig 3.14.(error: ± 5%)

Mol% Na_2O (x)	Q^0ppm FWHM Area	$Q^{1,1}$ppm FWHM Area	$Q^{1,2}$ppm FWHM Area	Q^2 ppm FWHM Area	$Q^{1,2}/Q^2$	K_d
0	3.70	-10.61	-15.18	-28.46	0.907	0.028
	9.66	11.42	11.07	13.56		
	7.04	52.9	19.1	21.05		
6.7	4.90	-8.20	-13.70	-25.0	1.18	0.0172
	9.98	9.64	9.64	13.7		
	6.17	57.51	19.68	16.64		
13.3	6.27	-6.20	-10.39	-21.1	1.48	0.0132
	8.94	8.4	8.87	13.7		
	6.32	60.21	19.98	13.5		
20	7.60	-4.69	-8.5	-19.5	1.8	0.010
	8	7.9	8.3	13		
	6.04	62.45	20.25	11.26		
26.6	8.46	-3.2	-7.42	-18.5	1.853	0.008
	8	6.87	6.75	10.8		
	5.75	64.8	19.13	10.32		
33.3	9.24	-2.22	-6.63	-16.70	1.98	0.006
	7.7	6.5	6.54	10.5		
	5.2	66.8	18.6	9.4		
40	9.72	-1.31	-4.79	-16.19	1.993	0.005
	7.1	6.1	6.94	8.6		
	3.99	68.26	18.5	9.28		
46.6	10.72	-0.23	-2.89	-15.06	1.941	0.004
	7.6	5.9	6.87	7.9		
	3.2	69	18.35	9.45		

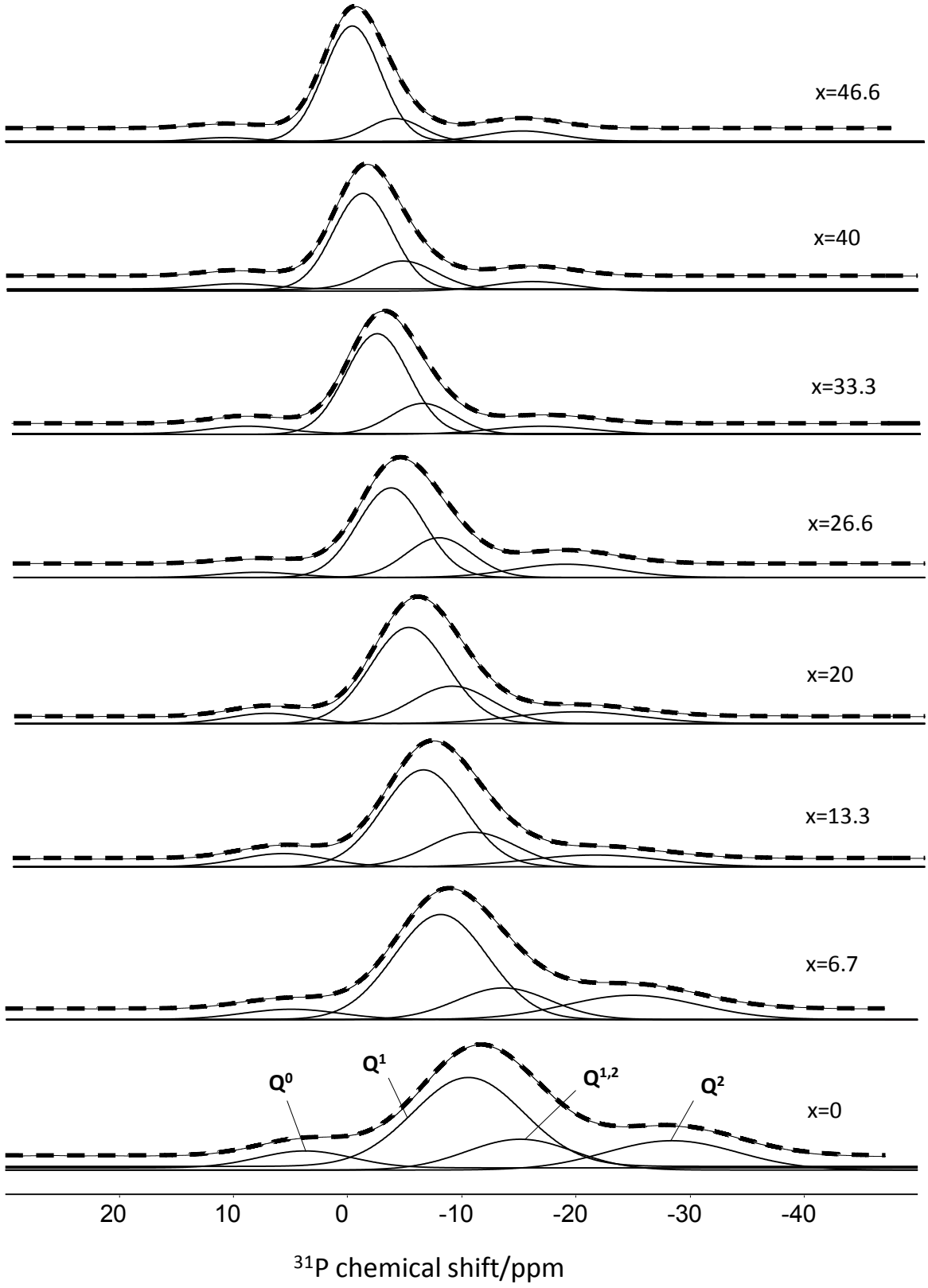

Fig. 3.14 Decomposed ^{31}P MAS spectra for (66- x) ZnO- x Na_2O-33.4 P_2O_5 {0≤ x ≤ 46.6} glasses, showing the Q^n components.

The fits of the ^{31}P spectra are sketched in *Fig. 3.14* and the relative proportions of the different species deduced from the fits including spinning side bands (not shown in the figure) are reported in *Tab. 3.6*. A number of samples were run in duplicate and the estimated uncertainty of the respective site concentrations were within ±4%.

The glass structure and the impact of substitution of Zn^{2+} by Na^{+} on the structure will thus be discussed using the precise Q^n distribution, the $Q^{1,2}/Q^2$ ratio (that can be used to determine the averaged chain length) and the K_d constant.

The Q^n distribution (including Q^0, $Q^{1,1}$, $Q^{1,2}$ and Q^2) versus the composition has been plotted in *Fig. 3.15*.

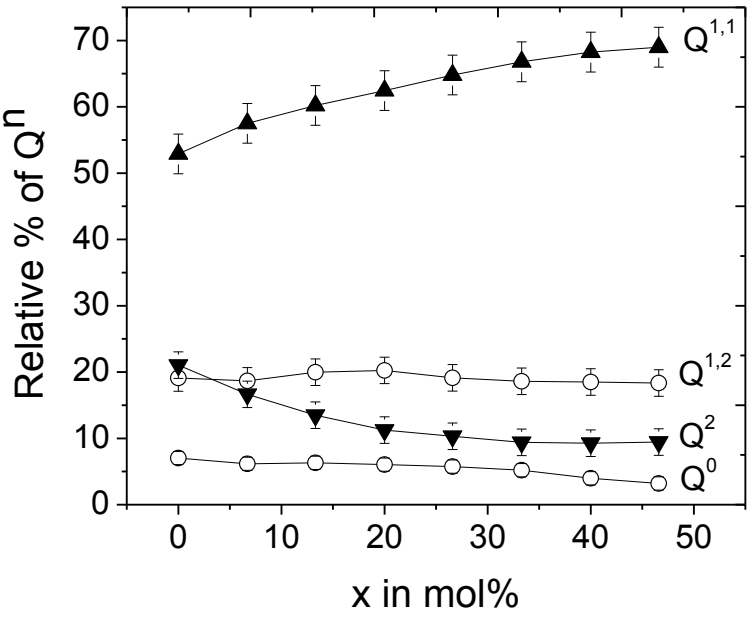

Fig. 3.15 The distribution of the phosphate tetrahedra on (66.6- x) ZnO- x Na_2O-33.4 P_2O_5 glasses determined from the NMR spectra.

The Q^0 species experiences a very weak decrease with a relative proportion shifting from 7 to 3 %. The isolated species is thus present as a minor feature within the glass structure of our system.

The figure show that the principal feature is the $Q^{1,1}$ species that is the building block forming the $P_2O_7^{4-}$ dimer. This result thus indicates that the glass network is principally

constituted by dimeric units. The proportion of this structural features increases with the Na_2O content from 52.9 to 69 %. This evolution suggests that additional structural features are present in low Na_2O (and thus high ZnO) content glasses, confirming that the topological disorder is higher in ZnO dominated formulation, owing to its intermediate oxide nature. Zinc oxide is thus more prone to create disorder than sodium oxide.

The $Q^{1,2}$ units amount appears to be constant and close to 20% all along the composition line. If the proportion of 'end of chain' species is constant, the proportion of 'middle of chain' (or cycle) units Q^2 strongly decreases when sodium oxide is inserted in the formulation. The global proportion shifts from 21 to 9 % all along the composition line.

The glass structure thus contains isolated phosphate, dimer and higher length phosphate chains and / or cycles. Detailed analysis of the $Q^{1,2}/Q^2$ ratio values could be used to discuss the averaged length of phosphate chains. The only assumptions required to do this calculation is that all the Q^2 participate to chains and are thus not involved in cycle formation. If the principal structural unit is the $P_3O_{10}^{5-}$ trimers, the $Q^{1,2}/Q^2$ ratio will be equal to 2, lower ratio will indicate higher chain length (1 for $P_4O_{13}^{6-}$ tetramers and 0.67 for $P_5O_{16}^{7-}$ pentamers).

The ratio evolution versus the composition is reported in *Fig. 3.16* and the values are regrouped in *Tab. 3.6*. It turns out that the ratio increases with the Na_2O proportion indicating that the averaged chains length is reduced when Zn^{2+} is replaced by Na^+ ions. The values is close to 1 in the x =0 sample, indicating that the averaged chain length is around 4 and that the most probable structural unit is a tetramer. For the x = 46.6 composition, the ratio reaches the values of 2 indicating that the most probable structural unit is a trimer. Between the two compositions, the ratio continuously decreases, showing that the averaged chain length evolved from 4 to 3.

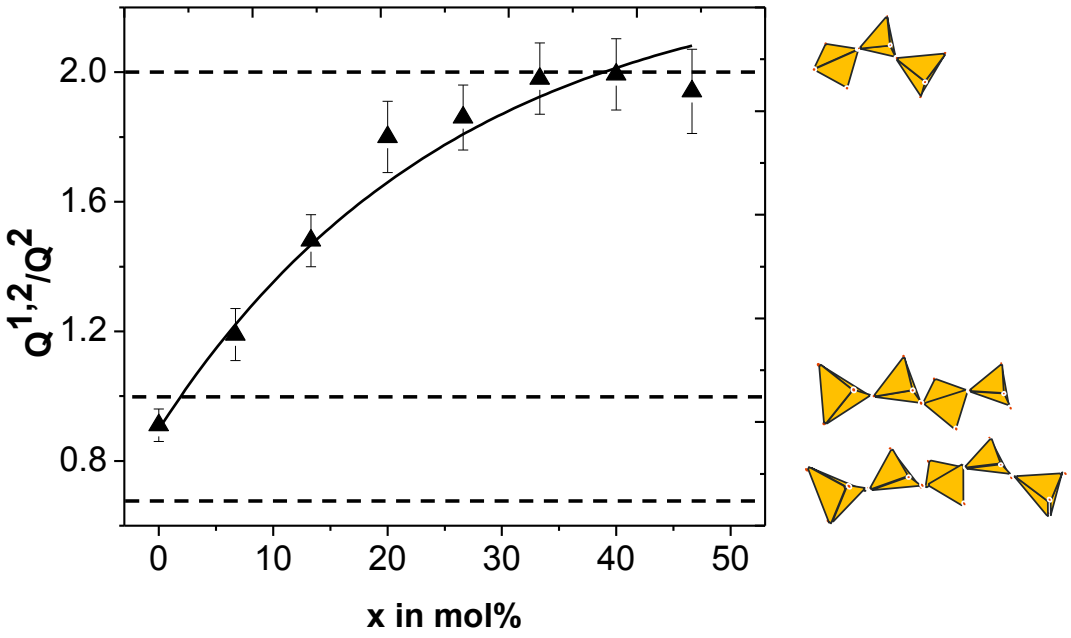

Fig. 3.16 The evolution of $Q^{1,2}/Q^2$ versus the composition.

Of course, the calculation only gives the averaged chain length and do not take into account the possible distribution centered around the most probable structural unit. If tetramer is determined to be the most probable feature ($Q^{1,2}/Q^2=2$), the presence of trimer and pentamers cannot be ruled out, the relative proportions of chains leading to the averaged values. Distinction between tri-, tetra- and penta-mers would require a precise analysis of the Q^2 distribution leading to the differentiation between $Q^{2,11}$, $Q^{2,21}$ and $Q^{2,22}$ characteristic of trimer, tetramers and pentamers units, respectively (Witter 1998). Due to the low concentration of Q^2 within our samples, this investigation has not been performed and the structural model will only be based on the averaged chain length calculation.

However, the relative proportion deduced from the 1D ^{31}P NMR spectra and the averaged chains length deduced from the $Q^{1,2}/Q^2$ ratio were used to describe the phosphate network in terms of P_n chains distribution, where n represent the number of P involved in the chain formation, P_1 being an isolated phosphate, P_2 a dimer, P_3 a trimer, P_4 tetramer and P_5 pentamer.

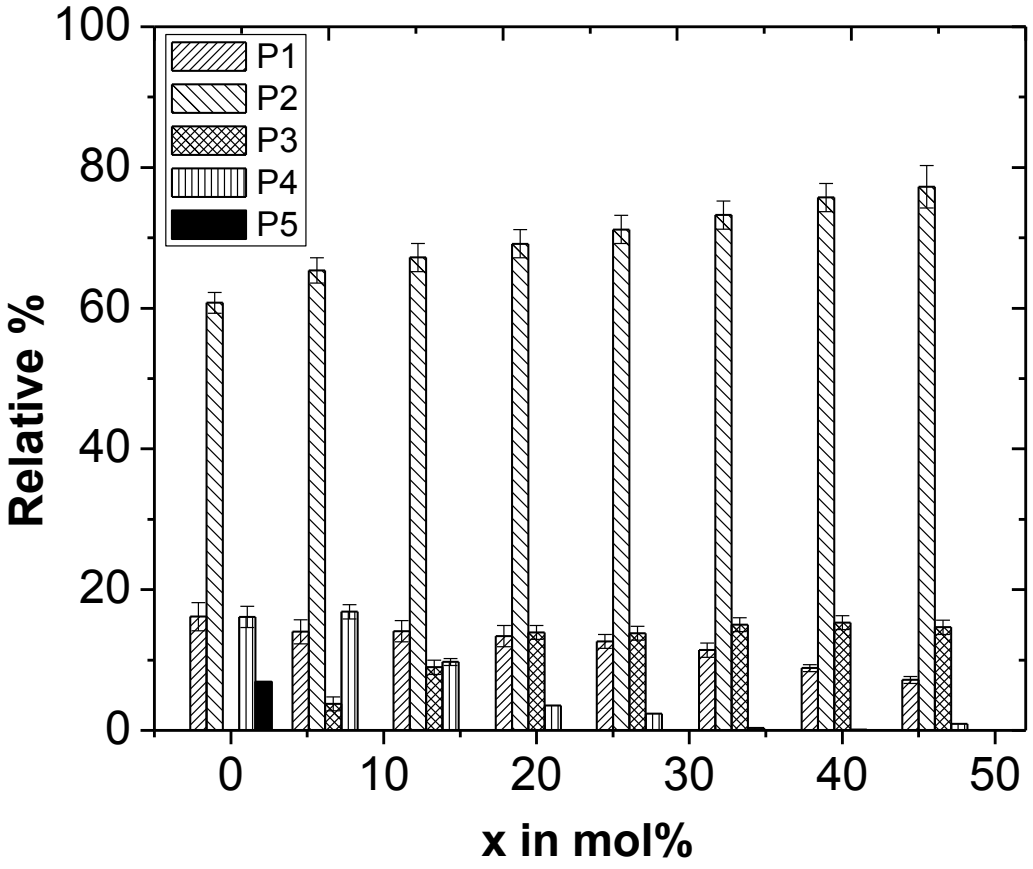

Fig. 3.17 The distribution of chain lengths as a function Na_2O content in the glass formulation.

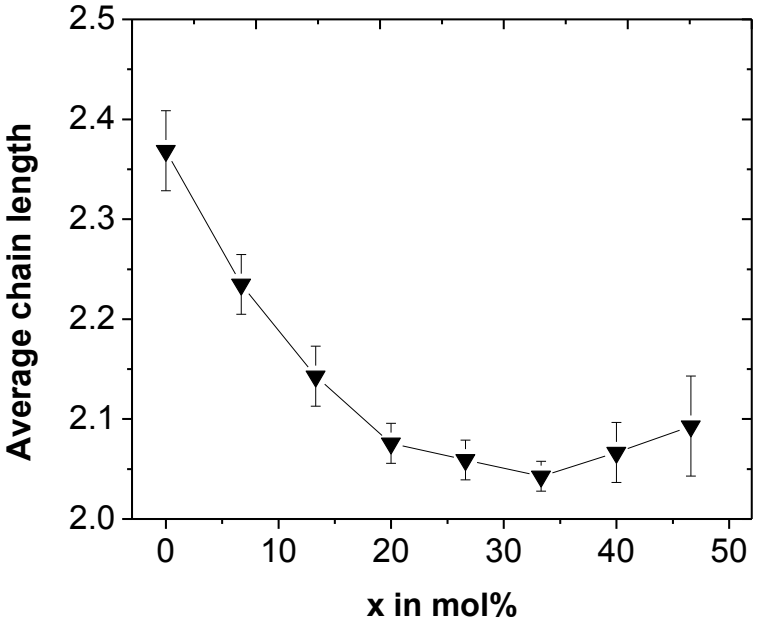

Fig. 3.18 The global averaged chain length (calculated from chain length distribution) versus the glass compositions.

Fig. 3.17 present the results obtained from the calculations and give a new insight onto the extent of topological disorder within the glass network. As previously mentioned, the 'unusual' distribution observed for the $x = 0$ sample comes from the averaged chain length used for the calculation. Even if the model is not complete, the decreases of disorder induced by the Zn/Na substitution is clearly highlighted through the largest distribution of phosphate chains involved in the formation of the glass network of high ZnO content materials. *Fig 3.18* shows the averaged chain length of the glass samples calculated by averaging the distribution of the chains (P_1, P_2, P_3, P_4 and P_5). The figure shows that the progressive substitution of Zn^{2+} by Na^+ eventually reduced the longer chains into shorter ones (from 2.37 for $x = 0$ to 2 for $x = 46.6$) increasing the relatively higher population of shorter chain lengths. It is worthy to note that the global averaged chain length slightly increased for high Na_2O content which is possibly due to the small error in the measurements.

The last parameter supporting this loss of disorder all along the composition line is the disproportionation constant K_d. The values have been calculated for each composition and are reported in *Tab. 3.6*. The evolution versus the composition is depicted in *Fig. 3.19* that shows a decrease of K_d when Zn is substituted by Na. The $x = 0$ sample K_d was calculated (K_d= 0.028) and is identical to the one deduced on the same formulation by NMR (0.028) (Brow, 1995). The observed decrease of K_d constitutes an additional evidence of the sodium ability to produce a less constrained network and thus a less disordered network in line with its pure network-modifying nature.

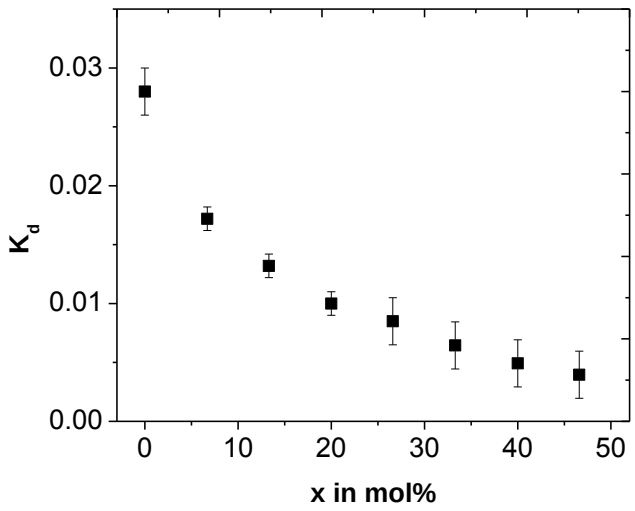

Fig. 3.19 The evolution of equilibrium constant (K_d) (66.6- x)ZnO- xNa_2O- 33.4 P_2O_5 glasses for the disproportionation reaction that occurs in the melt.

It is noteworthy that the Q^1 disproportionation reaction should theoretically produce equal proportions of Q^0 and Q^2 sites. However, ^{31}P MAS-NMR fittings do not provide similar proportions between the two units, the relative percentage of Q^2 being always higher than the Q^0 one. If changes in the formulation can be reasonably ruled out according to the very low $\Delta m/m$ observed during the preparation (and according to the fact that P_2O_5 volatilization should favor the formation of Q^0 site), we can tentatively explain this by the presence of a weak proportion of O^{2-} ions (between 2 and 4%) that are not participating to the phosphate network, i.e, they are bonded only to Zn^{2+} and/or Na^+ through Zn-O-Zn or (Na) bonds. These free oxygens (O^{2-}) will thus not be associated to the phosphate moieties and will lead to a more condensed phosphate species giving rise to the Q^2 increase. This kind of free O^{2-} is also observed in Na_2O-SiO_2 glasses (Nesbitt 2011). Of course, this assumption is far from being supported and additional experiments will be necessary to confirm this hypothesis.

IV. Conclusion

The zinc sodium pyrophosphate system (66.6-*x*)ZnO- *x*Na_2O- 33.4P_2O_5 was investigated in this chapter in terms of glass preparation, macroscopic properties and phosphate network structure.

Transparent glasses were prepared with the melt-quenching procedure up to a proportion of Na_2O equal to 46.6 mol%, higher Na_2O amount inducing melt crystallization.

If Raman and NMR have shown that the glass structure was dominated by dimeric species all along the composition line, the MRO analysis, provided by the 2D ^{31}P DQ-SQ experiment, has clearly shown that the Zn/Na substitution decreases the extent of disorder within the phosphate network, in a good agreement with the pure modifying-network of sodium oxide compared to the intermediate zinc oxide.

From a properties point of view, it has been shown that the progressive substitution of zinc by sodium induces a continuous decreases of the T_g, related to the replacement of covalent Zn-O-P bonds by ionic Na^+-O-P linkages. More opened structure is also created by the Zn/Na

substitution as indicated by the increases in the molar volume property. Two-domain regimes were observed for the thermal and chemical stability. The better thermal/chemical stabilities compromise was found for the x = 20 composition, that exhibits the most important K_A parameter ever reported for a low-T_g phosphate glasses.

The relativity low-T_g of this composition (339°C), far below the 400°C boundary, makes of this glass a perfect candidate for the doping procedure. It is noteworthy that additional formulation investigations have been performed within the frame of this Ph-D work. On the x = 20 sample, partial substitution of Zinc by Lead, Cadmium and Copper have been realized but does not provide any improvement of the stabilities. The mixed alkali effect, obtained by combining Li, Na and K, has also been tested in the x = 20 formulation in order to reduce the T_g and to improve the resistance against crystallization. If the T_g was significantly reduced when the three alkali oxide were used in combination (down to 309 °C), the thermal stability was always lower than in case of the pure sodium formulation. To summarize, none of the formulation among more than 50 different prepared glasses has exhibited better T_g/ stability compromise than the $46.6ZnO\text{-}20Na_2O\text{-}33.4P_2O_5$ composition. Therefore, for sake of clarity, the previously mentioned experiments have not been presented in this manuscript.

In addition to the x = 20 sample, a second formulation has also been chosen to continue this work. Owing to (i) its specific formulation (equal proportion of Na_2O and ZnO), (ii) its low-T_g (310°C) and intermediate thermal and chemical stabilities and (iii) the sharp and easily detectable crystallization peak observed on its DSC analysis, the x = 33.3 sample has also been selected for the doping procedure that will be described in the following chapter.

References

Abrahams, I, A Ahmed, C J Grommbridge, G E Hawkes, and T G Nunes. *J. Chem. Soc. Dalton Trans.*, 2000: 155-160.

Belharouak, I, P Gravereau, C Parent. J. *Solid State Chem.* 152 (2000): 466-473.

Bingham, P, R J Hand, O M Hannant, S D Forder and S H Kilcoyne. *J. Non-Cryst. Solids.* 355 (2009): 1526-1538.

Brow, R K, D R Tallant, S T Myers, and C C Phifer. *J. Non-Cryst. Solids.* 191 (1995): 23.

Cooper, E I, and C A Angell. *J. Non-Cryst. Solids*. 56 (1983): 75.

Elammani, L, J Durand, L Cot, and B Elouadi. *Z. Kristallogr.* 180 (1987): 137-140.

Ji, L N, H W Ma, and J B Li. *J. Solid State Chem.* 180 (2007): 2256-2261.

Koudelka, L, J Jirak, P Mosner, L Montagne, and L Delevoye. *Phys. Chem. Glasses: Eur. J. glass. Sci. Technol.* 48 (2007a): 33-38.

Koudelka, L, P Mosner, M Zeyer-Dusterer, and C Jager. *J. Phys. Chem. Solids.* 68 (2007b): 638-644.

Lakshmikantha R, R Rajaramakrishna, R V Anavekar, and N H Ayachit. *Mater. Chem. Phys.* 133 (2012): 249-252.

Lim, J W, M L Schmitt, R K Brow,and S W Yung, *J. Non-Cryst. Solids.* 356 (2010): 1379-1384.

Majling J, S Palco, F Hanic, and J Petrovic, *Chem. Zvesti* 28 (3), (1974): 294-297.

Manzani, D, R G Fernandes, Y Messaddeq, S J L Ribeiro, F C Cassanjes, and G Poirier. *Opt. Mater.* 33 (2011): 1862-1866.

Montange, L, R Delaval, and G Palavit. *J. Non-Cryst Solids.* 223 (1-2) (1998): 43-47.

Mosner, P, K Vosejpkova, and L Koudelka. *Thermochim. Acta*.. 522 (2011): 155-160.

Nalin, M, G Poirier, S L Ribeiro, Y Messadecq, and L Cescato. *J. Non-Cryst. Solids.* 353 (2007): 1592-1597.

Nesbitt, H W, G M Bancroft, G S Henderson, R Ho, K N Dalby, Y Huang, and Z Yan. *J. Non-Cryst. Solids.* 357 (2011): 170-180.

Petrova, M A, V I Shitova, G A Mikirticheva, V F Popeva, and A E Malshikov, *J. Solid State Chem.* 119 (1995): 219-223.

Quinn, C J, G H Beall, and J E Dickinson. *in:Proc. 16th Int. Congress on Glass.* 4 (1992): 79.

Stranford, G T, R A Condrate, and B C Cornilsen. *J. Molec. Struct.* 73 (1981): 231.

Subbalakshmi, P, and N Veeraiah. *J. Non-Cryst. Solids.* 298 (2002): 89-98.

Subcik, J, L Koudelka, P Mosner, L Montagne, G Tricot, L Delevoye, and I Gregora, *J. Non-Cryst. Solids.* 356 (44-49) (2010): 2509-2516.

Takebe, H, Y Baba, and M Kuwabara. *J. Non-Cryst. Solids.* 352 (2006): 3088-3094.

Varma, B R K. *B. Mater. Sci.* 9 (1) (1987): 1-5.

Walter, G, U Hoppe, J Vogel, G Carl, and P Hartmann. *J. Non-Cryst. Solids*.333(2004): 252-262.

Wazer, J R Van. "Phosphorus and its Compounds." *Interscience Publishers Ltd.* Vol. I (1958).

Weyl, W A, and E C Marboe. "The Constitution of Glasses." *Interscience, New york*, (1964): 578.

Witter, R, P Hartmann, J Vogel, and C Jager. *Solid State Nucl. Mag.* 602-603 (2002): 145-157.

Youssef, N H, M S Belkhiria, J Videau, and M B Amara. *Mater. Lett.* 44 (2000): 269-274.

Chapter D

Doping of zinc sodium phosphate compositions: effect of Al^{3+}, B^{3+} and Si^{4+} insertion on the properties, stability and structure.

Effect of Al-, B- and Si- doping of the two formulations derived from the previous chapter is investigated in this part. The first part will be devoted to the preparation of the glasses in which doping elements have been introduced in low amounts (1, 2 and 4 mol%). The effect of doping on the macroscopic properties will be treated in the second part. In addition to the previously studied properties (T_g, ρ, V_M), information about viscosity has also been reported. Benefic or unfavorable evolutions of thermal and chemical stabilities will also be investigated in this part. Definitive conclusions about the relevancy of the Al-, B- and Si- doping will then be deduced from the complete set of data. The preliminary results obtained on the doped glasses by Raman and 1D NMR spectroscopies will be presented in the last part of this chapter.

I. Glass preparation

Two series of doped glasses have been prepared using the two formulations derived from the previous chapter (20 and 33.3) and will be denoted as series I and II, respectively. In order to keep the T_g below our investigation boundary (T_g < 400°C), low amounts of doping oxide (1, 2 and 4 mol%) have been inserted in the formulation. Three oxides (Al_2O_3, B_2O_3 and SiO_2) have been used to dope the two based compositions, giving rise to 6 different systems. The glass series I corresponds to the samples obtained after doping of the $46.6ZnO\text{-}20Na_2O\text{-}33.4P_2O_5$ composition with Al_2O_3, denoted as I- *x*Al, B_2O_3, denoted as I- *x*B, and SiO_2, denoted as I- *x*Si, where *x* is the amount of doping oxide (1, 2 and 4 mol%). The glass series II has been obtained with the same doping procedure using the $33.3ZnO\text{-}33.3Na_2O\text{-}33.4P_2O_5$ glass composition.

Performing a standard addition of the Al_2O_3, B_2O_3 and SiO_2 doping oxides in the base formulation would have led to a progressive increase of the O/P ratio. In order to enable a more detailed structural investigation, and to limit the increase of T_g, the doping has been formulated to keep a constant polymerization degree of the phosphate network. Thus, to keep the constant phosphate network structure, all the doped glass formulation have been designed to produce constant O/P ratio (= 3.5) corresponding to a hypothetic pyrophosphate formulation. Therefore, the doping oxide additions have been made through a substitution between Zn^{2+} and Na^+ ions (in the relative proportions given by the base formulation) and the doping elements. In case of X_2O_3 oxide (X=Al or B), for which pure pyrophosphate corresponds to the $40X_2O_3\text{-}60P_2O_5$ formulation, the glasses have been thus designed as $y(40X_2O_3\text{-}60P_2O_5)\text{-}(100\text{-}y)(46.6ZnO\text{-}20Na_2O\text{-}33.4P_2O_5)$ and $y(40X_2O_3\text{-}60P_2O_5)\text{-}(100\text{-}y)(33.3ZnO\text{-}33.3Na_2O\text{-}33.4P_2O_5)$ systems for the glass series I and II, respectively. For SiO_2 doping oxide, which produce pyrophosphate structure with the $50SiO_2\text{-}50P_2O_5$ formulation, the glass series I and II have been designed within the $y(50SiO_2\text{-}50P_2O_5)\text{-}(100\text{-}y)(46.6ZnO\text{-}20Na_2O\text{-}33.4P_2O_5)$ and $y(50SiO_2\text{-}50P_2O_5)\text{-}(100\text{-}y)(33.3ZnO\text{-}33.3Na_2O\text{-}33.4P_2O_5)$ systems. For the sake of clarity, the formulation have been expressed in $ZnO\text{-}Na_2O\text{-}P_2O_5\text{-}X_nO_m$ where X=Al, B and Si and are reported in *Tab. 4.1*.

Tab. 4.1 Composition, melting temperature and weight loss of the glass samples.

Series-I								**Series-II**							
Sample	ZnO	Na_2O Mol%	P_2O_5		Melt(^oC) /t	Wt.%	Remarks	Sample	ZnO	Na_2O Mol%	P_2O_5		Melt/^oC/t	Wt.%	Remarks
I-0	46.6	20.0	33.4		1000/20mins	1.3	Clear	II -0	33.3	33.3	33.4		1000/20mins	1.8	Clear
				Al_2O_3								Al_2O_3			
I-1Al	45.5	19.5	34.0	1	1150/2hrs	1.5	Clear	II-1Al	32.5	32.5	34	1	1150/2hrs	1.3	Clear
I-2Al	44.4	19.0	34.6	2	1150/2hrs	1.9	Clear	II-2Al	31.7	31.7	34.6	2	1150/2hrs	1.4	Clear
I-4Al	42.0	18.0	36.0	4	1150/3hrs	1.9	Clear	II-4Al	30.0	30.0	36.0	4	1150/3hrs	2.0	Clear
				B_2O_3								B_2O_3			
I-1B	45.5	19.5	34.0	1	1000/20mins	1.6	Clear	II-1B	32.5	32.5	34	1	1000/20mins	1.4	Clear
I-2B	44.4	19.0	34.6	2	1000/20mins	1.4	Clear	II-2B	31.7	31.7	34.6	2	1000/20mins	1.2	Clear
I-4B	42	18.0	36.0	4	1000/20mins	1.5	Clear	II-4B	30.0	30.0	36.0	4	1000/20mins	1.5	Clear
				SiO_2								SiO_2			
I-1Si	45.7	19.6	33.7	1	1150/3hrs	2.0	Clear	II-1Si	32.6	32.6	33.8	1	1150/3hrs	1.6	Clear
I-2Si	44.7	19.2	34.1	2	1150/3hrs	1.9	Clear	II-2Si	32.0	32.0	34.0	2	1150/3hrs	1.4	Clear
I-4Si	42.9	18.4	34.7	4	1150/3hrs	2.1	Clear	II-4Si	30.6	30.6	34.8	4	1150/3hrs	1.7	Clear

All the glasses were prepared by the melt-quenching technique. Depending upon the compositions, melting temperatures of 1000-1150 ^{o}C and melting times of 20 minutes to 3.5 hours were used in order to yield clear and transparent glasses. The glasses were poured onto a brass plate and cooled at room temperature. All preparations produced clear and transparent glasses suggesting that dopants were solubilized homogenously into the melts. X-ray diffraction analysis were performed (not shown here) and confirmed that all the samples present an amorphous character, as expected from the slight formulation deviation compared to the undoped compositions. Weight loss measurements were carried out to check if significant amounts of P_2O_5 volatilizes during the preparation. With less than 2 % of weight loss, the chemical compositions of the glasses did not significantly deviate from the expected composition and the samples will be thus referred to 'as-batch' compositions. All the compositions and melting procedure parameters are reported in *Tab. 4.1*.

II. Effect of doping on glass properties and stabilities

In this section, we have investigated the doped glasses to determine how the macroscopic properties and stabilities evolve with the small quantity of doping elements. Evolution of density, molar volume, T_g will be first analyzed as well as the viscosity. Then, the effect of doping on the stabilities will be discussed. Finally, the global set of data will allow us assessing for the relevancy of each doping element for the development of low-T_g and stable phosphate compositions.

II.1. Density and molar volume

The density and molar volume of both glass series are summarized in *Tab. 4.2* and their plot against dopants mol% are shown in *Fig 4.1*.

Continuous but small decreases of density can be observed for all the different systems. This slight decrease can be related to the small changes in the glass compositions. Since one mole of ZnO is substituted by one mole of Al_2O_3, B_2O3 or SiO_2, the global replacement of Zn^{2+} (65.83 u) ion exceeds the mass of two Al^{3+}(2 x 26.9 u), two B^{3+} (2 x

10.81 u) or one Si^{4+} (28.08) ions leading to decrease in density (Fig 4.1). It is noteworthy that this decreasing trend in density is also reported by Metwalli with progressive substitution of barium by aluminium in the $BaO\text{-}Al_2O_3\text{-}P_2O_5$ system (Metwalli 2001).

Only slight modifications of density and molar volume have been observed in all the doped glasses. Doping procedure, independent of the nature of the doping element, seems thus to have a marginal effect on these properties.

Tab. 4.2 Density and molar volume of the glass samples.

	Series-I			**Series-II**	
Samples	ρ (gcm^{-3}) ±0.005	V_m (cm^3/mol) ±0.1	Samples	ρ (gcm^{-3}) ±0.005	V_m (cm^3/mol) ±0.1
I-0	3.218	30.38	II-0	3.006	31.67
I-1Al	3.193	30.83	II-1Al	2.999	31.98
I-2Al	3.175	31.21	II-2Al	2.968	32.43
I-4Al	3.129	32.13	II-4Al	2.940	33.07
I-1B	3.135	31.29	II-1B	2.950	32.40
I-2B	3.108	31.67	II-2B	2.932	32.73
I-4B	3.055	32.48	II-4B	2.917	33.22
I-1Si	3.184	30.80	II-1Si	3.000	31.85
I-2Si	3.158	31.16	II-2Si	2.983	32.17
I-4Si	3.109	31.91	II-4Si	2.924	33.14

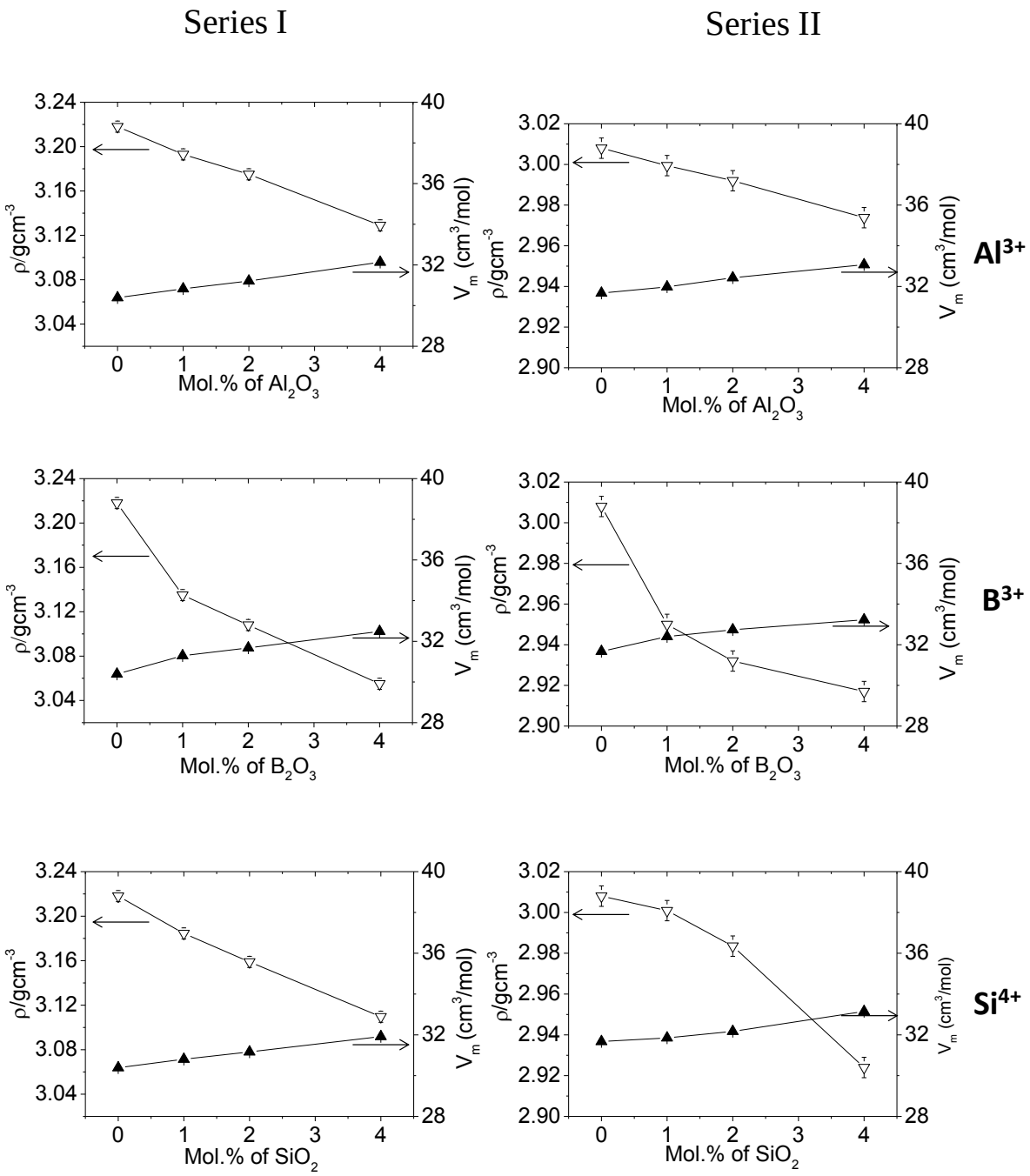

Fig 4.1 The evolution of density (down triangle) and molar volume (up triangle) with the insertion of Al, B and Si. (Arrows are provided for visual guidance).

▽ *:(Density),* ▲ *:(molar volume)*

II.2. Chemical stability

The effect of doping on the chemical durability was tested with the procedure used in chapter C and described in chapter B.

The weight losses obtained for each system after 24 hours of immersion in distilled water at 90 ^{0}C are reported in *Tab. 4.3* and sketched versus the doping content in *Fig. 4.2.*

Tab. 4.3 Chemical durability test: estimated weight loss percentage after 24 h of treatment in distilled water at 90 °C.

I-series	% Wt loss/24h	II-series	% Wt loss/24h(±1.5)
I-0	7.07 ±1.5	II-0	28.02 ±3.5
I-1Al	0.7 ±0.05	II-1Al	5.03 ±0.05
I-2Al	0.22 ±0.05	II-2Al	1.81 ±0.05
I-4Al	0.11 ±0.005	II-4Al	1.04 ±0.005
I-1B	10.9 ±1.5	II-1B	35.8 ±3.5
I-2B	15.7 ±1.5	II-2B	40.3 ±5
I-4B	30.3 ±3.5	II-4B	46.8 ±5
I-1Si	9.0 ±1.5	II-1Si	30.2 ±3.5
I-2Si	10.3 ±1.5	II-2Si	32.5 ±3.5
I-4Si	13.5 ±1.5	II-4Si	34.2 ±3.5

Doping with Al strongly improves the chemical durability, since samples containing 2 mol% of Al_2O_3 present an almost inexistent weight loss. This result is in perfect line with the papers showing the spectacular improvement of the chemical durability allowed by Al^{3+} insertions (Bunker 1984 and Brow 1993). Generally, B_2O_3 additions in phosphate glasses produce better chemical durability (Donald 2004, Tindyala 1978, He 1991 and Ray 1976). However, our results show that B-doping significantly decreases the resistance against water attack and its effect has thus to be considered as a negative one. It is noteworthy that this phenomenon has already been noted in alkali phosphate compositions (Peng 1991). SiO_2 has only a marginal effect on the chemical durability. However, Si-doping has to be considered as unfavorable for the chemical durability since a slight increase of the weight losses can be observed. Finally, the dopants can be ranked in terms of chemical durability as Al>>Si>B.

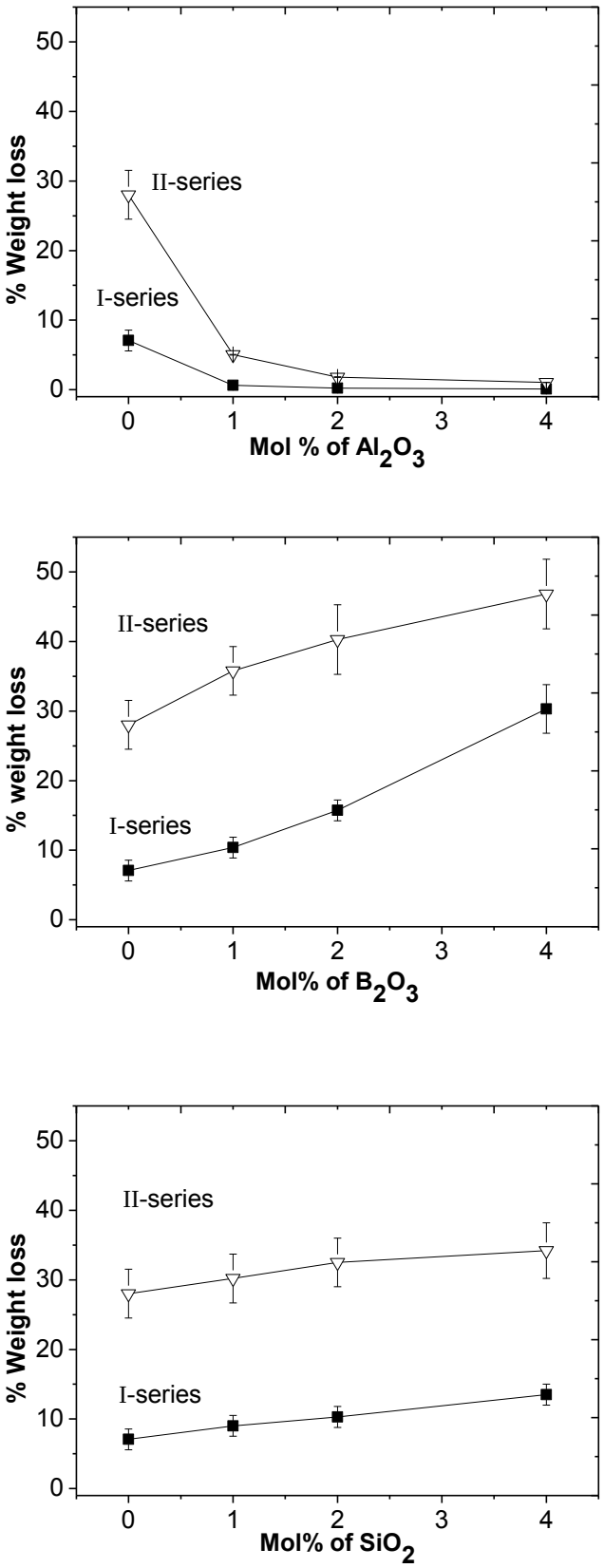

Fig. 4.2 Change in weight loss percentage as a function of increasing dopant content.

(▽ :Series II, ■ :Series I)

II.3. Effect on glass transition temperature:

The DSC patterns obtained on the systems are reported in *Fig. 4.3*. The T_g extracted from the analysis are reported in *Tab. 4.4*, accompanied by the T_x and T_C parameters.

The T_g evolutions induced by doping are reported in *Fig. 4.4* for both glass series. Different behaviors can be observed depending on the doping elements. It appears thus that Al_2O_3 insertion induces an important T_g increase on both glass series, 4 mol% of Al_2O_3 leading to T_g increase of 50°C. The increase due to B_2O_3 is not so important but can be considered as significant since addition of 4 mol% induces a 20°C increase. If both latter results are in line with data coming from the literature (Brow 1993 and Harada 2004), the most surprising result comes from SiO_2 that does not induce any increase of T_g. Glasses with 4 mol% of SiO_2 are even experienced a slight T_g decreases, not in line with the commonly admitted reticulating role of SiO_2.

Tab. 4.4 Thermal properties of the glasses (the estimated uncerntainty of T_g value is ±3 °C).

Samples	Thermal characteristics/°C				Samples	Thermal characteristics/°C			
Series-I	T_g	T_x	T_x-T_g	T_c	Series-II	T_g	T_x	T_x-T_g	T_c
I-0	339	535	196	550	II-0	310	440	130	461
I-1Al	351	-	-	-	II-1Al	325	460	135	479
I-2Al	365	-	-	-	II-2Al	335	494	159	522
I-4Al	385	-	-	-	II-4Al	368	540	172	580
I-1Si	342	-	-	-	II-1Si	312	452	140	490
I-2Si	341	-	-	-	II-2Si	312	451	139	476
I-4Si	340	-	-	-	II-4Si	309	468	159	511
I-1B	345	-	-	-	II-1B	315	460	142	462
I-2B	350	-	-	-	II-2B	320	490	170	522
I-4B	360	-	-	-	II-4B	330	542	212	-

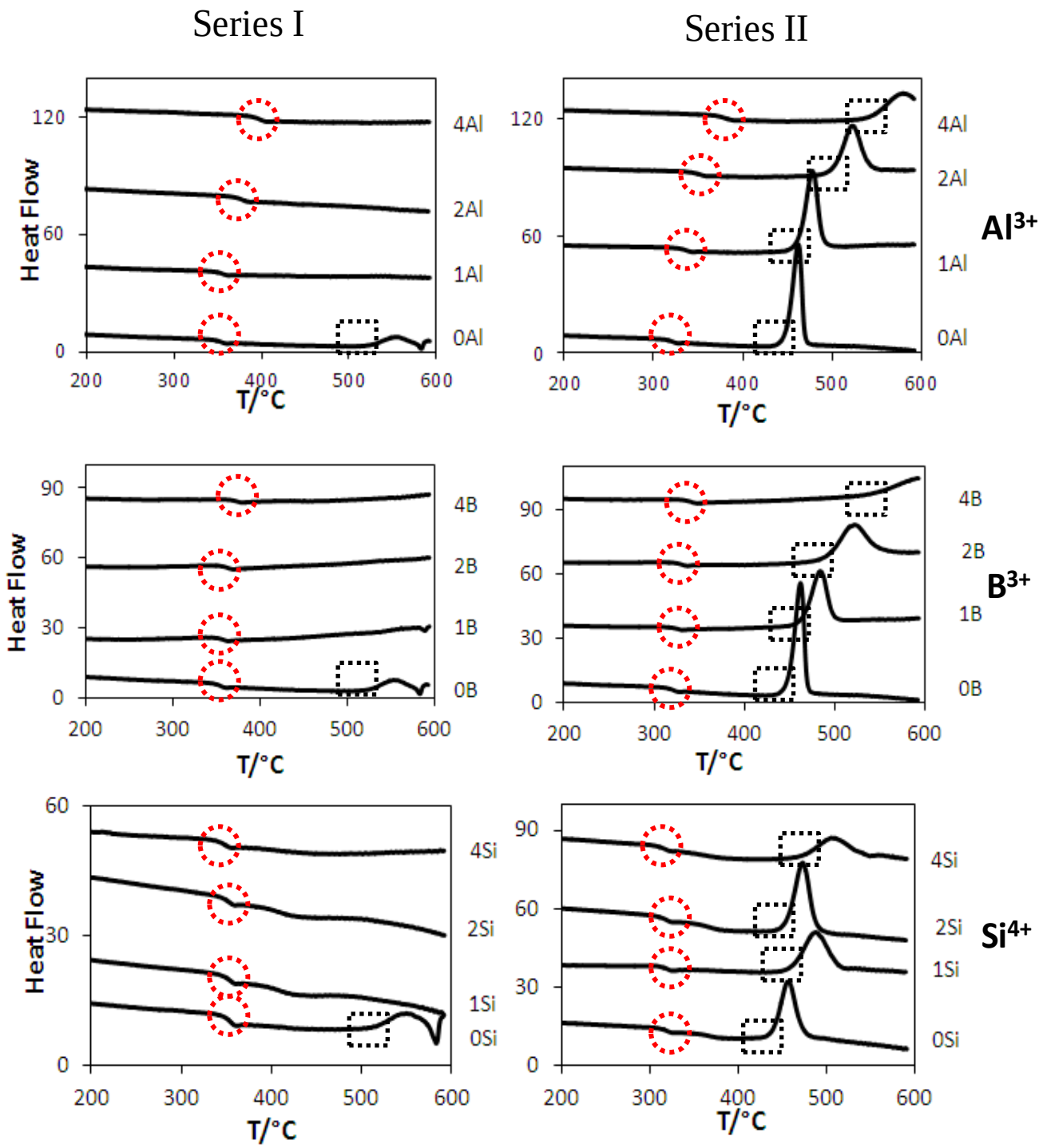

Fig 4.3DSC patterns obtained for the prepared glasses series I and series II.

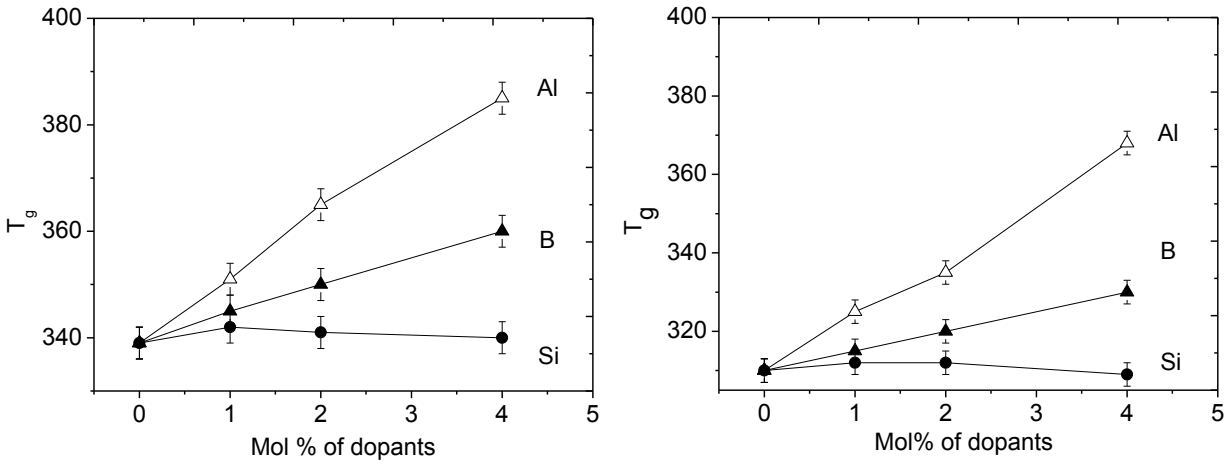

Fig 4.4 Evolution of T_g as a function of mol% of dopants.

Doping can thus significantly affect the T_g parameter, the effect being very important in case of Al_2O_3, moderate in case of B_2O_3 and surprisingly null in case of SiO_2. The doping ranking concerning the T_g is thus Si > B > Al. However, it is noteworthy that all our doped compositions fulfill the targeted T_g requirement (T_g < 400°C). The doping procedure used in this work appears thus not to be a limitation for the development of low-T_g and stable phosphate glasses. It is noteworthy that pure addition would have certainly lead to higher T_g increases as reported in literature (Lim 2010, Harada 2004, Takabe 2006 and Brow 1993).

II.4. Thermal stability

Effect of doping on the thermal stability of the glasses has been first evaluated through the Angell parameter (K_A) and further supported by isothermal crystallization studies. These latter analyses were used to determine if the doping procedure changes the nature of the crystalline phases and to estimate if the crystallization kinetic was limited or favored by the doping procedure.

II.4.1. Angell parameter

Doped glasses of series I perfectly illustrate the limitations of K_A, mentioned in chapter B. As observed in *Fig.4.3*, the very weak crystallization peak of the undoped composition is completely suppressed from all the Al-, B- or Si-doped compositions. If this

observation supports a thermal stability improvement, the results cannot be expressed in terms of Angell parameter, since it cannot be determined. Moreover, a complete suppression or a postponing beyond the DSC machine measurement limit (650°C) of the crystallization peak cannot be inferred from these analyses. Therefore DTA (Differential Thermal Analysis) with measurement limit of 1000 °C was also employed in order to monitor the crystallization peak temperature. No trace of Tc was highlighted in the analysis.

The glass series II allows for an easier and more complete analysis of the Angell parameter evolution, allowed by the clear and significant shifting of the crystallization peak observed on all the doped glasses thermal analysis (*Fig. 4.3*). The calculated K_A values are reported in *Tab. 4.4* and sketched in *Fig. 4.5*. Three different behaviors can be observed depending on the doping element. B_2O_3 insertions strongly improve the K_A, since the sample II-4B (containing thus 4 mol% of B_2O_3) presents a K_A of 212°C, 82° higher than the undoped composition. Higher thermal stability is also observed in case of Al_2O_3, but with a lower impact, since the K_A is only increased by 42 °C in case of the 4 mol% sample. SiO_2 induces a discontinuous evolution of the K_A parameter but finally produces a marginal increase of K_A (+28 °C) in the 4 mol% sample. Improvement of the thermal stability can also be discussed using the crystallization enthalpy parameter. As observed in *Fig. 4.3*, Al and B doping induce a concomitant increase of T_x and decrease of the intensity of crystallization peak, which supports their benefic effect on thermal stability. Insertion of SiO_2 does not provide a continuous and comprehensive evolution on this parameter.

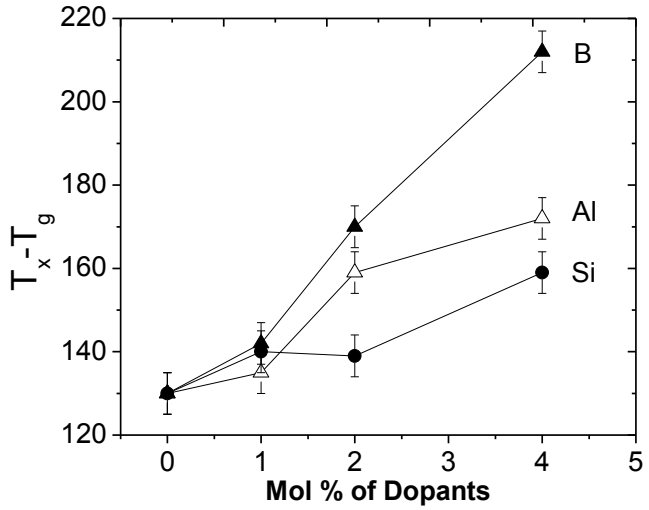

Fig 4.5 Angell Parameter K_A (T_x-T_g) as a function of mol % of dopants for the series-II glasses.

I.4.2. Isothermal treatment

The information deduced from the Angell parameter was completed by isothermal treatment investigations. The series I glasses were re-crystallized at 600 °C for 10 hours and series II glasses were re-crystallized at the crystallization temperature T_c and information about the effect of doping on the crystallization mechanism was obtained by XRD and ^{31}P NMR methods.

The nature of the phases formed during crystallization was investigated in a first time in order to determine if the doping procedure impacts this parameter. XRD analyses were thus performed on the annealed formulations. XRD patterns obtained on the Al-doped samples are reported in *Fig. 4.6*. As shown in the figure, the glass series I contain similar compounds than the undoped one (γ -$Zn_2P_2O_7$). Similar result was obtained for the glass series II, which crystallizes in γ-$Zn_2P_2O_7$ and $Na_2ZnP_2O_7$ independently of the doping content. The XRD analysis indicates thus that the Al doping procedure does not change the nature of the crystalline phase. Similar result was obtained with the B- and the Si- doped samples (not shown here). This study thus indicates that the doping elements do not enter into the crystalline compounds and do not participate in the formation of the crystalline phase. Their effect is thus only restricted to the remaining amorphous matrix. As a consequence, the amount of doping in the residual glass indirectly increases all along the crystallization process, since the doping elements do not participate to the formation of the crystalline phases that requires extraction of Zn, Na and P from the glass matrix.

The crystallization kinetic was also investigated. Since both the amorphous and crystalline compounds contain P, we use ^{31}P MAS-NMR analysis to quantify the proportion of P involved in the crystalline phase(s) versus the annealing time and thus to probe the crystallization kinetics. The temperature of annealing was different for each composition and was setup to 130 °C above the glass T_g. The decomposition of the ^{31}P MAS-NMR spectra, leading to the quantification of phosphorus involved in crystalline phase, obtained from an isothermally treated sample for various time, is illustrated in *Fig. 4.7*. The sharp and broad peaks in the spectrum represent crystalline and amorphous phase respectively, present in the sample

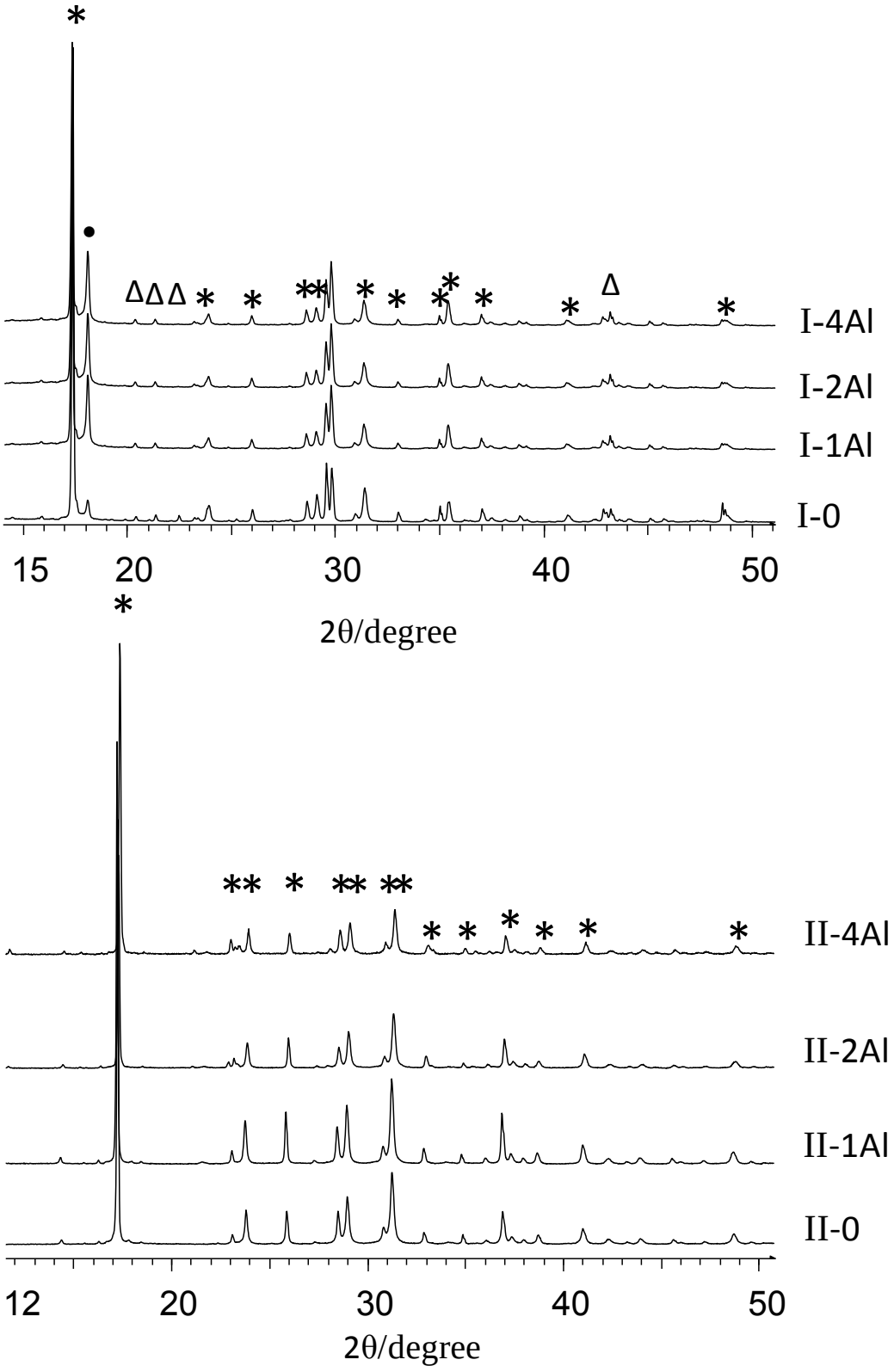

Fig. 4.6 XRD patterns obtained for the samples of series-I and II containing Al after crystallization where (*) $Na_2ZnP_2O_7$, (Δ) $Zn_2P_2O_7$, and (•)Teflon.

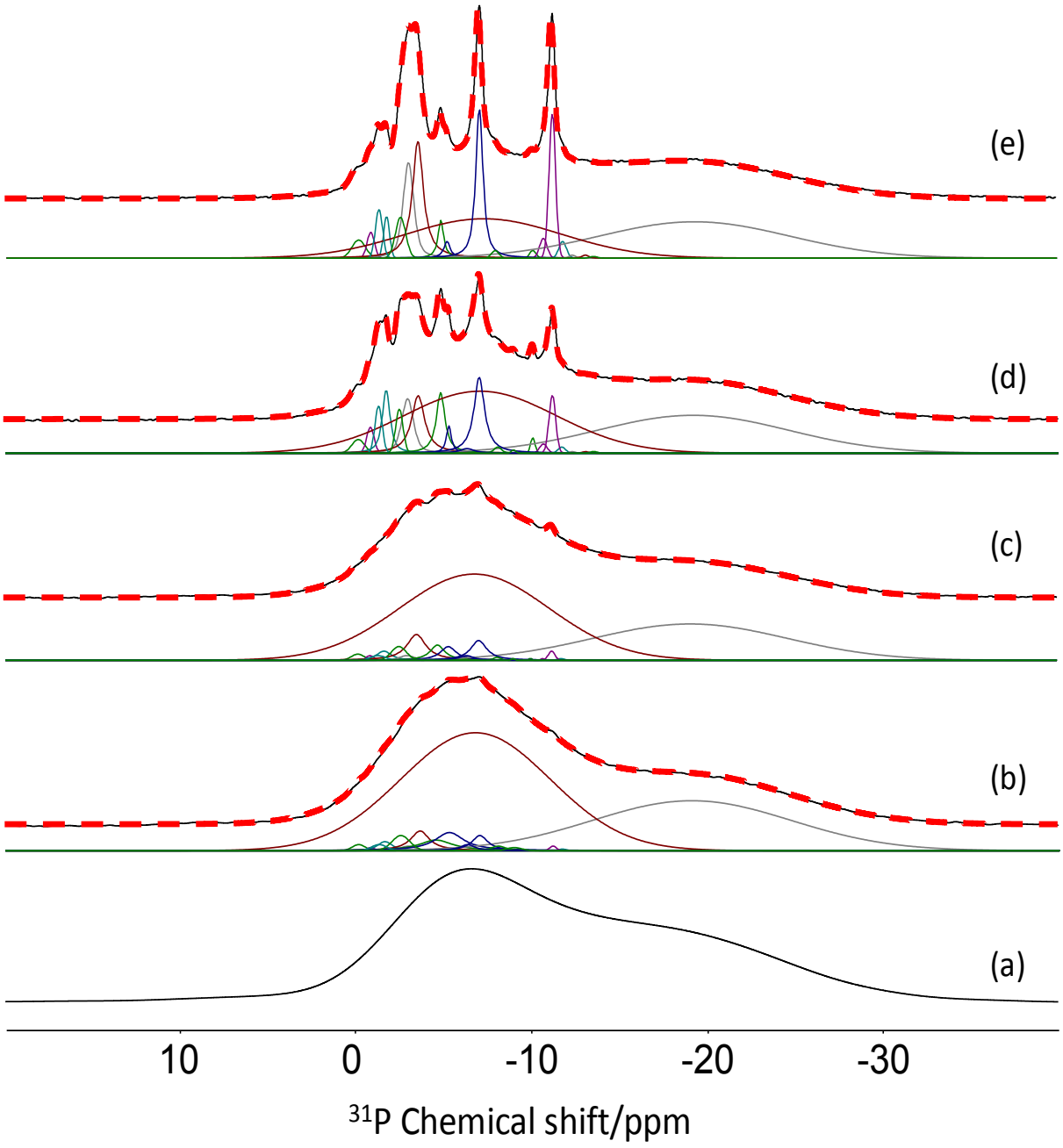

Fig. 4.7 ^{31}P MAS-NMR of the I-2B composition as quenched (a) and after being treated at 130 °C above T_g for 1h (b), 3h (c), 6h (d) and 10 h (e).

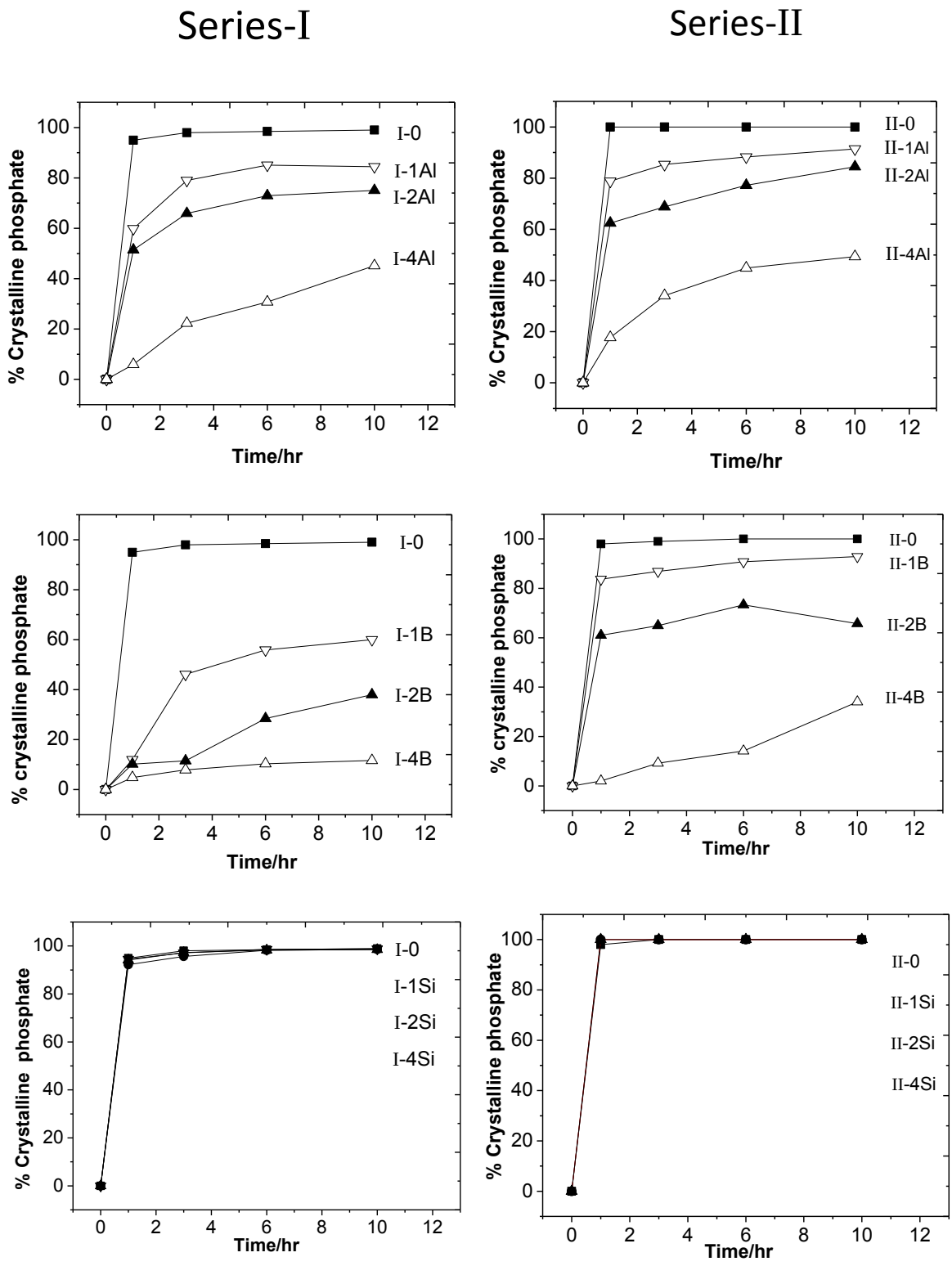

Fig. 4.8 Evolution of relative % of crystalline phase with the increase in B, Al, Si after treating isothermally for 1, 3, 6 and 10 hours. On the left series-I glasses and on the right series-II glasses.

The curves showing the proportions of P involved in crystalline phase(s) versus annealing time are reported in *Fig. 4.8* for the different systems. First, it has to be noticed that both undoped compositions experience a fast crystallization since the proportion of P in the crystallized phase(s) reaches 100% (that corresponds to an almost complete material crystallization) only after 1 hour. These results show that, in spite of their very important Angell parameter, these formulations do not resist against isothermal treatments, confirming thus the need for the formulations to be improved.

The insertion of Al and B doping elements within the glass matrix clearly has a limiting effect on the crystallization kinetic for both glass series. After 10 h of annealing, the proportions of P involved in the crystalline phases for glass series II decreases from 100% (complete crystallization) for the undoped glass down to 50% for the sample containing 4 mol% of Al_2O_3 and 30% for the sample doped with 4 mol% of B_2O_3. The results are even more spectacular for the glass series I that shows a decrease from 100 % (undoped) to 40 and 10 % for the Al- and B- doped sample (4 mol%), respectively. On the contrary, SiO_2 doping does not affect the curves, indicating that this latter doping element has no effect on the resistance against crystallization.

It appears thus that the doping does not change the chemical nature of the phases formed during the crystallization and are kept inside the glass structure. Taking into account the Angell parameter, the crystallization enthalpy and the crystallization kinetics, it turns out that B-doping strongly improves the resistance against crystallization. Al-doping also favors the thermal stability but in a less extent. Finally, Si doping has only a marginal effect. From a thermal stability point of view, the doping elements can thus be ranked as: B > Al > Si.

II.5 Viscosity measurements

Viscosity was analyzed in the range of $5 < \log \eta < 10$ with the parallel plate technique. We believe that this property could help explaining the changes observed in the crystallization kinetics since the structural rearrangements leading to crystallization are partially controlled by the viscous flow, higher viscosity leading to slower movements and slower kinetic.

The evolutions of $\log \eta$ versus the temperature are brought together in *Fig. 4.9* for all the systems. Insertions of Al- and B- doping elements lead to a viscosity increase, illustrated by the curves postponing. The effect of SiO_2 is lower since doping does not change the curves for glass series II and only produce a slight shift for glass series I, independently of the SiO_2 content.

If the short range of investigated viscosity does not allow us extracting activation energy, valuable information can be derived from these experiments. The temperatures corresponding to Log η = 7 Pa.s have been used to produce the data reported in *Fig. 4.10*. The curves express the differences in temperatures required to reach the same viscosity value and are reported versus the doping amounts. The tendency is similar for both glass series. Al-doping has the more important effect on ΔT since increases of 60 and 45 °C in temperature are required to reach the Log η = 7 Pa.s values in the 4 mol% Al-doped glass series I and II, respectively. B_2O_3 insertion has a lower impact on the ΔT parameter (+20 and 15°C for glass series I and II, respectively) whereas Si-doping does not induce any positive effect but a marginal negative one. It is noteworthy that this difference in tendency between Si and Al/B has already been observed for the T_g parameter.

The results indicate that Al_2O_3 and B_2O_3 have a significant impact on the glass organization since viscosity is affected by their insertion. SiO_2 does not seem to play a role in this structural organization since no effect on viscosity has been noticed. From a viscosity point of view, the doping elements can be ranked as: Al > B > Si.

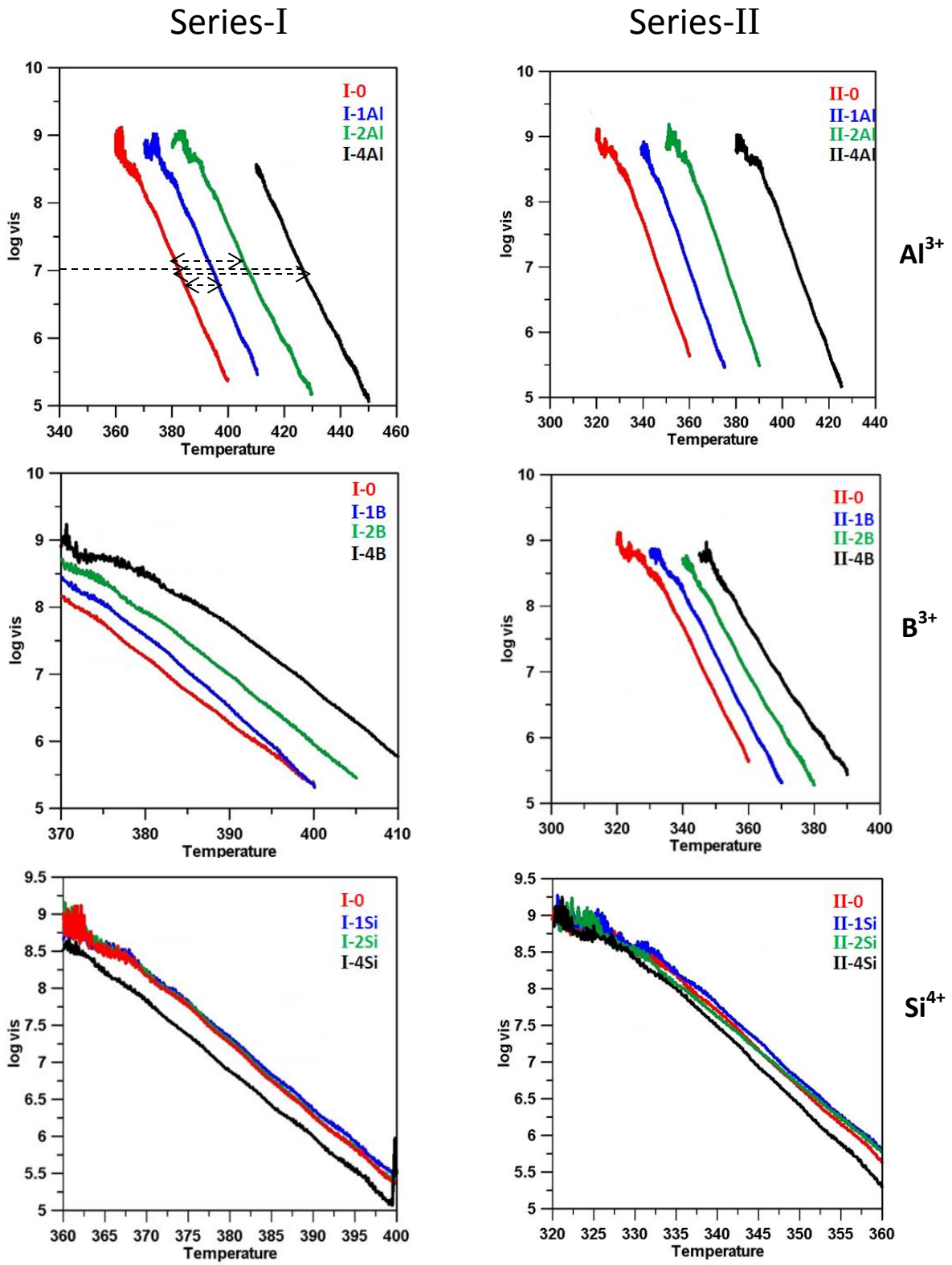

Fig. 4.9 Viscosity measurements Log (vis) Pa.s versus temperature of glasses. The temperature (Arrows showing the temperature difference measured at Log η = 7 Pa.s)

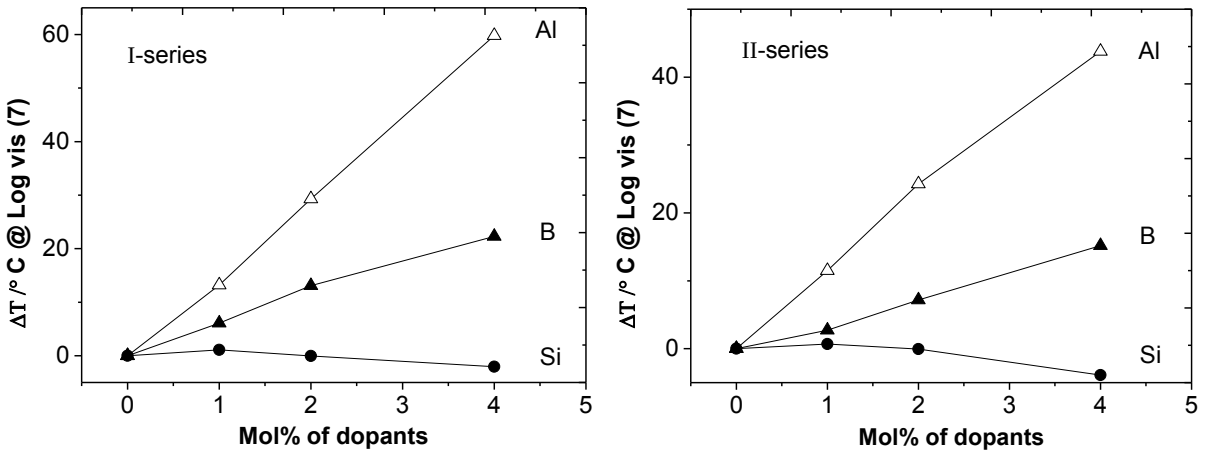

Fig. 4.10 Temperature shift measured at Log 7 as the function of mol% of dopants

II.6 Conclusion

The effects of Al-, B- and Si- doping on the macroscopic properties and stabilities of the two based zinc sodium pyrophosphate compositions have been analyzed in this part.

First, it is noteworthy that both compositions (x = 20 and 33.3) experience similar property and stability modifications when doping elements are inserted. Even if the modification extent can be different, this suggests that the results reported here can be considered as general ones, suitable for the complete zinc alkali pyrophosphate compositions line.

Al_2O_3 doping infers very interesting modifications. The most impressive one concerns the chemical durability improvement since only 2 mol% of Al_2O_3 are necessary to completely suppress the solubilization of our samples. Thermal stability is also significantly improved, since Angell parameter, crystallization enthalpy and kinetic experience 'positive' modifications indicating better thermal stability. Viscosity increase also supports the benefic effect of Al-doping. Finally, the only limitation comes from the significant increase of T_g relative to the Al-doping procedure. However, it is noteworthy than all the formulations present T_g lower than 400°C and can thus be considered as 'low-T_g' formulations in our study.

The insertion of B_2O_3 is also reflected in many property evolutions. The most important improvement has been observed for the thermal stability that is strongly improved in terms of K_A, crystallization enthalpy and kinetics. The B_2O_3 doped glasses present thus a

better resistance against crystallization. Moderate modifications have been observed for the viscosity and T_g parameters. Increasing thermal stability and maintaining an almost constant T_g can be thus obtained by B_2O_3 adding. This doping could thus be considered as a perfect procedure in order to develop low-T_g and stable formulations but, unfortunately, this doping also affects the chemical durability in a unfavorable manner by significantly decreasing it.

All the properties are only marginally affected by the SiO_2-doping procedure. If this tendency is positive for the T_g, it does not improve the thermal or chemical stabilities. SiO_2 insertion appears thus to be inefficient for the development of low-T_g and stable phosphate formulations.

All these above described effects are summarized in *Tab. 4.5*. This part indicates that all the parameters cannot be improved by the use of a single doping element. If it turns out that SiO_2 does not improve the formulation, it also appears that Al_2O_3 strongly improves the chemical durability whereas B_2O_3 has to be preferred if thermal stability is targeted.

Tab. 4.5 A summary of effect of dopants on the properties of the glasses.

Dopants	Low-Tg	Thermal stability	Chemical durability
Al_2O_3	Significant increase	Moderate increase	Remarkable increase
B_2O_3	Limited increase	Remarkable increase	Decrease
SiO_2	No change	Decrease	Decrease

The different behaviors observed for the three different doping elements might be related to different structural modifications induced during the doping procedure. Therefore, understanding the effect of the doping on the properties requires a structural characterization of the materials. Preliminary results retrieved from Raman ^{31}P, ^{27}Al, ^{11}B and ^{29}Si 1D MAS-NMR experiments will be presented and discussed in the next part.

III. Preliminary structural characterization by Raman and 1D MAS-NMR

Raman spectroscopy and 1D MAS-NMR spectroscopies have been used to investigate the structural changes inducing by the doping procedure. The Raman technique was used in a first time to investigate the global change induced by the doping procedure. Then, ^{31}P MAS-NMR was employed to specifically investigate the changes in the phosphate network structure, whereas the doping elements were accurately studied with ^{27}Al, ^{11}B and ^{29}Si MAS-NMR.

III.1. Raman Spectroscopy

Raman spectra obtained on doped glass series samples are shown in *Fig. 4.11*. We remind here that the spectra are mainly composed of 5 bands at 740, 970, 1040, 1140 and 1200 cm^{-1}, corresponding to P-O-P stretching mode, symmetric stretching of Q^0, symmetric stretching of Q^1, P-O stretching mode of Q^1 chain terminator and symmetric stretching mode of Q^2 units, respectively (Brow, 2000).

Similar changes are observed for both glass series. In case of Al- and B- doping procedures, the main bands are all affected by an intensity decrease and a broadness increase. Strong intensity decrease can be observed for the 1040 cm^{-1} band, corresponding to the Q^1 units, which suggest that this particular structural feature is strongly affected by the doping procedure. Interactions between the doping elements and the phosphate network could be highlighted through Raman bands at 1100 cm^{-1} coming from Al-O-P (Boucher, 2005) or B-O-P (Lee, 2007) linkages. Unfortunately, the spectra do not provide unambiguous evidence of such Raman bands. However, in case of 4 mol% B_2O_3 doped glasses, a new band appearing at 685 cm^{-1} that has been previously assigned to P-O-B bonds (Koudelka, 2007), suggests the interaction between the phosphate unit and the borate ions.

Additions of SiO_2 do not change the Raman spectra. The analysis present the same feature and no new signals can be observed, suggesting that SiO_2 interactions with the based glass network are marginal and that the glass structure is not modified.

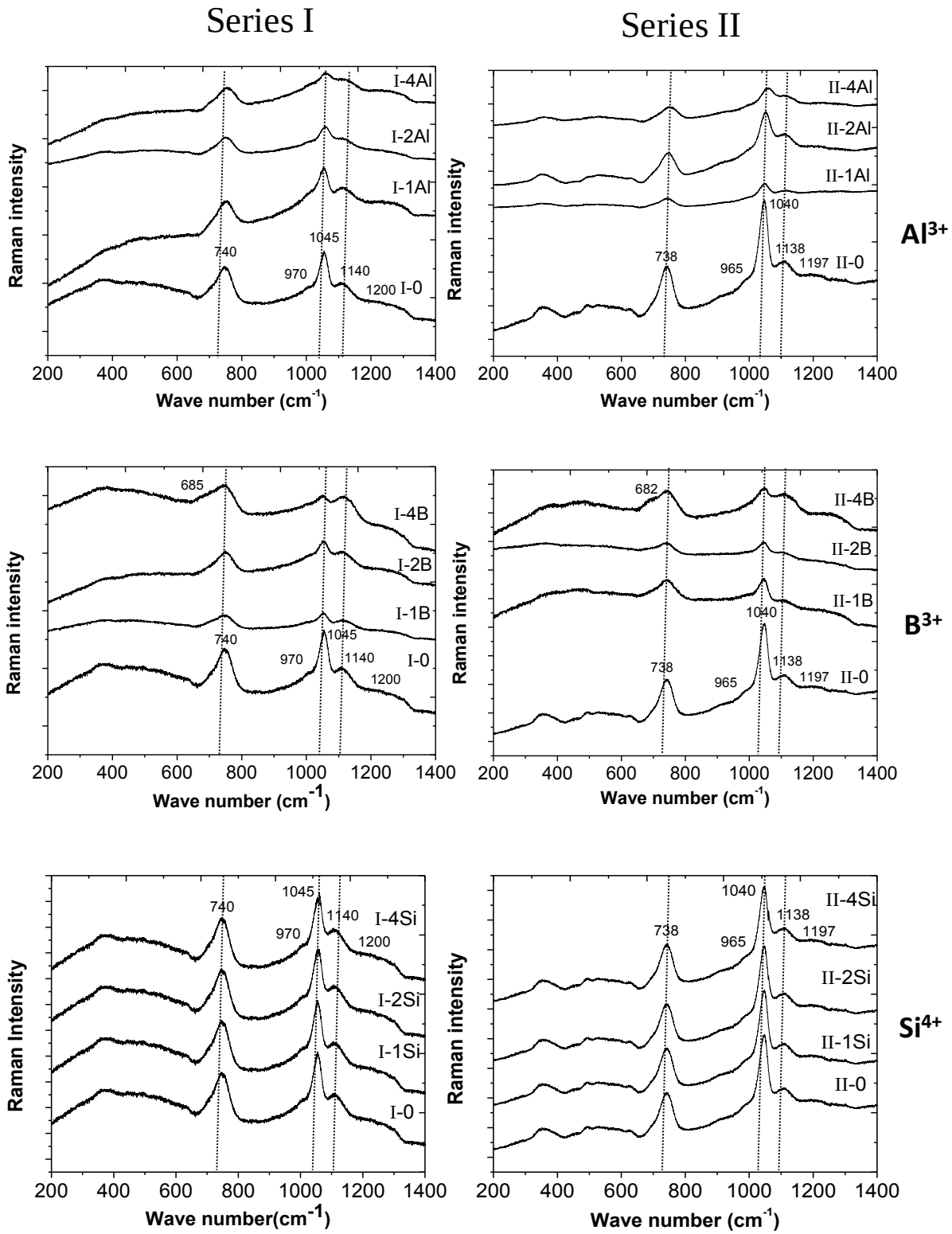

Fig. 4.11. The evolution of Raman spectra of glasses.

No definitive conclusion can be derived from the Raman analysis probably due to the very low amount of doping elements. However, linkages between the B doping elements and the phosphate structure as well as the lack of interaction between the glass network and the Si doping elements have been suggested by these analyses.

III.2. 1D ^{31}P MAS-NMR spectroscopy

1D ^{31}P MAS-NMR experiments were performed on the doped glasses to analyze the changes induced by doping in the phosphate network. All the spectra are reported in *Fig. 4.12*. It is reminded that the spectra of the undoped compositions indicate the presence of three Q^n species which are Q^0, Q^1 (separated in two signals coming from $Q^{1,1}$ and $Q^{1,2}$ species) and Q^2 that are centered around 8, -3 and -18 ppm, respectively. *Fig. 4.12* indicates significant changes, showing that the phosphate network is significantly affected by the three doping procedure. Moreover, it turns out that the three doping elements induce similar evolutions of the ^{31}P analysis that consist in the complete disappearance of the Q^0 signal and in an increase of the signal centered on the right side of the analysis around -20 ppm. It is noteworthy that if the increased signal superimpose with the Q^1 resonance in case of Al- and B- doping procedure, SiO_2 insertion leads to a well resolved and almost completely separated signal.

The signal increase in the -20 ppm region can originate from:

- the appearance of a new signal with a chemical shift close to the Q^2 units. The new signal will be without any doubt related to the interactions between the doping elements and the phosphate network;
- an increases of the Q^2 proportion induced by the doping procedure. Polymerization of the phosphate network is not expected to happen during the doping procedure and can only be explained using a phase separated glass model. Indeed, we can imagine that the doping elements are clustering to create a separated and isolated network with no interactions with the phosphate species. This separated network could attract some zinc and sodium ions necessary for its development. The zinc and sodium ions will thus be extracted from the phosphate network that will indirectly lead to a phosphate polymerization, reflected in the observed Q^2 increases.

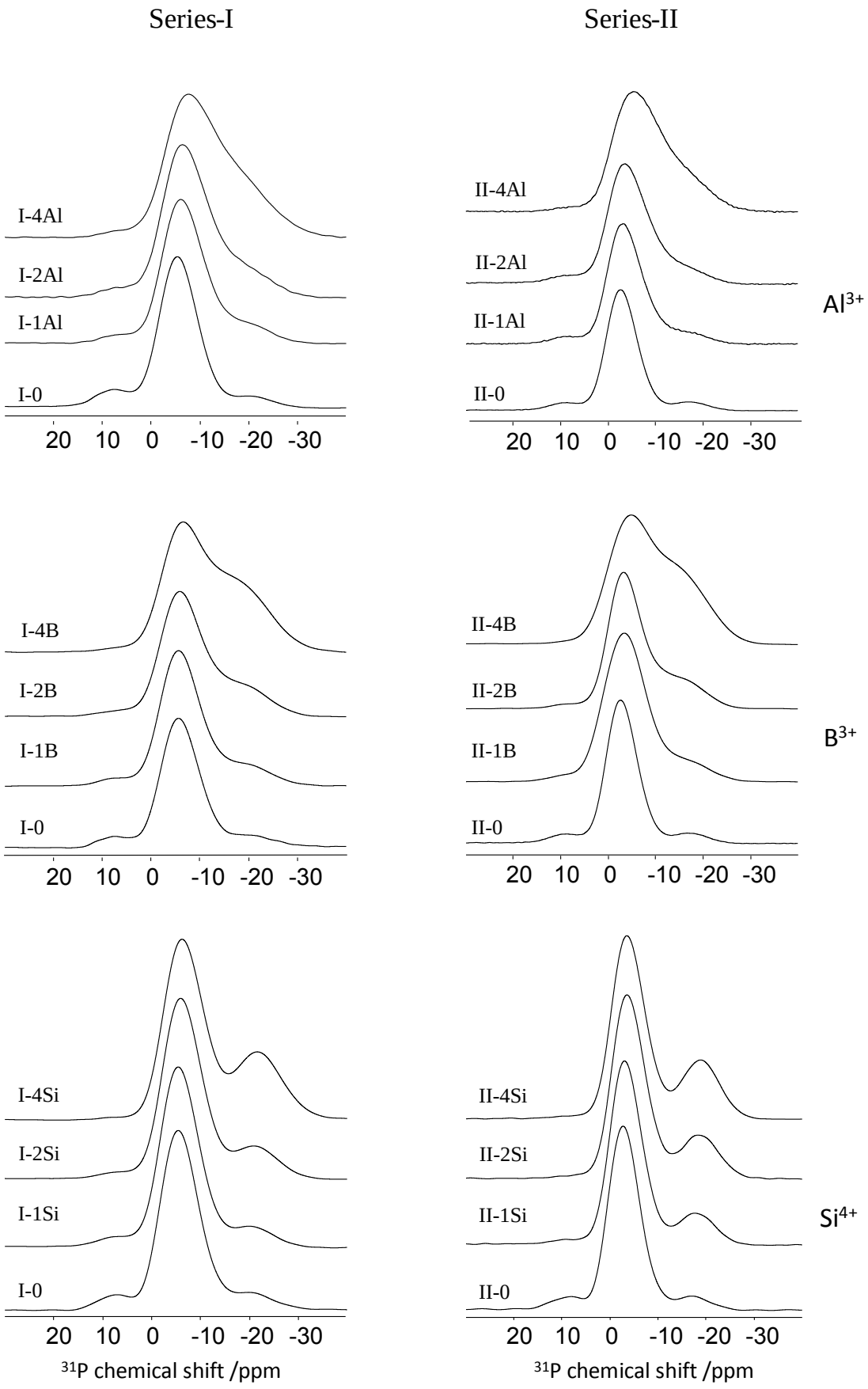

Fig. 4.12 1D ^{31}P MAS NMR spectra of glasses.

Definitive conclusion cannot be derived from the presented work based on 1D ^{31}P MAS-NMR analysis. However, the second scenario, implying a lack of interactions between the doping elements and the phosphate network, is not in line with the Raman analyses that suggest the formation of P-O-B bonds.

III.3. 1D MAS-NMR analysis of the doping elements

1D ^{27}Al, ^{11}B and ^{29}Si MAS-NMR experiments were performed on the doped glasses in order to investigate the doping element insertion within the glass network. Special emphasis will be paid to determine the coordination state of the doping element since Al^{3+} can be present under 4-, 5- and 6- fold, B^{3+} under 3- and 4-fold and Si^{4+} under 4- and 6- fold coordination states.

III.3.1. Coordination state of Al^{3+}

The spectra obtained from ^{27}Al 1D MAS NMR experiments are displayed in *Fig. 4.13*. Three different resonances at 39, 10, -15 ppm (series I) and at 41, 12, -14 ppm (series II) glasses are assigned to Al^{IV}, Al^{V} and Al^{VI} species respectively. These chemical shifts are consistent with the previous study (Brow 1993, Egan 2000 and Wullen 2007).

Among the three peaks (Al^{VI}, Al^{V} and Al^{IV}), the signal coming from Al^{VI} is dominant in all the cases as expected from the very low concentration of Al_2O_3 ($\leq$ 4 mol%) in the glass (Brow 1991). The relative proportion of 4-, 5- and 6-coordinated Al species were also determined, using DMfit software with Czjzek's model taking into account a distribution of the quadrupolar parameter (Czjzek 1981) (a simulation being shown in *Fig 4.14*) and the values are presented in *Tab 4.6*. With the increase in Al_2O_3 loading, the proportion of 6-coordinated species experienced a very important decrease in series I (by 20%) than in series II (by 3%). These evolutions of 4-,5- and 6-cordinatated Al versus Al/P ratio are further compared with the previous study on Na_2O-Al_2O_3-P_2O_5 system (Brow 1990) and sketched all together in *Fig. 4.15*.

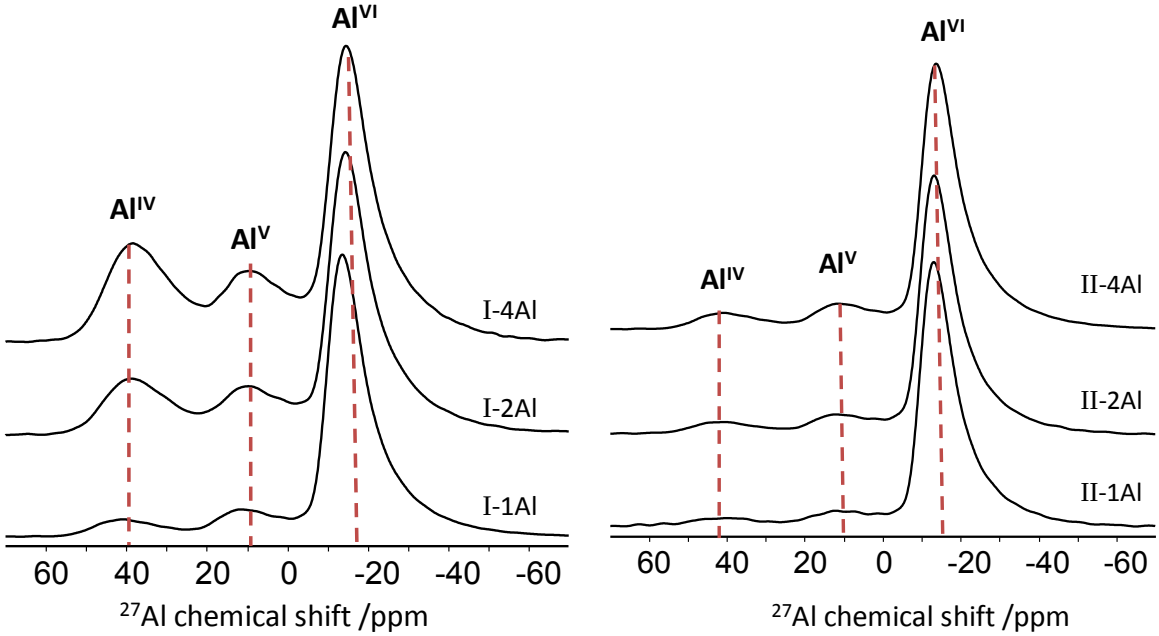

Fig. 4.13 1D ^{27}Al MAS-NMR spectra of series-I and series-II glasses.

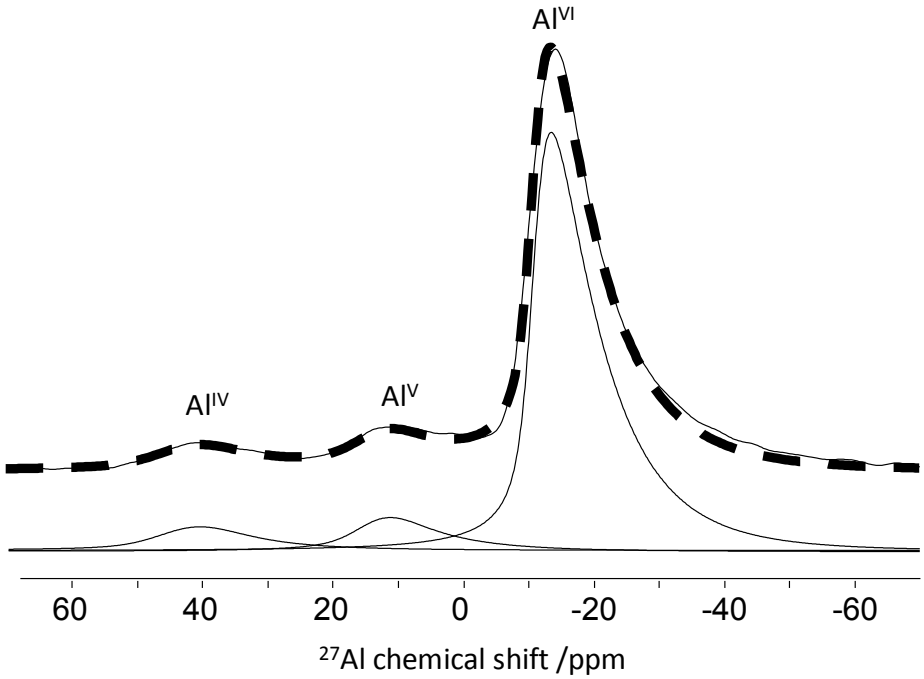

Fig. 4.14 Deconvolution of 1D ^{27}Al MAS-NMR spectra of representative glass sample II-4Al.

Tab. 4.6. The relative concentration of Al polyhedra as determined from the relative areas of the peaks in the ^{27}Al MAS NMR spectra.

Samples	Al^{IV} (Rel%)	Al^{V} (Rel%)	Al^{VI} (Rel%)
I-1Al	15	12.6	72.4
I-2Al	20.4	15.9	63.7
I-4Al	29.5	18.3	52.2
II -1Al	6	5.4	86.6
II -1Al	6.3	6.9	86.7
II -1Al	6.9	9.3	83.8

Series-I Series-II

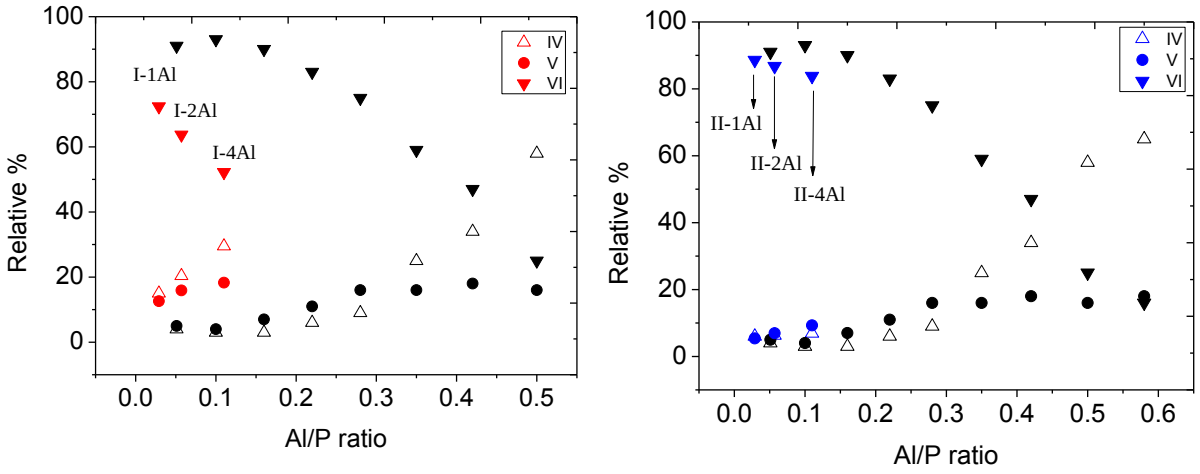

Fig. 4.15 The effect of composition on the relative concentration of Al polyhedral of the glasses compared with the evolution obtained from Na_2O-Al_2O_3-P_2O_5 system. Series I- ▼:Al^{VI}, ●:Al^{V}, △ :Al^{IV},; Series II-▼ :Al^{VI},● :Al^{V} △ :Al^{IV},

Referring to the *Fig. 4.15*, if data of series II are in line with the result of the literature, large deviation of the evolution of coordination state of Al in series I (zinc rich glasses) indicates that the higher coordination states of Al is less favored in those compositions. This is probably due to the stiffer and more disordered phosphate network induced by the formation of Zn-O bonds that might restrict Al^{3+} of higher coordination states. Nevertheless, the majority of Al polyhedra still exists as 6-coordinated species.

III.3.2. Coordination state of B^{3+}

A 9.4 T NMR spectrometer was used for ^{11}B 1D MAS NMR. The ^{11}B NMR spectra of the glasses from series-I and series-II are displayed in *Fig. 4.16*. A symmetric peak centered at -3 ppm is observed, which is the characteristic feature of tetrahedral boron sites. No peaks near 12 to 19 ppm are observed indicating the absence of trigonal boron. Thus the ^{11}B NMR spectra confirm that boron enters into the glass network only as tetrahedral units at addition of less than 4 mol% B_2O_3. In some study, trigonal boron starts to appear when B/P is ≥ 0.25 in ZnO-B_2O_3-P_2O_5-TeO_2 system (Vosejpkova 2012) and B/P $\geq$ 0.18 in Li_2O-B_2O_3-P_2O_5 (Raguenet 2011). Compared to these compositions, our glasses have lower B/P ratio of less than 0.1 and are thus in line with the previous studies.

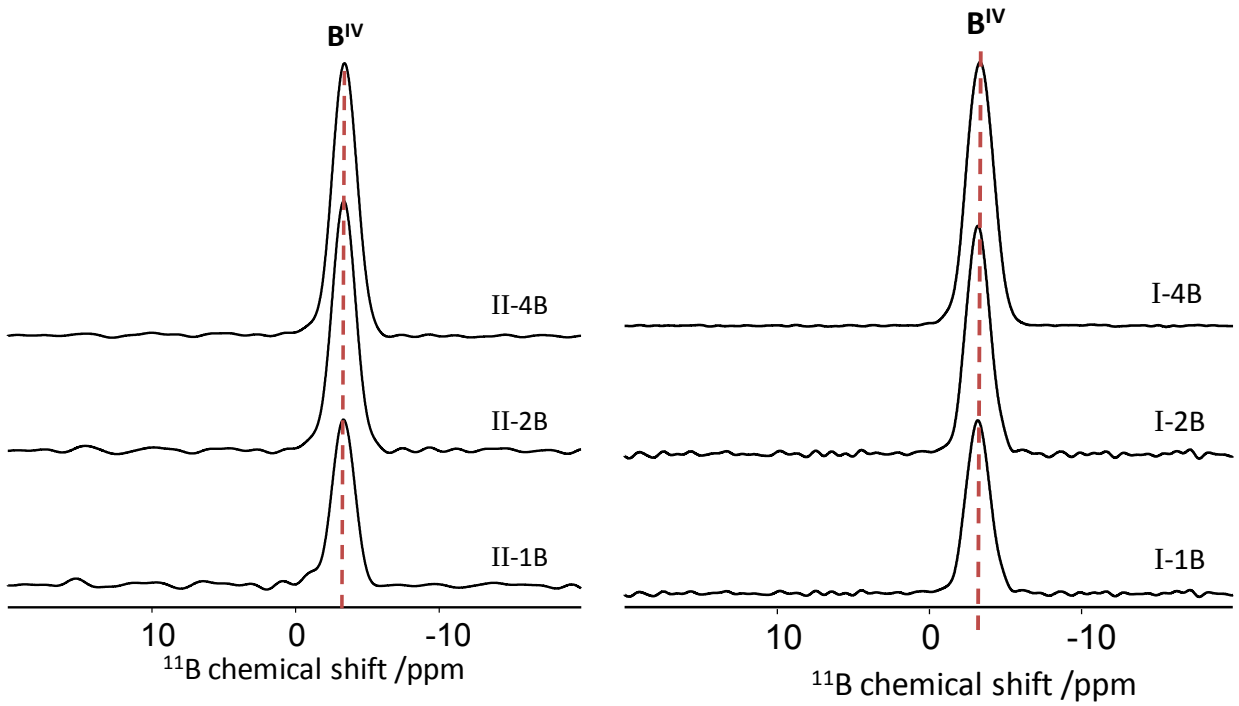

Fig. 4.16. 1D ^{11}B MAS-NMR spectra of series-I and series-II glasses obtained.

III.3.3. Coordination state of Si^{4+}

^{29}Si MAS-NMR spectra are reported in *Fig. 4.17*. It is reminded here that the glasses used for the experiments have been prepared using 100% ^{29}Si enriched SiO_2. The spectra obtained on the glass series I exhibit similar feature and are composed by a single peak countered at – 117 ppm. The first information that can be derived from these experiments is that Si^{4+} is present in the glasses under tetrahedral coordination state. No signal was observed in the Si^{VI} region (near -200 ppm), ruling out the presence of octahedral silicon as observed by Dupree in phosphate compositions doped with SiO_2 oxide (Dupree, 1987). In addition to the coordination state, the chemical shift values also indicates that the silicate species are in Q^4 configuration in which each Si^{4+} is connected to 4 other silicate tetrahedral. These structural units exclude the formation of P-O-Si bonds and indicate thus the silica ions do not enter into the phosphate network and do not interact with this latter. Doping with SiO_2 lead to the formation of an amorphous SiO_2 rich part separated from the phosphate network. The very high electrostatic field strength of both ions is probably at the origin of this lack of interactivity. The spectra obtained on the glass series II (not shown here) follow the same tendency and lead to the same conclusion.

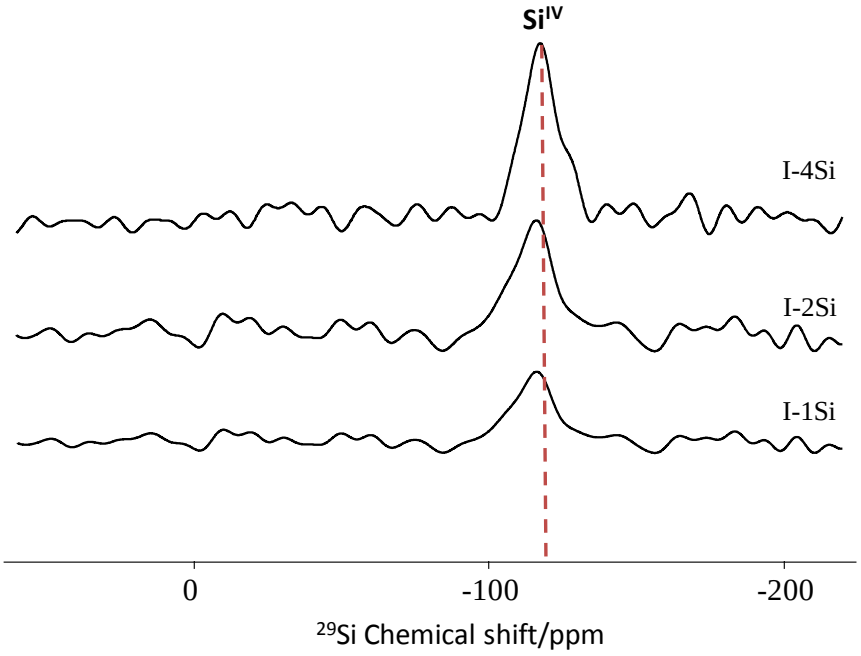

Fig. 4.17. 1D ^{29}Si spectra of series-I glasses.

The slight or inexistent evolution of the properties and stabilities observed during the Si-doping is thus explained by a non-insertion of this doping element. All the evolutions observed in this part are thus not due to the doping procedure but derive from the slight deviation from the undoped compositions induced by the $y(50SiO_2\text{-}50P_2O_5)\text{-}(100\text{-}y)(ZnO\text{-}Na_2O\text{-}33.4P_2O_5)$ composition lines as well as for the ^{31}P NMR spectra. It is noteworthy that higher preparation temperatures (up to 1300 °C) have been used to facilitate the silica insertion but no glasses containing dispersed tetracoordinated silicon ions that should appear as Q^0 units near -80 ppm or Si^{VI} near -200 ppm in the ^{29}Si MAS-NMR analysis, have been obtained.

IV. Conclusion

The effect of Al-, B- and Si- doping on the properties, stabilities and structure of the selected zinc sodium pyrophosphate glasses have been analyzed in this chapter.

The effects of each doping procedure on density, molar volume, chemical durability, T_g, thermal stability and viscosity have been determined. It turns out that:

(i) all the doped compositions can be considered as low-T_g formulation since this parameter never exceed 400°C;

(ii) macroscopic and molar volume are marginally affected by the doping procedure;

(iii) Al_2O_3 strongly improves the chemical durability, has a positive effect on the thermal stability but lead to a significant increase of T_g. Al-doping has thus to be considered to prepare materials presenting a good resistance against water attack;

(iii) B_2O_3 strongly improves the thermal stability without changing the T_g in a significant way. In our systems, the chemical durability is strongly altered by this doping. Therefore, B_2O_3 doping appears to be valuable in case of materials requiring high resistance against crystallization;

(iv) SiO_2 does not improve neither thermal nor chemical stability and doping using this element appears thus to be inefficient.

Preliminary structural investigations performed with Raman and 1D MAS-NMR spectroscopies also provide interesting results about the doping insertion mechanism that can be used to partially understand the doping procedure effect:

(i) the ^{31}P MAS-NMR spectra clearly show a modification of the phosphate network. Unfortunately, various speculations could be made to explain this structural change and no definitive conclusion can be derived about the interactions between phosphate and the doping elements. Correlation NMR will be used in the next chapter to address this particular point.

(ii) ^{29}Si MAS-NMR show that Si^{4+} is present as tetrahedral species in the doped samples. Moreover, the chemical shift value indicates that the Si elements present a Q^4 structure and thus do not interact with the phosphate network. The low impact of Si-doping on the properties and stabilities is thus explained by the fact that Si does not interact with the glass network but form a separated network. All the minor changes in the properties come from the minor evolution of the global glass compositions.

(iii) ^{27}Al and ^{11}B MAS-NMR show that Al^{3+} and B^{3+} enter into the network as octa- and tetra-hedral species, respectively. If the different coordination state adopted by the two doping elements appears to be a key information to understand the different effect on the properties and stabilities induced by the Al- and B- doping procedures, many other questions have to be addressed to provide a complete overview on that question. Questions about the presence or absence of Al-O-P and B-O-P bonds, the extent of mixing and about the clustering or complete dispersion of doping elements within the phosphate structure have to be answered.

All these questions will be addressed using correlation NMR in the next chapter.

References

Ahmadi Mooghari, H R, A Nemati, B Eftekhari Yekta, and Z Hamnabard. *Ceram. Int.* 38(4) (2012): 3281-3290.

Boucher, S, J Piwowarczyk, R F Marzke, B Takulapalli, G H Wolf, and W T Mcmillan. *J. Eur. Ceram. Soc.* 25 (8) (2005): 1333-1340.

Brow, R K. *J.Am. Ceram. Soc.* 76 (8) (1993): 913-918.

Brow, R K. *J. Non-Cryst. Solids.* 263/264 (2000): 1-28.

Brow, R K. *J. Non-Cryst. Solids.* 76 (1993): 913-918.

Brow, R K, R J Kirkpatrick, and G L Turner. *J.Am. Ceram. Soc.* 73 (8) (1990): 2293-2300.

Brow, R K, R J Kirkpatrick, and G L Turner. *J. Am. Ceram. Soc.* 8 (1991): 1430-38.

Bunker, B C, G W Arnold, and J A Wilder. *J. Non-Cryst. Solids.* 64 (1984): 291-316.

Czjzek, G, J Fink, F Gotz, H Schmidt, J M D Coey, J P Rebouillat, and A Lienard. *Rev. B.*23 (1981): 2513-2530.

Donald, I W, and B L Metcalfe. *J. Non-Cryst. Solids.* 348 (2004): 118.

Dupree, R. *Nature*, 328 (1987): 416-417.

Egan, J M, R M Wenslow, and K T Mueller. *J. Non-Cryst. Solids.* 261 (2000): 115-126.

Harada, T , H In, H, Takebe, and K Moringa, *J. Am. Ceram. Soc.* 87 (3) (2004): 408-411.

He, Y, and D E Day. *Glass. Technol.* 32 (1991): 166.

Koudelka, L, P Mosner, M Zeyer-Dusterer, and C Jager. *J. Phys. Chem. Solids.* 68 (2007): 638-644.

Lee, S, J Kim, and D Shin. *Solid State Ionics.* 178 (2007): 375-379.

Lim, J W, M L Schmitt, R K Brow,and S W Yung, *J. Non-Cryst. Solids.* 356 (2010): 1379-1384.

Liu, C H C, and G E Maciel. *J. Am. Chem. Soc.* 118 (1996): 5103-5119.

Massiot, D, et al. *Magn. Reson. Chem.* 40 (2002): 70.

Metwalli, E, and R K Brow. *J. Non-Cryst. Solids.* 289 (1-3) (2001): 113-122.

Peng, Y B, and D E Day. *Glass Technol.* 32 (1991): 166.

Raguenet, B, G Tricot, G Silly, G Ribes, and A Pradel. *J. Mater. Chem.* 21 (2011): 17693.

Ray, N H. *Phys. Chem. Glasses.* 16 (1975): 75.

Ray, N H, R J Plaisted, and W D Robinson. *Glass. Technol.* 17 (1976): 66.

Takebe, H, Y Baba, and M Kuwabara. *J. Non-Cryst. Solids.* 352 (2006): 3088-3094

Tindyala, M A, and W R Ott. *Ceram. Bull.* 57 (1978): 432.

Van Wazer, J R. *J. Am. Ceram. Soc.* 72 (1950): 644-647.

Vosejpkova, K, L Koudelka, Z Cernosek, P Mosner, L Montagne, and B Revel. *J. Phys. Chem. Solids.* 73 (2012): 324-329.

Wullen, L V, G Tricot, and S Wegner. *Solid State Nucl. Mag. Reson.* 32 (2007): 44-52.

Youssef, N H, M S Belkhiria, J Videau, and M B Amara. *Mater. Lett.* 44 (2000): 269-274.

Chapter E

New structural insights from correlation NMR

1D/2D correlation NMR techniques have been used in this chapter to analyze in details the interactions between the Al- and B- dopants and the phosphate network. The presence or absence of P-O-X (X= Al or B) bonds will be definitively addressed using the heteronuclear dipolar D-INEPT sequence. Then, the chemical environment of dopants will be investigated using the REDOR (tracing the X-O-P bonds) and the DQ-SQ (tracing the X-O-X bonds) technique. The glass structure will thus be discussed in terms of phosphate network modifications and doping element chemical environment. Finally, the material properties and structural information will be confronted.

I. Introduction

Preliminary information about the structural changes induced by doping was obtained by Raman and 1D MAS-NMR spectroscopies as reported in the previous chapter. The first level of information was related to the phosphate network modifications. The ^{31}P MAS-NMR spectrum evolution suggests direct (presence of P-O-X bonds) or indirect (phase separation mechanism) modifications but does not provide any unambiguous answer. Raman spectra suggest the formation of P-O-B but do not afford any clear evidence of such species in case of the Al-doping procedure. Then, 1D ^{27}Al, ^{11}B and ^{29}Si MAS-NMR lead to the determination of the coordination state of the doping element within the glass structure. The results show that Al^{3+}, B^{3+} and Si^{4+} enter into the glass network as mainly six-, four- and four- fold coordinated species, respectively. More information was obtained for ^{29}Si since the chemical shift indicates a Q^4 structure from which existence of P-O-Si can be ruled out. Therefore, it was concluded that the Si-doping procedure does not allow for interaction between the Si^{4+} ion and the glass structure but provide some separated networks. This behavior explains the weak impact of Si-doping on the properties and stabilities of the low-T_g phosphate glasses.

However, the structural characterization based on Raman and 1D MAS-NMR was far from being complete. Additional information on the P/doping element interactions was required in order to propose a clear and detailed structural picture of the doped glasses.

1D/2D correlation NMR techniques have been used to derive valuable information about these interactions. In a first time, the phosphate network modifications were investigated through the edition of P/X correlation maps from which the presence and absence of P-O-X bonds will be definitively inferred. The low doping element amounts require the use of a stable and sensible pulse sequence. The ^{31}P{X} D-INEPT sequence was chosen for this work. Then, the chemical environment around the doping element was investigated by the X{^{31}P} REDOR and X DQ-SQ sequence. The former gives access to the number of attached P around each doping element and the latter probes the possible linkages between the doping elements. All this information was then used to discuss about the extent of solubilisation or clustering of the doping within the glass matrix. The structural questions addressed in this part and the associated pulse sequences are reported in *Tab. 5.1*.

Tab. 5.1 Questions of structural order and NMR sequences that will be used to answer.

	Structural question	Associated correlation NMR technique (X= ^{27}Al, ^{11}B)
Phosphate network modifications	Presence / Absence of P-O-X bonds?	^{31}P {X} D-INEPT
Local environment of doping elements	How many attached P? X(OP)n	X{^{31}P} REDOR
	Presence / absence of X-O-X bonds?	X- DQ-SQ

II. Presence/ absence of P-O-X bonds? (D-INEPT sequence)

II.1. Application of the D-INEPT sequence

Correlation maps are used in this part to assess about the presence or the absence of P-O-X bonds in the glass structure. As previously mentioned the P/X interactions could be analyzed with different techniques as the CP (Cross-Polarization) (Hartmann 1962), the J- and D- Scalar HMQC (Scalar- and Dipolar- Hetero-nuclear Multiple Quantum Coherence) (Lesage 1998 and Trebosc 2007) or the J- and D- INEPT (Scalar- and Dipolar- Insensitive nuclei Enhanced by Polarization Transfer) (Morris 1979 and Trebosc 2007) sequences. In our case, due to the very low amount of doping elements, a robust, sensitive and easily optimized sequence was necessary. Among all the correlation techniques, the D-INEPT sequence appears to be the best compromise. Compared to J-HMQC and J-INEPT techniques, the D-INEPT sequence is based on the dipolar interaction that is larger than the scalar one (used in the above mentioned techniques) and thus easier to detect. Compared to the D-HMQC, the D-INEPT sequence produces a filtered ^{31}P spectrum whereas D-HMQC provides X spectrum. Obtaining the ^{31}P spectrum thus does not require the acquisition of the complete 2D leading to very long measuring time in our case. Compared to the CP experiment, the D-INEPT has proven to be more efficient and does not require time consuming process. When the complex

Hartmann Hahn conditions have to be fulfilled in case of the CP, simple rf strength calibration on the ^{31}P channel {vrf(^{31}P) = 2*vrot} is required to reintroduce the dipolar interaction with the $SR4^2_1$ method used in our experiments. Therefore, the $^{31}P\{^{27}Al\}$ and $^{31}P\{^{11}B\}$ D-INEPT technique were applied to the doped samples. The obtained filtered ^{31}P spectra, showing the phosphate units that have benefitted from the magnetization transfer (and that are thus involved in P-O-X bonds), are presented in *Fig. 5.1*.

All the spectra exhibits signal, independently of the nature and the amounts of the dopants, for both glass series. It is noteworthy that in spite of the low doping amount, good signal to noise ratio have been obtained, proving the excellent sensitivity of the D-INEPT technique. This global information indicates that P-O-X bonds exist within the glass structure. The doping elements are thus directly interacting with the phosphate network, leading to the observed evolutions of the ^{31}P spectra described in the previous chapter. The chemical shift values observed in the filtered spectra also explain the increase of the signal between -10 and -20 ppm observed in the global ^{31}P analysis. Therefore, we can conclude that the phosphate network is directly modified by the doping procedure through the creation of P-O-Al and P-O-B bonds. The phase separation mechanism proposed in the previous chapter can thus be excluded on the base of the results presented in *Fig. 5.1*.

The asymmetric line shape of the filtered spectra indicates the possible presence of more than one overlapping signals. Thus, these projections were simulated with the DmFiT software using minimum number of contributions and the results have been reported with the experimental data in *Fig. 5.1*.

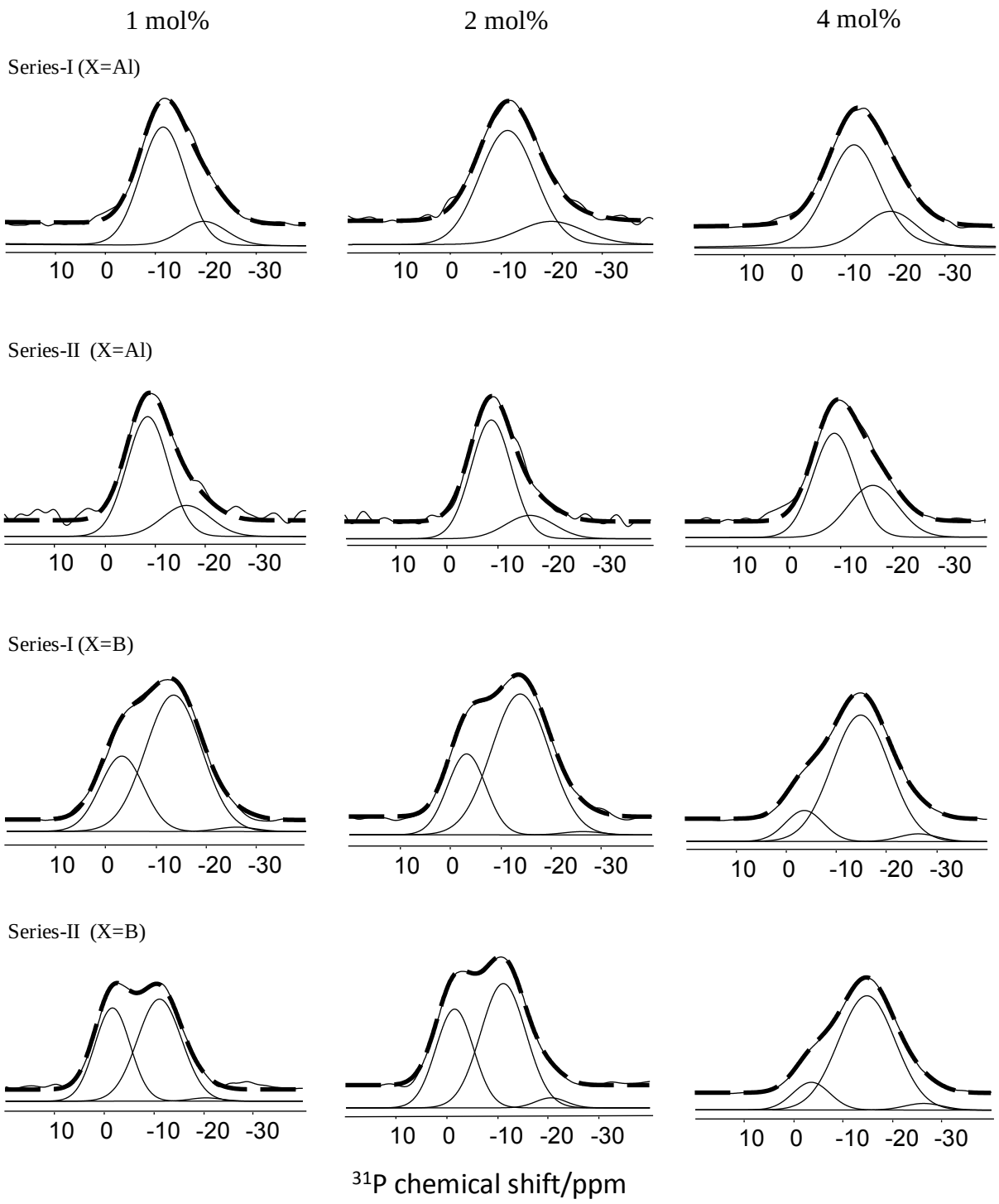

Fig. 5.1 1D ^{31}P{X} D-INEPT spectra obtained on both glass series. The experimental data are accompanied by the simulations (dashed line) performed with the DM-Fit software.

The Al-doped samples filtered spectra can be efficiently deconvoluted using a two-component system, indicating that two distinct phosphate units attached to Al co-exist within the glass structure. It is noteworthy that a 2D $^{31}P\{^{27}Al\}$ D-INEPT spectrum would have afforded a more detailed vision by distinguishing the P attached to Al^{VI}, Al^{V} and Al^{IV} through the indirect dimension. However, the Al^{IV} and Al^{V} low intensities led to low correlation signals that cannot be efficiently used for the structural characterization. Therefore, we will consider phosphate attached to global aluminium sites in the following and will denoted this species as P(Al).

The B-doped samples filtered spectra have been simulated using a three component system, including a very low intensity signal but necessary to reach a good fit. This result indicates thus that 2 main phosphate units attached to boron co-exist in the glass structure accompanied by a third one presenting very low proportion. Since only B^{IV} species are present in the glass formulations, P attached to boron will be denoted as $P(B^{IV})$ species.

The chemical shift values and full width at half maximum of each P(X) contribution have been derived from the simulations and are reported in *Tab. 5.2*. It is noteworthy that the chemical shift values of all the P(X) species are postponed towards more negative values in the glass series I in a good agreement with the highest electrostatic field strength presented by this composition owing to its higher ZnO content.

Recent literature about correlation NMR investigations on alumino- and boro-phosphate based systems (Van Wüllen 2007, Wegner 2008 and Raguenet 2011) were used to assign the P(Al) and P(B) based on their chemical shift values. All these studies have used the improved Q^{n}_{mX} notation to describe the phosphate units where n is the number of attached P and m the number of attached X elements.

In case of the Al-doped samples, the two P(Al) signals centered around -12 and -20 ppm for the glass series I and -9 and -16 ppm for the glass series II have been assigned to Q^{1}_{1Al} and Q^{1}_{2Al} sites, respectively (van Wüllen 2007 and Wegner 2008). Assuming that the majority of Al is in six-fold coordinated state, we can conclude that the glass structures contain phosphate connected to one phosphate and one octahedral alumina and phosphate connected to one phosphate and two octahedral alumina ions. It is noteworthy that both species are present independently of the Al_2O_3 content, showing that the proportions used in our system lead to the formation of these two mixed units only. Moreover, in all the three samples, the Q^{1}_{1Al} species appears to be the dominant mixed unit.

In case of the B-doped samples, the two main P(B^{IV}) signals are centered around -3 and -14 ppm and -2 and -11 ppm, for glass series I and II, respectively. These two signals were assigned to $Q^0{}_{1B^{IV}}$ (a P connected to one B^{IV} unit and no PO_4^{3-} species) and $Q^1{}_{1B^{IV}}$ (a P connected to one phosphate and to one B^{IV} unit). The third and low intensity signal centered at -26 and -21 ppm in glass series I and II, respectively, has been assigned to $Q^2{}_{1B^{IV}}$ species (a P connected to 2 other P and 1 B^{IV} units). Here again, the three signals are similar on the 3 samples, showing that the doping procedure used here produce only 3 mixed P units. All the glasses contain $Q^1{}_{1B}$ as the main component. The assignments of the P(Al) and P(B) species deduced from comparison with literature data have been reported in *Tab. 5.2*.

Tab. 5.2 Chemical shift, FWHM of the decomposed peaks of the glasses containing alumina and boron.

	δiso(ppm)/ FWHM			Assignment
Series-I	1 mol %	2 mol%	4 mol%	
Al_2O_3	-11.4 / 11.1	-11.4 / 11.1	-11.7 / 11.2	Q^1_{1Al}
	-19.8 / 14.4	-19.8 / 14.5	-19.8 / 15.0	Q^1_{2Al}
B_2O_3	-3.5 / 8.3	-3.2 / 8.3	-3.5 / 8.8	$Q^0_{1B^{IV}}$
	-13.8 / 13.0	-14.2 / 14.2	-15.5 / 14.4	$Q^1_{1B^{IV}}$
	-26.3 / 9.0	-26.3 / 9.0	-26.3 / 9.2	$Q^2_{1B^{IV}}$
Series-II	1 mol %	2 mol%	4 mol%	
Al_2O_3	-8.5 / 9.7	-8.6 / 9.3	-8.7 / 9.6	Q^1_{1Al}
	-16.0 / 11.2	-16.0 / 10	-16.3 / 11.2	Q^1_{2Al}
B_2O_3	-1.5 / 8.4	-1.5 / 8.7	-1.9 / 9.8	$Q^0_{1B^{IV}}$
	-11.1 / 10.4	-11.1 / 10.6	-12.2 / 12.5	$Q^1_{1B^{IV}}$
	-21.0 / 7.4	-20.5 / 7.2	-22.3 / 10	$Q^2_{1B^{IV}}$

It appears from these results that both doping procedures result in the formation of $Q^1{}_{1X}$ species as the main mixed unit. Both doping elements seem to interact with the dimeric structure through the formation of a P-O-X linkages base on a $Q^{1,1}$ site without destroying any POP bond. The formation of such linkage makes the dimeric structure unmodified. However, in addition to this main result, some differences on the additional species can be observed:

- in case of Al-doping, Q^1_{1Al} is accompanied by Q^1_{2Al} species. This latter comes from the attachment of two Al^{VI} species on the dimeric phosphate structure. No formation of mixed unit involves POP breaking.

- in case of B-doping, $Q^0_{1B^{IV}}$ and $Q^2_{1B^{IV}}$ are created in addition to the $Q^1_{1B^{IV}}$ unit. This time, the common feature among the three species is the number of boron attached to the phosphate units. The difference comes from the number of attached P. Formation of $Q^0_{1B^{IV}}$ could originate from attachment of B to a Q^0 site or from attack of a $Q^{1,1}$ site by B with breaking of POP bond replaced by POB one. If the former mechanism is unlikely owing to the very low amount of Q^0 in the undoped formulation, the second mechanism requires POP breaking and is thus based on a completely different mechanism than in case of Al-doping.

The mixed species identified in this part through their chemical shift values are sketched in *Fig. 5.2*, accompanied by the species previously observed in the undoped compositions.

II.2. Simulation of the 1D ^{31}P MAS-NMR spectra

The 1D ^{31}P MAS-NMR spectra, presented in *Fig. 4.12* in the previous chapter, have been re-analyzed at the light of the new information derived from the D-INEPT sequence. NMR parameters (δcs and FWHM) of $Q^{1,1}$, $Q^{1,2}$ and Q^0 sites (determined in the previous chapter) and the different P(X) species (*Tab. 5.2*) have been combined to produce complete fits of the ^{31}P MAS-NMR spectra from which the relative proportions between the different units have been derived. It is noteworthy that these fits were obtained by optimizing the intensity of each contribution while almost maintaining values for the chemical shifts and FWHM parameters. The simulations are presented in *Fig. 5.3-5.6* for the Al-doped glass series I and II and the B-doped glass series I and II, respectively. The NMR parameters deduced from these simulations are reported in *Tab 5.3 and 5.4* for the Al- and B-doped samples, respectively.

Fragments that are not connected to doping elements

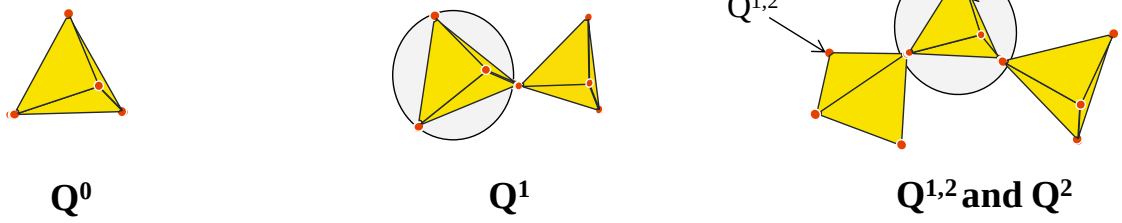

Q^0 **Q^1** **$Q^{1,2}$ and Q^2**

Fragments of Al-Doped glasses

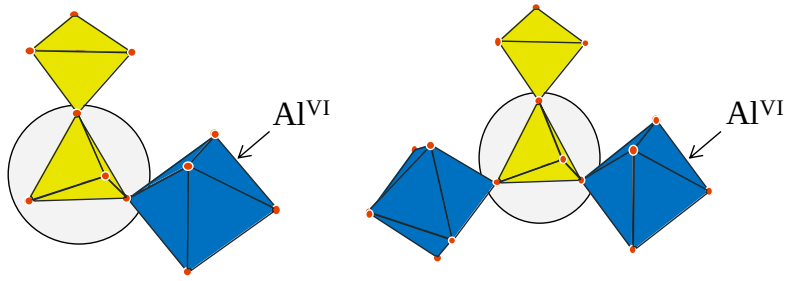

$Q^1{}_{1Al}{}^{VI}$ $Q^1{}_{2Al}{}^{VI}$

Fragments of B-Doped glasses

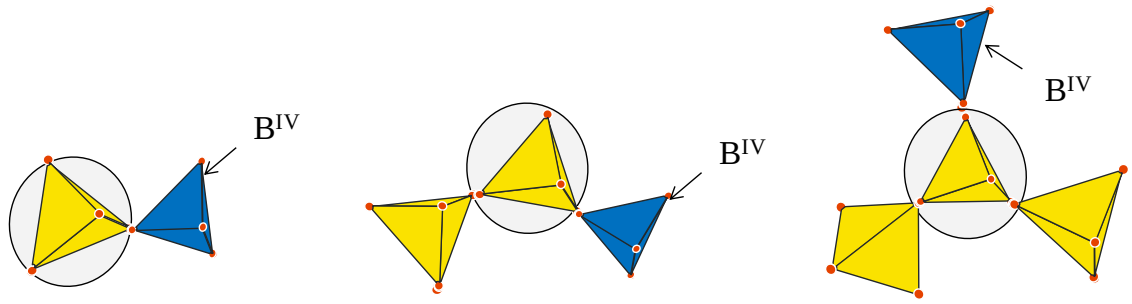

$Q^0{}_{1B}{}^{IV}$ $Q^1{}_{1B}{}^{IV}$ $Q^1{}_{1B}{}^{IV}$

Fig 5.2 Sketch of extended fragments glasses with Al_2O_3 and B_2O_3 derived from D-INEPT experiment.

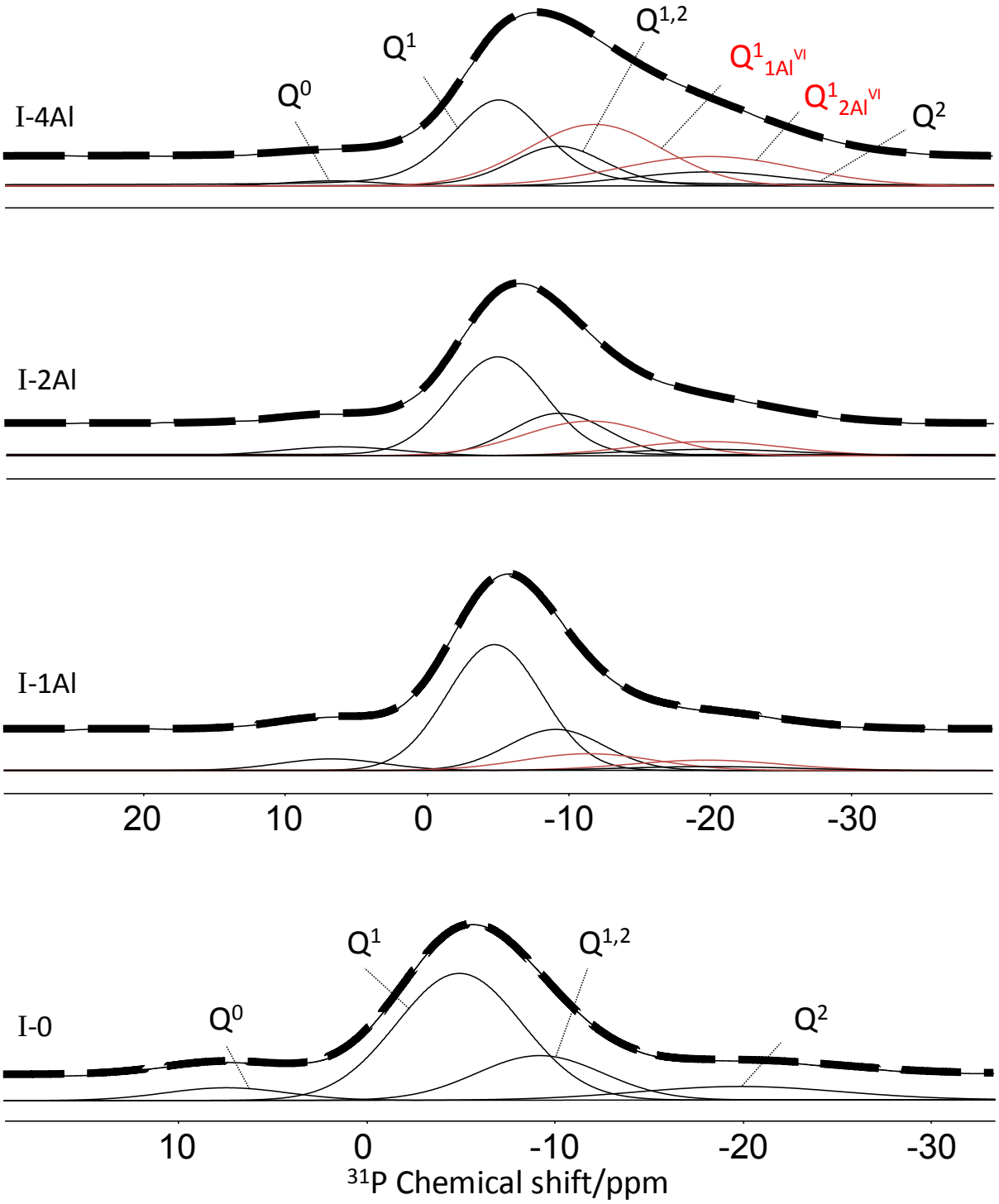

Fig. 5.3 Deconvolution of 1D ^{31}P spectra and the assignment of the sites for series I glasses doped with Al_2O_3.

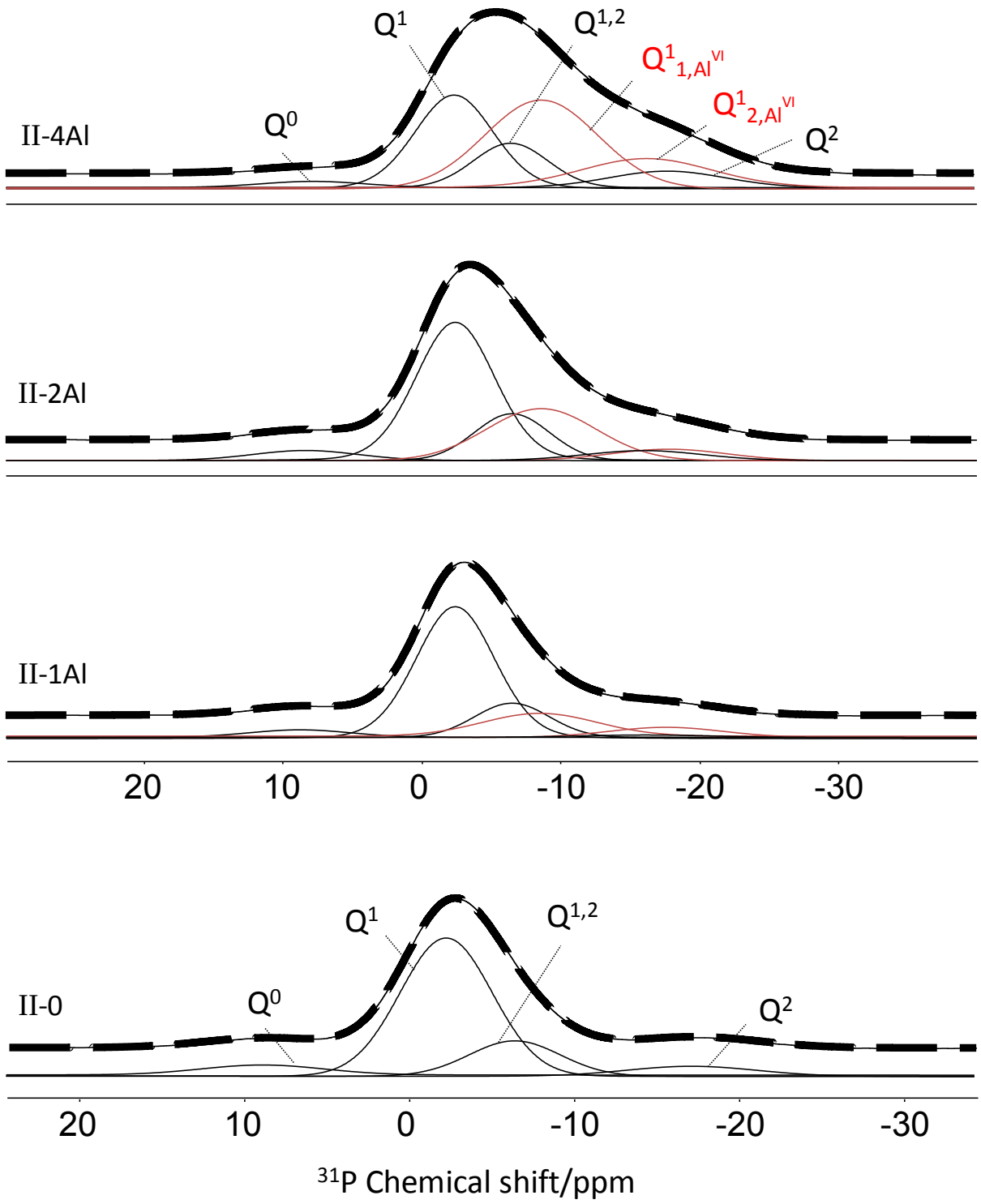

Fig. 5.4 Deconvolution of 1D ^{31}P spectra and the assignment of the sites for series II glasses doped with Al_2O_3.

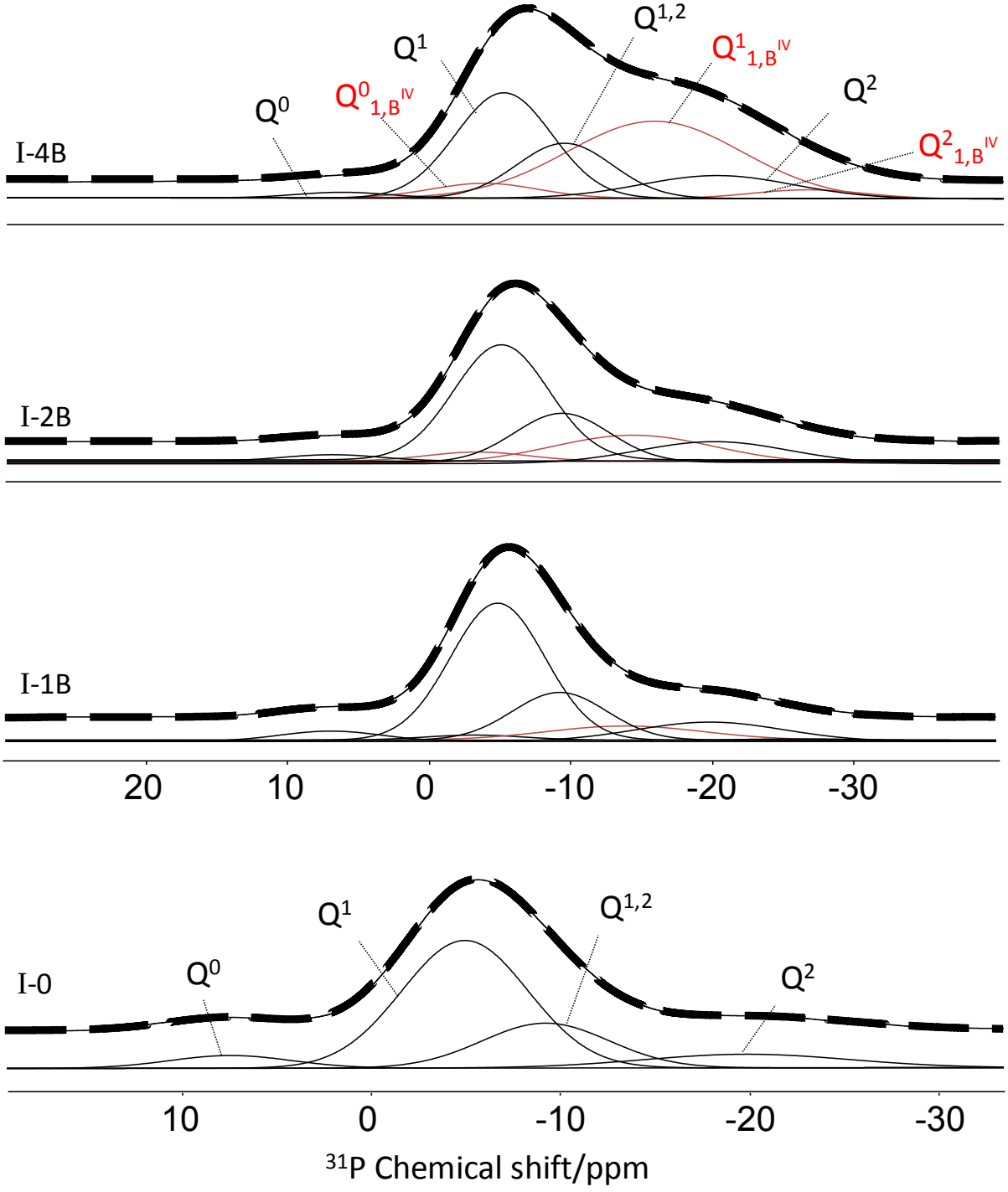

Fig. 5.5 Deconvolution of 1D ^{31}P spectra and the assignment of the sites for series I glasses doped with B_2O_3.

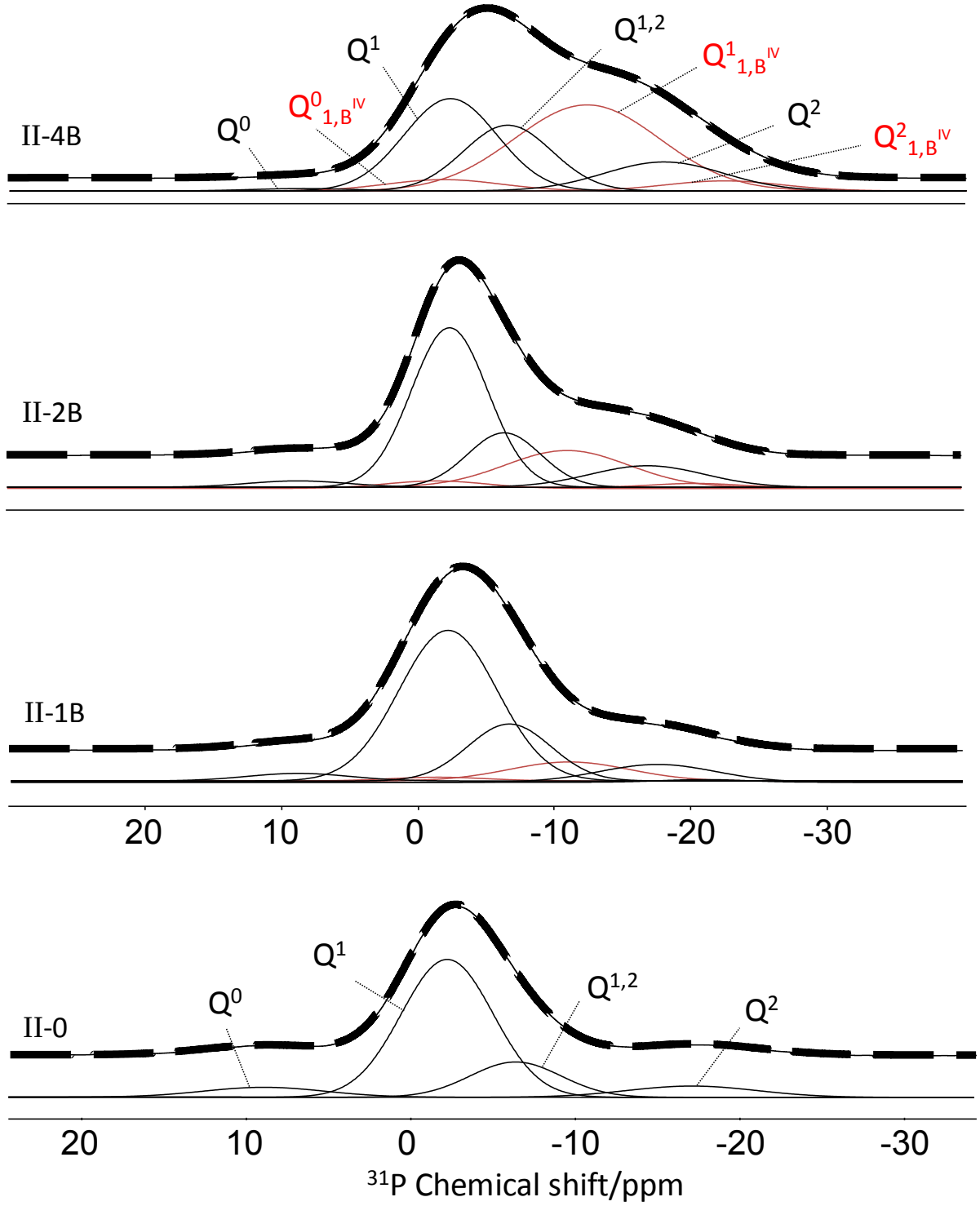

Fig. 5.6 Deconvolution of 1D ^{31}P spectra and the assignment of the sites for series II glasses doped with B_2O_3.

Tab. 5.3 Chemical shift, FWHM and relative percentage of the decomposed peaks of series-I glasses.

δiso(ppm)/ FWHM %																						
Series-I	Q^0			Q^1			Q^2			$Q^{1,2}$			$Q^1_{1Al^{VI}}$			$Q^1_{2Al^{VI}}$					
I-0	7.60	8.0		-4.69	7.9		-19.50	13.0		-8.8	8.3											
	6.04			62.45			11.26			20.25												
I-1Al	6.80	8.60		-4.75	7.90		-19.70	12.6		-9.10	7.98		- 11.40	11.1		-19.85	14.40					
	5.38			53.50			9.30			17.56			10.87			3.37					
I-2Al	6.30	9.93		-4.85	7.85		-19.70	12.8		-9.18	7.98		- 11.40	11.1		-19.85	14.50				
	4.59			40.61			9.44			17.98			20.48			6.9					
I-4Al	6.75	7.9		-5.0	7.80		-19.80	12.8		-9.20	7.85		- 11.78	11.22		-19.85	15.0				
	2.46			30.91			7.83			13.19			26.91			18.70					
	Q^0			Q^1			Q^2			$Q^{1,2}$			$Q^1_{1B^{IV}}$			$Q^2_{1B^{IV}}$			$Q^0_{1B^{IV}}$		
I-1B	7.0	8.5		-4.80	7.85		-19.8	12.30		-9.18	7.85		-13.8	13.0		-26.3	9.0		-3.15	8.30	
	4.19			53.73			11.74			18.86			9.20			0.42			1.86		
I-2B	7.0	7.98		-4.91	7.85		-19.9	12.4		-9.18	7.85		-14.2	14.2		-26.30	9.0		-3.2	8.3	
	2.39			43.22			12.9			18.81			18.13			0.89			3.62		
I-4B	6.41	7.67		-4.91	7.95		-19.9	12.6		-9.18	7.85		-15.5	14.42		-26.3	9.2		-3.55	8.82	
	1.48			28.54			9.96			14.78			37.91			2.76			4.57		

Tab. 5.4 Chemical shift, FWHM and relative percentage of the decomposed peaks of series-II glasses.

	δiso(ppm)/ FWHM %											
Series-II	Q^0		Q^1		Q^2		$Q^{1,2}$		$Q^1_{1Al^{VI}}$		$Q^1_{2Al^{VI}}$	
II-0	9.24	7.7	-2.22	6.5	-17.70	10.5	-6.63	6.54				
	5.2		66.8		9.4		18.6					
II -1Al	8.80	8.70	-2.40	6.70	-17.60	9.60	-6.49	6.33	-8.50	9.70	-16.0	11.25
	4.84		59.10		6.31		13.84		14.42		1.49	
II -2Al	8.40	9.0	-2.40	6.70	-17.80	9.80	-6.49	6.33	-8.60	9.30	-16.0	10
	3.87		46.97		6.49		14.0		23.54		5.13	
II -4Al	7.80	9.0	-2.40	6.70	-17.80	9.80	-6.49	6.33	-8.7	9.6	-16.30	11.25
	3.51		27.89		6.83		12.70		34.69		15.39	
	Q^0		Q^1		Q^2		$Q^{1,2}$		$Q^1_{1B^{IV}}$		$Q^2_{1B^{IV}}$	$Q^0_{1B^{IV}}$
II -1B	8.8	8.9	-2.2	8.45	-17.6	10	-6.7	7	-11.1	10.4	-21	7.41 -1.5 8.4
	3.28		57.68		8.31		18.85		9.53		0.67	1.68
II -2B	8.6	8.6	-2.5	6.6	-17	9.8	-6.5	6.3	-11.1	10.6	-20.5	7.21 -1.5 8.7
	2.64		48.02		7.9		16.77		18.07		1.42	3.18
II -4B	8.43	8.87	-2.3	8.0	-17.9	10.3	-6.49	7.60	-12.28	12.50	-22.3	10 -1.9 9.8
	2.36		32.15		6.95		12.95		37.8		3.68	4.10

The distribution of Q^n_{mx} species in both Al- and B- doped samples are sketched in *Fig. 5.7 and 5.*8, for glass series I and II, respectively. In these figures, all the mixed species have been regrouped and denoted as Q^1_{Al} and Q^n_{1B} species. The curves show a significant increase of the mixed Q^1_{Al} and Q^n_{1B} species at the expense of the $Q^{1,1}$ signal. The other species (Q^2, $Q^{1,2}$ and Q^0) experience slight decrease. This result confirm that the doping elements principally interact with the dimeric structure, exchange between the (Zn^{2+},Na^+) and one doping element leading to the formation of the Q^1_X moieties from the original $Q^{1,1}$ structure. The interactions between the doping elements and the phosphate network are significant since the 4 mol% doped samples present 50% of phosphate that have been modified by the doping procedures.

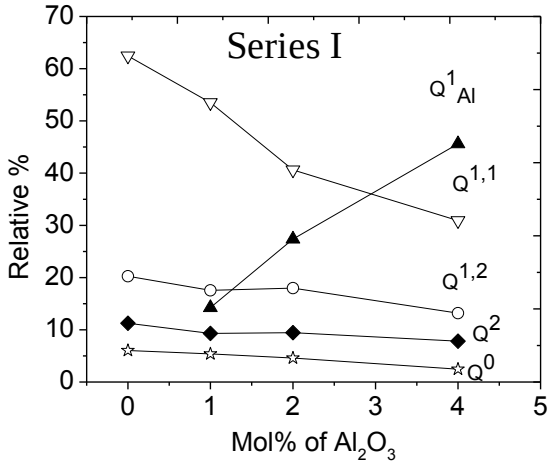

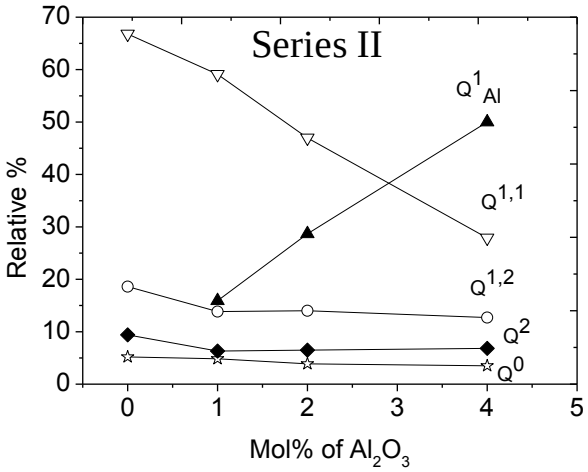

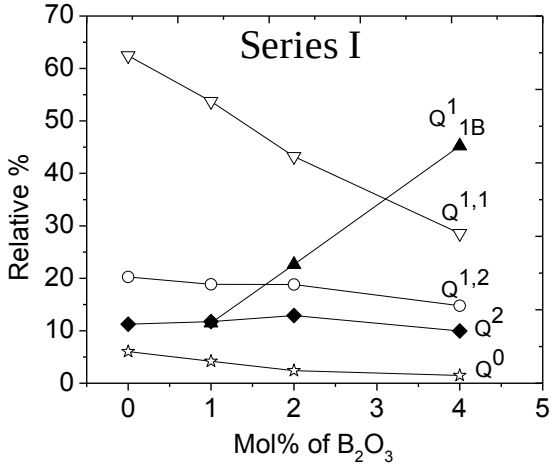

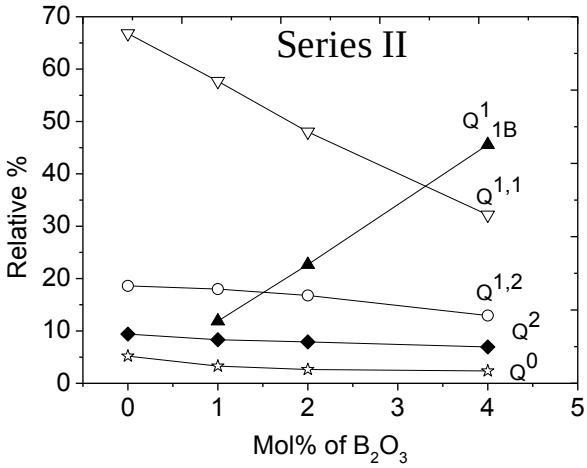

If Al- and B- doping procedures lead to similar amount of modified P species, difference appears when the number of P-O-X bonds is plotted versus the dopant content (*Fig. 5.8*). It appears that Al-doping induces high number of P-O-X bonds compared to B-doping. This result suggests that the network structure is modified in a deeper extent in case of the Al-doping procedure. Creation of Q^1_{2Al} species that provide 2 P-O-Al bonds per P atoms as well as the higher coordination state of Al (6-fold vs 4- fold for B) could explain this difference. However, additional information about the chemical environment of the doping elements will provide more information about that behavior.

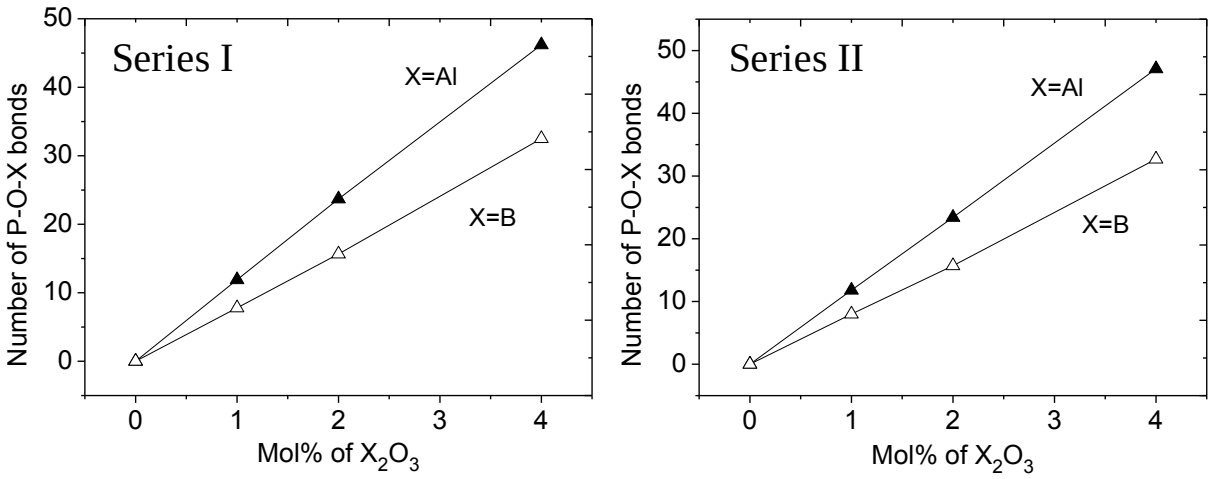

Fig 5.8 Number of P-O-X bonds versus the increase in dopants in glasses.

III. Clustering or perfect dispersion of the doping elements?

In addition to the phosphate network modifications, the doping element chemical environment has also been analyzed. If it has been clearly established that P-O-X linkages exist, the number of P attached to the doping element is still undetermined. However, this parameter is a key information because it could be used to determine if the doping elements only interact with P or if they also interact with the Zn^{2+} or Na^+ ions. The question of clustering or perfect dispersion has also to be answered to evaluate the efficiency of the doping procedures. It is crucial to determine if Al_2O_3 and B_2O_3 have been completely dissociated within the phosphate melts or not. This latter point is related to the presence or

absence of X-O-X bonds, the presence of such linkages would indicate partial doping clustering.

Two sequences were used to address these points. In a first time, the X{^{31}P} REDOR sequence was used to quantify the X/^{31}P dipolar interaction (Gullion 1989). Assuming constant P-X distance, the number of attached P will be derived from comparison with crystalline compound. Then, the presence / absence of X-O-X bonds will be highlighted by the modified DQ-SQ sequence (Wang 2009) using a particular protocol taking into account the low proportion of X elements in the investigated samples. Description of the chemical environment around the Al and B ions as well as the interactions between X/P, X/Zn and X/Na will be discussed.

III.1. REDOR (Rotational Echo Double Resonance)

The ^{31}P/X dipolar interactions have been quantitatively analyzed using the X{^{31}P} REDOR technique. The REDOR curves, expressing the dipolar interaction strength, have been constructed from these experiments and are reported in *Fig. 5.9* and *5.10* for both glass series doped with Al and B elements, respectively.

The 4 systems present the same tendency. The REDOR curves coming from the sample with different doping contents can be perfectly superimposed, indicating that the doping elements experience the same X/^{31}P dipolar coupling. The number of attached P is thus not modified by the increasing amounts of doping element. Al- doped glass series I and II exhibit the same REDOR evolution (*Fig. 5.9*), suggesting that the number of P attached to the octahedral aluminium is similar in both systems. Same conclusion can be derived from *Fig. 5.10* which shows that both systems experience the same ^{11}B/^{31}P dipolar coupling. The number of P attached to 4-fold coordinated boron is thus constant in all the B-doped samples.

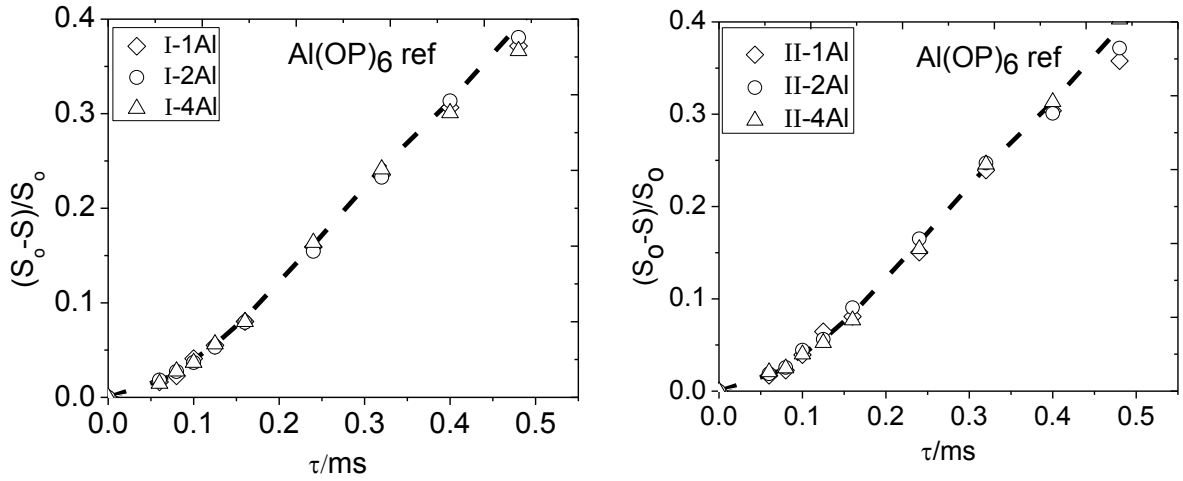

Fig. 5.9 REDOR curves of Al-doped glass series as indicated in the insert. The dashed line represents REDOR curve of $Al(OP)_6$ obtained from $Al(PO_3)_3$ crystalline reference.

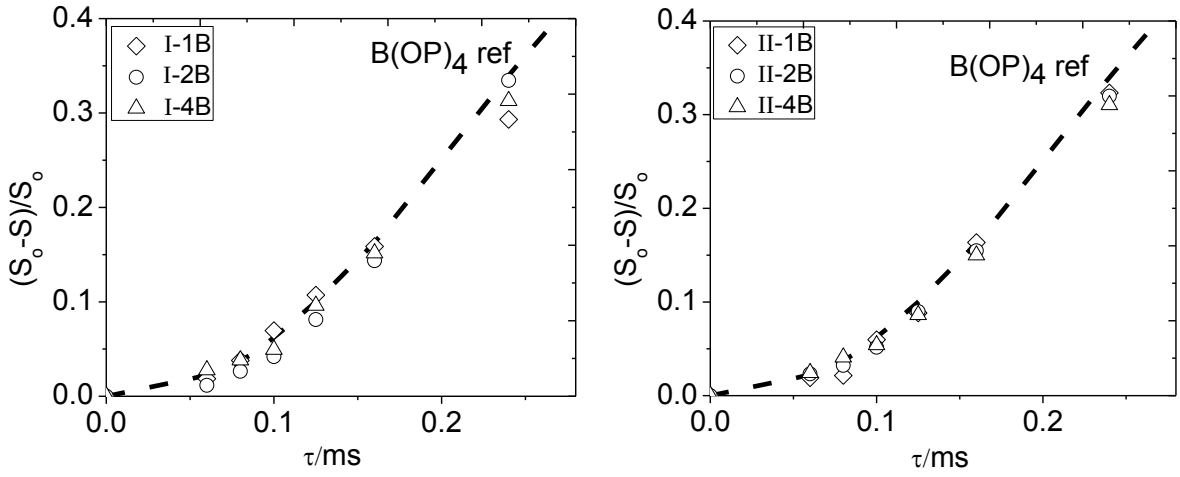

Fig. 5.10 REDOR curves of B-doped glass series as indicated in the insert. The dashed line represents REDOR curve of $B(OP)_4$ obtained from BPO_4 crystalline reference.

In a second step, REDOR curves were recorded on crystalline samples presenting identified X(OP)n structure. $Al(PO_3)_3$ and $AlPO_4$ compounds were used to calibrate the $Al(OP)_6$ and $Al(OP)_4$ chemical environment. Similarly, BPO_4 and $Na_5B_2P_3O_{13}$ compounds were employed to record $B(OP)_4$ and $B(OP)_3$ reference REDOR curves.

The reference curves with the best matching with the experimental data have been plotted in *Fig. 5.9* and *5.10*. It turns out that the Al-doped glasses data perfectly agree with the reference obtained on the $Al(PO_3)_3$ compound, indicating that the Al ions are surrounded by 6 P sites. In case of the B-doped samples, the REDOR curve obtained on the BPO_4 crystalline sample presents the best matching with the experimental data, indicating that the B ions are attached to 4 phosphate groups.

The REDOR experiments lead to the conclusions that octahedral alumina is attached to 6 P and that tetrahedral boron is attached to 4 P. The doping elements enter thus within the network as $Al(OP)_6$ and $B(OP)_4$ structural units. This information indicates that the extent of mixing between the dopants and the phosphate network is maximum. Moreover, it suggests that the doping elements are entirely associated to the phosphate network and do not interact with the Zn^{2+} or Na^{+} elements. Complete dispersion can also be assumed from this information since no Al-O-Al or B-O-B bonds can be present. The last point will be verified using the DQ-SQ technique.

III.2. DQ-SQ (Double Quantum Single Quantum)

The 1D X-DQ-SQ {X = ^{27}Al or ^{11}B} sequence is employed to determine the presence of X-O-X in the glass samples as it was used in the Chapter C to analyze the POP connectivity. It is noteworthy that, in addition to the Al- (and B-) doped glasses, reference samples composed by 99 mol% of undoped compositions and 1mol% of Al_2O_3 (or B_2O_3) have been prepared and analyzed by the DQ-SQ analysis to address the question of sensitivity.

Fig. 5.10 shows the 1D ^{27}Al DQ-SQ spectra obtained on the Al-doped and Al reference samples. Correlation signals observed in the Al-ref sample indicate the presence of Al-O-Al bonds coming from the Al_2O_3 present at 1mol%. The Al-doped glasses spectra do not show any signal. Since the signal absence cannot be related to the low Al^{3+} amount in the doped samples (Al-ref sample produces signal), the spectra indicate that the doped glasses do

not contain any Al-O-Al linkages. This result is in line with the previous part and support the complete dispersion conclusion.

Similar conclusion can be derived from the 1D ^{11}B DQ-SQ analysis (*Fig. 5.11*). The reference samples produces signal coming from the B-O-B linkages present in B_2O_3, but no signal is observed on the B-doped compositions. Lack of B-O-B bonds in the doped composition can thus be determined in a good agreement with the REDOR analysis conclusions.

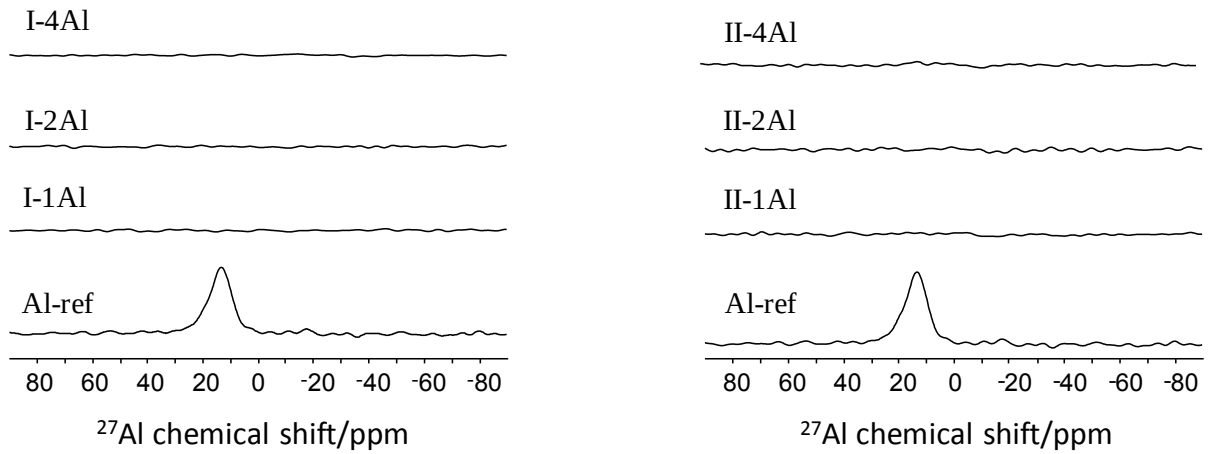

Fig. 5.10 1D ^{27}Al-DQ-SQ spectra.

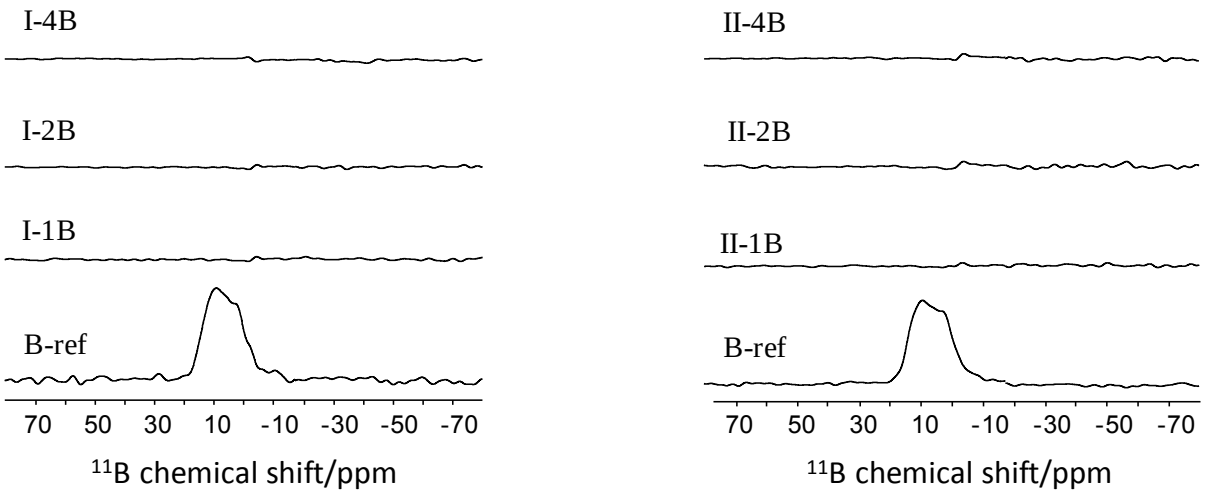

Fig. 5.11 1D ^{11}B-DQ-SQ spectra.

The chemical environment of the doping element was analyzed by REDOR and DQ-SQ NMR technique. The first sequence leads to the conclusion that Al and B elements are completely surrounded by phosphate groups and are only involved in linkages with P ions. Al and B are thus present inside the glass structure as $Al(OP)_6$ and $B(OP)_4$ groups (*Fig. 5.12*) and do not interact with the Zn^{2+} ions. This part shows that the effect of doping is only concentrated to the phosphate network structure.

The two levels of information (phosphate network modifications and chemical environment of doping elements) will thus be used to draw a complete structural model and to discuss the effect of doping on the global properties of the materials.

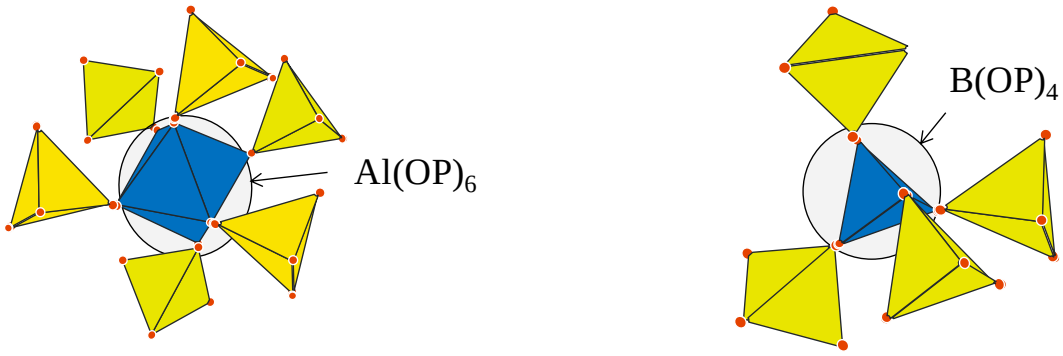

Fig. 5.12 Main Structural motif dominating the network for Al- and B-doped glasses.

IV. Conclusion

Correlation NMR techniques were used in this chapter to analyze in details the interactions between the Al and B doping elements and the phosphate network. The D-INEPT sequence was employed to produce correlation maps tracing the presence of P-O-Al and P-O-B linkages. Both doping procedures lead to the formation of such mixed species. In case of Al, two species assigned to Q^1_{1Al} and Q^1_{2Al} were highlighted whereas 3 species corresponding to Q^0_{1B}, Q^1_{1B} and Q^2_{1B} were determined for the B-doped samples. The number of P-O-X was found to be higher in case of Al-doping procedure in a good agreement with the higher coordination state of Al that offers thus larger possibility for P-O-X linkages.

In addition, the REDOR and DQ-SQ techniques were used to investigate the clustering or perfect dispersion of the doping elements. The first technique indicates the presence of $Al(OP)_6$ and $B(OP)_4$ groups within the glass structure, suggesting that the maximum P-O-X linkages are formed during the doping insertion. This result also indicates that Al^{3+} and B^{3+} ions do not interact with the Zn^{2+} and Na^{+} elements, restricting thus the doping effect to the phosphate network. Moreover, it suggests that the doping elements are totally dispersed within the glass matrix and that no X-O-X bonds exist. The last point was checked using the DQ-SQ technique, recently adapted to be suitable for quadrupolar nuclei. No signal coming from Al-O-Al or B-O-B bonds was detected, supporting thus the perfect dispersion of the doping elements.

The two levels of information (phosphate network modifications and chemical environment of doping elements) will thus be used to draw a complete structural model and to discuss the effect of doping on the global properties of the materials in the next chapter.

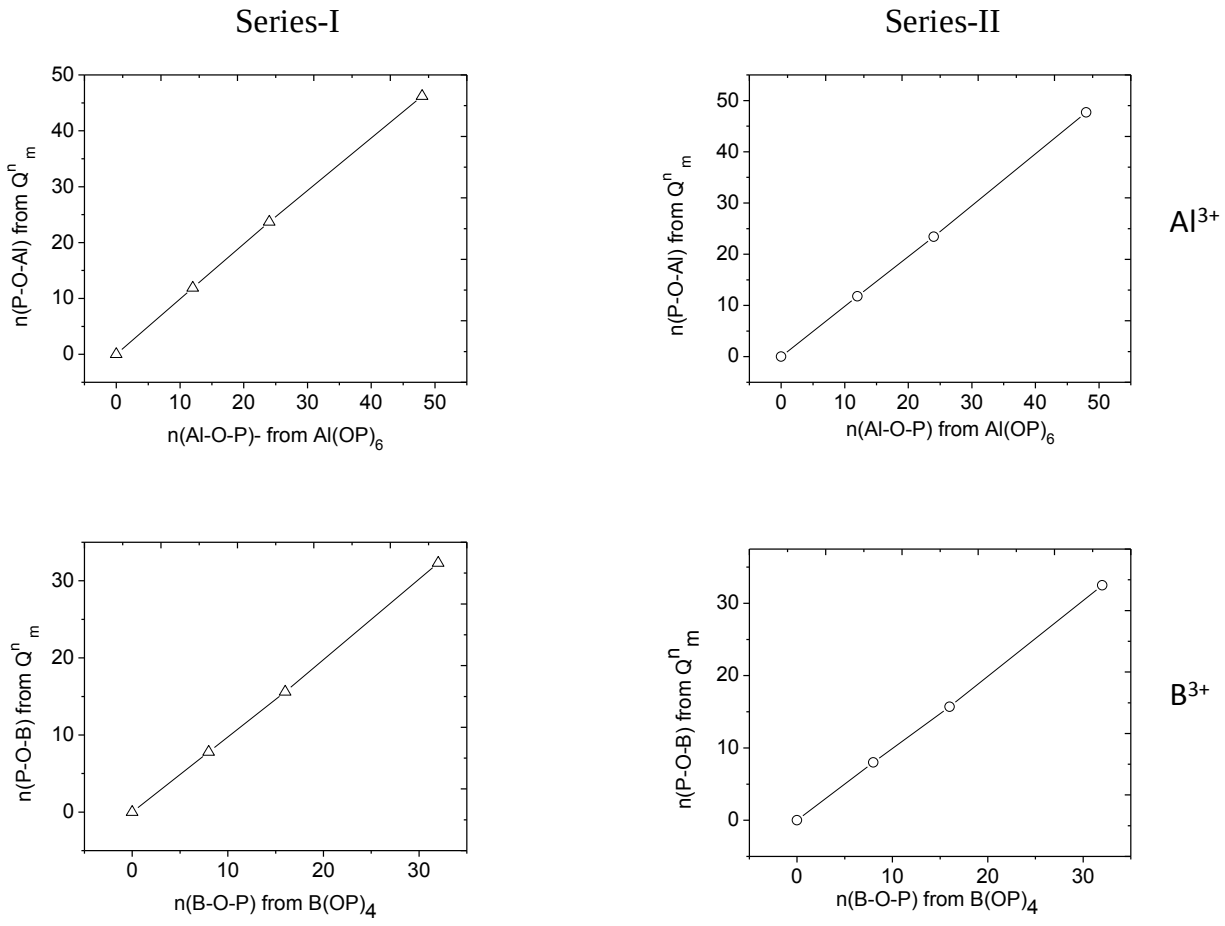

Fig. 5.13 The number of P-O-X bonds in Q^n_m (from D-INEPT) versus the number of X-O-P bonds in $X(OP)_n$ (from REDOR).

The interactions between Al- and B-doping and the phosphate network were thus analyzed using two different points of view. The D-INEPT sequence was first used to determine the number of P-O-X in the structure. Then, the REDOR and DQ-SQ results allow investigating the structure in terms of X-O-P. Of course the number of mixed linkages given by the two studies should be similar. Number of P-O-X versus number of X-O-P is reported in *Fig. 5.13*. Straight correlations close to a line presenting a slope of 1 indicate a very good correlation, assessing for the relevancy of our results.

It is noteworthy that other correlation technique could have been used in order to extend the structural information. ^{31}P DQ-SQ analyses have been done in order to analyze the interactions between the P(X) units and the species coming from the undoped compositions. Unfortunately, the low amounts of P(X) and the very complex spectrum feature (containing 6 and 7 components for the Al- and B-doped compositions, respectively) does not allow to derived clear and valuable information. Tentative specific analysis of the interactions between the P(X) units were performed using a combined ^{31}P{X} D-INEPT~BABA sequence. The global objective was to use in a first time the D-INEPT technique as a filter to cancel the signals corresponding to the P unconnected to the dopants and to analyze the interactions between the remaining P(X) species with the BABA pulse sequence. Additional information about the mixing between the $Q^1_{(X)}$ species could have been derived from these analyses. Unfortunately, the produced D-INEPT~BABA sequence does not present the robustness and stability expected to be used in this work.

References

Gullion, T and J Schaefer. *J. Magn. Reson.* 81 (1989): 196.

Hartmann, S R, and E L Hahn, *Phys. Rev.*, 128 (1962): 2042.

Lesage, A, D Sakellariou, S Steuernagel, and L Emsley. *J.Am.Chem.Soc,* 120 (1998): 13194.

Lu, X, J Trebosc, O Lafon, and J P Amoureux. *Cryst. Eng. Comm.* (2013) DOI: 10.1039/c3ce40557e.

Michaelis, K V, P Kachhadia, and S Kroeker. *Phys. Chem. Glasses: J. Glass Sci. Technol., 54(1)* (2013): 20-26.

Morris, G, and R Freeman. *J. Am.Chem.Soc.* 101 (1979): 760.

Raguenet, B, G Tricot, G Silly, M Ribes, and A Pradel. *J. Mater. Chem. 21* (2011): 17693.

Raskar, D, M T Rinke, and H Eckert. *J. Phys. Chem., 112*, (2008): 12530-12539.

Trebosc, J, B Hu, J P Amoureux, et Z Gan. *J. Magn. Reson.* 186 (2007): 220-227.

Wang, Q, B Hu, O Lafon, J Trebosc, F Deng, and J P Amoureux. *J. Magn. Reson.* 200 (2009): 251 260.

Wegner, S, V LWullen, and G Tricot. *J. Non-Cryst. Solids, 354*, (2008) 1703-1714.

Wullen, L V, G Tricot, and S Wegner. (2007). *Solid State Nucl. Magn. Reson. 32* (2007): 44-52.

Zeyer-Dusterer, M, L Montagne, G Palavit and C Jager, *Solid State. Nucl. Magn. Reson.* 27 (2005): 50.

Zielniok, D, C Cramer, and H Eckert. *Chem. Mat. 19* (2007): 3162-3170.

Chapter F

Discussion about the doping effect.

The general effect of doping is discussed in this part based on the results presented in the chapter C, D and E. General structural models are presented for the undoped and the Al-, B- and Si-doped compositions and the effect of doping in the structure is discussed in the first part. The different structural features are then used in order to explain how the doping procedures change the material properties and stabilities. Finally, optimized compositions combining two different dopants have been derived from this work and the preliminary results obtained on this sample are presented.

I. Impact of doping on the glass structure

The structure of undoped compositions has been investigated in Chapter C by means of 1D and 2D ^{31}P MAS-NMR. It turns out that the phosphate network is mainly constituted by dimeric entities $P_2O_7^{4-}$, as expected from the O/P=3.5 ratio of the composition line. We also show that the structure presents different extents of disorder depending on the Zn/Na relative proportions. At high Zn^{2+} content, the glass structure experiences significant Q^n dismutation leading to the presence of Q^0 and Q^2 sites within the structure. The Q^2 species organization induces the presence of 3- or 4- P chain length, increasing the distributions of phosphate entities and thus the topologic disorder. Typical phosphate structure found in our composition line is sketched in *Fig. 6.1*.

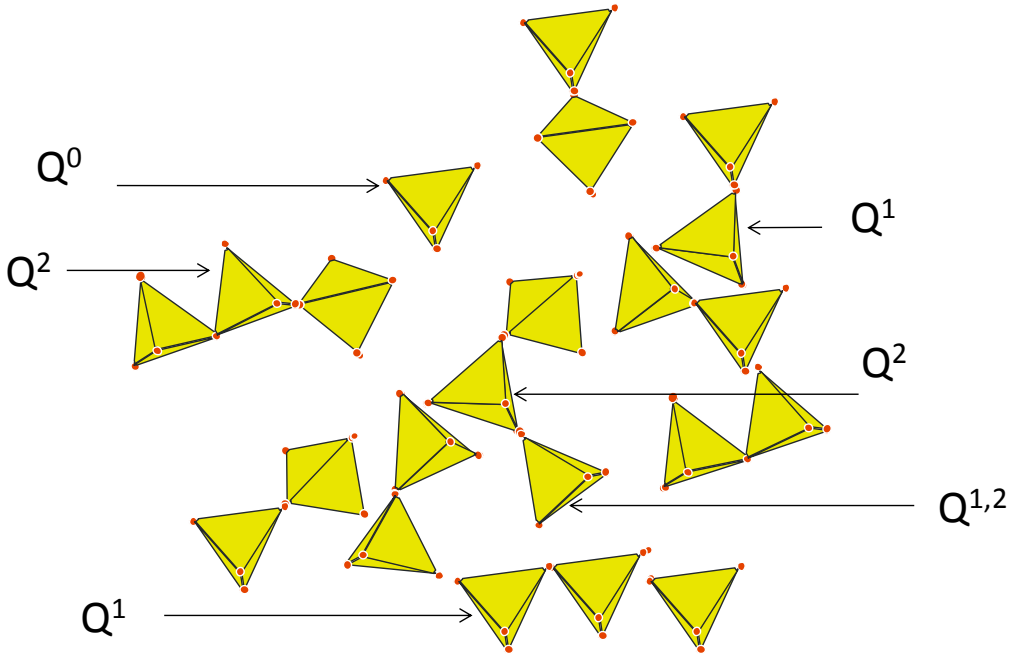

Fig. 6.1 Structural model for the undoped glass network visualization.

It is noteworthy that the Zn^{2+} ions are supposed to adopt a 4-fold coordination state in all glasses, due to the high O/P ratio as suggested by Walter and Hoppe (Walter 2004). Some neutron diffraction, EXAFS or ^{67}Zn NMR have been scheduled for this work but the proposals for the two former were not accepted. ^{67}Zn NMR (static) at 21.1 T performed on two samples (*Fig. 6.2*) show similar signal, suggesting that the chemical environment of zinc is not affected by the Zn/Na ratio. Of course these results need additional experiments to be confirmed. Nevertheless, Zn^{2+} ions will be assumed to be 4-fold coordinated in the following. ^{23}Na NMR was also used to investigate the chemical environment of this composition line. Constant signal (not shown here) was recorded but does not provide any valuable information on the Na^{+} ions local environment.

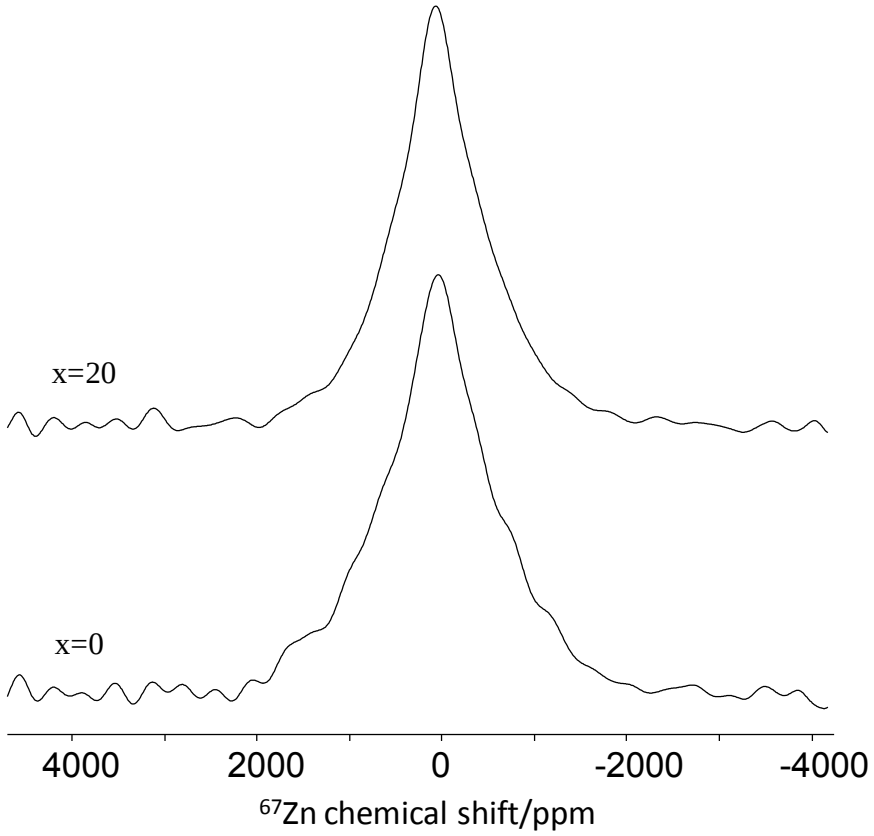

Fig. 6.2. ^{67}Zn NMR (static) of the (66.6-x)ZnO-xNa_2O-33.4P_2O_5 glasses

Structures of the doped compositions have been studied by 1D / 2D NMR techniques. The structural models derived from all the results are presented in *Fig. 6.3* for the Al-, B- and Si- doped compositions. The models take into account:

- the dopant coordination state deduced from 1D MAS-NMR: Al^{3+}, B^{3+} and Si^{4+} enter into the materials as 6-, 4- and 4-fold coordinated species;
- the presence of phosphate units interacting with the Al- and B- dopants: Al- and B-doping procedures lead to the formation of Q^1_{nAl} (n=1, 2) and Q^m_{1B} (m=0, 1, 2) as concluded from the X{^{31}P} D-INEPT sequence;
- the chemical environment of the doping element: X{^{31}P} REDOR and X DQ-SQ sequences show that the Al- and B- dopants are completely surrounded by P to form $Al(OP)_6$ and $B(OP)_4$ structural units ruling out any interaction between the dopants and the Zn^{2+} ions and indicating a complete dispersion of the dopant within the glass structure,
- the separation between the silicate and phosphate network suggested by the Q^4 speciation of the silicate units deduced from the ^{29}Si chemical shift values.

The effect of doping on the structure can thus be discussed based on the reported models.

Conclusions about the Si-doping are easy to derive. Silica and phosphate units do not interact to create mixed species, as expected from their respective high acidity and electrostatic field strength. The glass structure is thus composed by a phosphate rich part with a structure close to the undoped composition in which some SiO_2 rich part are embedded. In a similar way that P_2O_5 does not enter into the silicate network of bioactive glasses, our study shows that low SiO_2 amounts do not enter into the main phosphate network (Fayon 2013). Our system exhibits thus a different behavior than observed by Dupree in Na_2O-SiO_2-P_2O_5 system, in which silica is in octahedral coordination state but only when P_2O_5 concentration was greater than 40 mol% [$20Na_2O$-$40SiO_2$-$40P_2O_5$] (Dupree 1987). They could not trace the presence of any octahedral silica in the glass structure until 30 mol% of P_2O_5 [$23.3Na_2O$-$46.6SiO_2$-$30P_2O_5$]. It is noteworthy that P_2O_5 concentration in our system is also close to 30 mol%.

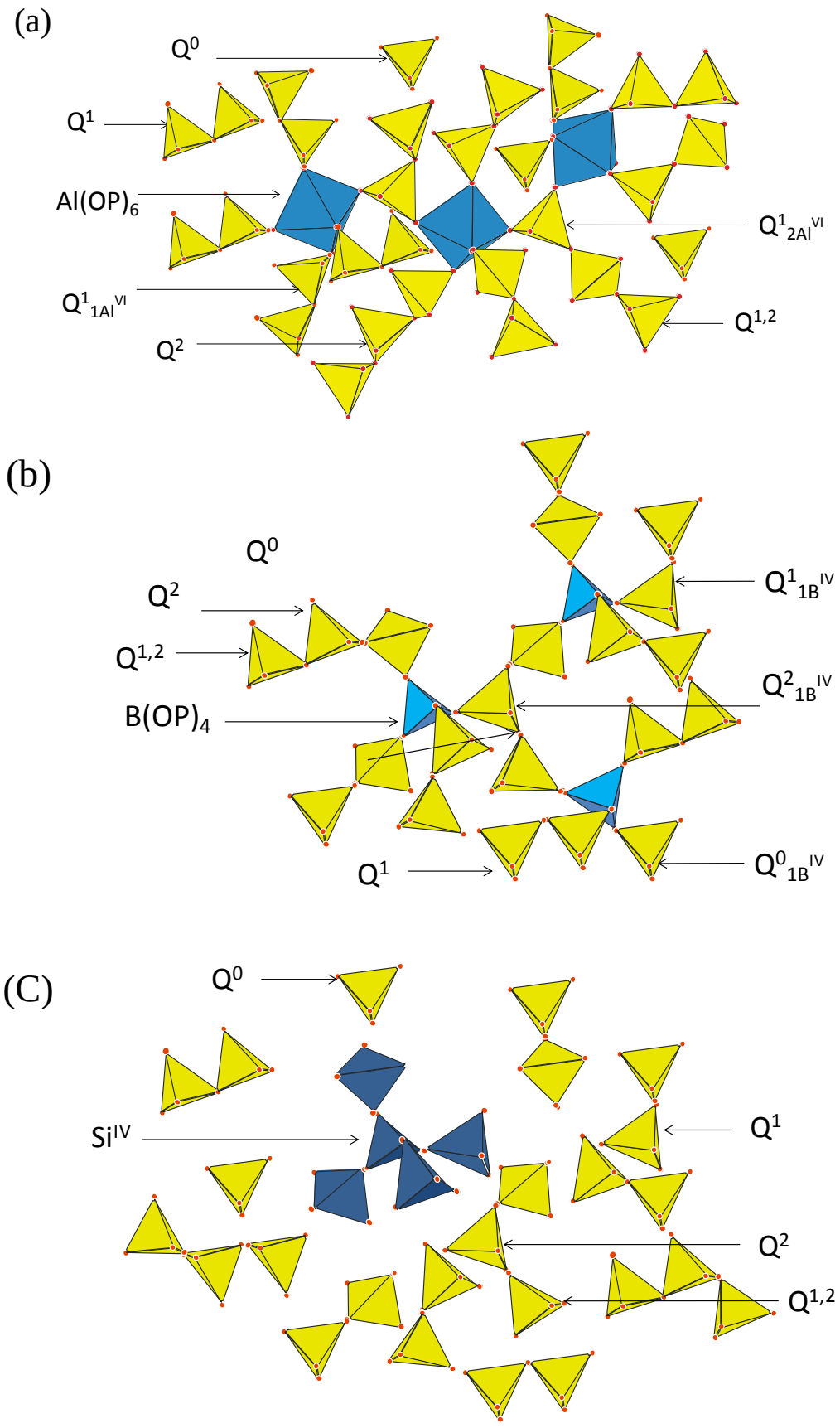

Fig. 6.3 Structural model for the Al-(a), B-(b) and Si-(c) doped glass network visualization.

As reported in *Fig. 6.3*, Al- and B-doping procedures strongly impact the phosphate network structure by forming P-O-X bonds. The structure is still mainly formed by dimeric entities but instead of being surrounded by Zn^{2+} and Na^{+} ions, the dimers are attached to Al- and B- polyedra presenting 6- and 4- fold coordinated character. These structural modifications can be analyzed on two levels:

(i) from an energetic point of view, both procedures lead to the replacement of weaker P-O-Zn or P-O^{-}-Na^{+} bonds (284 and 257 kJ/mol for O-Zn and O-Na, bonds respectively) by stronger P-O-Al or P-O-B linkages (512 and 806 kJ/mol for O-Al and O-B respectively), inducing thus the formation of a strengthened network (Cottrell, 1958, Benson 1965 and Kerr 1966).

(ii) from a topological point of view, the replacement of tetrahedral Zn^{2+} ions by $Al(OP)_6$ groups increases the global reticulation of the network, since 6 phosphate chains can be bring together around the Al^{3+} ion whereas only 4 chains were reticulated around the zinc element. B-doping resulting in $B(OP)_4$ group only has a moderate impact on the global reticulation. It is also noteworthy that both doping procedures do not affect the phosphate species nature in similar ways. In case of alumina, the dimeric phosphate structure is preserved, attachment of P and Al being produced without any POP breaking. The Al^{3+} ions create thus P-O-Al bonds using non bridging oxygens as reported in *Fig. 6.4*. Attachment of 1 or 2 Al^{3+} ions using this mechanism leads to the formation of the observed Q^{1}_{1Al} and Q^{1}_{2Al} species. In case of B-doping procedure, the formation of Q^{1}_{1B} is based on the previously described mechanism preserving the POP bonds. If the presence of Q^{2}_{1B} is explained by similar mechanism involving middle chains phosphate species, the significant amount of Q^{0}_{1B} can be hardly explained by Q^{0} conversion. Therefore, it has to be admitted that B^{3+} ions can also react with POP bonds to create the Q^{0}_{1B} species from a pure dimer, as depicted in *Fig. 6.4*.

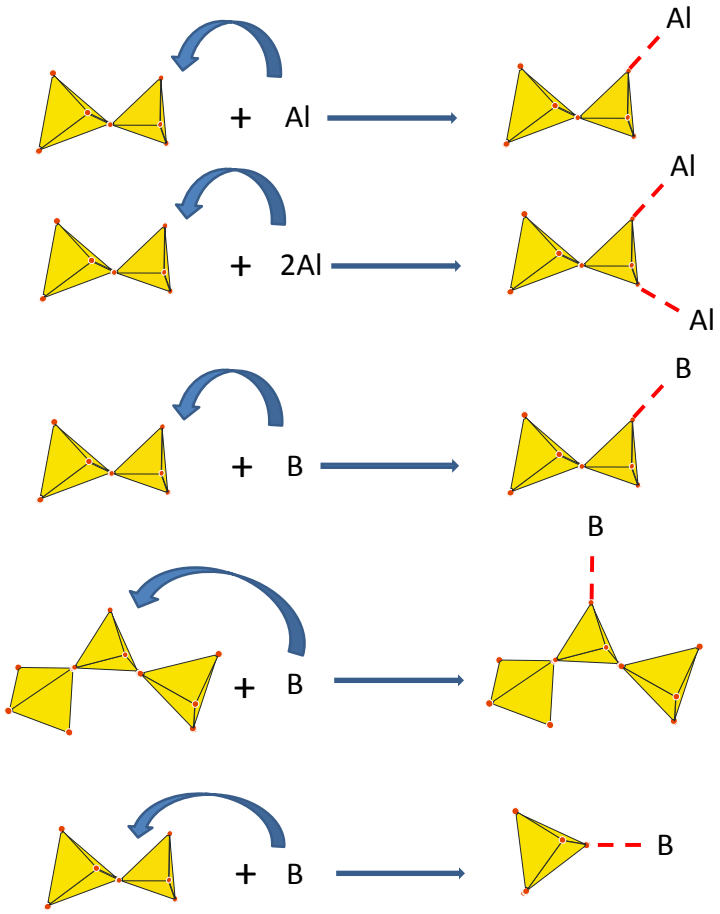

Fig. 6.4 Possible mechanisms of insertion of Al or B into the phosphate network.

A complete structural characterization would have required investigating the effect of doping on the Zn^{2+} coordination state. Indeed, if we have clearly evidenced that doping element only interact with the phosphate network, an indirect modification of the ZnO_n speciation induced by the re-arrangement of the phosphate chain structure cannot be completely ruled out. As previously mentioned, no EXAFS or neutron diffraction was allowed to be performed. ^{67}Zn NMR analyses do not provide any information supporting zinc coordination state evolution. The role of Na^+ ion in the structure has been investigated by ^{23}Na MAS-NMR. Indeed, in addition to its well known network modifying role, this ion is also known to act as a charge compensator in silicate glasses allowing for the evolution of Al^{VI} to Al^{IV} and B^{III} to B^{IV} species. If this feature can be considered as minor in case of Al-doped compositions, that contain low amount of Al^{IV} species, it could play a crucial role in B-doped samples owing to the 4-fold coordination adopted by 100% of the B^{3+} ions. Displacement of Na^+ ions from network modifier position in undoped compositions to charge

compensator in B-doped samples could also induce structural modifications. However, ^{23}Na MAS-NMR analyses (not shown) do not show any difference and are thus not relevant to investigate this structural question.

To summarize, B-doping leads to the formation of strong linkages without significantly changing the global reticulation scheme. In the opposite, Al-doping procedure produces lower energetic linkage but significantly increases the reticulation through the appearance of $Al(OP)_6$ groups. Using these two explanations, the impact of the doping procedures on the properties will be discussed in the next part.

II. Impact of doping on the glass properties and stabilities

The conclusions about the structural modifications induced by the doping procedures will be used now to discuss the properties and stabilities evolution observed in chapter D.

II.1 Macroscopic properties

If the density and Molar volume are not significantly affected by the doping procedure, the T_g parameter seems to be mainly controlled by the global reticulation of the phosphate network, since Al-doping produces the most important increases. It turns out that the presence of $Al(OP)_6$ induces higher effect than the highly strong BOP bonds on this property. In our study, B-doping appears thus to be advantageous since it does not induce significant increase.

Viscosity follows the same evolution and responds thus to the same structural features. Incorporation of $Al(OP)_6$ increases the amount of cross-linking giving rise to highly reticulated network. The structural rearrangements at the origin of the viscous flow require thus more energy (and thus higher temperature) to occur, explaining the viscosity curves postpone observed for the Al-doped samples. The moderate increases occurring in the B-doped samples results from the higher energy involved in the B-O-P linkages compared to the

Zn-O-P one. In this case again, this latter effect seems to be a lower impact than the global increase of the network reticulation.

II.2. Impact on stabilities

As observed in chapter D, the chemical durability was dramatically improved by the Al-doping whereas B-doping leads to an alteration of this property. One time again, it turns out that the resistance against water attack is governed by the global reticulation process rather than by the linkages energy. Nevertheless, if the improvement of chemical durability by Al-doping is perfectly in line with previous investigations (Kreidl 1941, Bunker 1984 and Brow 1993), some papers also state that insertion of B^{3+} ions also improves this property (Tindyala 1978, He 1991 and Lim 2006). Moreover, this improvement is generally explained by the formation of $B(OP)_4$ groups, as in our system. Therefore, the decrease of the chemical stability observed in our system cannot be completely explained.

Finally, the only property impacted in a higher extent by the B-doping procedure is the thermal stability. Clear evidences of better thermal resistance induced by B^{3+} insertion have been described in the chapter D. It appears thus that resistance against crystallization is principally governed by the bond energy. Crystallization of $Zn_2P_2O_7$ or $Na_2ZnP_2O_7$ compounds from the amorphous matrix requires P-O-X bonds breaking. The higher energy of P-O-B compared to Al-O-P bonds seems to limit this breaking, resulting in the slower crystallization kinetics for B-doped samples. Surprisingly, the viscosity increases induced by the Al-doping does not seem to limit the crystallization mechanism, even if it is generally admitted that higher viscosity induces slower structural rearrangements, that should result in a decreasing crystallization kinetic. In our system, the low viscosity impact could be explained by the structural similarity between the structural units present in the glass structure and in the crystalline compounds. Complex structural rearrangements would thus not be required to produce crystallization.

Different improvements are thus obtained with the Al- and the B-doping procedures. If the former clearly results in a better resistance against water attack, the latter has a clear positive impact on the resistance against crystallization. In the following part, simultaneous doping using B^{3+} and Al^{3+} ions will be tested in order to determine if a synergic or destructive

behavior is observed on the effect induced by each doping element. The two glass formulations will be doped with 2 mol% of Al_2O_3 and 2 mol% of B_2O_3.

The macroscopic properties, stabilities and structure of the glasses will thus be compared to 4 mol% of Al_2O_3 and 4 mol% of B_2O_3 in order to assess for the relevancy of using simultaneously both doping element in the same formulation.

III. Al- and B- doped composition

In one hand, insertion of B_2O_3 dramatically improved the thermal stability, while on the other hand, insertion of Al_2O_3 remarkably improved the chemical durability. Thus small amount of each element doped in a same sample may produce a glass with a good compromise between thermal and chemical stability. Therefore two doped compositions have been prepared with B_2O_3 (2 mol%) and Al_2O_3 (2 mol%). The initial results obtained on properties and structures are presented and then compared with samples containing 4 mol% of B_2O_3 and 4 mol% of Al_2O_3.

The two formulations will be as follows: $42ZnO\text{-}18Na_2O\text{-}36P_2O_5\text{-}2Al_2O_3\text{-}2B_2O_3$ (I-2Al2B) and $30ZnO\text{-}30Na_2O\text{-}36P_2O_5\text{-}2Al_2O_3\text{-}2B_2O_3$ (II-2Al2B) (*Tab.6.1*). Both batches were melted at 1100 °C for 20 minutes and quenched on a brass plate at room temperature to obtain clear and transparent glasses. X-ray diffraction analysis were performed (not shown here) and confirmed that the samples present an amorphous character. The weight loss measurements were also carried out and found under 2%, thus the glass composition can be referred to 'as-batch' compositions.

Tab. 6.1.Composition and thermal properties of the glass. samples.

Series-I	ZnO	Na_2O	P_2O_5	B_2O_3	Al_2O_3	O/P	T_g/°C	T_x/°C	T_x-T_g/°C	T_c/°C	Δm/m
I-0	46.6	20	33.4	0	0	3.5	339	536	197	555	0.9
I-4B	42	18	36	4	0	3.5	360				1.4
I-2Al2B	42	18	36	2	2	3.5	367	-	-	-	1.5
I-4Al	42	18	36	4	0	3.5	385				1.9
Series-II											
II-0	33.3	33.3	33.4	0	0	3.5	310	440	130	461	1.8
II-4B	30	30	36	4	0	3.5	330	542	212	-	1.2
II-2Al2B	30	30	36	2	2	3.5	341	542	201	-	1.5
II-4Al	30	30	36	4	0	3.5	368	540	172	580	1.8

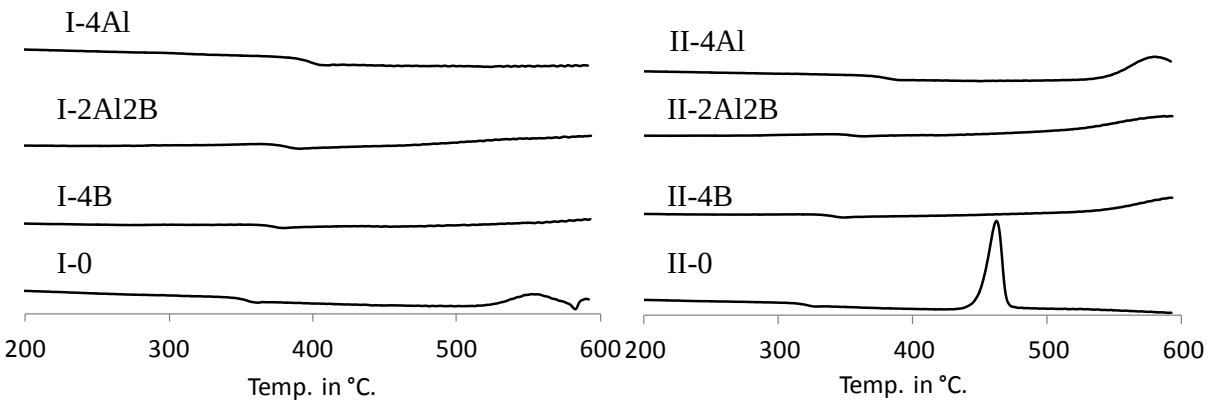

Fig. 6.5. DSC patterns of the glass samples.

III.1. Effect on T_g and stability

The DSC analysis of the glass with both Al^{3+} and B^{3+} is compared with samples containing 4 mol% of Al_2O_3 and 4 mol% of B_2O_3, as presented in *Fig. 6.5*. The thermal parameters (T_g, T_x, T_x-T_g and T_c) of these glasses are also regrouped in *Tab. 6.1*. In both series, the effect of (Al + B)-doping shows a moderate modification on T_g and stability parameters. The T_g and K_A values are nearly equivalent to B-doped glass with a marginal increase in T_g slightly higher (+7 °C and +11 °C respectively for series I and II). It is noteworthy that these T_g values are significantly lesser than Al-doped glasses by -18 °C and -27 °C respectively for series I and II. In addition, the crystallization peaks observed in series II glasses also exhibit same feature as B-doped glass suggesting similar resistance to crystallization. Moreover, K_A (201 °C) is also close to K_A of B-doped glass (212 °C). Thus it indicates 2 mol% of Al_2O_3+2 mol% B_2O_3 can thus produce nearly equivalent effect as 4 mol% of B_2O_3 in terms of T_g and thermal stability (*Fig. 6.5*).

If the T_g and thermal stability are marginally affected by (Al+B)-doping, a substantial effect on chemical durability is observed (*Fig. 6.6*). The weight loss of only 3 % is recorded for (series I) glass that lies between 30% (B-doped) and 0.1% (Al-doped) indicating an important positive effect on this property. Similar remarks can be applied to series II glasses. Owing to such simultaneous improvement of thermal and chemical stabilities of the glass, the ratio of B_2O_3/Al_2O_3 can thus be further optimized to produce better glass stability.

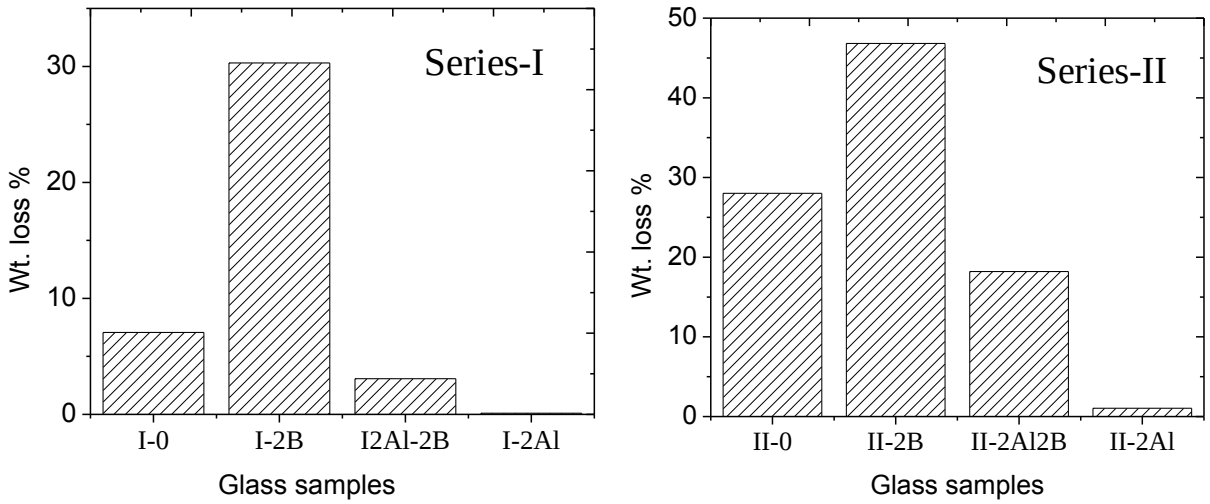

Fig. 6.6.Chemical durability test of the glass samples.

III.2. Effect on structure

^{27}Al and ^{11}B MAS NMR show the presence of Al^{VI} as dominant coordination state and only B^{IV} units respectively (*Fig. 6.7*), indicating no change in the coordination states. It is worthy to note that small amount of alumina did not change the coordination state of boron. This behavior is different from another study, in which addition of Al_2O_3 induced the transformation of B^{IV} to B^{III} units (Mascaraque 2011).

The 1D ^{31}P NMR spectra of the Al-doped, B-doped, and (Al+B)-doped, glasses are presented in *Fig. 6.8*. It suggests that the ^{31}P spectra of (Al+B)-doped glass also experiences significant changes, showing the effect of both Al^{3+} and B^{3+} ions in the phosphate network. However definitive conclusion cannot be derived due to the poor resolution of the spectra. Since the glass consists of both Al^{3+} and B^{3+} ions, the question of the presence of phosphate units with Al-O-P-O-B bonds or with separate P-O-Al and P-O-B linkages can be asked. Thus D-INEPT technique was applied to the glass sample to distinguish such phosphate species. *Fig. 6.9* shows the comparison between $^{31}P\{^{27}Al\}$ D-INEPT spectra and $^{31}P\{^{11}B\}$ D-INEPT spectra. The observed difference in chemical shift of the isotropic peak by +3 ppm in both series provides the strong evidence that these signals are definitely not coming from the same species (Al-O-P-O-B) but are from the separate species with P-O-Al and P-O-B linkages. Thereby the dominant P-O-Al and P-O-B environments provide an indicator of a very good

dispersion of Al^{3+} and B^{3+} ions within the glass structure. The presence of P-O-Al linkage thus explains the increase in chemical durability and the P-O-B maintains the thermal stability and T_g.

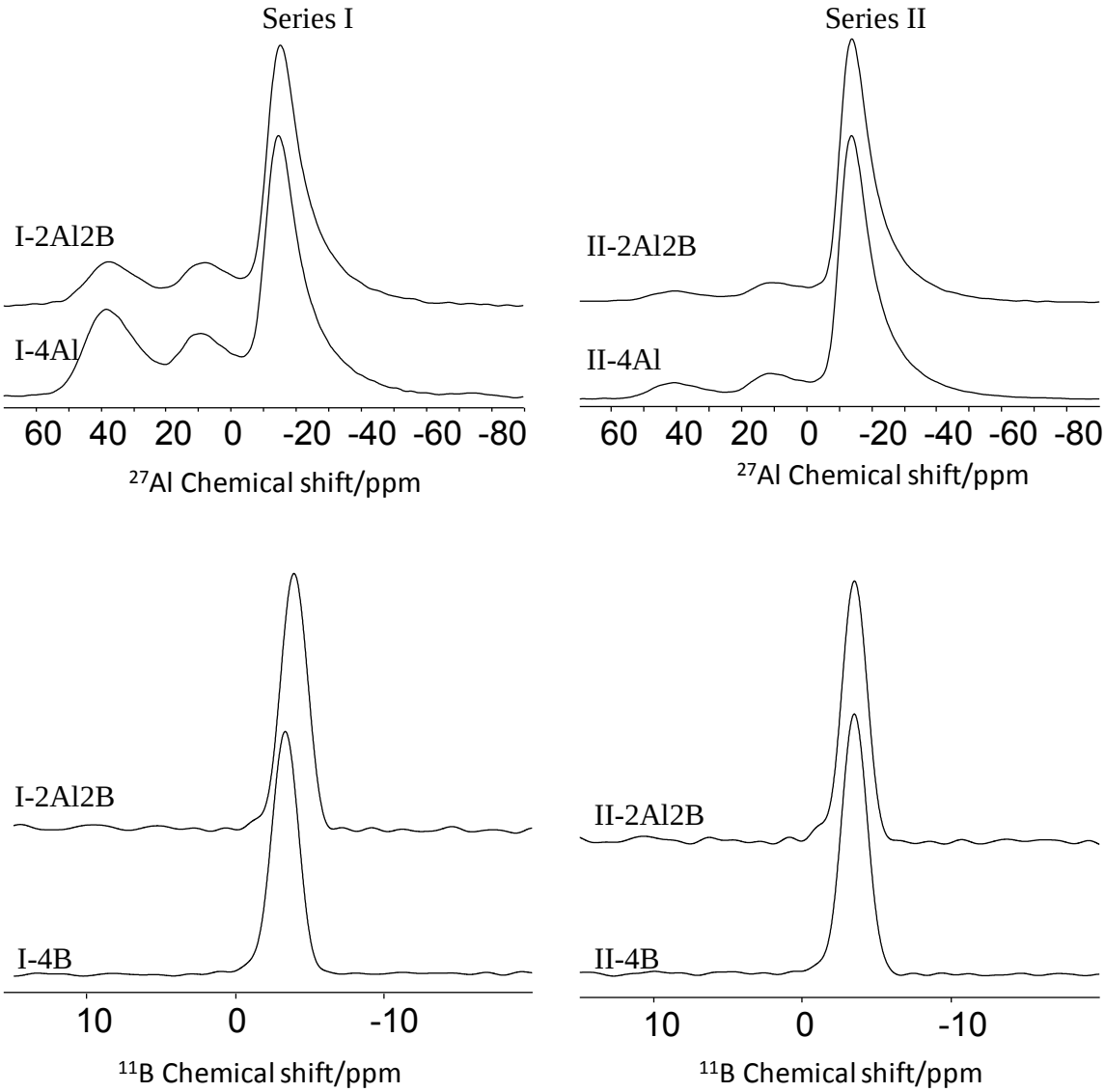

Fig. 6.7. Comparison of 1D ^{27}Al and ^{11}B MAS NMR of (Al+B)-doped glasses with B-doped and Al-doped glasses.

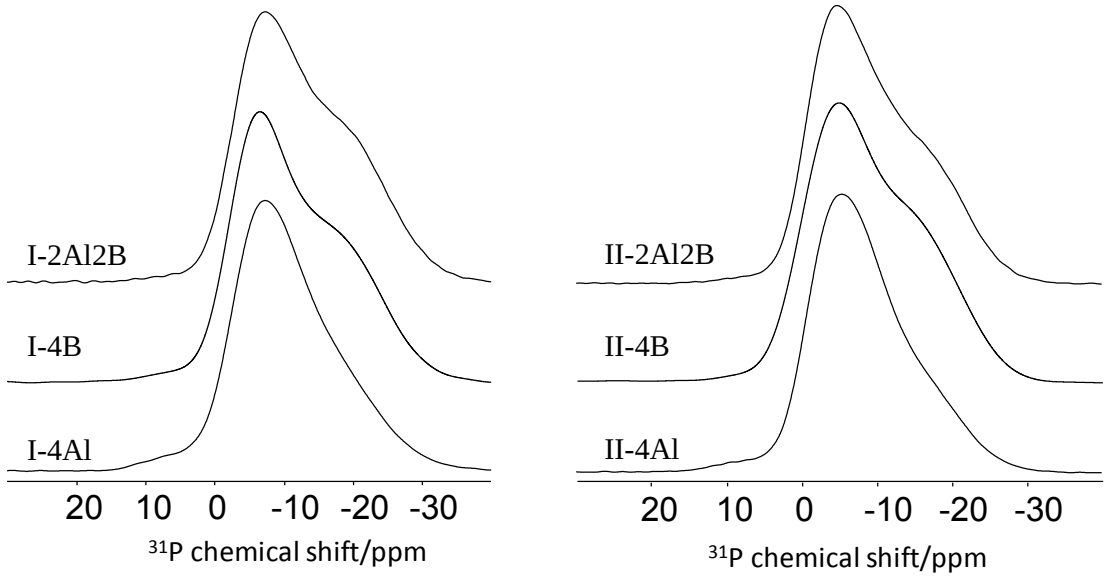

Fig. 6.8. 1D ^{31}P MAS NMR of the Al-,B- and (Al+B)-doped glasses.

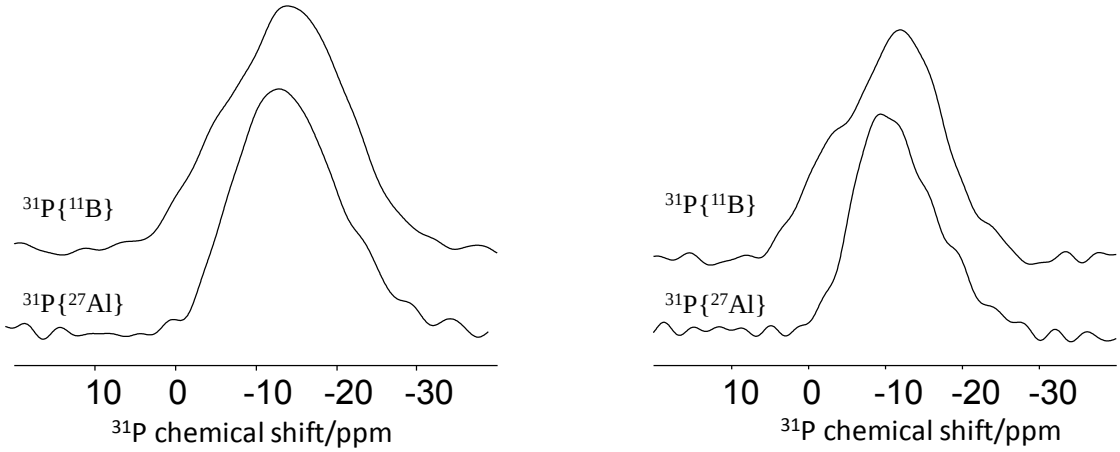

Fig. 6.9 Comparison of ^{31}P{^{27}Al} D-INEPT with ^{31}P{^{11}B} D-INEPT MAS NMR of (Al+B)-doped glasses.

Of course, the phosphate entity speciation and the determination of the percentage of phosphorus involved in P-O-X (X= ^{27}Al, ^{11}B) linkages as well as tracing out the presence of Al-O-Al and B-O-B bonds would be very useful and are recommended for the future work in order to obtain deeper structural insights.

References

Benson, S.W, *J. Chem. Educ.* 42 (1965):502

Brow, R K, *J. Am. Ceram. Soc.* 76 (1993):913-918.

Bunker, B C, G W Arnold, and J A Wilder. *J. Non-Cryst. Solids.* 64 (1984): 291-316.

Cottrell, T L, *The Strengths of Chemical Bonds*, 2nd ed. Butterworth, London, (1958).

Dupree, R. *Nature*, 328 (1987): 416-417.

Fayon, F, C Duée, T Poumeyrol, M Allix, and D Massiot. *J. Phys. Chem. C.* 117(2013):2283-2288.

He, Y, and D E Day. *Glass. Technol.* 32 (1991): 166.

Kerr, J.A, *Chem. Rev.* 66 (1966):465.

Kreidl, N J, W A Weyl, *J. Am. Ceram. Soc.* 24(1941): 372.

Lim, J W, M L Schmitt, R K Brow, and S W Yung, *J. Non-Cryst. Solids.* 356 (2010): 1379-1384.

Mascaraque, N, A Duran, and F Munoz, *J. Non-Cryst. Solids.* 357 (16-17) (2011): 3212-3220.

Tindyala, M A, and W R Ott. *Ceram. Bull.* 57 (1978): 432.

Walter, G, U Hoppe, J Vogel, G Carl, and P Hartmann. *J. Non-Cryst. Solids*.333(2004):252-262.

General conclusion

The effects of Al_2O_3-, B_2O_3- and SiO_2-doping (< 4 mol%) on the properties, stabilities and structure of low-T_g (< 400°C) phosphate glasses have been investigated in this work. The global objective was to optimize a formulation presenting low-T_g and high stabilities characteristics.

The first step within this work was to identify a suitable based (undoped) composition taking into account the low-T_g and acceptable stability parameters. A simple system (3 oxides) was derived from the literature and contains zinc, sodium and phosphorous oxides. More precisely, the system was designed to produce a pyrophosphate structure and can be expressed using the (66.6-*x*)ZnO- *x* Na_2O- 33.4P_2O_5 composition line.

The effects of the substitution of Zn^{2+} by Na^+ ions (*x* in the above-mentioned system) on the glass preparation, properties, stabilities and structure were investigated. Homogeneous glasses were prepared using the standard melt-quenching technique up to $x = 40$. The macroscopic properties of the (66.6- *x*)ZnO- *x*Na_2O- 33.4P_2O_5 system with $0 \leq x \leq 40$ experience classical evolutions encountered when a divalent ions is substituted by two monovalent ones: the T_g and density decreases whereas molar volume increases. Two-domain regimes were determined for the thermal and chemical stabilities. It turns out that the x =20 sample lies within the two domains for both stabilities. It presents the highest Angell parameter and is the highest Na_2O content sample belonging to the high chemical durability domains. The low T_g of this composition (339 °C) and the remarkable stabilities make of this sample a perfect formulation for the investigation of doping procedure effects. In addition to the x =20 sample, the x =33.3 was also considered for the doping procedure. The effect of the Zn/Na substitution on the glass structure was also studied. Raman and 1D ^{31}P NMR analysis indicate the presence of dimeric entities, as expected from the structure. 2D ^{31}P DQ-SQ analysis give new insights on the medium range order structure and show that high ZnO content samples exhibits higher disordered extent than the high Na_2O samples. In the former glasses, dimeric entities are accompanied by isolated monophosphate and 3- and 4- phosphate unit of chains. High ZnO compositions thus present a high topological disorder, in a good

agreement with the intermediate role of zinc oxide, compared to samples containing significant amount of the pure modifying network sodium oxide.

Insertions of low amounts (< 4 mol%) of Al_2O_3, B_2O_3 and SiO_2 in the x =20 and 33.3 samples were investigated in terms of properties and stabilities evolution. It turns out that Al-doping procedure significantly increases the T_g and viscosity parameters, leads to a moderate improvement of the thermal stability but dramatically increases the chemical durability. B-doping procedure has a moderate impact on T_g and viscosity, improve significantly the thermal stability but has a negative impact on the chemical durability. Si-doping procedure does not lead to significant change for any parameters and stabilities. Preliminary structural investigations by 1D MAS-NMR shows that Al^{3+}, B^{3+} and Si^{4+} ions are present in the materials as 6-, 4- and 4-fold coordinated species, respectively. The ^{29}Si chemical shift indicate a Q^4 speciation, suggesting that the Si^{4+} ions are clustered and do not enter into the phosphate network. This lack of interaction explains the insignificant impact of this doping procedure on the material characteristic. Si-doping has thus to be considered as inefficient in our low-T_g system.

1D/2D correlation NMR was used to analyse the correlations between the phosphate network and the doping elements (Al and B). The recently developed $^{31}P\{X\}$ D-INEPT technique proves the presence of P-O-Al and P-O-B linkages in the doped compositions, highlighting thus the interactions of the dopants with the phosphate structure. The main structural unit is a Q^1_{1X} (X=Al, B) species coming from the attachment of one doping polyedra to chain end of a dimeric phosphate group. In addition to this structural feature, it appears that Al^{3+} and B^{3+} ions interact differently with the phosphate structure, the former leading to Q^1_{2Al} groups and the latter producing Q^2_{1B} and Q^0_{1B} species. The chemical environment of the dopants was investigated with the $X\{^{31}P\}$ and X DQ-SQ NMR techniques. The results clearly indicate the Al^{3+} and B^{3+} are only attached to phosphate groups leading to the formation of $Al(OP)_6$ and $B(OP)_4$ groups. This indicates a perfect dispersion of the dopants within the phosphate melts and glasses (no Al-O-Al and B-O-B bonds were detected) and it rules out the interactions between the dopants and the Zn^{2+} ions. The doping procedure thus only affects the phosphate network.

The properties / stabilities modifications induced by doping were related to the structural changes and discussed. It turns out that the chemical durability is improved in Al-doped samples presenting a more reticulated structure owing to the presence of $Al(OP)_6$ groups. Thermal stability is better in B-doped samples due to the presence of higher energy P-O-B bonds. Each doping-procedure has thus proven its efficiency in the improvement of specific stability. Samples containing both Al_2O_3 and B_2O_3 oxides simultaneously have been prepared to determine if benefic effects of both doping procedures could be combined or if they cancel each other. The first results are in line with an additive effect, and no trace of a $Q^n_{Al,B}$ (Al-O-P-O-B bond) site has been detected in this preliminary study.

In the future, optimized formulations could be tested in order to open the way for new applications. Before considering that, the present project could be continued, improved and developed following the next topics:

(i) the Al- and B-doped composition could be analysis in a deeper way by optimizing the Al/B ratio and investigating the Al/B interactions though $^{27}Al/^{11}B$ correlation analysis. There are only a few papers focusing on interactions between two quadrupolar nuclei but this study could afford valuable information. Recently, $^{27}Al/^{11}B$ correlation spectrum was edited using a modified cross polarization technique on a magnesium alumino-borate glasses (Lu, 2013).

(ii) deeper insight onto the doped structure could be obtained by using combined NMR pulse sequences. D-INEPT-DQ-SQ technique could for example be used to determine if the Al-attached dimmers are formed by two Q^1_{1Al} or by a mixture of Q^1_{1Al} and Q^1_0 species. Up to now, combination of INEPT and other sequences were not successful. Use of other dipolar recoupling technique like the cross polarization could overcome this limitation.

(iii) ZnO is a major component of the glasses. It is thus clear that the coordination state of Zn^{2+} is a key parameter for understanding the global structure of the material. As mentioned in chapter C, we assume 4-fold coordination based on literature study. We also demonstrated that doping only interacts with the phosphate network. Nevertheless, an indirect change in the Zn^{2+} speciation cannot be completely ruled out. Additional ^{67}Zn MAS-NMR experiments, coupled with

EXAFS or neutron diffraction would afford valuable information. Moreover, Zn^{2+} speciation could also be investigated using an indirect procedure. In 2012, $^{13}C\{^{67}Zn\}$ RESPDOR NMR technique was used to derive the C-Zn distance in zinc acetate molecule (Lu, 2012). This technique could be used in zinc phosphate glasses to determine the P-Zn distance. Change in the global distance would indirectly trace evolution of the zinc coordination state.

(iv) other doping elements could be investigated. Glasses containing significant amounts of MoO_3 have shown high resistance against crystallization (Santagneli, 2007). However, insertion of low MoO_3 amounts is not well documented and sparce information are available about the chemical environment of Mo^{6+} within the glass matrix. Fe^{3+} could also be a very interesting doping element to study. However, significant reduction from Fe^{3+} to Fe^{2+} is likely to occur and NMR will not be suitable for the structural determination of such matrix. Doping with Ga^{3+} ions could also benefic for the development of stable glasses. Recently, we showed that Ga^{3+} speciation can be efficiently derived from ^{71}Ga MAS-NMR performed at very high field and very high spinning frequency (Caron, 2013).

References

Caron, A, Preparation, properties and structure of Ga_2O_3-$NaPO_3$ glasses, comparison with Al_2O_3 and B_2O_3 containing systems, Master thesis Lille 1, (2013).

Lu, X, A S L Tankamony, J Trebosc, O Lafon, and J P Amoureux, *J. Magn. Reson.* 228 (2013): 148-158.

Lu, X, O Lafon, J Trebosc, and J P Amoureux *J. Magn. Reson.* 215 (2012): 34-49.

Santanegli, S H, C C Araujo, W Strojek, H Eckert, G Poirier, S J L Ribeiro, and Y Messaddeq, *J. Phys chem. B*, 111 (2007): 10109-10117.

Caractérisation par RMN de l'effet des dopants Al_2O_3, B_2O_3 et SiO_2 sur les verres de phosphate de basse T_g.

Les verres de phosphates à faible température de transition vitreuse (T_g) et haute stabilité thermique ont été étudiés dans le système (66-x)ZnO- xNa_2O- $33.4P_2O_5$. Les mesures DSC ont montré un écart T_x-T_g de 197 °C et une T_g de 339 °C pour x = 20. La RMN ^{31}P 1D/2D révèle la diminution du désordre due à la substitution progressive de Zn par Na.

Les formulations x = 20 et x = 33 ont été dopées par Al_2O_3, B_2O_3 et SiO_2 (1-4 % mol.). Les effets du dopage sur les propriétés physiques comme la T_g, la stabilité thermique et la durabilité chimique ont été analysés. La DRX et la RMN ^{31}P ont été réalisés pour suivre le processus de cristallisation isotherme à 130°C au-delà de la T_g. La plus forte stabilité thermique a été identifiée pour les verres dopés au bore.

Les spectroscopies Raman et de RMN ont mis en évidence l'existence de liaisons P-O-X (X=^{27}Al ou ^{11}B) et la clusterisation des entités silicatées. L'utilisation de technique RMN de corrélation D-INEPT, REDOR et DQ-SQ ont permis d'approfondir nos connaissances sur la structure complexe de ces matériaux.

Key words: zinc pyrophosphate glasses, low-T_g, thermal stability, disordered structure doping of Al, B and Si, ^{31}P, ^{27}Al and ^{11}B NMR, ^{27}Al-^{31}P and ^{11}B-^{31}P NMR correlations.

Advanced NMR characterization of the effect of Al_2O_3, B_2O_3 and SiO_2 doping on low-Tg phosphate based glass.

Pyrophosphate glasses with low T_g and high stability have been investigated within the (66-x) ZnO- xNa_2O-33.4 P_2O_5 system. DSC measurement indicated T_x-T_g = 197 °C with T_g = 339 °C at x = 20. 1D/2D ^{31}P NMR revealed the decrease in extent of disorder with the progressive substitution of Zn by Na.

The x = 20 and x = 33 formulations were doped with (1-4 mol%) of Al_2O_3, B_2O_3 and SiO_2 and its effect on the physical properties such as the glass transition temperature, thermal stability and chemical durability is investigated. XRD and 1D ^{31}P solid state NMR were used to monitor the isothermal crystallization process occurring at 130 °C above T_g and the highest thermal stability is presented by the B-doped glasses.

Raman and ^{31}P NMR suggested the existence of P-O-X (X = ^{27}Al or ^{11}B) bonds and the silicate segregation. The use of D-INEPT, REDOR and DQ-SQ helped in producing deep insights onto the glass structure about the P-O-X connectivity, the wide range of phosphate speciation.

Key words: zinc pyrophosphate glasses, low-T_g, thermal stability, disordered structure doping of Al, B and Si, ^{31}P, ^{27}Al and ^{11}B NMR, ^{27}Al-^{31}P and ^{11}B-^{31}P NMR correlations.